Dual Inhibitors of ROCK-I and NOX2 to Attenuate Neuroinflammation in Neurological Disorders: High Throughput Virtual and Biological screening

THESIS

Submitted in partial fulfilment

of the requirements for the degree of

DOCTOR OF PHILOSOPHY

by

RESHMA CHOWDARY ALOKAM

ID No 2011PHXF018H

Under the Supervision of

Prof. P. YOGEESWARI

BITS Pilani

Pilani | Dubai | Goa | Hyderabad

BIRLA INSTITUTE OF TECHNOLOGY AND SCIENCE, PILANI

2015

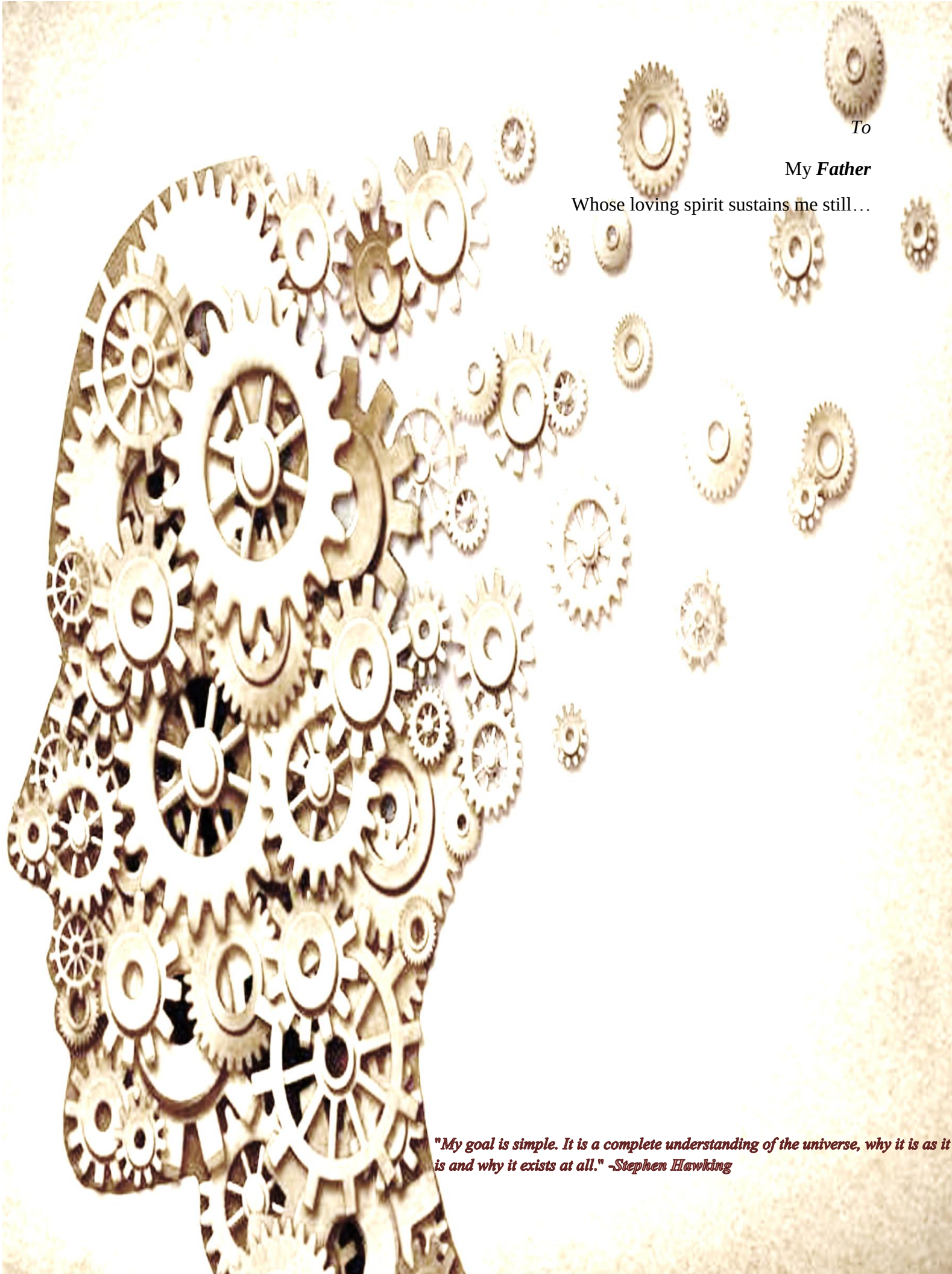

To

My ***Father***

Whose loving spirit sustains me still…

"My goal is simple. It is a complete understanding of the universe, why it is as it is and why it exists at all." -Stephen Hawking

BIRLA INSTITUTE OF TECHNOLOGY AND SCIENCE, PILANI

CERTIFICATE

This is to certify that the thesis entitled "**Dual Inhibitors of ROCK-I and NOX2 to Attenuate Neuroinflammation in Neurological Disorders: High Throughput Virtual and Biological Screening**" and submitted by **RESHMA CHOWDARY ALOKAM** ID No. **2011PHXF018H** for award of Ph.D. of the Institute embodies original work done by her under my supervision.

Signature of the Supervisor:

Name in capital letters : **P.YOGEESWARI**

Designation : **Professor**

Date:

ACKNOWLEDGEMENTS

It is done! Another exciting period in my life is accomplished. A bit more than a year after my post-graduation, I got a PhD position offered in Pharmacy Department, BITS-Pilani Hyderabad Campus which resulted in this book here. Of course this thesis was a fine piece of work and would be not the same without the support of many people. Thanks to all of you!

I would like to express my deepest gratitude to my mentor, ***Prof. P.Yogeeswari****, Professor and Associate Dean (Sponsored Research and Consultancy Division), Department of Pharmacy, BITS-Pilani Hyderabad Campus for the confidence she has placed in me by offering me a PhD position. I also thank her for the continuous guidance both personally and professionally, for her valuable suggestions and support. She was always an inspiration to me for my work. She was always an inspiration to me in research.*

I don't know how to thank ***Prof. D.Sriram****, Professor, Department of Pharmacy, BITS-Pilani Hyderabad Campus for introducing me in the wonderful world of neuropharmacology and keeping trust on my strengths and knowledge. Over the years you became more than just a DAC member to me. Your guidance made me the scientist that I am.*

I am thankful to acknowledge my DAC member ***Dr. Arti Dhar****, for her support and encouragement during this period.*

I am grateful to ***Prof. Bijendra N. Jain****, Vice-Chancellor, BITS-Pilani Campus and* ***Prof. V.S.Rao****, Director, BITS-Pilani Hyderabad Campus for allowing me to carry out my doctoral research work in the institute.*

I am thankful to ***Prof. M.M.S.Anand****, Registrar and* ***Prof. S.K.Verma****, Dean, Acamedic Research (Ph.D. Programme), BITS-Pilani for their support to do my research work.*

I would like to ***Prof. M.B.Srinivas****, Dean, Administration and* ***Prof. Vidya Rajesh****, Associate Dean, Academic Research (Ph.D Programme), BITS-Pilani Hyderabad Campus for their continuous support and encouragement during my research work.*

I would like to express my gratitude to ***Prof. Srikanth Charde****, Associate Professor & Head, Department of Pharmacy, BITS-Pilani Hyderabad Campus for providing me with all necessary laboratory facilities and for having helped me at various stages of my research work.*

I sincerely acknowledge the help rendered by ***Prof. Punna Rao****,* ***Prof. Sajeli Begum****, and other* ***Faculty members****, Department of Pharmacy, BITS-Pilani Hyderabad Campus.*

*Thanks to **Dr. Mallika**, without your help I would not have done my biological screening assays. Thanks a lot for helping me with the doubts and making me understand the underlying mechanism involved in the study.*

*I am grateful to express my sincere thanks to **Mr. Madhu**, **Mr. Saketh** and **Mr. Gangadhar** for their encouragement in establishing animal models and support given for my ideas and even to my annoying feats. **Ms. Brinda,** you were a great colleague and also became good friend. We went together through all ups and downsides of culturing HEK cell lines (mainly with the contamination) and I think we can proudly call ourselves as "trouble shooting team". It was a great time working and discussing with you. Also thanks to **Mr. Praveen**, **Mr. Ganesh P** and **Mr. Ganesh S** for sending me full text articles whenever I needed them. I am grateful to **Dr. Jean** and **Mr. Srikanth** for helping me with the compound synthesis. I thank **Dr. Mahesh** (from CCMB, Hyderabad) for making me understand histopathological studies. **Ms.Sridevi** and **Ms.Priyanka S**, thank you girls for making me to forget stressful work environment with all your laughter and movie outings. I would like to thank all other PhD scholars in the Pharmacy Department who suffered together with me in this journey. And of course I would like to thank all the students **Sarthak, Geetha Sai, Piyush** and **Sowmya** who helped me to accomplish this piece of work!*

*I express my thanks to our laboratory attenders and demonstrators **Mr. Rajesh, Mr. Seenu, Ms. Saritha** and **Ms. Rekha** for all their support.*

I deeply acknowledge the BITS-Pilani Hyderabad Campus, Hyderabad, India for providing me the fellowship and contingency.

*I would like thank my grandparents **Venkateswarlu** and **Sivamma** and close relatives **Naga Bhushanam** uncle, **Vani** aunt, **Bhavannarayana** uncle and **Bujji** aunt for all their support and prayers. And also special thanks to my cousins **Ranadheer**, **Nalini**, **Pooji**, **Chikki**, **Chintu** and **Sunny** for their support and for feeling proud of me and my doctorate.*

*At the end, but from my heart, I thank and deeply appreciate my family late **Mr. Pandu Ranga Rao** and **Mrs. Siva Naga Kalyani**, my brother **Mr. Narendra Nath** for their faith in me and allowing me to be as ambitious as I wanted. It was under their watchful eye that I gained so much drive and an ability to tackle challenges head on. No words can express how grateful I am for your love and support. You made my world beautiful.*

Lastly, and above all, I would like to thank the god almighty; for all that he has given to me.

Abstract

Neurological diseases (ND) associated with inflammation are the most common form of dementia among both infantile and elderly. The disease is characterized by amyloid-β (Aβ) plaques, synucleins, and neurofibrillary tangles, loss of synapses or neurons and chronic neuroinflammation. The significance of neuroinflammatory processes in attributed to both protective and damaging properties. However, patients systematically treated with anti-inflammatory drugs have been shown to develop ND to a lesser extent than average. This thesis focuses on four inflammatory related transcription factors, interleukin-6 (IL-6), interleukin-1β (IL-1β), tumor necrosis factor α (TNF-α) and nuclear factor κB (NF-κB) triggered by novel targets identified in neurological disorders.

Treating neuroinflammation in progressive neurological diseases is a remarkable strategy to obstruct superoxide generating inflammatory pathways. Two important targets identified to be crucial in progressive neuronal damage associated with neurodegeneration and neurodevelopmental disorders were ROCK-I and NOX2. NOX2 is a multi-enzyme component which is activated during host defence in phagocytes such as microglia, to catalyse the production of superoxide from oxygen. On the other hand ROCK-I is also an important mediator for fundamental cell processes like adhesion, proliferation and migration. Phosphorylated ROCK was found to activate NOX2 assembly *via* Ras related C3 botulinum toxin substrate (Rac) in inflammatory diseases. Thus, over expression of ROCK-I and NOX2 in microglial cells contributed to progressive neuronal damage early in neurodevelopmental and neurodegenrative disease development.

In the present study, a diverse set of molecules as possible ROCK-I and NOX2 dual inhibitors were identified using structure based drug design strategy utilizing interaction energy and shape of the crystal ligands reported. Lead molecules thus obtained from the structure based design and virtual screening of databases were experimentally validated with *in vitro* enzymatic assays, where, the most active lead compound from Asinex database (compound **RA6**) with ROCK-I IC_{50} of 1.8 nM, NOX2 ROS IC_{50} of 2.853 μM and in cell based assays, showed an EC_{50} of 3.03 nM against MeHg induced IMR-32 and EC_{50} value of 303 nM in LPS induced HUVE cell lines. This inferred that dual inhibition had beneficial effects. This compound was selected as best lead molecule from the Asinex database to test for the synergistic effect in combination with already

reported ROCK-I inhibitor Fasudil. **RA6** efficiently inhibited the cell motility and TNF-α and other inflammatory mediator's expression levels in cell lines. In *ex vivo* evaluation also, the inflammatory mediators were found suppressed when treated with the **RA6** in brain slices. **RA6** was found non- cytotoxic at the highest concentration tested (100 μM).

In the second phase, 37 molecules were selected from *in house* library through molecular docking studies and analyzed for the enzyme inhibition against ROCK-I and NOX2. All the 37 compounds were biologically evaluated for cytotoxicity (CC_{50}) and in cell based models (EC_{50}) to identify the best ROCK-I and NOX2 dual inhibitor in MeHg induced IMR-32 and LPS induced HUVE cell lines, using anti proliferative assays. Lead molecules were selected based on the selectivity index (CC_{50}/EC_{50}) and compound **RB12** with ROCK-I IC_{50} of 357 nM, NOX2 ROS IC_{50} of 817.2 nM and EC_{50} of 94.5 nM in MeHg induced IMR-32 cellines and EC_{50} of 88.5 nM in LPS induced HUVEC respectively emerged as a promising compound. **RB12** also showed synergistic effect but was found to be potent in ROS inhibition, lesser cytotoxic (reduced 10 fold) and more selective (2 fold) and exhibited greater cellular motility. **RB12** in combination with Fasudil also showed remarkable decrease in the inflammatory mediators expression in disease based cell lines (both MeHg and LPS) and *ex vivo* brain slices.

Finally **RB12** was taken up for *in vivo* studies to assess the neuroprotective activity in MeHg and LPS induced animal models using a cascade of behavioral assays including clasping assay, locomotor test and gait analyses. **RB12** was found to reduce MeHg induced neurodegenration in rats more efficiently than Fasudil and was also reascertained using histopathological studies.

There were no signs of demyelination or inflammatory mediators expression in **RB12** treated animals, in both MeHg and LPS induced animal models at transcript levels. Thus the present study was fruitful in utilizing computational tools in identifying dual inhibitors of novel targets invovlved in various neurological disorders.

Table of contents

List of Figures

List of Tables

Abbreviations

6-OHDA	:	6-Hydroxydopamine
A2 M	:	Alpha-2-macroglobulin
AD	:	Alzheimer's disease
ADME	:	Absorption, distribution, metabolism and excretion
AGC	:	Protein kinase A,G and C classes
AGE	:	Advanced glycation endproducts
ALS	:	Amyotrophic lateral sclerosis
APP	:	Amyloid precursor protein
ASD	:	Autism spectrum disorders
ATP	:	Adenosine triphosphate
AUC	:	Area under curve
BACE	:	β-secretase
BBB	:	Blood-Brain Barrier
BDNF	:	Brain derived neurotrophic factor
BEDROC	:	Boltzmann-Enhanced Discrimination of Receiver-Operating Characteristic
BrdU	:	5-Bromo-2-deoxyuridine
CADD	:	Computer-aided drug design
CBD	:	Coritco basal degeneration
CC_{50}	:	Cell cytotoxicity 50
CD 14	:	Cluster differentiation 14
cDNA	:	Complementary DNA
CGC	:	Cerebellar granule cells
CGD	:	Chronic granulomatous disease
ChP	:	Choroid plexus
CNS	:	Central nervous system
COX	:	Cyclooxygenase
CRMP2	:	Collapsin response mediator protein 2
CSF	:	Crebro-spinal fluid
CSPG	:	Chondroitin sulphate proteoglycans
CVO	:	Circumventricular organs
D	:	Day
DA	:	Dopaminergic Neurons
DCFH-DA	:	Dichloro flourescien hydrate diacetate
DMPK	:	Myotonic dystrophy kinase
DMSO	:	Dimethyl sulphoxide
DN-TNF	:	Dominent negative tumor necrosis factor

DPI	:	Diphenyleneiodonium
DTT	:	Dithiothreitol
EC_{50}	:	Effective concentration 50
ECGF	:	Endothelial cell growth factor
ED	:	Ectodermal dysplasia
EDTA	:	Ethylenediaminetetraacetic acid
EF	:	Enrichment factor
e-pharmacophore	:	Energy based pharmacophore
ERK1/2	:	Extracellular signal- regulated kinase 1/2
ERM	:	Ezrin/Radixin/Moesin
FAD	:	Flavin adenine dinucleotide
FBS	:	Fetal bovine serum
FGF	:	Fibroblast growth factor
FTD	:	Frontotemporal dementia
GAP	:	GTPase-activating proteins
GDI	:	Guanine nucleotide-dissociation inhibitors
GEF	:	Guanine nucleotide-exchange factors
GFAP	:	Glial fibrillary acidic protein
GST	:	Glutathione S-transferase
GTP	:	Guanidine tri phosphate
H	:	Hour
H_2O_2	:	Hydrogen peroxide
hAPP	:	Human amyloid precursor protein
HD	:	Huntington's disease
HEK	:	Human embryonic kidney epithelial cells
Hg	:	Mercury
HL-60	:	Acute myeloid leukemia cell line
HPA	:	Hypothalamic-pituitaryadrenal axis
Htt	:	Huntington gene
HTVS	:	High throughput virtual screening
HUVEC	:	Human umbilical vein endothelial cells
IC_{50}	:	Inhibitory concentation 50
ICV	:	Intracerebroventricular
IFNγ	:	γ-Interferon
IL-1	:	Interleukin-1
IP	:	Intraperitoneal
IPTG	:	Isopropyl β-D-1-thiogalactopyranoside
ITC	:	Isothermal titration calorimetry
IV	:	Intravenous
JNK	:	c-Jun N-terminal kinase

LBP	:	LPS-binding protein
LC3-I	:	Microtubule-associated protein 1A/1B-light chain 3
LINGO1	:	Low-affinity neurotrophin receptor
LPA	:	Lysophosphatidic acid
LPS	:	Lipo polysaccharide
LTP	:	Long Term Potentiation
MAG	:	Myelin-associated glycoprotein
MAP2	:	Microtubule-associated protein 2
MAPK	:	Mitogen activated protein kinase
MBP	:	Myelin basic protein
MeHg	:	Methyl mercury
MEM	:	Minimal essential medium
MHC	:	Major Histo compatability complex
Min	:	Minutes
MLC	:	Myosin light chain
MLCP	:	MLC phosphatase
MPE	:	Maximum possible effect
MPTP	:	1-Methyl-4-phenyl-1,2,3,6-tetrahydropyridine
MRCK	:	Myotonic dystrophy kinase-related CDC42-binding kinase
mRNA	:	Messenger RNA
MS	:	Multiple sclerosis
MTT	:	3-(4,5-Dimethylthiazol-2-yl)-2,5-Diphenyltetrazolium Bromide
MWM	:	Morris water maze
NADPH	:	Nicotinamide adenine dinucleotide phosphate
ND	:	Neurodegenerative Diseases
NF-kB	:	Nuclear factor kappa B
NGF	:	Nerve growth factor
NgR	:	NOGO receptor
Ni-NTA	:	Nickel-nitrotriaceticacid
Nm	:	Nano meters
nM	:	Nano molar
NMDA	:	N-methyl-d-aspartate
NO	:	Nitric oxide
NOGO-A	:	Neurite outgrowth inhibitor-A
NOX	:	Nicotinamide adenine dinucleotide phosphate-OXidase
NOX2	:	NADPH oxidase 2
Nrf2	:	Nuclear factor (erythroid-derived 2)-like 2
NSAID	:	Non-steroidal anti-inflammatory drugs
NT-3	:	Neurotrophin-3
NTR-3	:	Neurotensin receptor-3
OMgp	:	Oigodendrocyte myelin glycoprotein

OPC	:	Oligodendrocyte precursor cells
PB1	:	PHOX and Bem1
PD	:	Parkinson's disease
PHOX	:	Phagocyte oxidases
PiD	:	Pick's disease
PKN	:	Protein kinase N
PNS	:	Peripheral nervous system
PRK-2	:	Protein kinase C-related protein kinase 2
PRR	:	Proline rich region
PSP	:	Progressive supranuclear plasy
PtdIns(3)P	:	Phosphatidylinositol 3-phosphate
PTEN	:	Phosphatase and tensin homolog
PWD	:	Paw withdrawal duration
PWT	:	Paw withdrawal thresholds
PX	:	PHOX homology
QPlogBB	:	Predicted brain/blood partition coefficient
QPlogPo/w	:	Predicted octanol/water partition coefficient
QPPCaco	:	Predicted apparent Caco-2 cell permeability in nm/sec using the Boehringer-Ingelheim scale
RBD	:	Rho-binding domain
RFU	:	Relative fluorescence unit
RGM	:	Repulsive guidance molecule
Rho GTPases	:	Small GTP-binding proteins of the Rho subfamily
RNA	:	Ribonucleic acid
ROS	:	Reactive oxygen species
RT Enhancer	:	Reverse transcriptase enhancer
RT-qPCR	:	Real Time quantitative PCR
Sec	:	Seconds
SeH	:	Selenol
SH	:	Thiol
SH3	:	Src homology 3 regions
siRNA	:	Silencing RNA
SNpc	:	Substantia nigra pars compacta
SNT	:	Partial sciatic nerve transection
SOD1	:	Superoxide dismutase I
SOD1	:	Superoxide dismutase-1
SP	:	Standard precision
SVZ	:	Sub ventricular zone
TBST	:	Tris-buffered saline Tween-20
Th1	:	T helper type 1
TIR	:	Toll/IL-1 receptor

TLR	:	Toll like receptor
TNFR1	:	TNF receptor 1
TNF-α	:	Tumor necrosis factor-α
TPR domain	:	Tetratricopeptide repeats
TRI reagent	:	TRIzol reagent
VEGF	:	Vascular endothelial growth factor
vROCS	:	Rapid Overlay of Chemical Structures
XP	:	Xtra Precision
X-ROS	:	NOX mediated reacive oxygen species
μM	:	Micro molar

Chapter 1

Introduction to neuroinflammation and methods of drug design

1.1 INTRODUCTION

The normal adult central nervous system (CNS) contains low or undetectable levels of most systemic inflammatory cell subsets or their products such as cytokines. The immune-competent cell intrinsic to the mature CNS, microglia, can be found in their normal state to be ramified in morphology, with processes that are quite evenly spread within the CNS parenchyma and with each microglia and its processes located in its own domain. In classic inflammatory disorders of the CNS, such as multiple sclerosis (MS), various immune cell subsets infiltrate from the periphery, and these include T and B lymphocytes, monocytes that become macrophages in tissue, and the less well-documented professional antigen-presenting cells, dendritic cells. Also, microglia becomes activated, and converge at lesion areas where they transform into ameboid shaped cells [Kreutzberg GW., *et al.,* 1995]. The latter are hard to differentiate morphologically and phenotypically from macrophages that have invaded from the circulation, and these cells are thus commonly and collectively referred to as microglia/macrophages.

Microglia/macrophages and neutrophils are not antigen specific, they respond quickly to injury, and they are referred to as innate immune cells. T and B lymphocytes are antigen specific, with each recognizing a cognate set of amino acid sequence/conformation designated “antigen,” and they are referred to as the adaptive immune response [Town T., *et al.,* 2005]. Thus, from the

above descriptor, both innate and adaptive immune responses are represented in classic immune-mediated neurological conditions and in acute traumatic or vascular neurological disorders

Even when there is no evidence of prominent infiltration of leukocyte subsets into the CNS, such as in Parkinson or Alzheimer disease, microglial activation is prominent around areas of neurodegeneration. As with infiltrating innate and adaptive immune cells, the activated microglia are a rich source of several cytokines, chemokines, free radical species, proteases, and other potential mediators of injury [Gao HM., *et al.,* 2008]. With the occurrence of microglial activation in classic neurodegenerative conditions that are not associated with significant influx of systemic leukocytes, it is fair to state that neuroinflammation is a feature of virtually all neurological conditions.

1.1.1 The impact of neurological disorders in the global population

The population of our world is ageing and an ever-increasing number of elderly are affected by neurodegenerative diseases. In the developed world, about 2% of the population is afflicted at any time [Hardy J., *et al.,* 2006]. The neurodegenerative diseases include Alzheimer's disease (AD), Parkinson's disease (PD), amyotrophic lateral sclerosis (ALS), progressive supranuclear palsy (PSP), coritco basal degeneration (CBD), Huntington's disease (HD), multiple sclerosis (MS), frontotemporal dementia (FTD), Pick's disease (PiD) and prion diseases. Recently, the "World Neurodegenerative Diseases Market 2009-2024" forecasted that the overall neurodegenerative disease drug market currently estimated at reaching US$20 billion by 2017 (https://bccresearch.wordpress.com/tag/global-pharmaceuticals-industry/).

The overall neurodegenerative diseases market is growing at over 8.5% for each five years. With an increase in life expectancy and the number of old people, along with advances in treatments of neurodegenerative diseases, this increase is set to continue. According to Alzheimers association (www.alz.org), the global data report estimates AD to rise rapidly in emerging nations such as China and India. Throughout the forecast period, US and China would have the highest number of prevalent cases of AD, with high numbers than the five EU (France, Germany, Italy, Spain, the UK) countries combined, while India could demonstrate the fastest growth rate.

The case fatality of ND in india was 27% in Trivandrum, Kerala, 30%in Mumbai, and 42% in Kolkata, following ND and a matter of serious concern is early deaths of 20% in Kerala and 33%

in Kolkata. The lower case fatality rate in Kerala reflects better healthcare than in Kolkata. In the recent long term study in Kolkata over 7 years, the case fatality was 59% at 5 years and 61% at 7 years [Gourie-Devi M., *et al.,* 2014]

The neurodegenerative disease cost the US economy billions of dollars each year in direct healthcare costs and lost opportunities; it is estimated that $100 billion per years is spent on the AD alone. In addition to financial costs, there is an immense emotional burden on patients and their caregivers. As the number of elderly citizen increases, these costs to society would also increase [Brown RC., *et al.,* 2005]

1.1.2 The environmental risk factors for neurological diseases

Neurodegenerative diseases are characterized by progressive nervous system dysfunction. These disorders result from the gradual and progressive loss of neural cells, leading to nervous system dysfunction, neurodegenerative diseases can affect abstract thinking, skilled movements, emotional feelings, cognition, memory and other abilities [Soto C., *et al.,* 2003]. Known risk factors for neurodegenerative diseases include certain genetic polymorphisms and increasing age. Other possible causes may include gender, poor education, endocrine conditions, oxidative stress, inflammation, stroke, hypertension, diabetes, smoking, head trauma, depression, infection, tumors, vitamin deficiencies, immune and metabolic conditions, and chemical exposure like mercury, copper and iron. Because the pathogenesis of many of these diseases remains unknown, the role of environmental factors in neurodegenerative diseases has to be considered [Brown RC., *et al.,* 2005]. Although there is a growing body of evidence suggesting that a large proportion of the non-familial cases are significantly influenced by genetic factors, it is likely like the environmental risk factors play a part in the etiology of some of these conditions. MeHg (Methyl mercury) exposure has been implicated in PD. MeHg poisoning is characterized by severe neurological deficits due to brain lesions and disruptions of neurotransmitter systems, and both PD and MeHg poisoning present resting tremors and alterations in motor functioning. MeHg exposure occurs through seafood consumption, due to the global cycling and accumulation of Hg (mercury) from industries that reaches the aquatic environment. Several studies have shown an association between increase prevalence to PD and fish consumption or occupational exposure to Hg [Aschner M., *et al.,* 2005]. Despite the enormous effort put into searching causes for these diseases, epidemiological evidence for an association between

environmental agents and neurodegenerative diseases remains inconclusive [Brown RC., *et al.*, 2005].

1.2 Neuroinflammation and cognition

1.2.1 Effect of cytokines on cognition

Excessive activation of the glial cells such as microglia and astrocytes was reported to significantly increase the production of cytokines such as IL-1β and TNF-α [Block ML., *et al.*, 2007]. Elevation of cytokines has been associated with cognitive deficits where in ND and mild cognitive impaired patients, a stage described as a pre-clinical stage of ND an increased levels of inflammatory cytokines were observed in blood samples [Magaki S., *et al.*, 2007, Guerreiro R., *et al.*, 2007]. Furthermore, it was recently reported that an increase in TNF-α induced by acute and chronic inflammation were associated to a decrease in the performance of ND patients in cognitive tasks [Holmes C., *et al.*, 2009]. In PD patients elevated levels of IL-6 were also observed in the nigrostriatal region and cerebrospinal fluid (CSF). In addition, transgenic animals that overexpressed IL-6 exhibited neuropathological changes that were closely correlated with the cognitive deficit reported [Akiyama H., *et al.*, 2000], thus suggesting a possible correlation between inflammation and cognitive deficits.

Under normal physiological conditions however, these cytokines may play an important role in cognitive processes. In studies using TNF knock out animals, it was shown that TNF-α was essential for normal functions of learning and memory. These animals under immunologically non-challenged conditions, performed significantly worse in cognitive tasks [Baune BT., *et al.*, 2008]. In addition, under specific conditions, TNF-α might play a role against neuronal death where TNF-α treatment can protect against focal cerebral ischemia [Nawashiro H., *et al.*, 1997]. *In vitro*, TNF-α through the activation of nuclear factor kappa B (NFκB) may protect neurons against metabolic, excitotoxic or oxidative insults by upholding maintenance of intracellular Ca^{+2} homeostasis and inhibition of reactive oxygen species (ROS) [Pickering M., *et al.*, 2007]. The dysregulation of microglia and astrocytes, leading to the excessive production of the pro-inflammatory cytokines, has since been suggested to prevent the proper function of normal cognitive processes to the extent of dire consequences. Many labs have tried to induce cognitive deficits in rodent model by increasing the levels of cytokines in the CNS. In rodents, Oitzl MS., [

Oitzel MS., *et al.,* 1993] had shown that direct intracerebroventricular (ICV) infusion of IL-1β was able to induce a transient deficit in rodent spatial learning and memory task such as the morris water maze (MWM). Although animals treated with IL-1β did not show any deficit in acquiring the location of the platform, they were unable to recall the location of the hidden platform, when tested 24 h later.

Not limited to centrally infused cytokine, peripheral administration of cytokine was also shown to be able to induce cognitive deficit. The intraperitoneal (IP) injection of 100 ng IL-1β was shown to be effective in disrupting spatial learning and memory [Gibertini M., *et al.,* 1995]. Mice treated with IL-1β showed a significantly higher latency in finding the hidden platform location. It was hypothesized that the administration of IL-1β significantly affected memory acquisition suggesting that central and peripheral administrations of IL-1β may have differing effect on learning and memory. IL-1β was also shown to induce a deficit on long-term memory in contextual fear [Pugh CR., *et al.,* 1998]. These neuroinflammatory mediators have been shown to be able to induce cognitive deficit through several mechanisms that affect the cell survival and neuronal properties.

1.2.2 Effect of inflammation on long term potentiation

Long term potentiation, a form of synaptic plasticity that is widely touted as a model of learning and memory is characterized by a persistent enhancement of neurotransmission following an appropriate stimulus. There is evidence to suggest that cytokines are able to abrogate the action of LTP where peripheral LPS injection was able to impair LTP in the hippocampus [Vereker E., *et al.,* 2000]. LPS was shown to impair LTP through IL-1β activated pathway by increasing the activity of the stress-activated kinases, c-Jun N-terminal kinase (JNK) and p38 mitogen activated protein kinase (MAPK) by increasing the phosphorylation of these kinases, ultimately leading to the impairment in neuronal function [O'Donnell E., *et al.,* 2000].

LPS was also shown to disrupt glutamate release by the activation of p38 and NFκB [Kelly A., *et al.,* 2003]. As glutamate is an important player in the propagation of LTP, disruption of glutamate release would inevitably lead to the impairment of LTP. By studying the glutamate release in synaptosomes of dentate gyrus from rats treated with IL-1β, it was shown that IL-1β

reduces the amount of glutamate release after being tetanized. In addition, peripheral administration of an immunogenic property such as LPS was sufficient to induce, not only neuroinflammation but also impairment in LTP that is reflected in the cognitive deficit observed in animal behavior tests.

1.2.3 Effect of inflammation on neurite outgrowth

Activation of microglia has also been shown to induce cell death at high concentrations of endotoxins such as LPS and advanced glycation end products (AGEs) *in vitro* [Münch G., *et al.,* 2003]. Albeit, it is known that activated microglia could produce various factors that are cytotoxic. However, the exact mechanism through which these reactive glial cells induce neuronal death was completely understood. At a sublethal dose of LPS or AGEs, it was reported that these immunogenic properties were able to induce activation of microglia that can lead to a reduction of neurite outgrowth [Münch G., *et al.,* 2003]. More specifically, TNF-α has been shown to reduce neurite outgrowth and branching in the hippocampal neurons via small GTPase Rho proteins [Neumann H., *et al.,* 2002]. The reduction of neurite outgrowth during a mild inflammation (with an absence of T cell amplified systemic inflammation) with factors secreted by the activated microglia could interfere with the cytoskeleton reorganization. This change in synaptic reorganization was sufficient to induce learning and memory deficits even in the absence of cell death [Gallagher M., *et al.,* 1996]. Reduction of neurite outgrowth has since then been linked to NO and NO-derived products. NO directly regulate actin reorganization in the neurite, by inducing signaling cascades involved in growth cone collapse and through regulation of gene transcription.

1.2.4 Effect of inflammation on oxidative stress generation

Oxidative stress is a prevalent feature in numerous in numerous neurodegeneration diseases albeit the source of ROS was still debatable [Block ML., *et al.,* 2007]. In the microglia, the ROS production is catalysed by the nicotinamide adenine dinucleotide phosphate oxidase (NOX) enzyme complex that converts oxygen to superoxide. Distributed in both the cell membrane and membrane of organelles, the ROS generated under normal conditions has some beneficial functions as plays a vital role in host defense. ROS are involved in cell defence against pathogens, but also in reversible regulatory processes in most cells and tissues [Bedard K., *et al.,*

2007]. Hence, like the proinflammatory cytokines as discussed previously, the beneficial or detrimental effect of ROS lies on a fine balance. In normal aging humans, the level of ROS increases with age as predicted by the "free-radical theory of aging" [Harman D., *et al.,* 1956] and this increase in ROS levels is usually accompanied by a decline in cognitive and motor functions although not associated with a significant loss of neurons [Dröge W., *et al.,* 2007]. Furthermore, a decrease in antioxidant enzymes and concentrations of small-molecular-weight antioxidants in blood and tissue cells, also induce an age-dependent elevation in the proportion of ROS and free radicals that are normally being "removed" [Wei YH., *et al.,* 2002]. The involvement of NOXs in aging has been linked to the increased level of ROS in the CNS [Krause KH., *et al.,* 2007]. More interestingly neural damage induced by extracellular secretion of ROS has been shown to be mediated by NOX through the activation of microglia [Walder CE., *et al.,* 1997]. These oxidative conditions are able to induce irreversible damage to proteins, lipids, carbohydrates and nucleic acids.

In AD and PD patients, NOXs were reported to be upregulated in the CNS [Block ML., *et al.,* 2007]. In addition to the reduction in the concentrations of antioxidants present in the system, most patients suffering from AD and PD also experience an increase in ROS production, further uncoupling the redox balance in the CNS. The excessive ROS in the system could ultimately trigger the mitochondrial apoptosis pathway, inducing a mitochondrial dysfunction by the release of cytochrome C into the cytoplasm [Dean E., *et al.,* 2008]. Thus, during chronic neuroinflammation, the increases in ROS production induced by the upregulation of ROS producing enzymes induce cognitive deficits and neuronal death. The generation of ROS, is reported to act as a common signaling mechanism for phagocytes where the gangliosides activate microglia through protein kinase C and NOX [Min KJ., *et al.,* 2004]. Furthermore, changes in the morphology and proliferation of microglia (microgliosis) were found to be regulated by H_2O_2 produced from NOX [Block ML., *et al.,* 2007]. In return, higher levels of ROS in the intracellular positively regulate the inflammatory response where an increase production of pro-inflammatory response is able to affect cell survival by increasing lipid peroxidation and protein nitration [Engelhardt JF., *et al.,* 2001]. Hence, it seems that the catalytic events of NOX in the activated microglia are essential contributors of oxidative stress and inflammation that in extreme conditions could lead to neuronal damage and ultimately affect cognitive ability.

1.2.5 Effect of inflammation on neurogenesis and differentiation

Neuroinflammation has also been shown to induce a blocakade in neurogenesis [Monje ML., *et al.,* 2003]. Neurogenesis refers to the birth of new neurons that occur within the CNS. In the hippocampus, birth of new neurons continues throughout life and the amount of neurogenesis correlate closely with the hippocampal functions of learning and memory [Monje ML., *et al.,* 2003]. Any disruption to these proliferating neural stem or progenitor could lead to a disruption of neurogenesis and ultimately cognitive deficits. For example, in patients receiving cranial radiation therapy a decline in cognitive function has been reported as the therapy is known to ablate cell proliferation in the CNS [Monje ML., *et al.,* 2003]. To illustrate the effect of an altered microenvironment, it was reported that in rodent model, peripheral administration of LPS, induced an increase in central pro-inflammatory cytokine production, which was sufficient to induce a 35% decrease in hippocampal neurogenesis [Monje ML., *et al.,* 2003]. Disruption of neurogenesis by LPS was also shown to be able to induce spatial learning and memory deficits task [Wu CW., *et al.,* 2007]. The direct mechanism as to how neuroinflammation is able to induce a disruption to neurogenesis has yet to be fully elucidated. However it is hypothesised that inflammatory cytokines such as IL-6 and TNF-α were able to indirectly inhibit cell proliferation and neurogenesis in the dentate gyrus by increasing the levels of circulating glucocorticoids via centrally stimulating the hypothalamic-pituitary adrenal (HPA) stress axis [Vallières L., *et al.,* 2002]. It was thus suggested that glucocorticoids could affect cell proliferation by directly repressing the transcription of cyclin D1, a common cell-cycle regulator that controls G1-S phase transition, by binding to the promoter and affecting the β-catenin/TCF pathway [Boku S., *et al.,* 2009].

In a separate study, it was also reported that peripheral administration of LPS could induced cognitive deficits *via* COX-2. An increase in COX-2 expression in the granular cell layer and blood vessels, areas that were known to be neurogenic in the dentate gyrus was observed after LPS administration. The involvement of COX-2 was associated with a decrease in newborn cell survival but not cell differentiation where the number of 5-bromo-2-deoxyuridine (BrdU) labelled cells decreased significantly after LPS injection. COX-2 might modulate neurogenesis in the dentate gyrus through the generation of prostaglandins such as prostaglandin (PG) E2 and PGD2 that are able to induce apoptosis in a variety of cell types [Bastos GN., *et al.,* 2008].

However, the involvement in COX-2 in reducing cell proliferation is still under investigation as other studies have reported that the reduction of the number of newborn neurons were associated with neuronal differentiation rather than neuronal proliferation. Inflammatory mediators such as IL-6, TNF-α and IL-18 were reported to induce an increase in glial differentiation [Liu Y., *et al.,* 2005, Cacci E., *et al.,* 2008]. This suggests the complexity of the effect of neuroinflammation in neurogenesis in the dentate gyrus.

1.3 Neuroinflammation in various neurological disorders

Neuroinflammation is a common feature in most neurodegenerative diseases. Elevated levels of cytokines have been seen in most AD and PD patient and these cytokines have been shown to have an effect on cognition. Furthermore transgenic animals that overexpressed specific cytokines such as IL-6 and TNF-α have been shown to perform worse in cognitive tasks [Akiyama H., *et al.,* 2000].

Infusion of LPS into the fourth ventricle in young rats produced a chronic neuroinflammation with an activation of microglia and astrocytes within the hippocampus, piriform and entorhinal cortex. [Hauss-Wegrzyniak B., *et al.,* 1998]. This was due to induction of the expression of IL-1β, TNF-α and β-amyloid precursor protein mRNA levels in the hippocampus. Furthermore, these animals displayed impaired hippocampal-dependent memory task such as the T-maze but not object recognition memory [Hauss-Wegrzyniak B., *et al.,* 1998].

Peripheral administration of LPS was also to elicit similar cognitive deficits. In a study conducted by Arai *et al.* [Arai K., *et al.,* 2001], LPS, administered intraperitoneally (IP), was able to elicit a deficit on spatial learning performance in the water maze. The LPS induced animals had a higher escape latency and path length compared to the vehicle treated animals and at the same time performed much worse in the Y-maze test. Hence, this suggested that systemic administration of LPS could induce neuroinflammation in the CNS mediated by the activation of microglia. This activated microglia would in turn produce inflammatory mediators such as cytokines to drive the cognitive impairment as seen in centrally administered LPS.

1.3.1 Alzheimer's disease and neuroinflammation

All neurodegenerative diseases are accompanied by activated inflammatory and neuroinflammatory systems. The notion that inflammatory processes are involved in the pathogenesis of AD is also strongly supported by epidemiological studies, indicating that chronic use of non-steroidal anti-inflammatory drugs (NSAIDs) reduces the risk of developing AD [Stewart WF., *et al.,* 1997]. The neuroinflammatory process involves astrocytes, microglia, the complement system and to a lesser extent neurons [Akiyama H., *et al.,* 2000]. Senile plaques are known to be associated with activated microglia and reactive astrocytes. Microglia interaction with these amyloid deposits triggers the phenotypic activation and as a consequence a number of proinflammatory immune receptors and cell surface proteins become overexpressed, such as the leukocyte antigen CD45, complement receptors such as CR3, CR4 and LFA-1, MHC II surface antigens and the immunoglobulin receptors Fcγ RI, RII and RIII. Moreover, the acute phase proteins amyloid P and C-reactive protein and the protease inhibitors α1-antichymotrypsin and α1-antitrypsin are elevated [Tuppo EE., *et al.,* 2005]. There is also a large body of evidence reporting that fibrillar Aβ peptides induce the synthesis and release from microglia of pro-inflammatory cytokines interleukin-1 (IL-1), IL-6 and tumor necrosis factor-α (TNF-α) and the chemokines macrophage inflammatory protein-1 and IL-8 [Yates SL., *et al.,* 2000]. TNF- α is one of the most prominent pro-inflammatory cytokines that is significantly increased in AD. It plays a central role in initiating and regulating the cytokine cascade during inflammatory responses [Akiyama H., *et al.,* 2000, Fillit H., *et al.,* 1991]. For example, TNF- α increases the expression of adhesion molecules on the vascular endothelium, which allows leukocytes and immune cells to infiltrate areas of tissue damage and infection [Perry RT., *et al.,* 2001]. TNF- α exerts its biological functions via two distinct receptors: TNF receptor 1 (TNFR1) and TNF receptor 2 (TNFR2). The 55 kDa TNFR1 (p55/60) is a membrane-receptor and is expressed in most tissues where it can be stimulated by both the membrane-bound and the soluble form of TNF- α. The functions of TNFR1 range from inducing apoptosis and differentiation to NF-κB-mediated cell survival [Hu X., *et al.,* 2003]. Similar to TNFR1, also the 75 kDa TNFR2 (p75/80) is a membrane-receptor, but because of its low affinity to soluble TNF-α it can be fully activated only by membrane-bound TNF-α. The functions of TNFR2 are as complex as those of TNFR1 and are still not fully clear in all its detail. It is known that the action of the TNF receptors is strongly dependent on the cell type. For instance, TNFR2 is able to amplify apoptotic signals

from TNFR1 in cancer cell lines [Wajant H., *et al.,* 2003] but has also been reported to mediate protection of nerve cells, as shown in a model for glutamate-induced excitotoxicity [Marchetti L., *et al.,* 2004]. TNFR2 exerts its protective properties when pre-stimulated with TNF-α, which suggests a neuroprotective role in the CNS [Marchetti L., *et al.,* 2004, Dolga AM., *et al.,* 2008]. In AD patients, TNFR1 levels are increased [Fillit H., *et al.,* 1991], whereas TNFR2 [Taoufik E., *et al.,* 2007] levels are decreased. Recently, it was demonstrated that overexpression of TNFR1 promotes Aβ-induced neuronal death in an APP overexpressing mouse model for AD [Li R., *et al.,* 2004]. In contrast, such APP overexpressing mice lacking TNFR1 have a decreased amyloid plaque burden, lower expression of β-secretase (BACE), and improved learning abilities compared to controls [He P., *et al.,* 2007]. Interestingly, the stimulation of both TNF receptors can lead to the activation of NF-κB, which has binding sites in the promoter regions of both the APP and the BACE gene [Grilli M., *et al.,* 1996]. Mutations in the NF-κB promotor region of BACE lead to a significant decrease in promotor activity of TNF-α activated glia cells or Aβ exposed neurons, which indicate an activating role of NF-κB in BACE expression [Bourne KZ., *et al.,* 2007]. In this way, NF-κB activation can lead to increased APP expression and enhanced amyloidogenic APP processing. Elevated APP and BACE expression will ultimately lead to increase in Aβ production, which can in turn activate glia cells and enhance neuroinflammatory processes.

1.3.2 Parkinson ’s disease and neuroinflammation

Classically, the neuropathological hallmark of idiopathic PD is the presence of α-synuclein-positive inclusions in the cell body (Lewy bodies) and processes (Lewy neurites) of specific neurons of the brainstem and a classic motor phenotype resulting from substantial loss of dopaminergic neurons from the substantia nigra pars compacta (SNpc) [Litvan I., *et al.,* 2007]. A number of studies have confirmed the presence of inflammatory mediators (including TNF, IL-1β, IL-6, and IFNγ) in the cerebrospinal fluid (CSF) of patients with PD as well as in the post-mortem SNpc in PD patient brains [Banati RB., *et al.,* 1998, Gerhard A., *et al.,* 2006, Hunot S., *et al.,* 1999, McGeer PL., *et al.,* 1988]. Significantly elevated levels of TNF mRNA and protein can be detected in the rodent midbrain substantia nigra within hours of in vivo administration of two neurotoxins widely used to model parkinsonism in rodents, 6-hydroxydopamine (6-OHDA) [Nagatsu T., *et al.,* 2006] and 1-methyl-4-phenyl-1,2,3,6-tetrahydropyridine (MPTP) [Barcia C.,

et al., 2005, Ferger B., *et al.,* 2004]. Consistent with a role of TNF in contributing to dopaminergic neuron death in chronic parkinsonism, plasma TNF levels were shown to remain elevated in MPTP-treated non-human primates one year after administration of the neurotoxin [Ferger B., *et al.,* 2004]. In contrast, studies involving mice deficient in TNF or both TNF receptors have yielded conflicting results in that one group reported lack of TNF receptors altered dopamine metabolism and reduced survival of dopaminergic terminals [McGeer PL., *et al.,* 1988] and other groups reported TNF-deficient mice to have reduced sensitivity to MPTP-induced neurotoxicity [Hunot S., *et al.,* 1999, Vawter MP., *et al.,* 1996].

Additional evidence that inflammation (and in particular TNF) is involved in nigral DA neuron degeneration comes from two endotoxin rat models. In the first model chronic low dose lipopolysaccharide (LPS) infusion into SNpc of rats results in delayed, selective and progressive loss of nigral DA neurons [Barcia C., *et al.,* 2005]. In the second model exposure of pregnant rats to LPS and thus, in utero exposure of embryos to the endotoxin, caused a loss of DA neurons in postnatal brains [Ferger B., *et al.,* 2004]. Most importantly, chronic infusion of dominant negative TNF inhibitor proteins into SNpc of adult rats protected nigral DA neurons from LPS and 6-OHDA induced degeneration [McCoy MK., *et al.,* 2006] as did a single nigral injection of a lentivirus encoding DN-TNF in 6-OHDA hemiparkinsonian rats [McCoy MK., *et al.,* 2008]. Given that TNF receptors are expressed in nigrostriatal dopamine neurons [Boka G., *et al.,* 1994, Tartaglia LA., *et al.,* 1993] and these neurons are selectively vulnerable to TNF-induced toxicity, these early genetic studies and the more recent chronic inflammation models of PD strongly implicate TNF and its downstream targets in neurotoxin- and endotoxin-induced loss of nigral DA neurons. However, because it is clear that the permeability of the BBB increases with age increases the likelihood of peripheral immune cell infiltration into the CNS, TNF produced by brain-resident microglia may not be acting alone in mediating DA neuron cell death but in concert with other circulating neurotoxic factors to increase the inflammatory susceptibility of nigral DA neurons and development of PD. Another link between inflammation and neurodegeneration comes from studies of single nucleotide polymorphisms that are associated with over-production of cytokines, chemokines and acute phase proteins. These polymorphisms are over-represented in specific cohorts of individuals affected with PD and may confer increased susceptibility for the disease [Håkansson A., *et al.,* 2005a, Håkansson A., *et al.,* 2005b, Krüger R., *et al.,* 2000, Nishimura M., *et al.,* 2005, Nishimura M., *et al.,* 2001]. However, most

of these findings have not been replicated in independent studies and a meta-analysis of multiple association studies is needed to assess the overall genetic effect of cytokine gene polymorphisms on neurodegenerative disease.

1.3.3 Huntington's disease and neuroinflammation

Huntington's disease (HD) is an autosomal dominant neurodegenerative disorder that has been linked to mutations in the Huntington gene (htt) [Group TH., *et al.,* 1993]. CAG repeat expansions in the htt gene result in an increased number of glutamine residues in the huntingtin protein (polyglutamine expansion). Mutant htt causes degeneration of neurons, predominately in the caudate putamen and cortex, causing HD patients to suffer from uncontrolled movements, emotional disturbances and dementia. While the mechanism by which mutant htt causes neurodegeneration remains obscure, evidence supporting inflammation as an important player in HD is accumulating. Recent studies have demonstrated that inflammation appears both peripherally and in the central nervous system (CNS) during the progression of HD and HD-like pathology. The R6/2 mouse model of HD displays increased serum levels of IL-6 and in downstream IL-6 effectors, such as alpha-2-macroglobulin (A2M) and complement components [Dalrymple A., *et al.,* 2007]. In the CNS, microarray profiling of several brain regions from HD patients and controls revealed increased gliosis and expression of inflammation-related genes, including GFAP and complement proteins. Clinical plasma samples from HD gene carriers contain increased levels of pro-inflammatory cytokines involved in the innate immune response, such as IL-6 [Bjorkqvist M., *et al.,* 2008].

A number of studies indicate that the altered immune profile in HD occurs before onset of clinical HD symptoms, suggesting that striatal and cortical neurodegeneration could be exacerbated by inflammation. For example, plasma samples from HD gene carriers contain increased levels of pro-inflammatory cytokines involved in the innate immune response before the onset of clinical symptoms and investigators have been able to discriminate controls from presymptomatic HD mutation carriers by measuring the levels of 3 cytokines, IL-5, IL-6, and IL-10 in plasma [Bjorkqvist M., *et al.,* 2008]. In brains of mutant htt carriers, microglia are activated before onset of symptoms and increased microglial activation correlates with an increased chance of developing HD symptoms in 5 years [Tai YF., *et al.,* 2007]. Once symptoms have manifested, microglial activation correlates with disease severity [Pavese N., *et al.,* 2006, Sapp

E., *et al.,* 2001]. In the 3-nitroproprionic acid neurotoxin model of HD in rats, treatment with Celastrol, an anti-inflammatory and antioxidant compound derived from plants, reduced striatal lesion volume [Cleren C., *et al.,* 2005], indicating that controlling an inflammatory response could be therapeutically beneficial as HD progresses. However, treatment with acetylsalicylate or rofecoxib, anti-inflammatory drugs commonly used in the clinic, was not neuroprotective in either the R6/2 or N171-82Q transgenic mouse models of HD [Norflus F., *et al.,* 2004]. The presence of increased inflammatory mediators in periphery and in CNS beg the question of whether CNS inflammation "leaks" into periphery to alter the peripheral immune profile or whether inflammation is triggered in the periphery and immune modulators are allowed to cross the BBB to trigger or contribute to a central inflammatory response. Another possibility is that an inflammatory response could be triggered in the periphery and the CNS by an analogous mechanism. These alternatives are just beginning to be explored.

1.3.4 Autism spectrum disorders and neuroinflammation

Increasing evidence indicates that brain inflammation is important in the pathogenesis of neuropsychiatric disorders [Hagberg., *et al.,* 2012]. Autism spectrum disorders (ASD) are pervasive neuro-developmental disorders characterized by varying degrees of deficiencies in social interactions, intelligence, and language, as well as the presence of stereotypic behaviors [Johnson CP., *et al.,* 2007]. Recent results from the Centers of Disease Control in the USA indicate that as many as 1/80 children have ASD. Many such children regress at about age 3 years, often after a specific event such as reaction to vaccination, infection, trauma, toxic exposure or stress, implying the importance of some environmental triggers. Increasing evidence points to some immune dysfunction/inflammation in ASD. The markers of inflammation identified in the brain and cerebrospinal fluid (CSF) of many ASD patients include TNF, IL-6 and monocyte chemotactic protein 1 (MCP-1), the latter of which also is chemotactic for mast cells. Pro-inflammatory cytokine mRNA (IL-1α, IL-1β, IL-6 and TNF-α) is increased in brain inflammation and has been associated with hippocampal and cerebral damage. Mast cells are a rich source of IL-6 and TNF. In fact, mast cells are the only immune cells that store pre-formed TNF and can release it rapidly upon stimulation [Goines PE., *et al.,* 2013].

Mast cells and cytokines such as IL-6 and TNF are also implicated in disruption of the blood–brain barrier (BBB), which may be malfunctioning or leaky in ASD as evidenced by the presence

of circulating auto-antibodies directed against the fetal brain proteins [Theoharides TC., *et al.,* 2008]. We had reported that the cytokine IL-33 synergizes with inflammatory neuropeptides to stimulate mast cells and result in increased vascular permeability. IL-33 has been considered an alarmin; acting through mast cells to alert the innate immune system, and has recently been linked to brain inflammation [Pitchery M., *et al.,* 2012]. Neurotensin (NT) and corticotropin-releasing hormone (CRH), secreted under stress, synergistically stimulate mast cells, leading to increase vascular permeability and contribute to BBB disruption [Carraway R., *et al.,* 1973; Carraway RE *et al.,* 1985]. NT stimulates mast cell secretion of vascular endothelial growth factor (VEGF), which is also vasodilatory. NT also increases expression of CRH receptor-1 (CRHR-1), activation of which by CRH increases allergic stimulation of human mast cells.

NT has additional actions that are relevant to ASD, induces intestinal secretion and mobility, stimulates glial cell proliferation, and can facilitate seizures through activation of glutamate receptors. In fact, the glutamate receptor mGluR5 was reported to be overactive in fragile X mice, a condition associated with high risk of ASD. In other words, NT could contribute to ASD pathogenesis through different mechanisms [Martin S., *et al.,* 2003].

Mast cells can produce both pro- and anti-inflammatory mediators and may have immuno-modulatory functions [Barrocas AM., *et al.,* 1999]. It is, therefore, of interest that allergic-like reactions are common in ASD children implying activation of mast cells by non-allergic triggers. The richest source of mast cells in the brain is the diencephalon that regulates behavior, while the highest concentration of NTR is in the Broca area, which regulates language, known to be lost in many children with ASD. Mast cells are responsible for eliciting neutrophil infiltration that promotes inflammation. Mast cell-microglial interactions are important in neuroinflammatory diseases. Microglia is the innate brain immune cells that are increasingly implicated in a number of neuropsychiatric diseases. In fact, abnormal microglial growth and activation was recently reported in the brain of ASD patients. Microglia expresses NTR3, activation of which leads to their proliferation.

1.4 Toxin induced neuroinflammation

1.4.1 MeHg induced neurotoxicity

With emphasis on the neurotoxicity induced by MeHg, experimental evidence indicates that oxidative damage to proteins [Rocha JB., *et al.,* 1993], lipids [Stringari J., *et al.,* 2006] and nucleic acids [Belletti S., *et al.,* 2002] represents an important consequence of exposure to this toxicant. However, the critical role of oxidative stress in MeHg neurotoxicity has been identified; the precise molecular mechanisms underlying MeHg-mediated oxidative stress are not yet fully understood. Farina, *et al.,* 2011 proposed, the initial oxidative damage caused by MeHg in living organisms occurs via its reaction with thiol (-SH) and/or selenol (-SeH) groups from endogenous molecules, resulting in the formation of a very stable complex of the type $RSHgCH_3$ or $RSeHgCH_3$ [Farina M., *et al.,* 2011]. Chemically MeHg is classified as a soft electrophile and consequently it reacts preferentially with soft nucleophiles [Pearson RG., *et al.,* 1967]. Indeed, MeHg has high affinity for thiol and selenol groups that finding free MeHg inside a living organism is highly unlikely [Onyido IN., *et al.,* 2004]. In fact, thiol groups can be found in low molecular (mainly cysteine and reduced glutathione) and high molecular weight proteins, whereas selenol groups are found only in restricted group of selenoproteins (i.e. glucose-6-phosphate dehydrogenase, creatine kinase, glutathione reductase, glutathione peroxidase, thioredoxine reductase, among others) [Lobanov AV., *et al.,* 2009]. The absorption of MeHg from the gut is high; however, there are no experimental data regarding the speciation of MeHg that is absorbed im mammalian gastrointestinal tract. It is possible that cysteinyl-bound MeHg can be released after the digestion of fish protein, and that it can be transported as mimetic of the amino acid methionine [Bridges CC., *et al.,* 2011]. Super oxide anion, a by-product of normal functioning of the mitochondrial respiratory chain, is a ROS that is produced after the one-electron reduction of molecular oxygen [Chance B., *et al.,* 1979]. It is generated by complex I and III in respiratory chain and is readily converted to H_2O_2 by mitochondrial respiratory chain. Additionally, super oxide is a product of NADPH-oxidase, which is particularly important in the CNS during microglial activation [Lavigne MC., *et al.,* 2000]. Although most of the studies examining the various ROS which are produced as a result of MeHg exposure have focused on H_2O_2, super oxide anion has also been reported to play an important role in the oxidative damage induced by MeHg. Shanker *et al.,* 2004 using a specific probe for super oxide, observed increase

levels of ROS in MeHg-treated cultured astrocytes [Shanker G., *et al.*, 2004] (**Figure 1.1**). Although MeHg may induce pro-inflammatory events [Eskes C., *et al.*, 2002, Chang JY., *et al.*, 2007, Ni M., *et al.*, 2010], as well as toxicity and the activation of microglial cells, a potential relationship between MeHg, microglial activation and increased superoxide production is lacking in the literature.

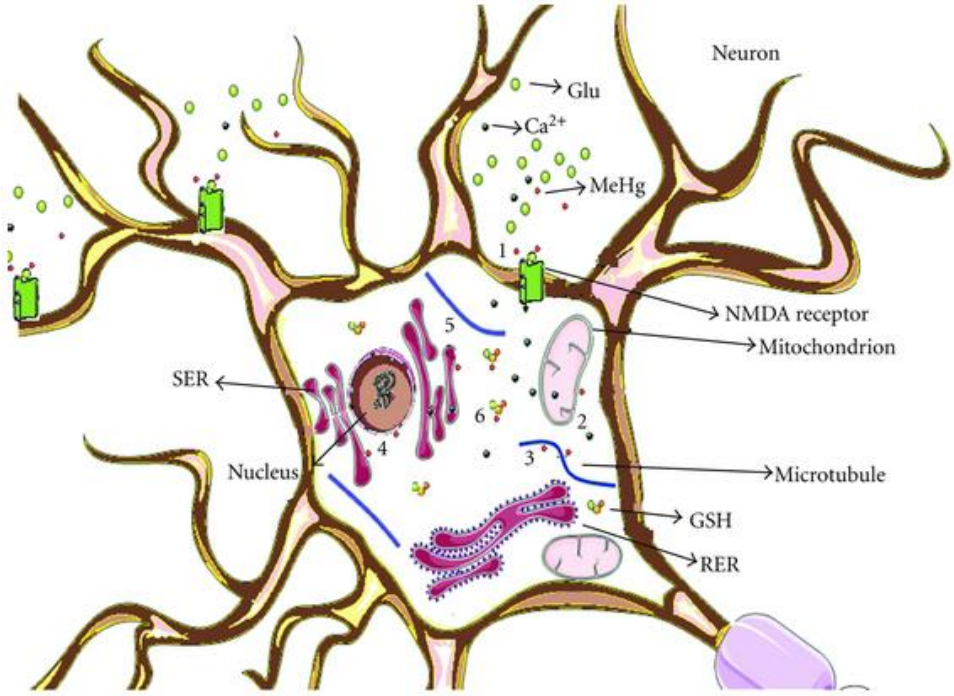

Figure 1.1 Schematic representation of possible mechanisms and cellular targets involved in the neurotoxicity MeHg-induced: (1) glutamate dyshomeostasis and Ca2+ intracellular dysregulation; (2) mitochondrial dysfunction; (3) cytoskeletal disruption; (4) DNA damage; (5) SER dysfunction; (6) thiol depletion (especially glutathione). This scheme is adapted from [Ni M., *et al.*, 2010], SER- soft endoplasmic reticulum, GSH- Glutathione, RER- rough endoplasmic reticulum, NMDA- N-methyl-D-aspartate.

1.4.2 LPS induced neurotoxicity

LPS is derived from the outer membrane of gram-negative bacteria such as Escherichia coli. LPS molecules consist of two main components: a well-conserved hydrophobic biphosphorylated lipid (lipid A) and a hydrophilic polysaccharide (PS). The PS has two regions, a non-repeating core oligosaccharide and a polysaccharide chain known as the O-chain [Caroff M., *et al.*, 2002]. The O-chain confers serotype specificity on a species or strain of bacteria. The lipid A moiety

binds to a variety of receptors including CD 14 that can initiate activation of the innate immune system.

LPS-binding protein (LBP), a 65kDa protein, binds LPS circulating in the bloodstream via the lipid A moiety [Ulevitch RJ., *et al.*, 1995]. LBP behaves as a lipid transfer protein acting to convert aggregates of LPS to monomers to accelerate the binding of LPS to CD 14. Soluble CD 14 (sCD14) aids activation of cells that do not express the membrane glycosylphosphatidylinositol-anchored CD 14 [Bazil V., *et al.*, 1989]. Membrane-bound CD 14 (mCD14) lacks a cytoplasmic domain and in order to induce intracellular signals, CD 14 forms a complex recognised by TLR4 [Dobrovolskaia MA., *et al.*, 2003]. The adaptor protein MD-2, expressed by dendritic cells and monocytes, was originally identified by Shimazu et al, 1999 [Shimazu R., *et al.*, 1999]. Co-expression of MD-2 is essential for the binding of LPS and translocation of the TLR receptor to the cell surface [Fujimoto T., *et al.*, 2004]. Studies using radiolabelled LPS have illustrated a physical interaction between LPS (**Figure 1.2**), MD-2 and TLR4 can only occur in the presence of CD 14 irrespective of the role of MD-2 in complexes with LPS or TLR4. Although the CD14/MD-2/TLR4 complex is well recognised, LPS may also activate CD64, CD 16, CD32, CD36, CD55 and CD 11 c/CD 18 [Ingalls RR., *et al.*, 1995] cell surface receptors, depending on cell type and activation state.

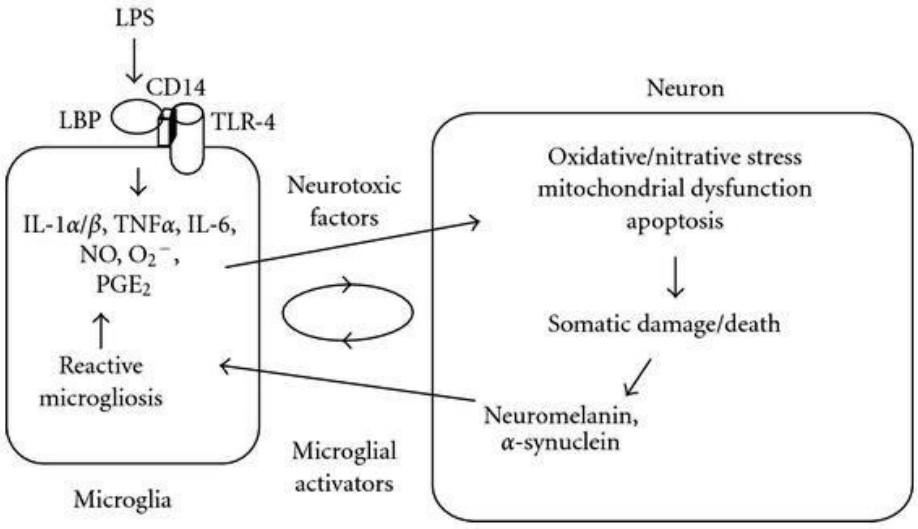

Figure 1.2 LPS induces progressive neurotoxicity [Fujimoto T., *et al.*, 2004].

In response to LPS stimuli, microglial cells are readily activated. It is demonstrated that LPS binds to specific receptors, for example, CD14/TLR4/LBP receptor complex on the microglia, to induce microglial activation. Uncontrolled microglial activation produce a variety of neurotoxic factors such as proinflammatory cytokines (IL-1, TNF-α, IL-6), NO, PGE2, which lead to neuronal damage or death through a cascade of events such as oxidative/nitrative stress, mitochondrial dysfunction, and apoptosis. Moreover, damaged neurons may emit injury signals to cause microglia activation, which is defined as reactive microgliosis. The injury signals could be neuromelanin and α-synuclein released by injured dopaminergic neurons. This microglial-neuronal interaction will be reinforced and become a self-amplifying cycle of neuronal injury and microglial activation, which may finally result in the neurodegenerative disease [Mei Liu., *et al.,* 2011].

1.4.2.1 Communication between periphery and CNS

Peripheral inflammation may be sensed by the brain via two pathways, namely the neural and humoral mechanisms. Evidence supports a major role for humoral pathways during systemic inflammation [Szelenyi J., *et al.,* 2000]. Bloodborne cytokines can bind to endothelial receptors in brain tissue or cross the blood-brain barrier (BBB) through a saturable carrier-mediated mechanism that is most likely to initiate when very high cytokine concentrations exist in the blood. Much of the communication from periphery to brain occurs via the circumventricular organs (CVOs), areas of minimal BBB, since cytokines in the blood can initiate the synthesis and release of soluble mediators including prostaglandins and nitric oxide at CVO sites. Circulating LPS can bind to TLR4 located on endothelial cells of the circumventricular organs (CVOs), leptomeninges and choroid plexus (ChP) of the brain and on the surface membrane of monocytes, mast cells and neutrophils. TLR4 activation causes transcription of cytokine target genes within immune cells, particularly microglia, firstly at the CVOs, choroid plexus and leptomeninges and then eventually throughout the brain tissue [Nadeau S., *et al.,* 1999]. Expression of mCD14 also increases dramatically in microglia, CVO regions and then throughout the brain following intravenous (IV) or intraperitoneal (IP) LPS. This leads to NF-kB translocation and proinflammatory cytokine production, firstly at areas easily reached by the systemic circulation and then subsequently throughout the brain tissue. IP LPS injection induces rapid IL-6 expression in the CVOs and ChP, however, IV injection of pro-inflammatory

cytokines IL-lβ and TNF-α fail to stimulate IL-6 transcription. There is also evidence to suggest that intraperitoneal LPS may cause mild breakdown of the microvasculature allowing diffusion of LPS through the barrier. Entry of molecules into the brain following breakdown of the BBB is molecular weight dependent with molecules of approximately <340Da entering brain tissue [Singh AK., *et al.*, 2004]. The molecular weight of LPS is l0kDa so it is possible, but unlikely, that sufficient LPS can enter the brain to elicit a central response.

1.5 Introduction to drug discovery using computer-aided drug design (CADD)

Molecular modeling and computational chemistry are assuming an increasingly important role in understanding the basis of drug-receptor interactions and assisting the medicinal chemist in the design of new therapeutic agents. Computer graphics have emerged as a cost-effective tool, and adequate computational power is now available, which removes limitations that have crippled computational chemistry. These advances have stimulated the development of software tools for probing the three dimensional aspects of specificity.

1.5.1 Strategies in drug discovery process

Strategies for molecular modeling vary depend on the extent of structural and other information available regarding the target (enzyme/receptor) and the ligands. "Direct and indirect" designs are the two major modeling strategies currently used in the drug design process. In the indirect approach the design is based on comparative analysis of the structural features of known active and inactive compounds. In the direct design the three-dimensional features of the target are directly considered.

1.5.1.1 Structure based drug design

Structure-based drug design relies on the knowledge of the three dimensional structure of the biological target obtained through methods such as x-ray crystallography or NMR spectroscopy [McCarthy JD., 1999]. Using the structure of the biological target, candidate drugs that are predicted to bind with high affinity and selectivity to the target may be designed using interactive graphics and the intuition of a medicinal chemist. Alternatively various automated computational procedures are used to suggest new drug candidates. The receptor-based (direct) approach to CADD can be used when a reliable model of the receptor (preferentially complexed with a

ligand) is available from x-ray diffraction. If the receptor structure is available, a primary challenge in lead discovery and optimization is to predict both the ligands orientation and binding affinity, and is referred as 'molecular docking'. [Taylor RD., et al., 2002].

1.5.1.2 Molecular docking and virtual screening

Molecular docking (direct approach) is a computational tool and represents a crucial component of many drug discovery projects, from hit identification to lead optimization. In particular, it is employed in approaches such as structure-based design and virtual screening techniques, widely used in many discovery efforts: such as, prediction of binding modes and selection from virtual large databases of putative ligands into the binding site of biological target. The docking methodology was pioneered during the early 1980s and remains a current and highly active area of research, thanks also to its short time and low computational cost. In particular, it is a multi-step process in which each step introduces one or more additional degrees of complexity.

Initially, the process begins with the application of algorithms that sample the several degrees of conformational freedom of small molecules "posing" them in the binding site. The algorithms are complemented by scoring functions that are designed to describe the biological activity through the evaluation of interactions between the ligand and the potential target as well as the entropic cost of the ligand conformation. Some of these scoring functions adopted for molecular docking try to estimate the free energy of binding of the ligand-target complex. Unfortunately, this estimation is not always reliable because of the high error associated to it. However, the molecular docking represents a useful technique in the CADD and discovery context towards delicate issues such as the identification of molecular features that are responsible for specific biological recognition and/or the prediction of chemical modifications to improve potency of ligands. This is achieved by minimizing a scoring function, which describes the interactions between ligand and target with respect to the atomic positions of the two moieties. In this work, Glide (Schrodinger, LLC) and vROCS (Rapid Overlay of Chemical Structures) (Open eye systemic software) programs were used to predict ligand-protein interactions and large database screening.

Glide uses a series of hierarchical filters to search for possible locations of the ligand in the active-site region of the receptor. The shape and properties of the receptor are represented on a

grid by different sets of fields that provide progressively more accurate scoring of the ligand pose. (By "pose" we mean a complete specification of the ligand: position and orientation relative to the receptor, core conformation, and rotamer group conformations.) These fields are generated as preprocessing steps in the calculation and hence need to be computed only once for each receptor. The next step produces a set of initial ligand conformations. These conformations are selected from an exhaustive enumeration of the minima in the ligand torsion-angle space and are represented in a compact combinatorial form. Given these ligand conformations, initial screens are performed over the entire phase space available to the ligand to locate promising ligand poses.

ROCS is a shape based method for rapid similarity analysis of molecules. Thereby, the volume overlap of molecules is assessed by Gaussians, which are parameterized according to the hard sphere volume of heavy atoms. The use of gaussians allows for fast calculation of overlaps between two atoms. The basic scoring function implemented in ROCS is the Shape Tanimoto Score, which is a quantitative measure for the shape overlap of two molecules. In order to obtain activity on a certain target, not only shape but also appropriate chemical functionality is crucial for a compound, which is why ROCS has implemented a color score to support the alignment process and evaluate chemical feature based similarity. The ROCS color force field is composed of SMARTS patterns for the characterization of chemical functions in combination with a rule set that describes how much functions interact. ROCS provides two color force field, the Implicit Milis Dean and Explicit Milis Dean force field. In this way, ROCS is able to maximize both molecular shape overlay and chemical functionality overlap. The ComboScore function puts exactly equal weights on its both components, the ShapeTanimoto and the ScaledColoreScore. Both components obtain values between 1 and 0 and are summed up to combo score that is tanimoto combo score.

Chapter2

Review of Literature

Inhibition of both Rho kinase (ROCK-I) and NOX (NOX2) to treat neuroinflammation in progression of neurodegenerative diseases is a remarkable strategy to obstruct superoxide generating inflammatory pathway. Where, NOX2 is a multi-enzyme component which is activated during host defence in phagocytes such as microglia, to catalyse the production of superoxide from oxygen, and ROCK is an important mediator for fundamental cell processes like adhesion, proliferation and migration. Phosphorylated ROCK further activates NOX2 assembly *via* Ras related C3 botulinum toxin substrate (Rac) in inflammatory pathway. Over expression of ROCK-I and NOX2 in innate immune cells like microglial cells contribute to progressive neuronal damage early in neurodegenerative disease development. Thus in order to facilitate our work on these two targets, an extensive literature survey was carried out on these two targets to understand the underlying and known mechanisms and pathways involved with these targets in neurological disorders. As drug discovery efforts for neurological disorders still continue to be a challenge, the targets of our interest (ROCK-I and NOX2) were considered attractive as these were relatively new for various neurological conditions.

2.1 RHO KINASE AS A TARGET

One of the best-characterized effectors of the small GTP-binding proteins of the Rho subfamily (Rho GTPases) is Rho-associated coiled-coil-containing protein kinase (hereafter simply referred to as ROCK). RhoGTPases, a subfamily of the Ras superfamily of GTPases, function as molecular devices that control multiple signalling pathways in a very precise and coordinated

way by switching between a biochemically inactive (GDP-bound) and an active (GTP-bound) state [Van Al., *et al.,* 1997, Burridge K., *et al.,* 2004, Bishop A., *et al.,* 2000]. The cycling between GDP- and GTP-bound states is controlled by two classes of proteins: GTPase activating proteins (GAPs), which enhance intrinsic GTPase activity; and guanine nucleotide-exchange factors (GEFs), which catalyze the exchange of GDP to GTP [Rossman KL., *et al.,* 2005]. Furthermore, a third set of regulatory proteins, the guanine nucleotide-dissociation inhibitors (GDIs), sequester GTPases in the cytosol in the inactive, GDP-bound state. In the active, GTP-bound state, Rho GTPases activate numerous downstream effectors. The current understanding of the pathophysiological consequences of ROCK activation in the CNS has to be summarized and the potential therapeutic use of ROCK inhibitors for the treatment of various neurological disorders, including spinal-cord injury, AD, ASD, stroke, MS and neuropathic pain.

2.1.1 ROCK isoforms and tissue distribution

ROCK is a serine/threonine (Ser/Thr) protein kinase that was identified about ten years ago as a RhoGTP binding protein with a molecular mass of ~160 kDa [Matsui., *et al.,* 1996, Ishizaki., *et al.,* 1996, Leung T., *et al.,* 1996]. Two isoforms encoded by two different genes of ROCK have been described: ROCKI (also known as ROKβ or p160ROCK) and ROCKII (which is also known as ROKα) [Nagawa O., *et al.,* 1996]. These two proteins share an overall sequence similarity at the amino-acid level of 65% and in their kinase domains of 92% [Amano M., *et al.,* 2000, Riento K., *et al.,* 2003]. ROCKs are most homologous to other members of the group of AGC KINASES, such as myotonic dystrophy kinase (DMPK), myotonic dystrophy kinase-related CDC42-binding kinase (MRCK) and citron kinase. In general, the catalytic domain of all these kinases is located at the amino terminus, followed by a coiled-coil-forming region and a pleckstrin-homology domain with a cysteine-rich repeat at the carboxyl terminus. In the case of ROCK, the carboxy-terminal coiled-coil region also encompasses the Rho-binding (RBD) domain. Despite the striking similarity of the protein sequences of the two ROCK isoforms, significant differences regarding their respective tissue distribution have been reported, which indicates distinct functions of each isoform *in vivo*. ROCK-II is preferentially expressed in brain, whereas ROCK-I shows the highest expression levels in non-neuronal tissues, including heart, lung and skeletal muscles. ROCK-II expression in bovine brain was mainly observed in the pyramidal neurons of the hippocampus and cerebral cortex, and in the Purkinje cells of the

cerebellum [Hashimoto R., *et al.,* 1999]. Interestingly, during postnatal development of the mouse brain, ROCKII expression levels gradually increased [Komagome R., *et al.,* 2000].

2.1.2 Regulation of ROCK activity

It has been previously demonstrated that the C terminus of ROCK negatively regulates its kinase activity [Komagome R., *et al.,* 2000]. Similar to DMPK and MRCK, the C-terminal domain of ROCK folds back onto the kinase domain, thereby forming an auto-inhibitory loop that maintains ROCK in an inactive state. Binding of GTP-bound Rho to the RBD is believed to disrupt the negative regulatory interaction between the catalytic domain and the auto-inhibitory C-terminal region, which results in activation of the enzyme in response to extra cellular signals. The activation mechanism of ROCK is illustrated schematically in **Figure 2.1**. Rho binds to ROCK only in the biochemically activated, GTP-bound form [Leung T., *et al.,* 1996]. Recently, the crystal structure of RhoA bound to the RBD has been investigated by two groups [Bush EW., *et al.,* 2000, Shimizu TI., *et al.,* 2003], and it indicates the formation of a parallel coiled-coil dimer of the RBD domain and provides strong evidence that the full-length kinase is also a dimer. Consistent with these conclusions, it has been shown that protein oligomerization might regulate ROCK activity [Dvorsky R., *et al.,* 2004], possibly through N-terminal transphosphorylation [Doran J., *et al.,* 2004]. Other direct activators include intracellular second messengers such as arachidonic acid [Turner M., *et al.,* 2002] and sphingosyl phosphorylcholine [Fu X., *et al.,* 1998] which can activate ROCK independently of Rho. Furthermore, ROCKI activity can also be induced during apoptosis. Cleavage of the auto-inhibitory C terminus of ROCK-I by caspase 3 gives rise to a constitutively active ROCK-I [Shirao S., *et al.,* 2002, Sebbagh M., *et al.,* 2001]. During apoptosis, caspase cleavage occurs specifically to ROCK-I, although other apoptosis-related mechanisms can also modify ROCK-II. In conclusion, the complexity of the regulation mechanisms of the kinase activity could represent a crucial feature for the maintenance of a proper balance of ROCK function *in vivo*.

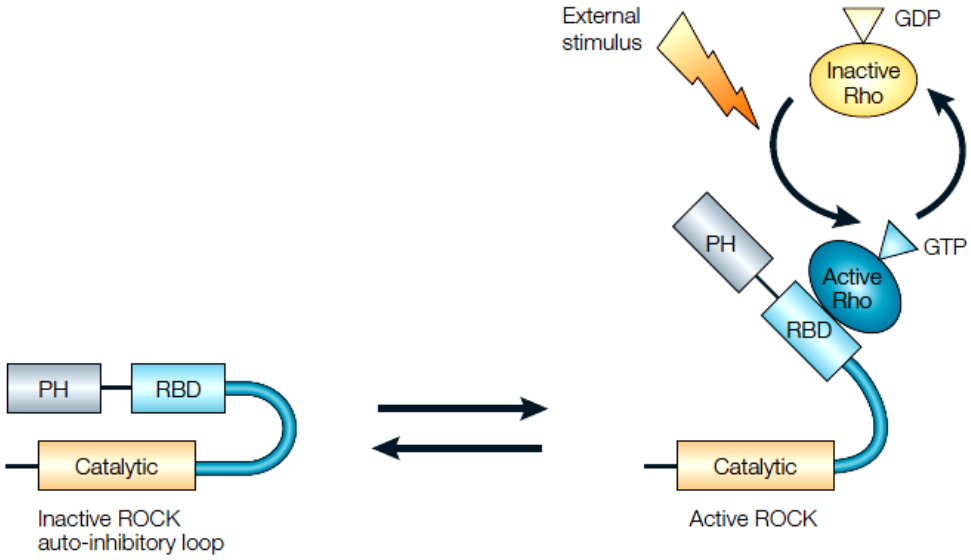

Figure 2.1 Activation mechanism of Rho kinase (ROCK). The carboxy terminus of ROCK folds back onto the kinase domain, thereby forming an auto-inhibitory loop that maintains the enzyme in an inactive state. Binding of GTP-bound, biochemically active Rho to the Rhobinding domain (RBD) disrupts the negative regulatory interaction between the catalytic domain and the autoinhibitory C-terminal region, resulting in activation of the enzyme in response to extracellular signals. PH, pleckstrin-homology domain [Leung T., *et al.*, 1996].

2.1.3 Substrates of ROCK

Activation of ROCK by GTP-bound Rho or by the aforementioned lipid mediators leads to phosphorylation of various target proteins. One of the main substrates of ROCK is myosin light chain (MLC). In fact, ROCKs were initially characterized according to their roles in mediating the formation of RhoA-induced cytoskeletal rearrangements, including stress fibers and focal adhesions, through their effects on MLC [Coleman ML., *et al.*, 2001, Leung T., *et al.*, 1996]. Phosphorylation of MLC subsequently results in stimulation of myosin–actin interactions. Furthermore, ROCK can indirectly regulate the amount of phosphorylated MLC by inactivating MLC phosphatase (MLCP) [Somlyo AP., *et al.*, 2000]. Although recent observations indicate that the inactivation of myosin phosphatase, rather than the direct phosphorylation of MLC, would contribute to the elevation of MLC phosphorylation, the exact contribution of the two pathways is not clear and needs to be elucidated.

Other downstream targets of ROCKs include the Ser/Thr kinases LIM kinases 1 and 2 (LIMK1 and LIMK2) [Kimure K., *et al.*, 1996, Sumi T., *et al.*, 2001]. As shown in **Figure 2.2**, Phosphorylation of LIMKs by ROCKs inhibits cofilin-mediated actin-filament disassembly,

which leads to an increase in the number of actin filaments. In addition to LIMK, ROCK phosphorylates the ezrin/radixin/moesin (ERM) protein complex and other proteins involved in cytoskeletal regulation. Further substrates of ROCK include intermediate filament proteins such as vimentin, glial fibrillary acidic protein (GFAP) and neurofilaments, which upon phosphorylation by ROCK undergo depolymerization [Ohashi K., *et al.*, 2000, Goto H., *et al.*, 1998, Kosako H., *et al.*, 1997, Hashimoto R., *et al.*, 1998]. Several other candidates for ROCK substrates include microtubule-associated protein 2 (MAP2) and tau. Phosphorylation of tau decreases its activity to promote microtubule assembly in vitro [Amano M., *et al.*, 2003]. In addition, ROCKII phosphorylates collapsin response mediator protein 2 (CRMP2) [Arimura n., *et al.*, 2000], a neuronal protein with a role in semaphorin-3A-mediated axon guidance during development of the nervous system. ROCKII therefore seems to be an integration point for various signaling pathways, particularly that regulating actin–myosin contractility.

2.1.4 The Role of ROCK in regulating vascular tone

Although data from knockout mice should be interpreted with care and cannot always be extrapolated to human beings, the results of the ROCK-knockout studies are encouraging and consistent with the experiences gathered in clinical trials with the first ROCK inhibitor, Fasudil. Neither the deletion of any of the ROCK genes in mice nor the inhibition of ROCK proteins in humans by Fasudil caused any serious adverse effects, indicating that ROCK is a valuable drug target. Fasudil (AT877 or HA-1077; Asahi Kasei), initially characterized as an intracellular calcium antagonist, has been marketed in Japan since 1995 for the treatment of cerebral vasospasm after hemorrhage in the subarachnoid space. A subarachnoid hemorrhage-induced cerebral vasospasm, characterized by increased constriction of cerebral arteries, results in delayed cerebral ischemia, and is a frequent cause of morbidity and mortality of brain hemorrhages [Thumkeo D., *et al.*, 2003]. Fasudil given orally or intravenously only had modest effects on systemic blood pressure, and in mouse models systolic blood pressure was not significantly different in mice lacking ROCKI compared with wild-type mice [Shimizu Y., *et al.*, 2005]. To date, more than 30,000 patients have been treated with Fasudil and, despite the ubiquitous expression of ROCK; reported side effects are usually minimal and acceptable.

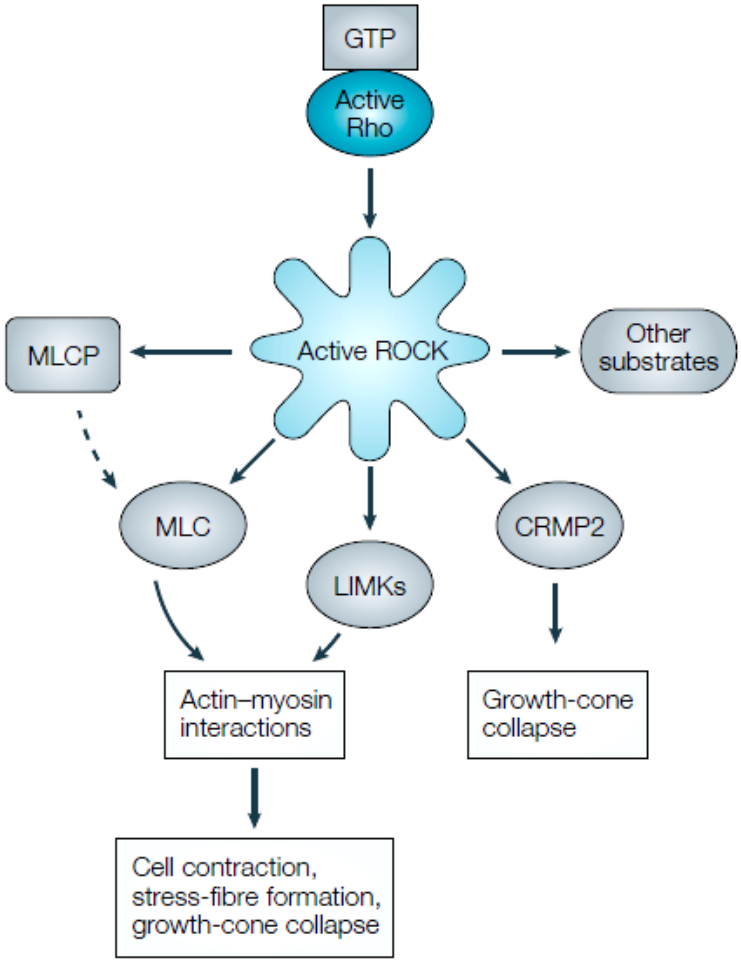

Figure 2.2 Major ROCK substrates. Activation of ROCK by GTP-bound Rho leads to phosphorylation of various target proteins, particularly those that regulate actin– myosin contractility. One of the main ROCK substrates is myosin light chain (MLC). Phosphorylation of MLC results in stress-fibre formation and increased cellular contractility. ROCKII also phosphorylates collapsin response mediator protein 2 (CRMP2), a neuronal protein with a role in growthcone collapse. MLCP, myosin light chain phosphatase; LIMK, LIM kinase [Arimura N., *et al.*, 2000].

2.1.5 ROCK-I and disease pathogenesis

2.1.5.1 Alzheimer's disease

Alzheimer's disease today is still lacking a disease-modifying treatment and represents a huge medical need there are currently more than 12 million people suffering from Alzheimer's disease worldwide [Honing H., *et al.*, 2004]. Most often the disease begins in patients in their sixth to eighth decade of life with mild cognitive impairments such as memory deficits. It progresses rapidly within 4–5 years to severe dementia, and death usually occurs less than 10 years after

diagnosis. Neurofibrillary tangles contain aberrantly phosphorylated tau protein, a microtubule-associated protein and substrate for ROCK, whereas the amyloid aggregates are formed primarily by toxic 42-amino-acid long amyloid-β (Aβ) peptides. Aβ peptides are generated by secretases from a much larger plasma transmembrane protein, the amyloid precursor protein (APP). Cleavage of APP by α-secretases and subsequently by γ-secretases is a process that occurs throughout life and does not yield toxic Aβ42 peptides, which are instead generated by cleavage of APP by β- and γ-secretases. Large data sets from human genetic studies with mutations that increase Aβ42 levels have highlighted an important role of Aβ42 in disease pathology. In addition, significant correlations in humans have been reported between levels of soluble Aβ42, the formation of small aggregates (oligomers) and the extent of cognitive impairment [Kakulas BA., *et al.,* 1999]. Therapeutic approaches are therefore focused on lowering the amount of soluble, oligomeric Aβ42 by raising Aβ-specific antibodies, by developing inhibitors of β- or γ-secretases or by stimulating the α-secretase pathway. One possible approach to lowering Aβ42 levels was recently demonstrated by interfering with the RhoA–ROCK pathway. Some non-steroidal anti-inflammatory drugs (NSAIDs) have been shown in epidemiological studies to be linked to reduced prevalence of Alzheimer's disease among NSAID users [Melendez-Vasquez CV., *et al.,* 2004, Minagar A., *et al.,* 2004] and an explanation for these data was provided with the observation that a subset of NSAIDs (ibuprofen, sulindac sulphide and indomethacin) reduced Aβ42 levels, independent of their effects on cyclooxygenase (COX) activity [Trapp BD., *et al.,* 1998, Toshima Y., *et al.,* 2000]. However, the mechanism of Aβ42 lowering remained elusive until an investigation by Zhou and colleagues showed that in cells secreting Aβ42 and in transgenic PDAPP mice producing large amounts of Aβ42, some NSAIDs lowered Aβ42 by inhibiting the RhoA-ROCK pathway [Satoh S., *et al.,* 2001]. Inhibition of RhoA by the clostridial c3 transferase or by dominant-negative RhoA resulted in a decrease of Aβ42 levels in cell culture. The ROCK inhibitor Y-27632 was effective in lowering Aβ42 levels both in cell culture and in PDAPP transgenic mice after intra-cerebroventricular injection. Activation of Rho by geranyl geranyl pyrophosphate, a lipid required for the membrane attachment of Rho, increased Aβ42 levels; this increase was completely prevented by Y-27632. The ROCK inhibitor Y-27632 used in animal Alzheimer's disease models was efficient in lowering the amount of the toxic Aβ42 levels, but had no effect on total Aβ levels and this effect of Rho or ROCK inhibitors is at least one mechanism by which

NSAIDs reduce Aβ42 levels. It remains to be shown whether these results are confirmed in different cellular systems or transgenic animals that overexpress APP. The NSAID-induced inhibition of the RhoA-ROCK pathway seems to be specific for the RhoA-ROCK pathway. How NSAIDs inhibit this pathway is currently not known, but interfering with membrane attachment of RhoA is a non-specific mechanism of inhibition, as opposed to the specific and direct inactivation of RhoA activators, such as RhoGEFs.

In AD, ROCK inhibitors could prove beneficial in slowing down the degenerative process by reducing toxic levels of Aβ42, possibly by increasing ectodomain shedding via the α-secretase pathway [Kitaoka Y., *et al.,* 2004]. In addition to many other therapeutic interventions, these inhibitors have the well-documented advantage of stimulating regenerative growth of neurites and it is therefore possible that the inhibition of this pathway could result in repair of the amyloid-damaged neural circuitry.

2.1.5.2 Inflammatory, demyelinating CNS diseases

MS, a debilitating autoimmune neurological disease, affects more than 1.5 million people worldwide [Lee JK., *et al.,* 2004]. Most important in disease pathogenesis is the migration of leukocytes beyond the brain endothelium into the CNS and the inflammatory cascade stimulated by these cells, which finally results in demyelination of CNS fiber tracts and in neurite damage and loss. Several inhibitors (the statin lovastatin, the flavonoid luteolin, and the prenyltransferase inhibitors FTI-276 and GGTI-298) directly interfere with RhoA activation and might therefore block ROCK activation. Such a mechanism prevents or reduces leukocyte migration into the CNS and ameliorates or attenuates the disease process in animal models of multiple sclerosis [Wiessner C., *et al.,* 2003, Schwab JM., *et al.,* 2015, Ji RR., *et al.,* 2004]. Obviously leukocytes require active RhoA and ROCK for their journey beyond brain endothelium, because their trans-endothelial migration was prevented by the ROCK inhibitor Y-27632 [Inoue M., *et al.,* 2004].

Not much is known about the role of the Rho-ROCK pathway in CNS myelination. Myelination in the CNS is performed by oligodendrocytes, whereas in the peripheral nervous system Schwann cells are responsible for myelinating peripheral nerves. In humans suffering from spinal-cord injury, remyelination of central fibre tracts by Schwann cells has been observed [Inoue M., *et al.,* 2004] and transplanted human Schwann cells have been shown to remyelinate

demyelinated CNS fibre tracts in the rat spinal cord [Ramer LM., *et al.,* 2004]. Recent data indicate that ROCK regulates myelination by Schwann cells and that ROCK inhibition by two different inhibitors results in a myelination pattern in a Schwann cell neuron co-culture system reminiscent of the myelination pattern created by oligodendrocytes [Tatsumi S., *et al.,* 2005]. It is currently not known whether ROCK inhibition stimulates CNS myelination by oligodendrocytes in an animal multiple sclerosis model. Blocking ROCK by specific inhibitors not only interferes with the most relevant pathological process of multiple sclerosis the migration of leukocytes beyond brain endothelium but also stimulate neurite regrowth. Axonal loss in multiple sclerosis is regarded as the major factor underlying the progressive neurological disability of patients [Uehata M., *et al.,* 1997] and ovoid-like axonal structures, similar in shape to the retraction bulbs of injured or collapsed axons in spinally injured patients have been documented [Uehata M., *et al.,* 1998]. Such neuroregenerative potential of ROCK inhibitors might offer the chance of inducing functional recovery of autoimmune-damaged CNS circuitry.

2.1.5.3 Stroke and excitotoxicity

Neuroprotective effectives of the ROCK inhibitors Fasudil and hydroxy-Fasudil are not restricted to spinal-cord injury models, but have also been reported in cerebral multi-infarct models in gerbils and rats, and in an excitotoxicity rat model in which N-methyl-d-aspartate (NMDA) was injected intravitreally into the rat eye [Inoue M., *et al.,* 2004]. The ROCK inhibitors were given within 5 minutes of infarct induction or in parallel with NMDA injection. However, it has not been shown whether these inhibitors are still neuroprotective when the delivery of the ROCK inhibitors is delayed by several hours after induction of the infarct or after NMDA injection, a therapeutic treatment window that more closely mimics the human stroke situation. In rodent stroke models, several regeneration inhibitors, such as the ROCK-activating NgR1 complex and one of its ligands, NOGO-A, have been neutralized 24 hours or even 1 week after induction of a cerebral stroke and improved functional recovery has been observed [Lee JK., *et al.,* 2004, Wiessener C., *et al.,* 2003]. Other ROCK activators, such as the neurite-growth inhibitor repulsive guidance molecule, have been described in the infarct and penumbra area of humans dying from cerebral stroke [Schwab JM., *et al.,* 2015]. Blocking ROCK is therefore a feasible neuroregenerative strategy; furthermore, such a strategy has the advantage that the

therapeutic treatment window for the use of these inhibitors might be larger than for thrombolytic or neuroprotective stroke treatment options.

2.1.5.4 Neuropathic pain

Neuronal injuries in the peripheral nervous system (PNS; peripheral nerves, dorsal root ganglia (DRG) and dorsal roots) or in the CNS (thalamus or spinal cord) of humans can lead to a chronic pain state known as neuropathic pain [Ji RR., *et al.*, 2004]. This type of pain is difficult to treat and therapeutic outcomes are usually poor. One of the reasons for such a poor therapeutic situation is that neither the initiation nor the maintenance of neuropathic pain is completely understood. Inflammatory mediators produced in response to injury are potential candidates for the induction of neuropathic pain and one candidate, lysophosphatidic acid (LPA), has recently been shown to be involved in initiation of neuropathic pain in a mouse model of peripheral nerve injury [Inoue M., *et al.*, 2004].

LPA is present at lesion sites in the PNS and CNS, and exerts its function by binding to G-protein-coupled LPA receptors. Binding of LPA to the LPA1 receptor results in activation of the RhoA–ROCK pathway. In this study, intrathecal injection of LPA or peripheral nerve injury (partial sciatic nerve injury) in wild-type mice induced allodynia and hyperalgesia, symptoms characteristic of neuropathic pain. Blocking ROCK (with Y-27632) or RhoA (by Clostridium botulinum C3 transferase) prevented the initiation of neuropathic pain after nerve injury or LPA injection. These results were further substantiated by the data from LPA1- receptor-knockout mice, which showed no neuropathic pain after peripheral nerve injury [Inoue M., *et al.*, 2004].

Activation of RhoA and ROCK downstream of the LPA1 receptor was involved in induction of neuropathic pain but it is currently unclear whether this reversible model of neuropathic pain, in which the LPA-induced demyelination of the dorsal root is an important mechanism, is reflecting the persistent nature of human neuropathic pain. In another study of dorsal root injury (rhizotomy) performed in mice, pain resolution and sprouting of serotonergic spinal axons was accelerated by Y-27632 [Ramer L.M *et al.*, 2004]. One of the ROCK inhibitors, H-1152, relieved neuropathic pain in an L5 spinal-nerve-transection model [Tatsume S., *et al.*, 2005]. The results of these studies indicated ROCK as a potential drug target responsible for the induction and also maintenance of persistent pain states.

2.1.5.5 Amyotrophic lateral sclerosis

Fasudil was found to be effective in preventing motor neuron degeneration through inhibition of ROCK activation in ALS transgenic mice and also in *in vitro* studies. The activation of ROCK by SOD1G93A down-regulated phosphorylated Akt by enhancing the phosphorylation of PTEN, and these resulted in neuronal cell death. Here, it was evidenced suggesting that Fasudil suppressed the activation of ROCK and thereby reduced phosphorylation of PTEN, resulting in neuronal protection *via* increasing phosphorylated Akt. Fasudil and M3 protected motor neuron cells against SOD1G93A-induced neurotoxicity and modulated the PTEN/Akt pathway *via* inhibition of ROCK activation by SOD1G93A. Previous research has shown that the ROCK/PTEN/Akt pathway regulates cell death in neurons. Moreover, the PTEN/Akt pathway was linked to motor neuron survival in human SOD1-related ALS indeed, up-regulation of phosphorylated Akt *via* the inactivation of phosphorylated PTEN leads to motor neuron survival in ALS patients and in transgenic mouse models. A recent study showed that Fasudil prevented neuronal apoptosis by regulating ROCK activity and the PTEN/Akt pathway in cerebral ischaemia in rats. These findings suggested ROCK might play an important role in neuronal cell death, and that ROCK may have potential as a new treatment target in ALS [Rosen DR., *et.al*., 1993].

2.1.5.6 Autism spectrum disorders

Autism spectrum disorders (ASD) are genetically heterogeneous diseases, which has been made difficult in the understanding etiology. However, several genes implicated in the etiology of ASD are part of common molecular pathways, indicating that different genetic alterations could cause similar effects during neurogenesis. One of such common mechanisms was the cytoskeleton dynamics regulation, which is essential for organization of dendritic spines and axonal growth and guidance. However, the relationship between these mechanisms and the etiology of ASD has been poorly explored in the literature, especially in their functional aspects. The disturbance in cytoskeleton dynamics in cells have observed from autistic patients. Thus, the actin cytoskeleton dynamics regulation in stem cells from human exfoliated deciduous teeth (SHED) from ASD idiopathic patients. Researchers has been reported studies by incubating the cells of 13 patients and 8 controls for 24h using Rho kinase inhibitor (ROCKi) in order to depolymerize the microfilaments. To induce actin reconstruction, ROCKi was washed out and

cells were treated with drugs that activate specifically Rac2, Cdc42 or RhoA. The percentage of cells presenting actin filaments were counted at 15, 30, 45 and 60 minutes after drugs application. The results showed that 5 out of the 13 patients presented a significant lower percentage of cells with recovered actin filaments at all-time points compared to controls when treated with Rac2 or cdc42 activator, and among these, 2 patients respond abnormally to RhoA activation (unpaired t-test $p<0.05$). Also treated the cells with a drug that directly activates the three RhoGTPases, making them constitutively activated. Upon this treatment, 4 patients responded abnormally compared to controls. Interestingly, these are the same patients that had responded abnormally to the specific activactors. We tested all the five patients that presented abnormal actin reconstitution for expression of Rac2, cdc42 and RhoA and we found that one of them has lower expression of these three RhoGTPases. These results suggest that, at least for a group of ASD patients, the dynamics of actin polymerization is slower compared to control individuals and that for one of them this could be due to lower expression of RhoGTPases. [Inoue M., *et al.,* 2004] believe that this study can contribute for the understanding of the common molecular mechanisms involved in ASD etiology.

2.1.5.7 Cancer

Increased expression of Rho GTP-binding proteins has been reported for a wide variety of cancers. Although the mechanisms leading to elevated Rho expression have not been widely investigated, it was recently reported that metastatic breast cancer cells overexpress a microRNA that increases the expression of RhoC. In addition to increased levels of Rho proteins, specific examples of elevated expression or mutation of Rho activating guanine nucleotide exchange factors and downregulation or deletion of Rho inactivating GTPase-accelerating proteins have been detected. These findings suggest that there may be increased ROCK activity associated with cancer. Consistent with this possibility, elevated expression of ROCK I and ROCK II were observed in bladder and testicular cancer. In the case of bladder cancer, elevated expression was significantly correlated with poor survival. The increased expression and activity of ROCK could contribute to cancer initiation and progression in several ways. [Das S., *et al.,* 2011].

2.1.6 Small-molecule inhibitors of ROCK

2.1.6.1 Chemical structures and binding data of ROCK inhibitors

Fasudil (**Figure 2.3**, compound 1) and Y-27632 (**Figure 2.3**, compound 5) were the first small-molecule ROCK inhibitors discovered [Uehata M., *et al.,* 1997, Uehata M., *et al.,* 1998]. Originally, their mode of action was characterized as intracellular calcium antagonism. Since then, several laboratories have initiated research programmes for ROCK inhibitors to develop drugs for a variety of therapeutic indications, and at least eight distinct chemotypes have been described as ROCK inhibitors. A selection of their structures and ROCK activity data are summarized in **Table 2.1** and **Figure 2.3**. A more general assessment of all data is discussed below.

2.1.6.2 Isoquinoline series

Fasudil was shown to be a moderate inhibitor of ROCK with a Ki of 330 nM [Uehata M., *et al.,* 1997]. Characteristic features of the structure are the isoquinoline and the homopiperazine ring, connected by a sulphonyl group. Hydroxy-Fasudil (**Figure 2.3**, compound 2), the main metabolite of Fasudil *in vivo*, was slightly more active than the corresponding drug [Uehata M., *et al.,* 1997]. Optimization in the isoquinoline-sulphonamide series led to H-1152 [Hidaka H., *et al.,* 1997] (**Figure 2.3**, compound 3), so-called dimethyl-Fasudil, which is one of the most potent ROCK inhibitors reported so far. Due to its potency and commercial availability this compound represents an excellent tool for the investigation of ROCK inhibition *in vitro*. ROCK inhibitors containing the related 5-aminoisoquinoline backbone were recently disclosed, of which compound 4 (**Figure 2.3**) showed nanomolar potency [Iwakubo M., *et al.,* 2004].

2.1.6.3 4-Aminopyridine series

Y-27632 (**Figure 2.3**, compound 5) is widely used in biological and pharmacological experiments and is therefore the most prominent representative of the 4-aminopyridine series. Additional characteristic features of this series include a central cyclohexyl or phenyl moiety and, optionally, a basic side chain in the 4-position of the cyclohexyl ring. Optimization of Y-27632, which displayed only moderate inhibition of ROCK, led to a series of very potent compounds, such as Y-30141 (Figure 2.3, compound 6), compound 7 (**Figure 2.3**) and compound 8 (**Figure 2.3**).

Table 2.1 Potency of Rho kinase (ROCK) inhibitors

Compound and code	Ki or IC_{50} values (nM)			Source
	ROCK	ROCK-I	ROCK-II	
1 (Fasudil, HA-1077, AT877)		330	--	Full-length ROCKI expressed in COS cells
2 (HydroxyFasudil)	170	--	--	GST-Rho-kinase-CAT expressed in Sf9 cells
3 (H-1152, DimethylFasudil)	1.6	--	--	Purified Rho-kinase from bovine brain gray matter with GTPγS-GST-RhoA column
4	23*	--	--	Catalytic subunit of ROCK fused with GST and purified from baculovirus
5 (Y-27632)	--	140	300	ROCKI expressed in COS cells ROCKI and II expressed in HeLa cells
6 (Y-30141)	--	220	--	ROCKI expressed in COS cells ROCKI and ROCKII expressed in HeLa cells
7	--	13*	--	ROCKI expressed in Sf9 cells
8	--	23*	--	Human ROCKI purified from baculovirus
9	1*	--	--	Bovine ROCK catalyst region and glutathione S-transferase expressed in insect cells
10	Nobiologicaldata			
11	--	--	1*	Rat ROCKII expressed in Sf21 insect cells (bought from Upstate)
12	69*	--	--	Bovine ROCK catalyst region and glutathione S-transferase expressed in insect cells
13	--	--	22*	Immunoprecipitation of ROCKII from bovine grey-matter extract

*IC_{50} value

Incorporation of 1H-pyrrolo[2,3-b]pyridin-4-amine or 1H-pyrazolo[3,4-b]pyridin-4-amine instead of 4-amino-pyridine raised the activity against ROCK by an order of magnitude (for example, Y-30141 versus Y-27632). The combination of a hydrogen-bond donor and an acceptor in the bicyclic ring system seems to fit very well in the hinge-binding region. Investigating the chirality of Y-27632 revealed that the R-enantiomer was only slightly more potent than the corresponding S-enantiomer [Uehata M., *et al.,* 2003, Gingras K., *et al.,* 2004].

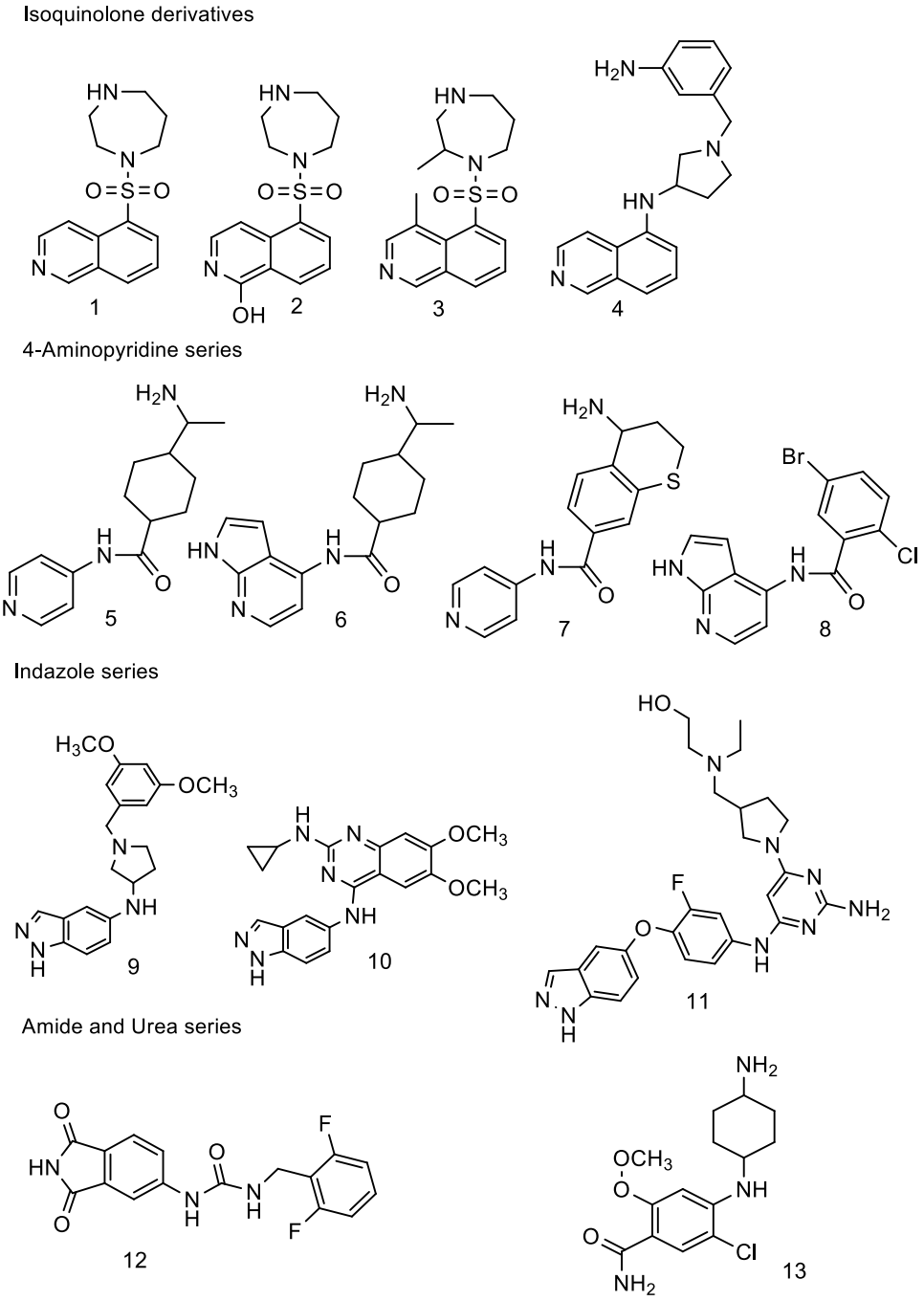

Figure 2.3 Structures of Rho kinase (ROCK) inhibitors. The ROCK inhibitors can be grouped into four classes according to their hinge-binding scaffold: isoquinolines, 4-aminopyridines, indazoles, and amide and urea derivatives. This mode of binding is proven for Fasudil, H-1152 and Y-27632, and presumed for the others. The selection of examples from patent applications is based on disclosed biological data, showing the most active compound(s) described.

2.1.6.4 Indazole series

Incorporation of 5-amino- or 5-alkoxy- 1H-indazole as scaffolds also led to a number of very potent ROCK inhibitors for example, compound 9 (**Figure 2.3**), compound 10 (**Figure 2.3**) and compound 11 (**Figure 2.3**) [Hirooka Y., *et al.,* 2005]. Attached to this scaffold are either substituted benzyl-pyrrolidine, aminoquinazoline or pyrimidine-aniline residues.

2.1.6.5 Amide and urea series

Urea-based pharmacophores have been described in numerous and diverse kinase inhibitors. However, this type of backbone seems to be of minor use in the case of ROCK inhibitors, and only a few examples have been described in the literature so far. A representative of this class is compound 12 (**Figure 2.3**) [Lu M., *et al.,* 2004], which comprises a phthalimide and a urea group as potential hinge-binding partners.

The structural diversity of the ROCK inhibitors might open up avenues for the development of inhibitors with different profiles, increased cell penetration and tissue specificity, but no systematic study has been reported so far.

2.1.6.6 Crystal structures

X-ray crystallography, in conjunction with homology modelling, is a powerful tool for structure-based rational design of regulatory domain inhibitors. Crystal structures have been determined for 35 protein kinases, which represent only a fraction of the more than 500 protein kinases encoded by the human genome. A crystal structure of the kinase domain of ROCK has not been published yet. In recent years, PKA was used as surrogate system for designing ROCK inhibitors as there were no crystal structures. In early years of 2000, many crystal complexes of ROCK were available with many inhibitors available which make them easy to analyze their mode of binding [Hirooka Y., *et al.,* 2005]. The hetero-aromatic hinge-binding pharmacophore of the inhibitors occupy the adenine sub site, whereas the linker and the saturated rings reside in the ribosyl su bsite. The phosphate sub site is not used by any of the inhibitors. Sequence alignments of 491 human kinases were used to calculate the frequency of certain amino-acid residues and their combinations within the regulatory domain binding site. These studies indicate that ROCK has a combination of five specific residues within its regulatory domain binding site that form a

uniquely shaped inhibitor-binding pocket with unique electronic properties [Hirooka Y., *et al.*, 2005]. These residues are also among those showing the largest numbers of contacts to the inhibitors, especially in the case of H-1152 (**Figure 2.4**) which could explain the high potency and selectivity for ROCK observed with this compound. Co-crystal structures of ROCK with inhibitors are needed to verify and possibly refine the model.

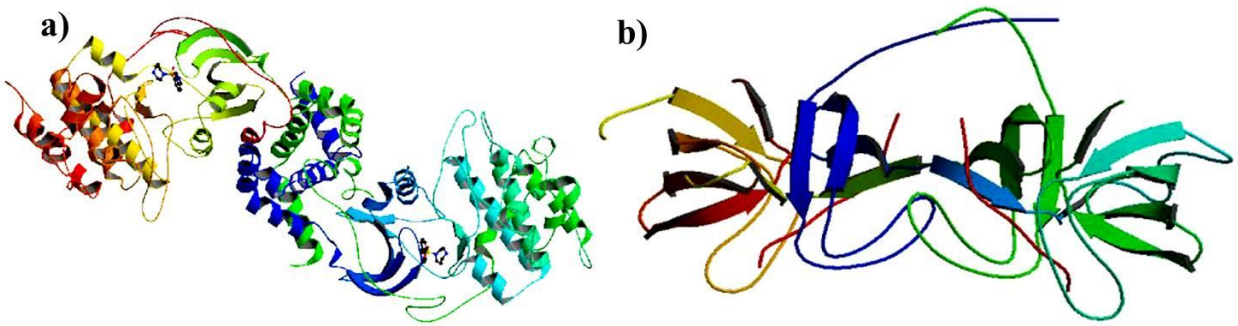

Figure 2.4 Crystal structures for a) ROCK-I and b) NOX2 obtained from PDB.

2.1.6.7 Therapeutic effect of ROCK inhibitors

Fasudil has been marketed in Japan and so extensive data are available on its safety profile and pharmacokinetic behaviour. All the available evidence indicates that the drug is well tolerated in humans. Fasudil has also shown beneficial effects in a number of other cardiovascular diseases, including angina pectoris, hypertension, coronary vasospasm, restenosis after percutaneous coronary intervention and arteriosclerosis [Lu M., *et al.*, 2004]. It is active after oral administration [Takanashi Y., *et al.*, 2001] but has a very short half-life in vivo because it is rapidly metabolized to hydroxy-Fasudil. The brain penetration of Fasudil and hydroxy-Fasudil seems to be poor. Therefore increasing the drug concentration in the cerebrospinal fluid by using a liposomal Fasudil formulation for intrathecal injection was beneficial in increasing therapeutic efficacy and reducing side effects in a rat acute ischaemia model [Nagatoya K., *et al.*, 2002].

Y-27632 has been much less investigated in vivo. Similarly to Fasudil it is active after oral administration [Wei L., *et al.*, 2001] but is also metabolized very rapidly. Its brain penetration might also be too low to achieve therapeutic levels for CNS diseases. Y-27632 was administered intracerebroventricularly to PDAPP mice to assess its Aβ42-lowering effect.

Y-27632 has been extensively studied in a number of cellular assays and showed activity at 1–100 μM. For example, Y-27632 inhibited the phosphorylation of the ROCK substrate MARCKS (myristoylated alanine-rich C-kinase substrate) in NT-2 cells, which were stimulated by the Rho activator LPA. This cellbased phosphorylation was only weakly inhibited by Fasudil, Y-27632 and H-1152 (IC_{50} values of 25, 12.8 and 2.5 μM, respectively), despite their more potent in vitro activities (IC_{50} values of 330, 140–300 and 1.6 nM, respectively) as depicted in **Table 2.1**. Such a 100–1,000-fold decrease in activity is typical for kinase inhibitors that bind to the ATP site of the enzyme, due to competition with intracellular micromolar ATP concentrations. Non- ATP-binding ROCK inhibitors have not been reported in the literature, to date.

Only a few ROCK inhibitors have been investigated for their kinase selectivity. On the basis of their low-to-moderate selectivity for PKN, citron kinase, MSK1 and MAPKAPK1b, Fasudil and Y-27632 are not optimal tool compounds. Better tool compounds are therefore needed. In addition, drugs based on inhibition of ROCK for neurological indications must meet additional criteria, such as enhanced brain availability and longer half-life [Feurer A., *et al.*, 2004]. In vivo data for other ROCK inhibitors besides Fasudil, Y-27632 and H-1152 have not been published so far.

2.2 NADPH oxidase 2 (NOX2) as a target

The NOXs are a group of plasma membrane associated enzymes found in a variety of cells of mesodermal origin. The most thoroughly studied of these is the leukocyte NOX, which is found in professional phagocytes and B lymphocytes. It catalyzes the production of superoxide (O_2^-) by the one-electron reduction of oxygen, using NADPH as the electron donor:

$$2O_2 + NADPH \rightarrow 2O_2^- + NADP^+ + H^+$$

The O_2^- generated by this enzyme serves as the starting material for the production of a vast assortment of reactive oxidants, including oxidized halogens, free radicals, and singlet oxygen. These oxidants are used by phagocytes to kill invading microorganisms, but they also cause a lot of what the military would call ‘‘collateral damage’’ to nearby tissues, so their production has to be tightly regulated to make sure they are only generated when and where required.

In the 40 years since first reported findings suggesting the existence of such an enzyme in neutrophils, a great deal has been learned about the leukocyte oxidase. Research over this period of time has shown that the core enzyme comprises five components: $p40^{PHOX}$ (PHOX for PHagocyte OXidase), $p47^{PHOX}$, $p67^{PHOX}$, $p22^{PHOX}$ and $gp91^{PHOX}$. In the resting cell, three of these five components $p40^{PHOX}$, $p47^{PHOX}$ and $p67^{PHOX}$ exist in the cytosol as a complex. The other two components $p22^{PHOX}$ and $gp91^{PHOX}$ are located in the membranes of secretory vesicles and specific granules, where they occur as a heterodimeric flavohemoprotein known as cytochrome b558. Separating these two groups of components by distributing them between distinct subcellular compartments guarantees that the oxidase is inactive in the resting cell [Babior BM., *et al.,* 1999].

2.2.1 NOX subunits

The NOX consists of six hetero-subunits, which associate in a stimulus-dependent manner to form the active enzyme complex and produce O_2^-. This activity has to be spatially and temporally restricted to the closed phagosome in order to prevent destruction of host tissue in what has been previously described as 'collateral damage' [Heyworth PG., *et al.,* 2003]. Tight regulation of enzymatic activity is achieved by two mechanisms: separation of the oxidase subunits into different subcellular locations during the resting state (cytosolic and membrane-bound) and modulation of reversible protein–protein and protein–lipid interactions. These can either enforce the resting state or allow translocation to the membrane in response to appropriate stimuli. Two NOX subunits, $gp91^{PHOX}$ and $p22^{PHOX}$, form as integral membrane proteins. They form a heterodimeric flavocytochrome b558 ('cyt b558') that constitutes the catalytic core of the enzyme, but exists in a dormant state in the absence of the other subunits. These play mostly regulatory roles, and are located in the cytosol during the resting state. They include the multi domain proteins $p67^{PHOX}$, $p47^{PHOX}$ and $p40^{PHOX}$, as well as the small GTPase Rac, which is a member of the Rho family of small GTPases.

2.2.1.1 gp91^{PHOX}

The gp91^{PHOX} subunit (also called the β-subunit of the cytochrome) consists of 570 amino acids and has a molecular mass of 65.3 kDa, but runs as a broad smear of approx. 91 kDa on SDS/polyacrylamide gels due to heterogeneous glycosylation pattern of three asparagine residues (Asn132, Asn149 and Asn240) [Wallach TM., *et al.*, 1997]. The N-terminal 300 amino acids are predicted to form six transmembrane α-helices, while the C-terminal cytoplasmic domain contains the binding sites for FAD and NADPH, shown experimentally through cross-linking studies and the observation that flavocytochrome alone can generate O_2^-. In addition, gp91PHOX is responsible for complexing the two non-identical heme groups of the NOX via two histidine pairs [Doussiere J., *et al.*, 1993]. Hence gp91^{PHOX} contains all co-factors required for the electron transfer reaction which occurs in two steps. First, electrons are transferred from NADPH on to FAD and then to the haem group in the second step to reduce O_2 to O_2^- in a one electron- transfer reaction [Yu L., *et al.*, 1998]. At present, no information is available on the three-dimensional structure of gp91^{PHOX} or fragments thereof, although a model for the structure of the cytoplasmic domain of gp91^{PHOX} has been suggested based on sequence homology with the FNR (ferredoxin–NADP reductase) family. Significant insight into the topology of the cytochrome and the sites of interaction with other oxidase components has been gained through the use of a number of techniques, including epitope mapping or random sequence peptide phage analysis [Taylor WR., *et al.*, 1993]. Additionally, the study of cytochrome isolated from patients with X-linked CGD has contributed to our current understanding of its function.

2.2.1.2 p22 PHOX

p22^{PHOX} (also called the α-subunit) contains 195 amino acids and has a molecular mass of 21.0 kDa. It associates with gp91^{PHOX} in a 1:1 complex, and contributes to its maturation and stabilization [Yu L., *et al.*, 1997]. Its N-terminal portion is predicted to contain three transmembrane α-helices, while the C-terminal cytoplasmic portion appears to be devoid of any secondary structure and its only recognizable motif is a PRR (proline-rich region) that contains a consensus PxxP (Pro-Xaa-Xaa-Pro) motif around Pro156. This motif is known to be a target of the SH3 (Src homology 3) domains of p47^{PHOX} and Pro156 has been found mutated in a CGD patient. Studies using a reconstituted cell-free system for NOX activation show that p22^{PHOX} becomes phosphorylated in a phosphatidic-acid-dependent manner on a threonine residue

(Thr132 or Thr147) [Leto TL., *et al.,* 1994]. The physiological role of these events is not understood at present, but it is interesting to note that Thr147 is close to the region of $p22^{PHOX}$ that is involved in the interaction with the cytosolic regulatory subunit $p47^{PHOX}$.

2.2.1.3 The GTPase Rac

It was first suspected in the late 1980s that a GTPase might play a role in NOX activation when it was demonstrated that guanine nucleotides were able to stimulate oxidase activity. The GTPase was subsequently identified as Rac1 or Rac2, and it is now clear that its presence is absolutely required for full oxidase function [Seifert R., *et al.,* 1989] (reviewed recently in [Dinauer MC., *et al.,* 2003]. Rac belongs to the Rho-family of small GTPases, which act as molecular switches and regulate a large variety of signalling pathways, including cytoskeletal remodelling and chemotaxis. Their activity is determined by the type of guanine nucleotide to which they are bound: GDP maintains the protein in the inactive state, while GTP induces the active state, thereby allowing interaction with downstream effectors and propagation of a signalling response. The conversion between the active and inactive states is tightly regulated by GEFs (guanine-nucleotide-exchange factors), which promote the release of GDP and allow GTP to bind, and by GAPs (GTPase-activating proteins) that increase the rate of GTP hydrolysis by several orders of magnitude and hence down regulate GTPase signaling [Bourne HR., *et al.,* 1990].

Structural studies on many small GTPases over the last 15 years have shown that they all share a common fold consisting of a six-stranded β-sheet and five α-helices (reviewed in [Sprang SR., *et al.,* 1997]. The conformational changes that occur during the interconversion between the active and the inactive states are by and large confined to two regions of the protein, which have been termed the switch I and switch II regions. Not surprisingly, these regions are generally recognized by regulatory proteins [GDIs (GDP-dissociation inhibitors), GEFs and GAPs] or downstream effectors, and they can therefore be viewed as the docking stations for GTPase-binding proteins. The remainder of the GTPase, including the insertion helix (amino acids 123–135), which is found only in Rho-family GTPases, stays unaltered during GDP–GTP cycling. Rac, however, is an exception to this rule, because its switch II region does not change its conformation upon GTP binding, as shown by crystallographic studies on (**Figure 2.5**) GTP- and GDP bound forms of Rac. Both Rac1 and Rac2 are geranyl geranylated at the C-terminus, which

facilitates their association with membranes. Nevertheless, both isoforms are kept cytosolic in the resting state due to an association with the GDI protein RhoGDI, to which Rac binds mainly through its switch II region and a hydrophobic pocket of the GDI that accommodates the geranyl geranyl moiety of the GTPase. Appropriate stimuli induce the dissociation from RhoGDI, allowing membrane translocation independent of the other oxidase subunits [Price MO., *et al.*, 2002] and exchange of GDP against GTP catalyzed by GEFs such as the phosphoinositide-activated exchange factor P-Rex1 and the haematopoietic cell-specific GEF Vav1 [Kim C., *et al.*, 2003].

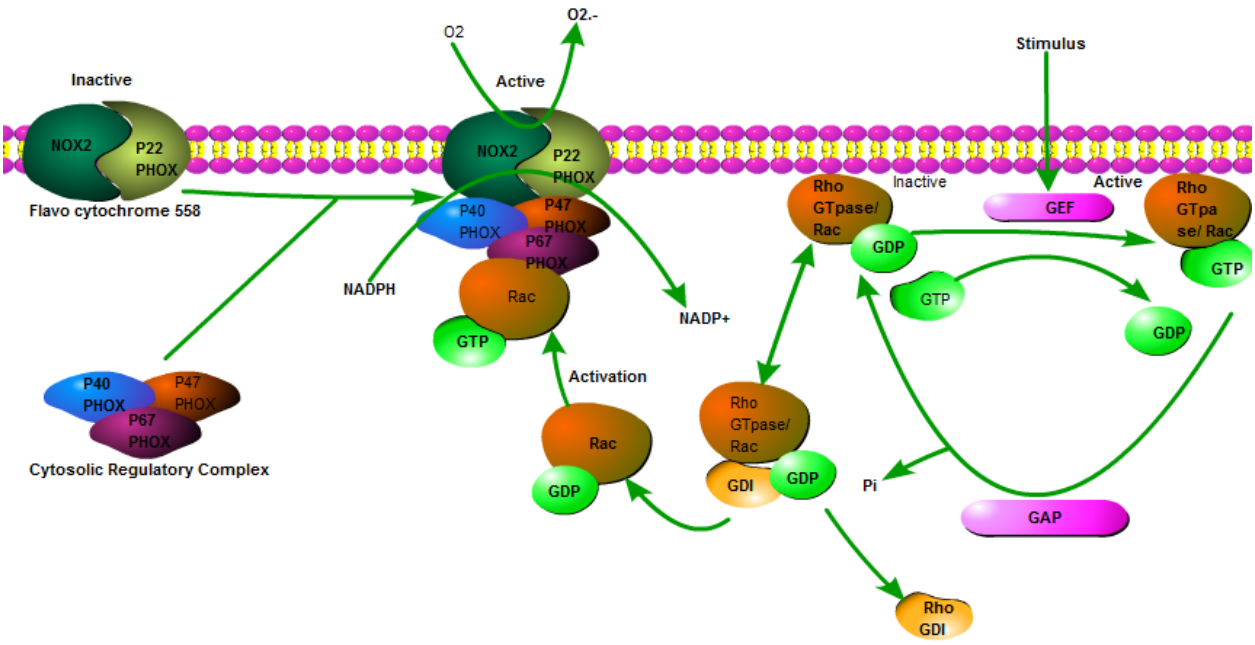

Figure 2.5 Hypothetical pathway interrelates between ROCK-I and NOX2 in neuroinflammatory conditions.

Two regions of Rac are of particular interest to NOX regulation: the insertion helix and the hyper variable C-terminus, where most of the differences between Rac1 and Rac2 occur. Rac1 is expressed ubiquitously, while Rac2 expression is restricted to haematopoietic cells [Gu Y., *et al.*, 2001]. Both proteins consist of 192 amino acids and share 92%sequence homology, and, importantly, no amino acid substitutions occur in the switch regions or the insertion helix. Their ability to support $O2^{-}$ production is similar in reconstituted cell-free systems using purified proteins. However, functional differences between Rac1 and Rac2 have been found in assays using neutrophil [Heyworth PG., *et al.*, 1993]. Interestingly, the two isoforms are found in different subcellular micro-environments in activated neutrophils. This distribution has been

shown recently to be regulated by the hyper variable C-terminus and Asp150 of Rac2, and might explain apparent differences in oxidase regulation [Ponting CP., *et al.,* 1996].

2.2.1.4 The cytosolic regulatory subunits

The activity of the phagocytic NOX is tightly regulated by three cytosolic components $p67^{PHOX}$, $p47^{PHOX}$ and $p40^{PHOX}$. These regulatory factors feature a number of protein–protein and protein–lipid interaction modules, sometimes in multiple copies, and undergo a variety of controlled protein–protein interactions at different stages during the activation process. Some of these interactions are modulated by reversible phosphorylation of serine or threonine residues, while others are targeted by phospholipids.

2.2.1.4.1 $p47^{PHOX}$

$p47^{PHOX}$ is a 390-amino-acid protein with a molecular mass of 44.7 kDa that consists of a PX (PHOX homology) domain, two adjacent SH3 domains, a region rich in arginine and lysine residues (the polybasic region) and a PRR (**Figure 2.6**). The PX domain was first identified in 1996 as a novel domain that is present in the NOX subunits $p40^{PHOX}$ and $p47^{PHOX}$, and has since been shown to specifically recognize phosphoinositides. In the case of $p47^{PHOX}$, it recognizes preferentially PtdIns(3,4)P2 and thereby contributes to membrane anchoring of $p47^{PHOX}$ after activation-induced translocation. The two SH3 domains of $p47^{PHOX}$ have been shown to mediate a number of protein–protein interactions in both the resting and the active states, some of which are targeted by phosphorylation [Quinn MT., *et al.,* 2004]. In fact, $p47^{PHOX}$ is the most extensively phosphorylated subunit of the NOX, and a total of 11 phosphorylation sites have been identified to date, all of which map to the region C-terminal of SH3 domain B [Kobayashi T., *et al.,* 2001]. Pure, recombinant $p47^{PHOX}$ is a monomeric protein free in solution as shown by analytical ultracentrifugation and neutron scattering, and there is no indication that post-translational modifications might change this state. A number of reports have suggested that the actin cytoskeleton might play a role in NOX regulation, most likely through an interaction with $p47^{PHOX}$ and possibly other oxidase components [Zhan Y., *et al.,* 2004]. Specifically the PX domains of $p47^{PHOX}$ and $p40^{PHOX}$ have been shown to bind moesin, which belongs to the ERM (ezrin/radixin/moesin) family of actin-binding proteins [Nisimoto Y., *et al.,* 1997]. The precise effect of association of PHOX components with the cytoskeleton remains unknown, but it has recently been suggested that the moesin–p47 PX domain interaction might be responsible for

membrane translocation of p47^{PHOX}. Such an interaction is difficult to reconcile with the phosphoinositide-binding function of PX domains, which is well documented by biochemical and structural evidence. Clearly, additional data are required to clarify the physiological role of the actin cytoskeleton in oxidase assembly.

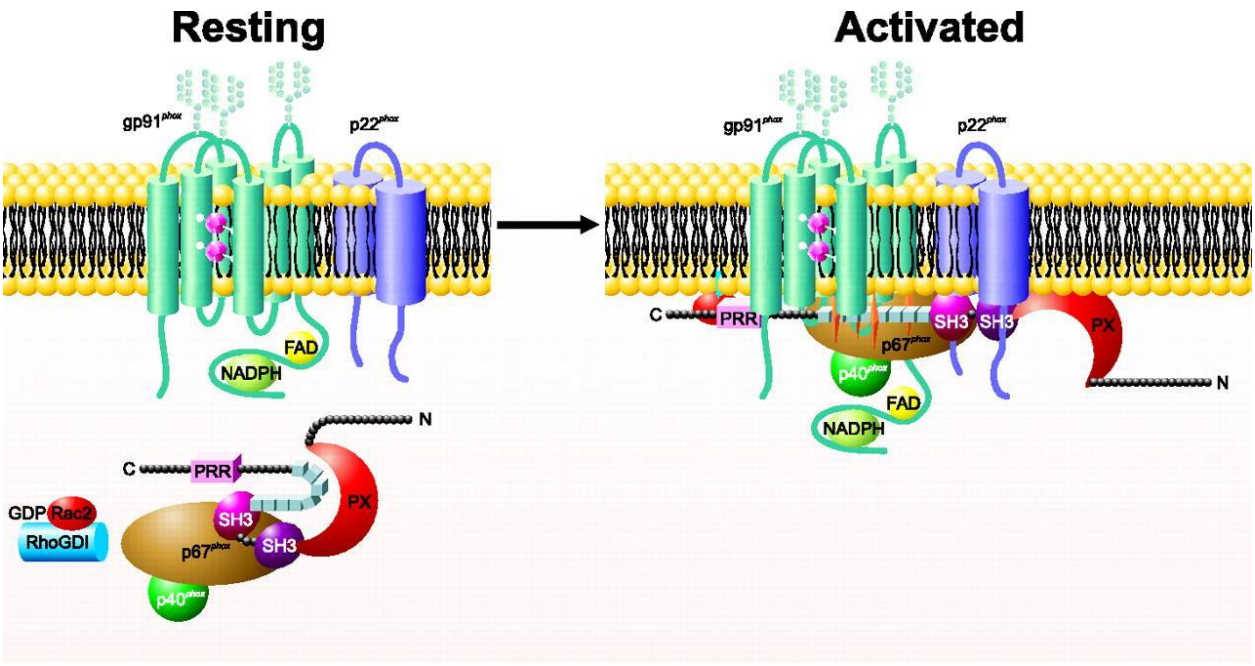

Figure 2.6 Assembly and activation of the phagocyte NOX. In resting phagocytes, hetero dimeric gp91^{PHOX}-p22^{PHOX} resides in the membrane, whereas the complex of p47^{PHOX}-p67^{PHOX}-p40^{PHOX} is cytosolic. Agonist-triggered phosphorylation of the autoinhibitory domain of p47^{PHOX} (series of small boxes) releases a conformational restriction, making interactive protein motifs, including the PX domain, Src homology 3 regions (SH3), and proline-rich regions (PRR), in p47^{PHOX} accessible to associate at the membrane and to mediate oxidase assembly [Wientjes FB., *et al.*, 1996].

2.2.1.4.2 p67^{PHOX}

p67^{PHOX} is a 526-amino-acid protein with a molecular mass of 59.8 kDa, which consists of a four TPR (tetra tri co peptide repeat) motif-containing domain, a PRR and two SH3 domains that are separated by a PB1 (PHOX and Bem1) domain (**Figure 2.6**). The N-terminal portion of p67PHOX that encompasses the TPR domain is responsible for mediating the interaction with Rac in a GTP-dependent manner [Das AK., *et al.*, 1998]. TPR domains are known to promote protein–protein interactions and are often found in proteins that are part of multi-protein assemblies. In addition, recent reports have suggested that the TPR domain of p67^{PHOX} may also bind NADPH and exhibit weak dehydrogenase activity in spite of the absence of any homology with NADPH-binding sites in other proteins. The significance of this observation is not

understood at present, since it is generally accepted that the cytochrome contains the binding sites for all the co-factors that are necessary for efficient oxygen reduction. No binding partner has yet been identified for the PRR in $p67^{PHOX}$ nor is it established if SH3 domain A participates in the regulation of NOX activity. The PB1 domain is a novel protein–protein interaction module that interacts with other PB1 domains and has been named after its occurrence in the phagocytic oxidase and Bem1 [Ito T., *et al.,* 2001]. In the case of $p67^{PHOX}$, it forms a heterodimer with the PB1 domain of $p40^{PHOX}$. In addition to its protein interaction modules, $p67^{PHOX}$ contains an 'activation domain', which encompasses amino acids 199–210 and has been shown to be absolutely required for $O2^-$ production in a reconstituted cell free system. It is believed that this region might interact directly with the flavocytochrome and thereby participate in the regulation of electron transfer [Tsunawaki S., *et al.*, 1994].

The shape and oligomerization state of $p67^{PHOX}$ in solution is controversial. Based on neutron scattering data in combination with analytical gel filtration, it was suggested that it exists as a dimer; however, the protein used in those studies had a propensity to aggregate even at low protein concentrations. Analytical ultracentrifugation data instead indicated that it is an elongated monomer, which could explain its apparent high molecular mass on gel filtration. On the other hand, phosphorylation studies of $p67^{PHOX}$ using different kinases including p38 MAPK (mitogen-activated protein kinase) and ERK1/2 (extracellular signal- regulated kinase 1/2) suggest that it might exist in an auto-inhibited state. A new phosphorylation site in the C-terminal part (amino acids 244–526) of $p67^{PHOX}$ appears after removal of the N-terminal portion of the protein [Sathyamoorthy M., *et al.*, 1997], suggesting a conformation in which the C-terminal phosphorylation site is masked by an N-terminal fragment containing the TPR domain.

2.2.1.4.3 $p40^{PHOX}$

$p40^{PHOX}$ is a 339-amino-acid protein with a molecular mass of 39.0 kDa and consists of a PX domain, an SH3 domain and a PB1 domain (in the context of $p40^{PHOX}$, previously described as a PC domain, where PC is PHOX and Cdc24) (**Figure 2.6**). $p40^{PHOX}$ was the last NOX subunit to be identified by co-immunoprecipitation and co-purification with $p47^{PHOX}$ and $p67^{PHOX}$ [Yoshinaga S., *et al.,* 2003]. It interacts with $p67^{PHOX}$ via its PB1 domain, while its SH3 domain has been suggested to interact with the PRR in $p47^{PHOX}$. However, this interaction is very weak in comparison with that between $p47^{PHOX}$ and $p67^{PHOX}$, and its physiological relevance is not

clear at present. The PX domain of $p40^{PHOX}$ binds specifically to PtdIns(3)P, which accumulates in phagosomal membranes, and could thus facilitate oxidase assembly at this location. The overall function of $p40^{PHOX}$ in oxidase regulation is still controversial, and it has been described as both activator and inhibitor [Kami K., *et al.,* 2002].

2.2.1.5 Protein–protein interactions in the resting state

Reversible protein–protein interactions mediated by modular protein interaction domains are key to NOX assembly, and much effort has been put into identifying the regions that are responsible for mediating complex formation during the different stages of the activation process. The interactions have been examined using a variety of techniques including phage display, yeast-two hybrid assays, oxidase reconstitution assays, GST (glutathione S-transferase) pull-down experiments, fluorescence spectroscopy and ITC (isothermal titration calorimetry). In addition, several crystal and NMR structures of NOX fragments and complexes thereof have been solved recently. The focus on the interactions of the cytosolic proteins in the resting state as these are the best characterized at present, and later give an overview of our current understanding of protein interactions occurring at the membrane in the fully assembled enzyme.

Early isolation of a complex of the regulatory oxidase subunits from the cytosol of resting neutrophils detected a molecular mass of 240–300 kDa by analytical gel filtration and showed that this complex contained $p47^{PHOX}$ and $p67^{PHOX}$ [Wientjes FB., *et al.*, 1996]. $p40^{PHOX}$ had not been identified at that time, and it was only appreciated later that it was part of the cytosolic complex. The large apparent molecular mass suggested that one or more oxidase subunits exist in multiple copies in this complex. However, recent biophysical studies employing ITC and analytical ultracentrifugation have shown that $p40^{PHOX}$, $p47^{PHOX}$ and $p67^{PHOX}$ associate with a 1:1:1 stoichiometry, and that the high molecular mass of the cytosolic complex is likely to be due to a non-globular shape. This trimeric complex is generally believed to constitute the resting state of the cytosolic components. However, a recent report by Yaffe [Kanai F., *et al.,* 2001]and co-workers suggested that $p47^{PHOX}$ may actually exist separately from the p40–$p67^{PHOX}$ complex in resting cells, and that formation of the trimeric complex requires stimulation. Hence this would constitute the first step along the activation pathway.

2.2.1.6 Oxidase assembly

Activation of the NOX requires conformational changes in the cytoplasmic complex to allow the assembly of the hetero hexameric enzyme at the membrane. Docking of the p47– p67–$p40^{PHOX}$ complex to the membrane bound cytochrome b558 is supported by an interaction between the tandem SH3 domains of $p47^{PHOX}$ and the cytoplasmic tail of $p22^{PHOX}$ [Ago T., *et al.,* 1999]. The crystal structure of the tandem SH3 domains of $p47^{PHOX}$ in complex with a peptide derived from the C-terminal tail of $p22^{PHOX}$ (amino acids 149–166) revealed that both SH3 domains cooperate to mediate this interaction [Huang J., *et al.,* 1999]. As observed in the auto-inhibited structure of $p47^{PHOX}$, (**Figure 2.6**) the tandem SH3 domains act in conjunction to form a SuperSH3 domain and bind the peptide simultaneously through conserved residues from both domains. SH3 domain A makes a larger contribution to complex formation, as demonstrated by its ability to interact with the peptide in the absence of SH3B. However, the interaction between $p47^{PHOX}$ and $p22^{PHOX}$ is strengthened significantly through additional contacts made with SH3B [de Mendaz I., *et al.,* 1997].

Once at the membrane, additional contacts between $p47^{PHOX}$ and the cytochrome take place, which are believed to either help position $p67^{PHOX}$ correctly or possibly induce a conformational change within the cytochrome. These interactions have been mapped to the first cytoplasmic loop of $gp91^{PHOX}$, and to two regions in the cytoplasmic domain of $gp91^{PHOX}$: to amino acids 450–457 adjacent to the NADPH-binding site and to the extreme C-terminus of the molecule as highlighted in **Figure 2.6**. Studies using atomic force microscopy support the notion that oxidase assembly, and specifically association with $p67^{PHOX}$, induce a conformational change in the cytochrome [Koshkin V., *et al.,* 1996]. In contrast, no evidence has yet been found for a direct interaction between $p40^{PHOX}$ and the cytochrome.

2.2.2 Therapeutic indications for NOX2

2.2.2.1 Parkinson's disease

Parkinson's disease (PD) is a neurodegenerative disorder characterized by a progressive loss of dopaminergic neurons in the nigrostriatal pathway of the brain, which triggers complex functional modifications within the basal ganglia circuitry, leading primarily to motor dysfunctions. Although the etiology of PD is unknown, a common element of most theories is

the involvement of oxidative stress, either as a primary or secondary event of the disease. Research on the pathogenesis of PD suggested that mitochondrial dysfunction is the major source of oxidative stress in this disease however, increasing evidence has been also found for a role of NOX enzymes in the process.

The research on the mechanisms involved in PD disease has relied on the development of animal models that reproduce the pathological and behavioral characteristics of the disease. Classically, these models are based on the systemic or intracerebral administration of neurotoxins capable of selectively degenerate the nigrostriatal system. A very useful model is based on systemic administration or striatal injection of 1-methyl-4-phenyl-1,2,3,6-tetrahydro-pyridine (MPTP), which causes a PD-like syndrome highly similar to the human disease [Shibuya M., *et al.*, 1992]. As demonstrated under in vivo conditions, translocation of $p67^{PHOX}$ was induced by MPTP in mouse brain and prevented by the tetracycline derivative minocycline. More recently, it has been demonstrated that $p47^{PHOX}$ phosphorylation and $p47^{PHOX}$–$gp91^{PHOX}$ complexes are significantly increased in mice substantia nigra (SN) after systemic injections of MPTP.

In addition, MPTP induced increases of both $gp91^{PHOX}$ and 3-nitrotyrosine in the SN of ageing mice, which were inhibited by oral treatment with the NO-donating derivative of flurbiprofen [2-fluoro-α-methyl (1,1'-biphenyl)-4-acetic-4-(nitrooxy)butyl ester (HCT1026)]. In line with these findings, degeneration of dopaminergic neurons induced by MPTP was attenuated in $gp91^{PHOX}$-/- mice as compared to Wt littermates [Pollitt SK., *et al.*, 2003]. In the same PD model, $gp91^{PHOX}$ immunoreactivity colocalizes with microglial cell markers but not with astrocyte markers, confirming a microglial origin for NOX. In vitro overnight MPP+ (a MPTP metabolite) treatment of N27 rat dopaminergic cells was able to induce NOX2 protein expression and $O2^{\cdot -}$ generation, as measured by flow cytometric detection. This effect was inhibited by siRNA silencing of $p22^{PHOX}$ [Machida Y., *et al.*, 2006]. Thus, it appears that activation of NOX2 plays a relevant role in the loss of dopaminergic neurons in the MPTP-induced PD model.

Another commonly used procedure for obtaining experimental nigrostriatal lesion in rodents is based on local infusion of 6-hydroxydopamine (6-OHDA). The biological effects of 6-OHDA are mainly related to the massive oxidative stress caused by the toxin that, once accumulated in the cytosol, seems to be auto-oxidated, promoting a high rate of free radical generation. As detected by dihydroethidium fluorescence, the treatment of primary mesencephalic cultures with

6-OHDA induced a significant increase of the intracellular generation of $O_2^{\cdot -}$ in dopaminergic neurons, as well as in microglial cells. There is evidence to implicate NOX-derived ROS in this process, but the mechanisms involved are poorly understood. For instance, data from our laboratory suggest a relevant role for NOX2 in 6-OHDA-induced PD. In this study, the membrane protein levels of $p67^{PHOX}$ were markedly elevated in the SN of 6-OHDA lesioned mice, suggesting that the $p67^{PHOX}$ subunit translocated from the cytosol to the plasma membrane, thus forming a NOX entity capable of producing superoxide after 6-OHDA injection. Tyrosine hydroxylase immunolabeling indicated that $gp91^{PHOX}$-/- mice appear to be protected from dopaminergic cell loss in the SN and from dopaminergic terminal loss in the striatum. Moreover, wild type mice treated with apocynin, a NOX inhibitor, and $gp91^{PHOX}$-/- mice all exhibited significantly ameliorated apomorphine-induced rotational behavior after 6-OHDA lesion [Nagatsu T., *et.al*., 2006]. These results are corroborated by some in vitro observations. In rat primary mesencephalic cultures, 6-OHDA induced a significant increase of $gp91^{PHOX}$ and $p47^{PHOX}$ immunolabeling. Confocal microscopy revealed that both $gp91^{PHOX}$ and $p47^{PHOX}$ were intensely expressed in microglia cells. Microglial activation and $O_2^{\cdot -}$ generation in dopaminergic neurons were significantly reduced by apocynin. Six-OHDA also induced increased expression of $gp91^{PHOX}$ in human dopaminergic neuroblastoma cells.

Nevertheless, the role of NOX enzymes in 6-OHDA-induced PD might not be only limited to the NOX2 isoform. As recently demonstrated, striatal administration of 6-OHDA increased NOX1 expression in dopaminergic neurons of the SN. Furthermore, adeno-associated virus-mediated NOX1 knockdown reduced 6-OHDA-induced oxidative DNA damage and dopaminergic neuronal degeneration in the rat SN [Zhang L., *et al.*, 2007].

The involvement of NOX in PD has also been revealed through other, unrelated PD models. In mesencephalic primary cultures, activated microglia generated NOX derived superoxide and enhanced lipopolysaccharide-elicited dopaminergic neurodegeneration. Furthermore, microglial NOX but not neuronal NOX, renders dopaminergic neurons more sensitive to rotenone, an herbicide able to reproduce features of PD in rats. In mesencephalic neuron-glia cultures from gp91PHOX-/- mice the deleterious effect of microglia induced by substance P on tyrosine hydroxylase-positive neurons was significantly attenuated. The NOX involvement in the cytotoxic action of paraquat, another widely used parkinsonism inducing agent, has also been

recently described. Apocynin attenuated paraquat-induced dopaminergic degeneration, NOX activation, cytochrome c release and caspases-9/-3 and microglia activation. According to the authors, paraquat induces oxidative stress through NOX activation and depletion of glutathione, which in turn activate the apoptotic machinery leading to dopaminergic neurodegeneration. It has been also reported that the NOX inhibitor diphenyleneiodonium (DPI) blocked the paraquat-induced ROS production and subsequent dopaminergic neurodegeneration [Mudo G., *et al.*, 2012].

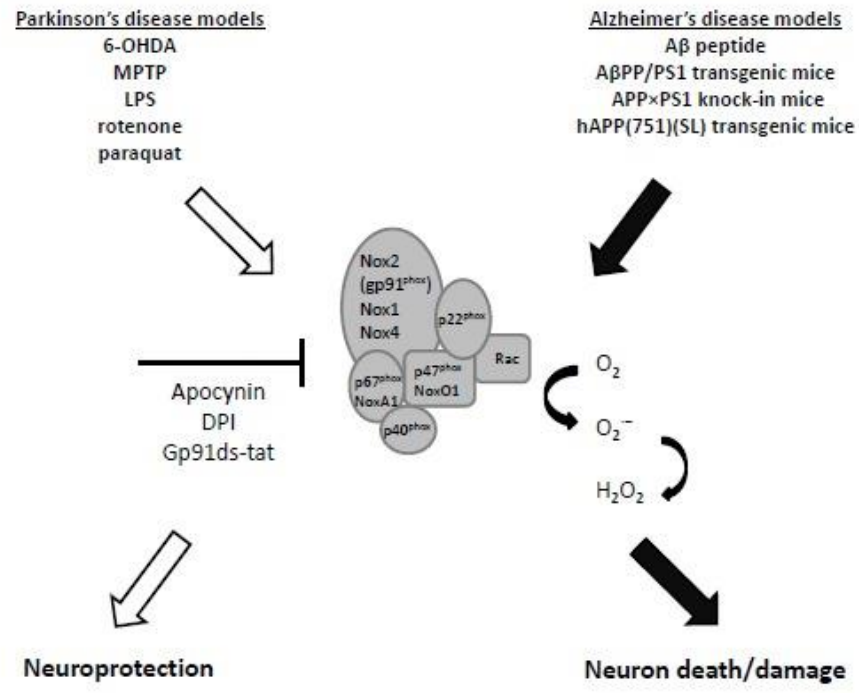

Figure 2.7 NOX activation, neurodegeneration and neuroprotection. In Parkinson´s and Alzheimer´s disease rodent models, increased activation of the NOX family of ROS-producing proteins contributes to neurodegeneration. Blockade of NOX generates neuroprotection in some instances. Abbreviations: 6-hydroxydopamine (6-OHDA); 1-Methyl-4-Phenyl-1,2,3,6-Tetrahydropyridine (MPTP); Lipopolysaccharide (LPS); amyloid-β peptide (Aβ); superoxide ($O2^{\cdot-}$); hydrogen peroxide (H2O2) and diphenyleneiodonium (DPI) [Zhang L., *et al.*, 2007].

2.2.2.2 Alzheimer's disease

Alzheimer's disease (AD) is characterized by an initial mild cognitive impairment that progressively develops into a loss of higher cognitive functions, resulting in dementia. Accumulation of amyloid-β peptide (Aβ) in the brain is considered one of the main pathological features of AD. Other AD microscopic hallmarks include abnormal protein folding, exacerbated

activation of glial cells, and synaptic and neuronal loss. Importantly, a growing body of evidence supports a role for abnormal NOX activation in this pathology. Activation of NOX2 in the brain of AD subjects has been demonstrated, as evaluated by the translocation of NOX2 subunits. In addition, analysis of frontal lobe tissue of AD patients demonstrated significantly increased levels of NOX1 and NOX3 mRNAs, suggesting that other isoforms beyond NOX2 can contribute to that neuropathology. There is also evidence that NOX-associated redox pathways might participate in the early pathogenesis of AD. By using a luminescent assay to detect NOX-dependent ROS production, it was shown that NOX activity is increased in the superior/middle temporal gyri over control levels at the earliest clinical manifestations of disease, but not in late-stage AD. The observed increases of NOX activity were associated with increased expression of $p47^{PHOX}$ and $gp91^{PHOX}$ in both microglia and neurons [Huh SH., *et al.*, 2011].

However, in vitro and in vivo studies have generated most of the information related to the role of NOX enzymes in AD pathogenesis. It has been recently shown that the cholesterol oxidation product, 24-hydroxycholesterol, markedly potentiates the pro-apoptotic and pro-necrogenic effects of Aβ. This effect depends on its strong enhancement of the intracellular generation of NOX-derived ROS, mainly H_2O_2, and the consequent impairment of the neuronal redox state, measured in terms of the GSSG/GSH ratio. Gp91ds-tat, a NOX2 inhibitory peptide, decreased both oxidative stress and AD pathology in aged mice. Also, It has been recently shown that feeding AβPP/PS1 double transgenic mice, a mouse model of AD, with a diet containing phenolic antioxidant tert-butylhydroquinone, inhibits NOX2 protein expression and suppressed lipid peroxidation in the cerebral cortex and hippocampus. It was also found that age-dependent increases of Aβ had a significant linear relationship with both NOX4 activity and cognitive performance in "humanized" APP×PS1 knock-in mice. Apocynin treatment reduces Aβ deposition and the number of microglial cells in the cortex and hippocampus of aged transgenic mice overexpressing the human amyloid precursor protein (hAPP), but it failed to inhibit cytosolic $p67^{PHOX}$ translocation to the membrane and to reduce the levels of TNF-α. Similarly, apocynin did not improve cognitive and synaptic deficits, and did not decrease Aβ deposition, microgliosis and hyperphosphorylated tau in transgenic AD mice. In vitro exposure of hippocampal neuronal/glial co-cultures to Aβ peptides resulted in activation of glial NOX, followed by neurodegeneratio. In another in vitro study using a co-culture of microglia and neuroblastoma cells over-expressing the Aβ precursor protein (APP), ROS generated by

microglia induced neurodegeneration. This effect was attenuated by ROS-scavengers and was dose-dependently inhibited by DPI, suggesting that APP-dependent microglia activation and subsequent ROS generation by NOX play a crucial role in neuronal degeneration [Reiter RJ., *et al.*, 2010]. In addition, some studies demontrated that Aβ-induced NOX2 activation in astrocytes contributes to neurodegeneration. Aside from its involvement in neurodegeneration, production of H_2O_2 from NOX2 regulated microglial proliferation induced by Aβ, as demonstrated in a primary mixed glial culture obtained from rat cerebral cortex. This effect was prevented by apocynin and catalase, a H_2O_2 degrading enzyme. In summary, strong evidence indicates that oxidative stress in AD involves ROS generation by NOX enzymes, in particular NOX2.

2.2.2.3 Neuropathic pain

There is a growing body of evidence supporting a causal role of microglia activation in the development of nerve injury-induced neuropathic pain; yet the mechanisms are far from being understood. The ROS production in spinal cord microglia is required for the nerve injury-induced microglia activation and subsequent development of pain hypersensitivity. A previous study has implicated ROS in neuropathic pain, in which (spinal nerve transection) SNT injury induced superoxide production in spinal cord neurons at 7 d postinjury. The ROS production in spinal cord microglia immediately after nerve injury is critical for the induction of pain hypersensitivity. ROS are generated mainly in microglia at early time points (1 and 3 d postinjury). These data show that, after SNT, ROS production in dorsal horn microglia precedes ROS generation in neurons. Pain hypersensitivity develops within 3 d after SNT, which indicates that microglial ROS are involved in the induction of neuropathic pain.

The mechanism underlying SNT induced ROS generation, we found that NOX2 is induced in spinal cord microglia after SNT. NOX2 generates superoxide that can be converted to other ROS molecules, including hydrogen peroxide. Currently, it is not clear how peripheral nerve injury induces NOX2 transcript expression in spinal cord microglia. Thus far, various molecules, e.g., fractalkine, glutamate, and ATP, have been implicated in the signal transmission from injured peripheral nerve to spinal cord microglia. Tolllike receptor 2 (TLR2) is involved in nerve injury-induced spinal cord microglia activation, suggesting the possibility that damaged neuron-derived endogenous TLR2 agonist may activate microglia via TLR2. Although it is pure speculation, that

an endogenous TLR2 agonist released from the damaged sensory neurons might induce NOX2 transcripts in spinal cord microglia.

The fact that SNT-induced mechanical allodynia and thermal hyperalgesia were attenuated in NOX2-deficient mice suggests that microglial ROS contribute to neuropathic pain induction. Although these data do not formally exclude the contribution of NOX2 in other cell types, NOX2 immunoreactivity in the spinal cord was detected mainly in microglia and not in neurons [Bertoni A., *et al.,* 2010]

TNF-α and IL-1β expression in the spinal cord after SNT was reduced in NOX2-deficient mice and also in sulforaphane-injected WT mice [Nita DA., *et al.,* 2001]. The data from primary spinal cord glial cells suggest that ROS generation is required for expression of these proinflammatory cytokines. TNF-α and IL-1β have been implicated in the development of neuropathic pain, as these cytokines are expressed in spinal cord microglia after peripheral nerve injury. Blocking these cytokines using neutralizing antibodies or inhibitors decreased neuropathic pain induced by nerve injury. In isolated spinal cord slices, TNF-α and IL-1β enhanced the frequency of spontaneous excitatory synaptic transmission in lamina II neurons, and IL-1β reduced inhibitory synaptic transmission, as well. Excitatory synaptic transmission in lamina II neurons is regulated by MCP-1. Based on these reports, it was proposed that TNF-α and IL-1β released from activated microglia after SNT induces MCP-1 expression in astrocytes, which, in turn, regulates the excitability of pain transmission neurons in the dorsal horn. Regardless of the exact mechanism for TNF-α/IL- 1β–induced central sensitization, microglial ROS generated after SNT may increase pain hypersensitivity, at least in part, by upregulating proinflammatory cytokine expression in the spinal cord. In conclusion, SNT induces the generation of ROS in spinal cord microglia via NOX2, and NOX2-derived ROS in the spinal cord microglia contribute to the development of neuropathic pain. In addition, [Chan EC., *et al.,* 2009] sulforaphane has a strong analgesic effect on neuropathic pain by inhibiting microglial ROS, which may have important therapeutic implications.

2.2.2.4 Amyotrophic lateral sclerosis

Amyotrophic lateral sclerosis (ALS) is a fatal neurodegenerative disease that can be caused by dominant mutations in superoxide dismutase-1 (SOD1). Great uncertainty remains as to the

precise mechanism of motor neuron death in ALS, although oxidative stress and inflammation are both believed to be involved. Transgenic mice overexpressing a mutant form of *SOD1* found in ALS patients (*SOD1*^{G93A}) develop motor neuron disease similar to that seen clinically in familial forms of ALS.

Redox stress is thought to be an important component of disease progression in ALS. Indeed, recent studies have shown that *SOD1*^{G93A} ALS transgenic mice produce elevated levels of NOX2 gp91^{PHOX} and superoxide in spinal cord microglia. Although NOX2 expression increases in microglia of the spinal cord of *SOD1*^{G93A} transgenic mice, deletion of *NOX2* on a *C57BL/6J* inbred background of *SOD1*^{G93A} transgenic mice led to only a marginal increase in survival (122 to 135 days). Hence, the possibility remains that other NOX genes may more significantly influence redox stress in ALS disease. NOX1 and NOX2 are closely related homologs in the NOX gene family and share many of the same regulatory characteristics including a requirement for Rac1 and p22^{PHOX} coactivators. To this end, studies comparing the contribution of NOX2 or NOX1 deletion on disease progression in mixed hybrid *SOD1*^{G93A} ALS mice. Because both NOX genes reside on the X chromosome, we evaluated all NOX genotypes for male (*WT, NOXX+/Y; and KO, NOXX–/Y*) and female (*WT, NOXX+/X+*; heterozygous [HET], *NOXX+/X–*; and *KO, NOXX–/X–*) mice on the *SOD1*^{G93A} transgenic background, using siblings from F2 generations. The onset and progression of motor neuron disease were monitored using rotarod performance, stride length, weight, motor neuron counts, and/or survival as indices. Disrupting either of these NOX genes (NOX1 or NOX2) significantly delayed the progression of motor neuron disease in a *SOD1*^{G93A} transgenic mouse model of ALS. Interestingly, female ALS mice lacking a single copy of the X-chromosomal NOX1 or NOX2 genes also exhibited significantly increased survival rates. Thus, we conclude that in the setting of random X-inactivation, a 50% reduction in NOX1- or NOX2-expressing cells has a substantial therapeutic benefit in ALS mice. These studies demonstrate that multiple NOX genes appear to contribute to the pathoprogression of ALS and expand potential therapeutic targets for this disease.

2.2.2.5 Cancer

NOX expression in colon cancer has been detected to reach a maximum level in well-differentiated adenocarcinoma and to decrease in poorly differentiated adenocarcinoma, implying that NOX expression does not correlate with the extent of malignancy. By the same

token, a recent study on patient samples concluded that NOX expression was not statistically higher in colon cancer than in normal colon tissues, arguing that NOX contributes to colon epithelial differentiation rather than tumorigenesis. By reevaluating the statistical analysis, Laurent et al. 2001, however, obtained the contrasting results that increased NOX mRNA expression correlated with activating mutations in Gly-12 and Gly-13 of K-Ras, and that the colon tumor phenotype was closely related to overexpression of NOX. Transgenic mice expressing K-Ras Gly12Val in the intestinal epithelium also elevated NOX expression in the intestine, which fits in very well with oncogenic Ras-induced upregulation of NOX transcription through an ERK–GATA-6 cascade in CaCO-2 cells. Because the number of patient samples surveyed was relatively small, more clinical and experimental data would be needed to make any definitive conclusion. Nevertheless, the study has significant implications in understanding a causal relationship between K-Ras activation and NOX expression in colorectal cancer with a high frequency (~45%) of K-Ras activation mutation. If NOX exerts cancer-promoting effects, it is most likely at an early stage, as NOX expression is diminished at a more advanced tumor stage. Another point is that while NOX1 expression predominates, persistent activation of NF-κB also occurs in well-differentiated adenocarcinoma. This supports the scenario where the enhanced production of NOX1-derived ROS activates NF-κB signaling, which in turn contributes to tumor promotion by inducing inflammatory cytokines or providing potent anti-apoptotic survival signals to the enterocytes. Additionally, NOX may be associated with gastric cancer. Earlier studies indicated that lipopolysaccharide from *Helicobacter pylori* induced NOX-derived ROS through TLR4 in guinea pig gastric pit cells, suggesting that activation of NOX is one of the initial innate immune responses against *H. pylori*. Given that infection with *H. pylori* is associated with development of gastric adenocarcinoma, one might expect activation of NOX to promote gastric carcinogenesis by enhancing inflammation or oxygen radical activity. However, it remains to be determined whether NOX is engaged in the pathology of *H. pylori* in human stomach, as NOX1 and NOXO1 were absent in normal or chronic atrophic gastritis cells. In contrast, significant levels of NOX1 and NOXO1 were detectable in gastric cancer cells (intestinal, diffuse, or signet-ring cell type) but not normal gastric cells, whereas NOXA1 was constitutively expressed in both normal and tumor tissues. This points to an intriguing possibility that gastric cancer undergoes aberrant control of NOX1 and NOXO1 expression. In addition to

gastrointestinal neoplasms, some correlation between ERK activation and increased NOX expression was also seen.

2.2.3 NOX inhibitors

2.2.3.1 Small molecule inhibitors

2.2.3.1.1 Pyrazolopyridine derivatives

There are no clinically available specific NOX inhibitors as of this writing. Recently, pyrazolopyridine derivatives have been reported as specific NOX inhibitors that show promising potential as new drugs. GenKyoTex identified pyrazolopyridine derivatives (general formula 1, **Figure 2.8**) as specific and potent chemical structures using a high-throughput screening system [Page P., *et al.,* 2013]. They discovered two promising hits (2 and 3 in **Figure 2.8**) among 136,000 compounds screened. The hit compound 2 (4-methyl-2-phenyl- 5-(pyridin-3-ylmethyl)-1H-pyrazolo[4,3-c]pyridine-3,6 (2H,5H)-dione) was the most potent inhibitor and showed selectivity for NOX4 and NOX1 isoforms with little activity for NOX2 in *in vitro* cell-free assays. The K_i value of compound 2 (**Figure 2.8**) against human NOX4 was 373 nM, and NOX4/ NOX2 selectivity was > 12-fold. Compound 3 (**Figure 2.8**), which is a derivative of compound 2 with acetyl group to R position of compound 2, showed similar degree of NOX4 inhibitory activity. However, since the hit compound 2 had shown high first-pass metabolism, and low oral bioavailability was revealed by *in vivo* pharmacokinetic study, their focus turned to two lead molecules (4 and 5 in **Figure 2.8**). One of the two lead compounds, GKT136901 showed strong specificity (5, **Figure 2.8**), pharmacological and safety profiles.

2.2.3.1.2 Pyrazolopyrimidine derivatives

Shionogi & Co. Ltd discovered and claimed pyrazolopyrimidine derivatives (general formula 1 in **Figure 2.8**) as NOX inhibitors [Seno K., *et al.,* 2010]. One of the derivatives is 3-(3-chlorophenyl)-N-(2-(piperazin-1-yl)phenyl)-6,7-dihydro-1H-pyrazolo[4,3-c]pyridine-5(4H)-carboxamide (compound 2, **Figure 2.9**).

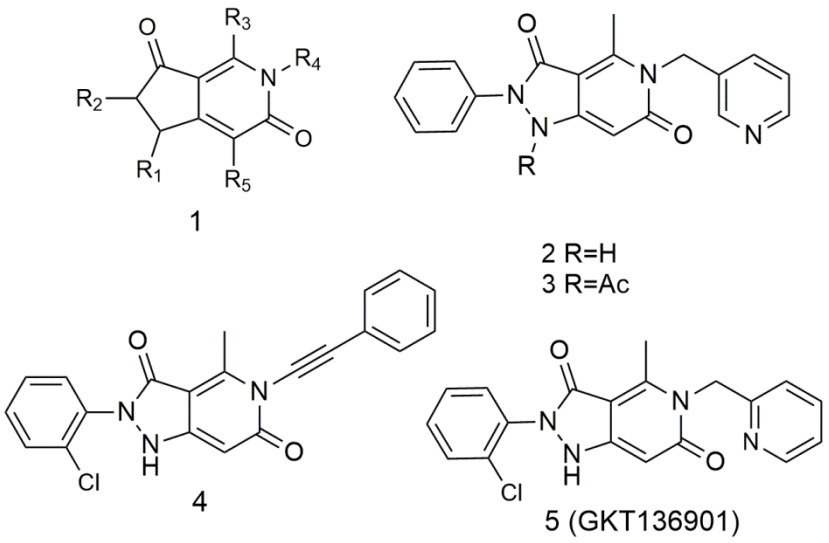

Figure 2.8 Pyrazolopyridine derivatives. GenKyoTex, SA. [Page.P *et al.,* 2013].

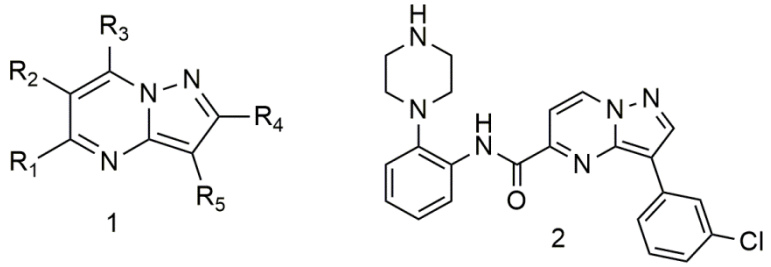

Figure 2.9 Pyrazolopyrimidine derivatives. Shionogi & Co. Ltd. [Seno.K., *et al.,* 2010].

2.2.3.1.3 Triazolopyrimidine derivatives

Vasopharm Biotech GmbH has investigated triazolopyrimidine derivatives (general formula 1, **Figure 2.10**) as NOX inhibitors and as the potential drugs for the treatment of cardiovascular diseases and stroke. The compounds listed in **Figure 2.10** had NOX2 inhibitory activity in HL60 cells, with IC_{50} values < 2 μM except compound 4 (**Figure 2.10**), which showed IC_{50} value of 12 μM. 3-Benzyl-7-(2-benzoxazolyl) thio- 1,2,3-triazolo [4,5-di] pyrimidine (VAS2870, compound 2, **Figure 2.10**) induced relaxation of aortas in hypertensive rats by blocking NOX1 and NOX2-mediated ROS production. A study [Tegtmeier F., *et al.,* 2005] demonstrated that protective effect of VAS2870 on ROS production in transient ischemic stroke was similar to the effect of NOX4 knockout in mice. In addition, VAS2870 attenuated not only PDGF-mediated vascular smooth muscle cell chemotaxis but also oxLDL-induced endothelial formation of ROS through

inhibition of NOX activation. Interestingly, VAS2870 diminished both autocrine and mitogen-dependent growth of tumor cells, which implicates promising therapeutic potential especially in hepatocellular carcinoma. VAS3947 (compound 3, **Figure 2.10**), a solubility-optimized derivative of VAS2870, effectively suppressed NOX-catalyzed ROS production in cell homogenates as well as *in situ* aortas from spontaneously hypertensive rats.

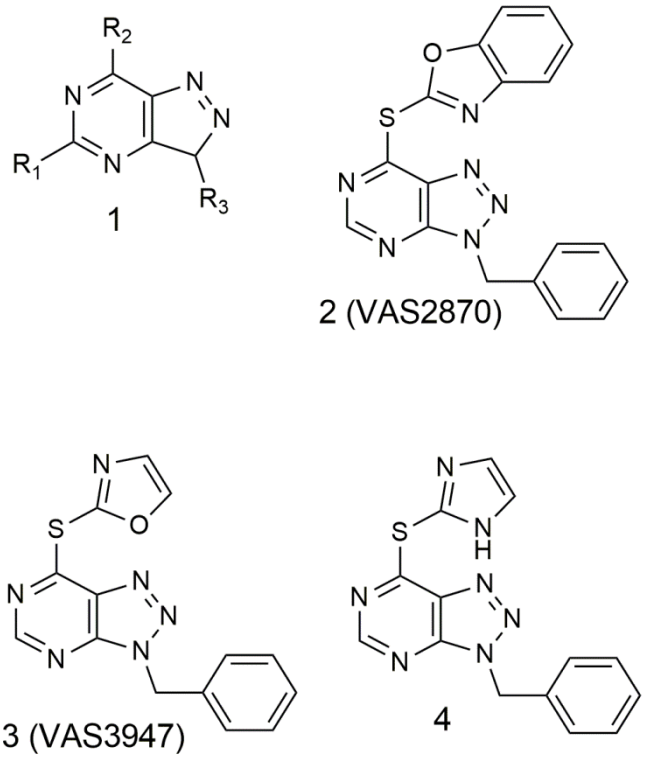

Figure 2.10 Triazolopyrimidine derivatives. Vasopharm Biotech GmbH, Germany. [Tegtmeier., *et al.,* 2005].

2.2.3.1.4 Tetrahydroindole derivatives

GenKyoTex also identified novel tetrahydroindole derivatives (general formula, **Figure 2.11**) as NOX inhibitors for the treatment and/or prophylaxis of diseases associated with NOX [Genkyo Tex SA., *et al.,* 2010]. The compounds have benzamide functionality or nitrogen molecule in tetrahydroindole moiety as a common skeleton. The inhibitory activity of these compounds was measured by Amplex Red using DMSO-differentiated HL-60 cells. The compound shown in **Figure 2.11** exhibited strong inhibition with IC_{50} values of 1.6 μM in the assay. (N-{3-[Cyclohexyl(methyl)amino]propyl}-4-(2-phenyl-4,5,6,7-tetrahydro-1H-indol-1-yl)benzamide) was the most potent with an IC_{50} of 1.6 μM.

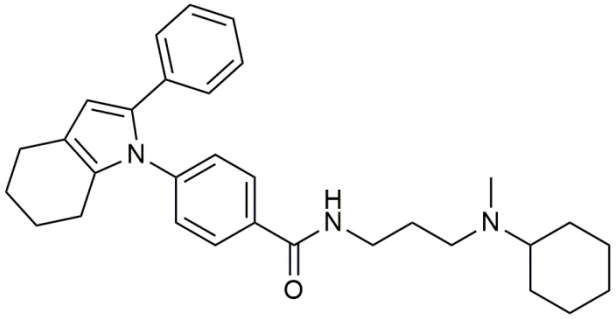

Figure 2.11 Tetrahydroindole derivatives. GenKyoTex. [Genkyo Tex S.A., *et al.,* 2010].

2.2.3.1.5 Fulvene and fulvalene analogues

A patent application from Emory University claimed fulvene and fulvalene analogues as NOX inhibitors that have the potential to be used for the treatment of cancers, and of inflammatory, degenerative and vascular ocular diseases [Arbiser JL., *et al.,* 2014]. Among the analogues, compound presented in **Figure 2.12** showed inhibitory activity against NOX2 in p47PHOX-transfected Cos cells. Especially, this compound (Fulvene-5) suppressed the loss of light-induced retinal function in in vivo ocular disease mice model. However, since the compounds were quite unstable and symmetric, they were not optimal for hit-to-lead optimization.

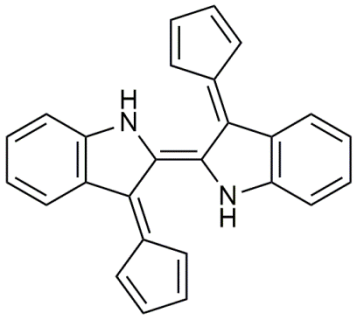

Figure 2.12 Fulvene and fulvalene derivatives. Emory University. [Arbiser.J.L., *et al.,* 2014].

2.2.3.1.6 Synthetic polyphenol

A synthetic polyphenol S17834 (compound in **Figure 2.13**) (6,8-diallyl-2-(2-allyl-3-hydroxy-4-methoxyphenyl)-5,7-dihydroxy-4H-chromen-4-one), which was originally discovered as an adhesion modulator for the treatment of venous insufficiency [Tony V., *et al.,* 2006], has been reported to inhibit endothelial NOX and thus suggested to have therapeutic potential in hypertension and other cardiovascular diseases [Tony V., *et al.*, 2006]. Since the mechanism of

action by which S17834 inhibits NOX was not known, additional studies were required to assess its use as a specific NOX inhibitor.

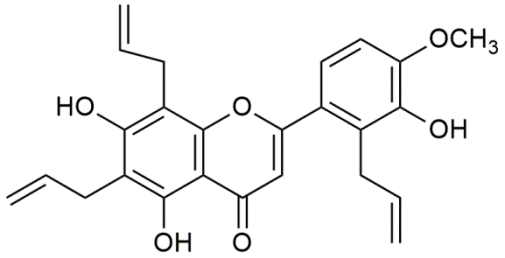

S17834

Figure 2.13 Synthetic polyphenol S17834,. Les Laboratoires Servier. [Tony.V *et al.*, 2006].

2.2.3.1.7 Apocynin and its derivatives

Apocynin (compound 1 in **Figure 2.14**) is a methoxycatechol extracted from the Picroria kurroa plant. The Research Foundation of the State University of New York discovered and claimed that apocynin derivatives, including apocynin dimers (compound 2, **Figure 2.14**) were NOX inhibitors that have the potential for prevention and treatment of diseases resulting from endothelial hyper permeability [Tony V *et al.*, 2006]. The anti-inflammatory effect of apocynin has been demonstrated in various disease models such as rheumatoid arthritis, inflammatory bowel disease, ischemic reperfusion lung injury and diaphragm dysfunction in endotoxin-induced sepsis. It also has preventive effects on diabetic nephropathy and dexamethasoneand adrenocorticotrophic hormone-induced hypertension. The mechanism of action by which apocynin inhibits NOX was thought to be blockage of enzyme assembly in the binding of $p47^{PHOX}$ to NOX2. The enzyme activity was more efficiently inhibited by apocynin dimmer, which is produced by myeloperoxidase-catalyzed oxidation of apocynin. Furthermore, a recent report showed that diapocynin inhibited NOX2 mRNA expression; its effect was much stronger than that of apocynin itself. However, there are reports showing that apocynin is not active in NADPH over-expressing cells, and that apocynin is not a NOX inhibitor but an antioxidant. Apocynin also showed other nonspecific effects.

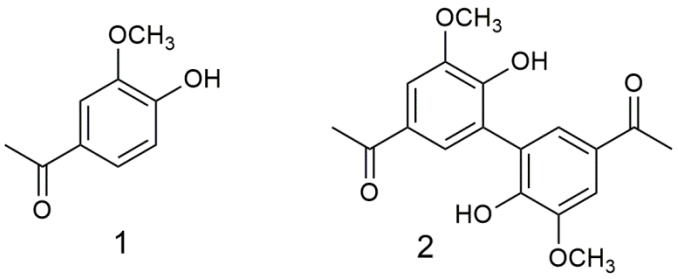

Figure 2.14 Apocynin and apocynin dimer. [Tony.V *et al.,* 2006].

2.2.3.1.8 Bicylic pyridazine derivatives

Mitsubishi Pharma Corp. disclosed bicylic pyridazine compounds (**Figure 2.15**) as specific NOX inhibitors that are effective on the over-expressed or activated enzymes in tissues such as aorta other than leukocytes. The major areas for the potential therapeutic applications of the compounds claimed were ischemic heart disease, atherosclerosis, stroke and diabetic complications. In cell lysates using HUVEC, the compounds 1 and 2 (**Figure 2.15**) showed inhibitory activity in in vitro IL-8 production, which had been produced by NOX in the presence of 44 mM glucose, with IC_{50} values of two-digit nanomolar concentrations, without significant inhibitory activity against leukocyte NOX [Yamamoto T., et al., 2004].

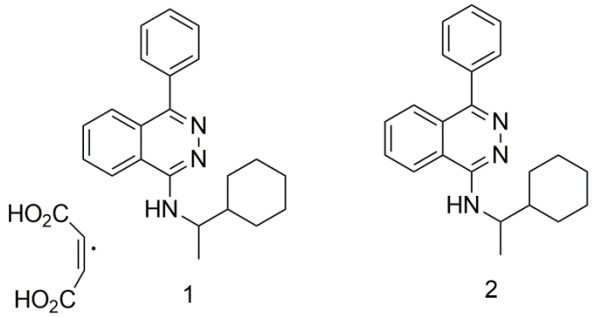

Figure 2.15 Bicylic pyridazine derivatives. Mitsubishi Pharma Corp. [Yamamoto.T., *et al.,* 2004].

2.2.3.1.9 AEBSF

AEBSF (Aminoethyl benzenesulfono fluoride, **Figure 2.16**), also known as Pefabloc, inhibits NOX by interfering with the binding of membrane fraction of NOX to $p47^{PHOX}$ [Supinski G., *et al.,* 1999]. It is a sulfonyl fluoride and a sulfonylating agent. It reacts with the hydroxyl group of the active site serine residue to form a sulfonyl enzyme derivative. This was extensively studied for the cholesterol regulatory genes in golgi apparatus.

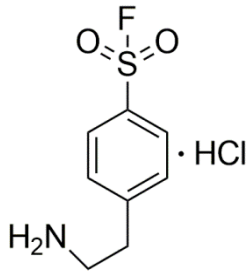

Figure 2.16 Aminoethyl benzenesulfono fluoride.

2.2.3.1.10 NOX siRNAs

Small interfering ribonucleic acids (siRNAs) are short doublestranded RNAs that inhibit, either partially or fully, the expression of mRNA of its endogenous counterpart or of an exogenous gene such as a viral nucleic acid. City of Hope (Duarte, California) claimed siRNA effector molecules, which post-transcriptionally down-regulate NOX1 gene [Quark Pharmaceuticals, *et al.,* 2008]. The siRNAs are designed to be used for the treatment of colon cancer. The siRNA contains 14-30 nucleotides of sense and complementary antisense strands, wherein the antisense strand has a complementary sequence to NOX1 mRNA. In the patent molecules, the sense and antisense strands are interconnected via a linker molecule such as a polynucleotide or non-polynucleotide linker.

Quark Pharmaceuticals, Inc. also claimed siRNAs that selectively down-regulate NOX genes from NOX4, NOX1, NOX2, NOX5, DUOX2, NOXO1, NOXO2, NOXa1 and NOXa2 for the potential treatment of various diseases related to NOX. Those siRNAs are composed of a sense strand which is 18-40 consecutive nucleotides derived from the mRNA sequence of the NOX genes, and an antisense strand that is complementary to the sense strand. The siRNAs also have stabilizing modifications such as a 2'-modification on the sugar moiety of at least one ribonucleotide (2'O-alkyl, 2'-fluoro, or 2'O-allyl) or others including additions (of lipids, peptides, sugars or others) to the 5' or 3' terminus of the oligonucleotides.

Chapter 3

Objectives and Plan of work

3.1. Objectives

As extensively reviewed, neuroinflammation seem to be a complex clinical syndrome indicated in several distinct common neurological disorders affecting the global population both in developed and in developing countries. Conventionally, major research on developing drug candidates to treat neuroinflammation was mainly focused on symptomatic and superficial management. The crucial role of ROCK-I and NOX2 in the regulation of pathophysiology of a number of neurological disorders, by their role in cell proliferation, motility and free radical generation in neurons, glial cells and astrocytes have been surveyed in literatures and patent databases. ROCK-I and NOX2 existed with unique contribution as enzyme targets involved in initiation and propagation of neurodegenerative and neurodevelopmental disorders.

After thorough review of the literature, design of small molecule inhibitors of human ROCK-I and NOX2 was considered important and hence the thesis work was focused with the following objectives.

I. Primary objective was to design new ROCK-I and NOX2 inhibitors utilizing rational structure based drug design.

II. High throughput virtual screening and *in vitro* screening commercial (Asinex database) and *in house* (~3000 molecules) libraries.

III. *In vitro* cell based and *ex vivo* tissue based evaluation for inflammatory gene expression analyses.

IV. *In vivo* pharmacological studies on neuroinflammatory models depicting diseases models for proof of concept.

3.2. Plan of work

The plan of work was classified into following stages

3.2.1. Design and development of new ROCK-I and NOX2 inhibitors using computational methods

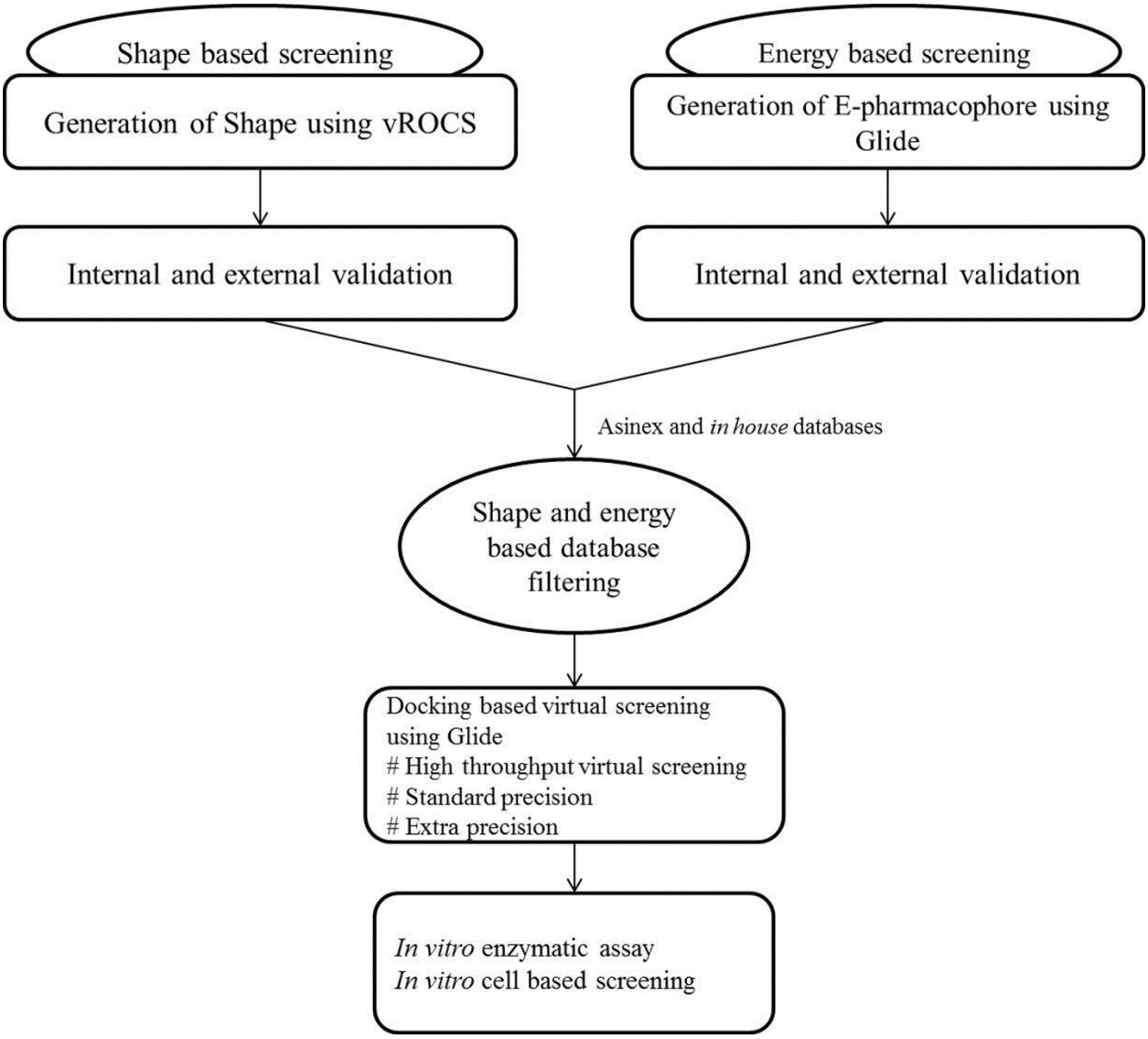

Table 3.1 Similarities and differences between ROCK-I and ROCK-II with NOX2

	ROCK-I	**ROCK-II**	**NOX2**
Family	AGC kinase	AGC kinase	Oxidase
Isoforms	1		4
Subunits	NA		5
Sequence similarity	92% (kinase domain)		2%
expression	Neurons, muscle, macrophages	Neurons, Heart, lungs	Endothelial cells, cancer tissues, macrophages, neurons
Upstream mediator	RhoA		Rho/Rac
Function	Motility, adhesion, replication	Also in migration	Oxidative stress maintanance, kill pathogens

3.2.2. *In vitro* ROCK-I enzymatic assay using conventional method and NOX2 enzymatic screening using X-ROS estimation in LPS induced HUVE cell lines using fluorescent dye.

3.2.3. *In vitro* cell based studies on cell lines like MeHg induced IMR-32, LPS induced HUVEC and cytotoxicity studies in HEK293 cells.

3.2.5. *In vitro,* and *ex vivo* gene expression analyses of inflammatory mediators using RT-PCR.

3.2.6. *In vivo* pharmacological studies.

3.2.6.1. Behavioral rodent model using LPS and MeHg.

3.2.6.2. Neurotoxicity assessment

3.2.7. Measurement of *in vivo* gene expression levels of various key regulators NFκB, IL-1β, IL-6 and TNF-α using RT-qPCR.

Chapter 4

Materials and Methods

4.1. Computational details

An Intel Core i7 2600, 3.40GHz capacity processor with memory of 12GB RAM running with the CentOS 6.1 X86_64 bit operating system was used to carry out all the computations. The e-pharmacophore models were generated using Glide (Glide, version 5.7, Schrodinger, LLC, New York, NY, 81 2011) and PHASE [Phase, version 3.0, Schrodinger, LLC, New York, NY] applications implemented in the Maestro 9.3 software package (Schrodinger, LLC, New York, 2012). In this study, we utilised crystal structure of ROCK1 (PDB code: 2ESM) bound to Fasudil. For NOX2, (PDB code: 1OV3) which was $p47^{PHOX}$ subunit bound to proline rich region of $p22^{PHOX}$ (peptide). The 3D coordinates of these enzymes were obtained from PDB and processed further by removing all the water molecules as well as other heteroatoms except the bound inhibitor or peptide in both structures. Hydrogens were added to the target protein by OPLS-2005 [Jorgensen, W. L *et al.,* 1996], and further minimized using Impref. The resultant target protein was used for molecular docking studies.

Using protein preparation wizard and impact energy minimization, the protein file was prepared. About 500 cycles of steepest descent (SD) and 5000 cycles of conjugate gradient (CG) methods with optimized potential for liquid simulations (OPLS) 2005 [Shivakumar D., *et.al*., 2010] force field using Schrodinger suite version 9.3 were employed. The active site of the protein was located and grid files were generated using receptor grid generation panel. The "Write XP descriptor information" option was selected and "Compute RMSD" option was enabled and rest of the parameters were kept as default. The XP Glide scoring function was used to order the best

ranked compounds and the important interactions like π-cation and π-π stacking were analysed using XP visualizer in Glide module. The input RMSD of the crystal ligand was also ascertained.

4.2 Structure based hypotheses generation

4.2.1 Shape based pharmacophore generation

ROCS (Rapid Overlay of Chemical Structures) [Grant JA., et *al.,* 1996] is a shape based method for rapid similarity analysis of molecules. In the first step, ROCS assesses the centers of mass of the query and candidate compound and subsequently starts aligning their principal components of intertia. In the second step, the initial orientations of the two molecules are optimized applying a solid-body optimization algorithm in order to maximize volume overlap. ROCS consider both shape and a colour force field for optimization of the overlap.

The basic scoring function implemented in ROCS was the shape Tanimoto Score, which is a quantitative measure for the shape overlap of two molecules. ROCS provides two color force field, the Implicit Milis Dean and Explicit Milis Dean force field. As the ImplicitMilisDean force field includes also a basic pKa model assuming pH 7, charges are assigned accordingly in an automated way, and users do not need to protonate molecules accordingly before virtual screening.

4.2.2 Energy based pharmacophore generation

4.2.2.1 Protein preparation

Coordinates for each structure were taken from the RCSB Protein Data Bank (PDB) 2ESM [Jacobs M., *et al.,* 2006] and 1OV3 [Groemping Y., *et al.,* 2003] for ROCK-I and NOX2 respectively and prepared using the Protein Preparation Wizard, which is part of the Maestro software package (Maestro, v8.5, Schrödinger, LLC, New York, NY). Bond orders and formal charges were added for heterogroups, and hydrogens were added to all atoms in the system. To optimize the hydrogen bond network, His tautomers and ionization states were predicted, 180° rotations of the terminal angle of Asn, Gln, and His residues were assigned, and hydroxyl and thiol hydrogens were sampled. Water molecules in all structures were removed. For structures with missing side-chain atoms, the refinement module in Prime [Jacobson MP., *et al.,* 2004] (Prime, v2.0, Schrödinger, LLC, New York, NY) was used to predict their conformations. For

each structure, a brief relaxation was performed using an all-atom constrained minimization carried out with the Impact Refinement module (Impref) (Impact v5.0, Schrödinger, LLC, New York, NY) using the OPLS-2005 force field to alleviate steric clashes that might exist in the original PDB structures. The minimization was terminated when the energy converged or the rmsd reached a maximum cutoff of 0.30 Å.

4.2.2.2 Ligand Docking/Refinement

Glide energy grids were generated for each of the prepared complexes. The binding site was defined by a rectangular box surrounding the x-ray ligand. Ligands were refined using the "Refine" option in Glide, and the option to output Glide XP descriptor information was chosen [Friesner RA., *et al.,* 2006] (Glide v5.0, Schrödinger, LLC, New York, NY). Default settings were used for the refinement and scoring.

4.2.2.2.1 Splicing of peptide for NOX2

For NOX2 as the PDB structure, 1OV3 was a crystal structure of SH3 domain of $p47^{PHOX}$ bound to proline rich region of $p22^{PHOX}$ (a 10 amino acid peptide). As a 10 amino acid peptide (Peptide-1) was long enough to screen peptide molecules to meet our interest to screen for small organic molecules. The 10 amino acid peptide was spliced into small fragments. These fragments were prepared using Ligprep [Greenwood J R., *et al.*, 2010] and were docked into the grid for 10 amino acid peptide to check the RMSD of the docked pose. Reproducing crystallographically observed conformation of the ligand was a minimum requirement to determine whether a docking setup is applicable to a given system.

4.2.2.3 Generation of energy based pharmacophores (e-Pharmacophores)

Starting with the refined x-ray ligand, pharmacophore sites were automatically generated with Phase [Dixon S L., *et al.,* 2006] (Phase, v3.0, Schrodinger, LLC, New York, NY) using the default set of six chemical features: hydrogen bond acceptor (A), hydrogen bond donor (D), hydrophobe (H), negative ionizable (N), positive ionizable (P), and aromatic ring (R). While Phase treat most cationic groups exclusively as positive ionizable, we chose to represent primary and secondary amines from guanidinium and amidine groups with a complementary set of hydrogen bond donors. Hydrogen bond acceptor sites were represented as vectors along the hydrogen bond axis in accordance with the hybridization of the acceptor atom. Hydrogen bond

donors were represented as projected points, located at the corresponding hydrogen bond acceptor positions in the binding site. Projected-points allow the possibility for structurally dissimilar active compounds to form hydrogen bonds to the same location, regardless of their point of origin and directionality.

Each pharmacophore feature site was first assigned an energetic value equal to the sum of the Glide XP contributions of the atoms comprising the site. This allows sites to be quantified and ranked on the basis of the energetic terms. Glide XP descriptors include terms for hydrophobic enclosure, hydrophobically packed hydrogen bonds, hydrophobically packed correlated hydrogen bonds, electrostatic rewards, π-π stacking, π-cation, and other interactions. ChemScore hydrogen bonding and lipophilic atom pair interaction terms were also included when the Glide XP terms for hydrogen binding and hydrophobic enclosure were zero. Sites with less than half of the heavy atoms contributing to the pharmacophore feature were excluded from the final hypotheses. Thus, if only two heavy atoms in a six-member ring exhibit energetic interactions, the ring is not considered as a pharmacophore feature. Variations in this rule, such as including features with fewer than half of the heavy atoms exhibiting energetic interactions, were tried and tested during the course of the work and ultimately did not show any improvements in enrichments (results not shown). The final procedure reported here led to a final energy optimized hypothesis (e-Pharmacophore).

Pharmacophore features were chosen for the final hypothesis based on a systematic analysis of receptor-ligand contacts. The contacts considered included hydrophobic or aromatic groups contacting the receptor, hydrogen bonds as measured in Maestro v8.5 (Maestro, v8.5, Schrödinger, LLC, New York, NY) or ionic interactions.

4.2.2.4 Pharmacophore validation

Enrichment factor (EF) [Halgren TA., *et al.,* 2010] was employed for the fraction of known actives recovered when a fraction of database was screened. EF could be defined as the ratio of number of actives retrieved relative to the number of database molecules tested. EF was often described with respect to a given percentage of the database screened. Decoy set consisted of 1000 molecules with an average molecular weight of 400 kDa was used. Ligand decoy sets were available for download (http://www.schrodinger.com/glidedecoyset). In decoy set 48 known

active molecules of both ROCK-I reported inhibitors were included for validation. For this, we focused primarily on EF (1%), the enrichment in the top 1% of the decoys, second enrichment metrics, the Boltzmann-enhanced discrimination of receiver operating characteristic (BEDROC) [Halgren TA., *et al.*, 2010] was also used as a way to ensure that the results and conclusions were significant. RIE (robust intial enhancement) [Halgren TA., *et al.,* 2010] was used as a metric using a continuously decreasing exponential weight as a function of rank of actives. The RIE metric was similar to EF since it also showed how many times better than random was the exponential average of the distribution generated by the ranking method. AUC (area under accumulation curve) [Halgren TA., *et al.,* 2010] was widely used to display ranking performances. However, the corresponding area under the curve, the AUC, was not as often used partly because it was believed to be largely dependent on the ratio of actives in the set. EF and goodness of fit (GH) were calculated using the following equations.

$$\mathrm{EF} = \frac{(\mathrm{H_a} \times \mathrm{D})}{(\mathrm{H_t} \times \mathrm{A})}$$

$$\mathrm{GH} = \left(\left(\frac{\mathrm{H_a}}{4\mathrm{H_t A}}\right) \times (3\mathrm{A} + \mathrm{H_t})\right) \times \left(1 - \left(\frac{\mathrm{H_t} - \mathrm{H_a}}{\mathrm{D} - \mathrm{A}}\right)\right)$$

Where ‘Ht’ was total number of compounds in the hit list

‘Ha’ was the total number of active molecules in the hit list

‘A’ was the total number of actives in the decoy set

‘D’ was the total number of molecules in the decoy set

4.3 Database screening for lead identification

4.3.1 Preparation of commercial database

Asinex database containing 500000 unique structures and BITS *in house* database of 2500 compounds were used in this study. Database molecules were prepared using LigPrep and Epik [Greenwood JR.., *et al.,* 2010] to expand protonation and tautomeric states at pH 7.0. Conformational sampling was performed for all molecules using the ConfGen search algorithm. We employed ConfGen with the OPLS-2005 force field and a duplicate pose elimination criterion of 1.0 Å RMSD to remove redundant conformers. A distance-dependent dielectric

solvation treatment was used to screen electrostatic interactions. A maximum relative energy difference of 10.0 kcal/mol was chosen to exclude high energy structures. Using Phase, the database was indexed with automatic creation of pharmacophore sites for each conformer to allow rapid database alignments and screening.

4.3.2 High-throughput virtual screening, docking studies and ADME predictions

For the e-pharmacophore approach, explicit matching was required for the most energetically favourable site (scoring better than 1.0 kcal/mol) that finds matching pharmacophores in the ligands. For filtering the database molecules, a minimum of 4-5 sites were required to match for hypotheses with 5-7 sites. The above criterion was followed in the present work to screen the databases. In order of their fitness score, database hits were ranked to measure how well the aligned ligand conformer matched the hypothesis based on RMSD, site matching, vector alignments and volume terms. Database ligands after e-pharmacophore filter were docked into the binding sites of the protein utilizing high-throughput virtual screening (HTVS) scoring function to estimate protein-ligand binding affinities. Ligands filtered from HTVS were subjected to Glide SP (standard precision) docking. The centre of the Glide grid was defined by the position of the co-crystallized ligand. Default settings were used for both the grid generation and docking. Post docking minimization was implemented to optimize the ligand geometries. Compounds with best docking and Glide scores were then subjected to Glide XP (extra precision) docking. Final short listing of possible hit compounds was based on visual inspection of the important amino acid residues in the active site cleft involved in binding and the hydrophobic interactions. Finally, top list compounds were subjected to ADME property predictions, where further checked predicted druggability and pharmacokinetic properties using QikProp module [Duffy EM., *et al.,* 2000] provided by Schrodinger, LLC.

4.4 Biological Assessments

4.4.1 ROCK-I inhibitory assay

4.4.1.1 Expression and purification of human ROCK-I

pET21(+)-ROCK recombinant obtained from NII, New Delhi was transformed into *E.coli* BL21 (DE3) for ROCK1 production based on IPTG induction. Transformed cells with recombinant

BL21 (DE3) were grown in LB medium supplemented with 50µg/ml of kanamycin and incubated at 37°C on shaking incubator with 150 RPM to an A_{600} ≈0.6. Protein synthesis was induced with 0.1 mM IPTG at 18°C overnight. Induced cells from culture of BL21 (DE3)/pET21(+)-ROCK recombinant (300mg of cells) were suspended in lysis buffer (137 mM NaCl, 2.7 mM KCl, 10 mM Na2HPO4, 1.8 mM KH_2PO_4, 1 mM DTT, protease inhibitors cocktail and 5% Glycerol). The cell suspension were sonicate for 12-15 cycles (20s pulse and 45s halt) and centrifuged at 8000 rpm at 4°C for 10minutes. Repeat the centrifugation of supernatant with 10000 rpm at 4°C for 35 mins consecutively to get clear lysate. Pre-equilibrate clarified lysate with Ni-NTA resin for 3.30 hrs at 4°C. Centrifuge whole content at 500 rpm for 5 min at 4°C, remove the sup as much as possible and load pre-equilibrated beads on to column. The column was equilibrated with lysis buffer and wash buffer(500 mM NaCl, 2.7 mM KCl, 10 mM Na_2HPO_4, 1.8 mM KH_2PO_4, 1 mM DTT, 1 mM PMSF and 5% Glycerol), each for 10min and centrifuged for 5 min at 4°C. Wash protein bound beads with elution buffer (140 mM NaCl, 25 mM Tris-Cl (pH 8.0), 1 mM DTT, 1 mM PMSF, 5% Glycerol and 200 mM Imidazole). The eluted protein was concentrated upto 3 mg/ml.

4.4.1.2 *In vitro* ROCK-I enzyme assay

The human ROCK-I enzymatic studies were performed as per the earlier reported literature [Doran JD., *et al.*, 2008]. A reaction mix was prepared with all components of the coupled assay except for ATP, which is added to initiate the assay. The final volume of each reaction will be 100 µL, of which 10 µL will be the ATP stock solution. The reagents should be mixed such that they are at the final concentrations listed below after the addition of ATP- 0.1 M HEPES, pH 7.6, 10 mM $MgCl_2$, 2.5 mM PEP, 0.2 mM NADH, 0.03 mg/mL PK, 0.01 mg/mL LDH, 2 mM DTT, 100-150 nM ROCK protein and 100 µM ROCK substrate (MBP).

90 µl of the reaction mix is added to each well in a 96-well plate. The reaction is then initiated by the addition of 10 µL ATP, giving a final volume of 100 µL. Mix the reagents well using a plate shaker for 1 min. The ROCK Km for ATP is 30 µM when using the ROCK peptide, so a final ATP concentration of 300 µM yields a high signal-to-noise ratio.

4.4.2 Thermofluor studies

The temperature at which protein melts was recorded as Tm, which was a measure of protein stability. Sypro orange fluorescent dye (Sigma-Aldrich Co. LLC) supplied as a 5000X solution in 100% DMSO was employed. First, the dye was diluted in 100 mM HEPES buffer to a concentration of 10X before adding to the protein, to prevent damage of protein with high concentrations of DMSO. 100 µg/ml of ROCK protein solution with 1 µM of inhibitor (total DMSO concentration is <0.1%) and diluted sypro orange to a total volume of 30 µl. Reference control wells (no ligand wells) containing the appropriate amount of DMSO were distributed on 96-well plate. Plate was stepwise heated from 25°C to 95°C to obtain Tm values. During heat process the fluorescence of Sypro orange increases as it starts interacting with enclosed hydrophobic residues with in the protein (unfolding state) [Niesen FH., *et al.,* 2007]. Fluorescence was measured 0.1°C rise for every 20sec using a BIO-RAD CFX CONNECT real time system. The recorded fluorescence reads were fitted to Boltzmann sigmoid function using CFX Manager Software 3.0.

4.4.3 NOX2 inhibitory assay

4.4.3.1 Intracellular X-ROS estimation

X-ROS is the novel signalling pathway seen in most of the cells [Prosser BL., *et al.,* 2011]. which arises when extra cellular matter triggers local ROS production by membrane located NOX2 . Human umbilical vein endothelial cells (HUVEC) are type of endothelial cells, in which NOX2 was over expressed upon stimulation with lipopolysaccharide (LPS) [Barth BM., *et al.,* 2010]. These were the generous gift from Incozen Therapeutics PVT Ltd. These cells were further sub cultured in T25 flasks in F12k medium supplemented with 10 µg/ml of ECGF (endothelial cell growth factor). Exponentially growing cells were seeded at the density (5.0×103 cells/well) in 96-well black flat bottom with p-lysine coated plates (HiMedia Laboratories). Cells were treated with different concentrations (100 µM to 0.01 µM) of compound for 2h and followed by stimulated with 5 µg/µl LPS (Sigma-Aldrich Co. LLC) for 3h before treating with 5 µM Dichloro-dihydro-fluorescein diacetate (DCFH-DA) (Sigma-Aldrich Co. LLC) for 1 h. After various treatments, LPS containing medium was removed and fresh medium was added. The fluorescence was read at excitation at 488nm and emission at 525nm by using fluorescence

microplate reader [Kim SY., *et al.,* 2010] (SpectraMax M4, Molecular Devices, Sunnyvale, USA).

4.5 *In vitro* studies using cell line models

4.5.1 Cytotoxicity studies on HEK 293 cell lines

Human embryonic kidney epithelial cells (HEK 293) were procured from NCCS, Pune. These were further grown in RPMI-1640 supplemented with 10% FBS, 100 IU/ml penicillin and 100 µg/ml streptomycin being maintained at 37^0C in 5% CO_2 by standard cell culture techniques. After culture of HEK 293, (5.0×103 cells/well) in 96-well p-lysine coated flat bottom (NEST Biotechnology Co.Ltd) in supplemented RPMI-1640 (200 µl) for 48h in presence of different concentrations of compounds (100 µM-0.01 µM). After incubation, MTT was added same as above for all wells [Buttke TM., *et al.,* 1993].

4.5.2 Determination of EC_{50} on MeHg induced IMR-32 cell lines

Human neuroblastoma cell lines (IMR-32) cells were procured from NCCS, Pune. These were grown on T25 flasks (NEST Biotechnology Co.Ltd) in supplemented MEM (with 10%FBS, 100 IU/ml penicillin and 100 µg/ml streptomycin) for 24h. After attaining 100% confluency, (5.0×103 cells/well) in 96-well p-lysine coated flat bottom (NEST Biotechnology Co.Ltd) in supplemented MEM (200 µl) for 2h in presence of different concentrations of compounds (100 µM-0.01 µM) and followed by 10 µM MeHg (Sigma-Aldrich Co. LLC) treatment for 3h and the cells were further allowed to grow for 48h. After incubation, 20 µl/well of (3-(4,5-dimethythiazol-2-yl)-2,5-diphenyl tetrazolium bromide (MTT) solution (5 mg/ml in phosphate buffered saline pH7.4) were added to cells and then incubated for additional 3h at 37^0C under 5% CO_2. Remove the medium from wells and dissolve MTT crystals with 200 µl/well and the absorbance determined at 570nm using spectrophotometer [Das S., *et al.,* 2011] (SpectraMax M4, Molecular Devices, Sunnyvale, USA).

4.5.3 Determination of EC_{50} on LPS induced HUVE cell lines

Human umbilical vein endothelial cell lines (HUVEC) cells were procured from NCCS, Pune. These were grown on T25 flasks (NEST Biotechnology Co.Ltd) in supplemented F12k (with 10% FBS, 100 IU/ml penicillin, 10 µg/ml of ECGF and 100 µg/ml streptomycin) for 24h. After

attaining 100% confluency, (5.0×103 cells/well) in 96-well p-lysine coated flat bottom (NEST Biotechnology Co.Ltd) in supplemented MEM (200 µl) for 2h in presence of different concentrations of compounds (100 µM-0.01 µM) and followed by 5 µg/ml LPS (Sigma-Aldrich Co. LLC) treatment for 3h and the cells were further allowed to grow for 48h. After incubation, 20 µl/well of (3-(4,5-dimethythiazol-2-yl)-2,5-diphenyl tetrazolium bromide (MTT) solution (5 mg/ml in phosphate buffered saline pH7.4) were added to cells and then incubated for additional 3h at 37^0C under 5% CO_2. Remove the medium from wells and dissolve MTT crystals with 200 µl/well and the absorbance determined at 570 nm using spectrophotometer [Kim SY., *et al.*, 2010] (SpectraMax M4, Molecular Devices, Sunnyvale, USA).

4.5.4 Clonogenic Assay

Clonogenic assay was performed according to Puck and Marcus [Puck TT., *et al.*, 1955]. The experiment was carried out by seeding approximately 1000 cells per well in 6 well plate. The optimum concentration of 10 µM of MeHg was selected from previous experiment; cultures were treated in as MeHg alone for 3h. For compounds, cultures were treated with 1 µM of compound for 2h before treating with MeHg for 3h. After various treatments, MeHg and compounds containing media were discarded and fresh MEM media was added and the cultures were left undisturbed for 14 days at 37^0C in 5% CO_2 incubator for colony formation and the colonies were washed with 1XPBS followed by staining with 0.5% gentian violet in methanol. Allow the colonies to absorb stain for 30minutes then slowly rinse off the stain without disturbing colonies and wash with tap water later allow it to air dry.

Plating efficiency $PE = \frac{No.Of\ Colonies\ formed}{No.Of\ cells\ seeded} X100$

Survival fraction $SF = \frac{No.Of\ colonies\ formed\ after\ treatment}{No.Of\ cells\ seeded\ X\ PE}$

4.5.5 Cell motility studies

For measuring cellular motility, 10^5 cells were plated on 6-well p-lysine coated plates (NEST Biotechnology Co.Ltd) with supplemented MEM for 2h in presence of compound and Fasudil at 1 µM and followed by 10 µM MeHg (Sigma-Aldrich Co. LLC) treatment for 3h. Using a sterile pipette tip (10 µl), scratch vertically on cell monolayer to make a wound. Rinse the cells with

1XPBS and replace with 1.5 ml of supplemented MEM [Liang CC., *et al.,* 2007]. Pictures were taken for 0h and 24h using 10X magnification in inverted microscope (OLYMPUS IX53).

4.5.6 Total RNA isolation and cDNA conversion

10^5 cells in 35 mm petridish were treated with 1 μM compound and Fasudil for 2h followed by 10 μM MeHg or 5 μg/ml LPS for 3h. Total RNA was extracted from the cells of MeHg induced, LPS induced, naïve, Fasudil treated and compound treated cells in triplicate. Cells were treated with TRI reagent [Chomczynski, P *et al.,* 1993] according to the protocol of the manufacturer (Sigma-Aldrich Co. LLC. USA). Concentrations and purity of RNA were quantified with Perkin Elmer VICTOR X3 (Perkin Elmer, Shelton, CT, USA) according to optical density. Purity of RNA was determined with $A_{260/280}$ ratio (1.8–2.0 was considered pure).

cDNA synthesis of respective samples were acquired according to the Verso cDNA synthesis kit (Thermo Fisher Scientific Inc. USA) protocol. Equal amount of RNA (about 1 μg) from the samples was suspended in 5 μl of RNAse-free water. RNA sample was further added to reaction mixture containing final volumes of 1X cDNA synthesis buffer, 500 μM of dNTP Mix, 500 ng of Anchored Oligo-dT primers, 1 μL of RT enhancer (to remove contaminating DNA), Verso enzyme mix (includes Reverse transcriptase) and the final volume was adjusted with water (PCR grade). Reverse transcription cycling program was set at the temperature 42 ºC in 1 cycle of 30 min and at 95 °C for 2 min for reaction termination using MJ Mini Thermal Cycler (Bio-Rad Laboratories, Inc. USA.).

4.5.7 Gene expression analyses of inflammatory mediators using Real Time PCR studies

Induced IMR-32 and HUVEC were trypsinised and centrifuge at 5000 rpm for 3 min. The cell pellet was taken and total RNA was isolated using TRIzol reagent (Sigma-Aldrich Co. LLC) according to manufacturer's instructions. Transcript levels of inflammatory mediators like IL-6, IL-1β and TNF-α were assessed using BIO-RAD CFX Connect Real Time System (BIO-RAD Laboratories, Inc). 1 μg of total RNA was used as a template to make the first strand cDNA by Anchored oligo dT priming using a commercial cDNA synthesis kit (Verso cDNA synthesis kit, Thermo Fischer scientific, Inc). Real time PCR was performed according to the manufacturer's instructions using a BIO-RAD CFX Connect with SYBR green (Kapa Biosystems) as the

fluorescent dye enabling real-time detection of PCR products. The synthetic gene specific primer sets used in PCR were shown in **Table 4.1**.

Table 4.1 Oligonucleotide sequences used for the RT-PCR in cells

Primer	Oligonucleotide sequence	Tm (°C)
Human-IL-6-FP	TTCGGTCCAGTTGCCTTCTC	61.7
Human-IL-6-RP	GAGGTGAGTGGCTGTCTGTG	
Human-TNF-α-FP	CTCCAGGCGGTGCCTTGTTC	60
Human-TNF-α-RP	CAGGCAGAAGAGCGTGGTG	
Human-IL-1β-FP	GCAAGGGCTTCAGGCAGGCCGCG	63.2
Human-IL-1β-RP	GGTCATTCTCCTGGAAGGTCTGTGGGC	
Human-NF-κB-FP	GCGCTTCTCTGCCTTCCTTA	60.8
Human-NF-κB-RP	TCTTCAGGTTTGATGCCCCC	
Human-GAPDH-FP	ACCACAGTCCATGCCATCAC	61.4
Human-GAPDH-RP	TCCACCACCCTGTTGCTGT	
Human-ROCK-I-FP	GAAGAAAGAGAAGCTCGAGAGAAGG	72
Human-ROCK-I-RP	ATCTTGTAGCTCCCGCATCTGT	
Human-p47PHOX-FP	ATCATATGGGGGACACCTTCATCCG	63
Human-p47PHOX-RP	GGATCCTCAGACGGCAGACGCCAG	

4.6 *Ex vivo* studies using rat brain

4.6.1 Isolation of brain cells

All animal experiments were approved by the institutional animal ethical committee (IAEC). Wistar rats weighing about 200 g were anaesthetized with diethyl ether and 0.9% ice-cold saline perfused through heart. Whole brains were removed from rats weighing 4 gms or more and placed in ice-cold MEM. Meninges and all visible blood vessels were removed. Tissue was minced with scissors into pieces small enough to pass through the tip of Pasteur pipette in disaggregation solution (0.5% (w/v) collagenase solution, MEM and 40 µg/ml of DNAse). Incubate for 1 hr at 37°C with 5% CO_2. Centrifuged the cells at 500g X 10min at room temperature. Supernatant was removed and add dissociated cells to the poly lysine coated flasks and allowed them to attach for 1hr. Remove cells with 0.1% trypsin and plated them on to (5.0×10^3 cells/well) 96-well p-lysine coated flat bottom (NEST Biotechnology Co.Ltd) supplemented with complete MEM (MEM with FBS and antiboitics) (200 µl) for 48 hrs in

presence of different concentrations of test compounds (100 µM-0.01 µM). After incubation, MTT was added similar to the above for all wells to determine the neurotoxicity in brain cells [Ahmed Z., *et al.,* 1983].

4.6.2 Brain slice preparation for *ex vivo* studies

Female wistar rats (200-250 g) were decapitated and brains were removed and submerged in ice-cold minimal essential medium (MEM). Each hemisphere of cerebral cortex was cut into coronal slices to attain approximate weight of 100 mg and placed in 12-well p-lysine coated plate [Nimmerjahn A., *et al*., 2005]. Culture media consisted of MEM with 10% fetal bovine serum, 100 µg/ml streptomycin and 100 U/ml penicillin. Slices were treated with 10 µM MeHg or 5 µg/ml lipopolysaccharide (LPS) reference (0111:B4, Santa Cruz Biotechnology, Inc) and both in combination with Fasudil and compound in combinations (LPS, LPS+Fasudil, LPS+test compound, MeHg, MeHg+Fasudil, MeHg+test compound) and all are at 1 µM individual concentration. All the combination of treatments was incubated simultaneously for 3 h in a humidified environment with 5% CO_2. Total number of three animals was utilized for the study and slices after test compound incubation were harvested to isolate total RNA using TRIzol reagent method explained in section 4.5.6. For cDNA synthesis and real-time quantitative polymerase chain reaction were performed with CFX CONNECT Real-Time System as explained in sections 4.5.6 and 4.5.7. The synthetic gene specific primer sets used in PCR were shown in **Table 4.2**.

Table 4.2 Oligonucleotide sequences used for the RT-PCR in Rat brain samples

Primer	Oligonucleotide sequence	Tm (°C)	Ref
Rat-IL-6-FP	GACTGATGTTGTTGACAGCCACTGC	65	[Haung Y., *et al.,* 2014]
Rat-IL-6-RP	TAGCCACTCCTTCTGTGACTCTAACT		
Rat-TNF-α-FP	CCACGTCGTAGCAAACCACCAAG	61	[Hagiwara N., *et al.,* 2005] [Visnagri A., *et al.,* 2014]
Rat-TNF-α-RP	CAGGTACATGGGTCATACC		
Rat-IL-1β-FP	ATAGCAGCTTTCGACAGTGAG	61.8	[Rantamaki T., *et al.,* 2013]
Rat-IL-1β-RP	GTCAACTATGTCCCGACCATT		
Rat-NF-κB-FP	CCTCTACACATAGCGGCTGG	66.7	[Hagiwara N., *et al.,* 2005]
Rat-NF-κB-RP	GCACCTTGGGATGCGTTTTT		
Rat-GAPDH-FP	GGTGAAGGTCGGTGTGAACGG	68.9	[Nagiwara N., *et al.,* 2005]
Rat-GAPDH-RP	CATGTAGTTGAGGTCAATGAAGGG		

4.7 *In vivo* pharmacology

Male wistar rats (200–250 g) for MeHg neurodegenerative model and swiss albino male mice (17-20 g) for LPS induced neurotoxicity were utilized and were kept under a 12h/12h light-dark cycle regimen, with free access to food and water. The Institutional Animal Ethics Committee approved all experiments. All the animals were acclimatized to the housing conditions for a period of one week before the start of experiments. For all experiments, animal groups were divided into vehicle control, naïve, standard drug control and test drug groups for optimal comparisons, where each group comprised of five animals.

4.7.1 Neurotoxicity assessment

Neurotoxicity was measured in mice by the rotarod test. Before drug administration, mice were trained in rotarod with 25 RPM. Neurotoxicity was the inability of the animal to maintain balance on rotating rod for at least one minute. All the animals were received a dose of 300 mg/kg and subjected for Rotarod assessment at 0 h, 1 h and 2 h after dosing [Asakura W., *et al.,* 1991].

4.7.2 MeHg induced neurodegeneration

4.7.2.1 Administration and dosage

Methyl mercury (MeHg) was procured from Sigma Chemical Co. Male wistar rats were given free access to water and food, and were maintained on a 12 hr light-dark cycle. Rats were randomly divided into four experimental groups: MeHg induced control (n=5), **RB12+**MeHg induced (30 mg/kg, n=5), Fasudil+MeHg induced (30 mg/kg, n=5) and Naïve (n=5). MeHg was dissolved in water and all animals were given a daily dose of 20 ppm (approximately 1.0 mg/kg) orally except naïve [Jin X., *et al.,* 2007]. Exposure was for 3 weeks in duration. **RB12** was dissolved in citrate buffer at pH 4.5 with 10% PEG400 where as Fasudil was dissolved in double distilled water with 10% PEG400

4.7.2.2 Observation of clasping and body weight

Rats were examined for mortality as a general protocol and also were tested for the degree of hind limb clasping phenomenon. Hind limb clasping was a marker of disease progression in a number of rodent models of neurodegeneration. To achieve dyskinetic posture, rats were suspended by holding them at the tail position, whereby rats clasped their hind limbs tightly into

their abdomen. The hind limb position was observed for 10 seconds. If the hind limb was consistently splayed outward, away from the abdomen, it is assigned a score of 0. If the hind limb was retracted toward the abdomen for more than 50% of the time suspended, it received a score of 1. If both the hind limbs were partially retracted toward the abdomen for more than 50% of the time suspended, it received a score of 2. If its hind limbs were completely retracted and touching the abdomen for more than 50% of the time, it received a score of 3. Body weight was measured daily before the observation [Whishaw IQ., *et al.,* 1985].

4.7.2.3 Rotarod test

Each animal separately was placed on rotarod. The latency to fall down was recorded with five minutes cutoff time. Rats were given three consecutive trials with a maximum trial time of 5 min and 15 min rest interval [Gralewicz S., *et al.,* 2009].

4.7.2.4 Open field locomotor activity

Open field tests were conducted between 10.00 a.m and 2.00 p.m. The spontaneous locomotor activity of each rat was recorded individually for 5 min using digital photo acto meter (Dolphin, India Cat.NO:1126) before the daily dosage. Locomotion of all rats were recorded. This method allowed for the examination of horizontal locomotor activity while ignoring small movements, such as breathing, head, tail actions and tremors [Asakura W., *et al.,* 1993].

4.7.2.5 Footprint analyses

The footprint test was used to qualitatively compare the stride and stance lengths of all groups. Footprint tests were performed on the last day before sacrificing. To obtain footprints, the hind and fore limbs were coated with blue non-toxic ink. The animals were then allowed to walk along a 40 cm long, 8 cm wide runway (with 20 cm high walls) [Head RJ., *et al.,* 2000] and analyzed by comparing among all the groups with naïve animals.

4.7.2.6 Nerve conduction velocity assessment

Caudal nerve conduction velocity studies were performed on all the animals. The animal was positioned ventrally for their tail to be completely loose and the tail was cleaned with 70% alcohol to remove debris. Stimulating electrode was placed proximally and recording electrodes were placed distally at a distance of 10 cm. The electrophysiological parameters studied were onset latency of nerve conduction velocity (m/s). Measurement was taken 3 times and averaged

together [Kang SH., *et al.,* 2013]. NCV was measured using data acquisition system (AD Insturments).

4.7.2.7 Histopathological analyses

Animals were anaesthetized with ether and 0.9% ice-cold saline perfusion through the heart. The brains were excised, fixed with 10% formalin, neutral buffered, (Sigma-Aldrich Co.LLC) and embedded in paraffin-wax; Further, 5-µm coronal sections were sliced out using a microtome (Medimeas Instruments, India). Paraffin sections were stained with hematoxylin and eosin (H&E). Images were taken using inverted microscope OLYMPUS IX53 at 10X magnification and the scale was set to 100 µm [Kang SH., *et al.,* 2013].

4.7.2.8 Gene expression analyses of inflammatory mediators using RT-PCR studies

Total number of four animals' brain samples was utilized for the study and were harvested to isolate total RNA using TRIzol reagent method explained in section 4.5.5. For cDNA synthesis and real-time quantitative polymerase chain reaction were performed with CFX CONNECT Real-Time System as explained in sections 4.5.6 and 4.5.7. The synthetic gene specific primer sets used in PCR were shown in **Table 4.2**.

4.7.3 LPS induced neuro inflammation

4.7.3.1 Administration and dosage

Mice were kept on fast for overnight before the day of experiment. All experiments were performed according to the guidelines of IAEC. All groups of mice except naïve were given *Escherichia coli* LPS (0111:B4, Santa Cruz Biotechnology, Inc) prepared in non-pyrogenic 0.9% sterile saline administered *i.p* by single injection at a dose of 50 mg/kg. Compound and Fasudil were administered 30 min before LPS administration at 30 mg/kg. Animals were studied 3 h after the LPS injection for peripheral nerve damage [Qin L., *et al.,* 2007, Li G., *et al.,* 2005] using following tests.

4.7.3.2 Assessment of peripheral nerve damage

Animals were tested at 0 h for the baseline values, and were dosed using *i.p* injection (30 mg/kg for **RB12** and Fasudil), Activity of test compounds were again tested 3 h post injection as described below and was compared with the baseline values.

4.7.3.2.1 Hot plate test

Mice were placed on a 16 cm height X 16 cm diameter heated surface of the plate. The temperature of the hot plate (Eddy's hot plate, Techno Electronics, Lucknow) was set to 55±0.5°C. The time of latency was defined as the time period between zero point when the animal was placed on the hot plate surface and the time when the animal licked its fore paw or jumped off to avoid thermal pain. Baseline latency was determined before experimental treatment for each mouse. To minimize the tissue damage, cutoff time was limited to 60 s. The latencies of both fore paws licking or jumping were measured for each animal at 0 and 3 h in order to calculate the percentage maximum possible effect (%MPE) for these time points [Duman EN., *et al.,* 2006]

4.7.3.2.2 Tail flick test

The lower 5 cm portion of each tail was immersed in a beaker of cold water (0-1°C). The time, in seconds for tail withdrawal from water was recorded as the reaction time. Measurement of threshold was taken at 30 and 60 min before and after administration of LPS [Qnais E., *et al.,* 2011]

4.7.3.2.3 Clasping assay

The experiment was performed as briefly described in the section 4.7.2.2.

4.7.3.2.4 Gene expression analyses of inflammatory mediators using Real Time PCR studies

Total RNA was isolated from the animal brain tissue using TRI reagent (Sigma-Aldrich Co. LLC) TRIzol reagent method explained in section 4.5.5. Transcript levels of inflammatory mediators like IL-6, IL-1β, TNF-α and NFκB were assessed using BIORAD CFX connect real time system (BIORAD Laboratories, Inc). For cDNA synthesis and real-time quantitative polymerase chain reaction were performed with CFX CONNECT Real-Time System as explained in sections 4.5.6 and 4.5.7. The synthetic gene specific primer sets used in PCR were shown in **Table 4.3**.

Table 4.3 Oligonucleotide sequences used for the RT-PCR in Mice brain samples

Primer	Oligonucleotide sequence	Tm (°C)	Ref
Mouse-TNF-α-FP	GACCCTCACACTCAGATCATCTTC	60.6	[Riekenberg S., *et al.*, 2009]
Mouse-TNF-α-RP	CCTCCACTTGGTGGTTTGCT		
Mouse-IL-1β-FP	CTGGTGTGTGACGTTCCCATTA	64	[Liu J., *et al.*, 2006]
Mouse-IL-1β-RP	CCGACAGCACGAGGCTTT		
Mouse-NFκB-FP	GGCGGCACGTTTTACTCTTT	61.2	[Walmsley SR., *et al.*, 2005]
Mouse-NFκB-RP	CCGTCTCCAGGAGGTTAATGC		
Mouse-IL-6-FP	GCCCACCAAGAACGATAGTCA	62.2	[Liu J., *et al.*, 2004]
Mouse-IL-6-RP	GAAGGCAACTGGATGGAAGTCT		
Mouse-GAPDH-FP	GACATGCCGCCTGGAGAAAC	58	[Tsujita., *et al.*, 2006]
Mouse-GAPDH-RP	AGCCCAGGATGCCCTTTAGT		

4.8 Statistical Analyses

All the statistically compared data were expressed as mean ± standard error in mean (SEM). The data were analyzed by one-way ANOVA in case of animal studies, statistical significance was determined for drug effects by Dunnett's multiple comparison post hoc test for individual comparisons with vehicle group. For gene expression studies, analyzed by one-way ANOVA followed by Tukey‘s multiple range post hoc test. Significance was assigned to a P value of less than 0.05. The statistical software package PRISM 6 (Graphpad Software Inc., San Diego, CA) was used for the analyses.

Chapter 5

Results and discussion: Design of Dual inhibitors of ROCK-I and NOX2

Dual inhibition of ROCK-I and NOX2 was attempted for the first time to estimate greater biological effects in inhibiting signaling pathways in neuroinflammatory disorders. To identify the dual inhibitor we employed different approaches using *in silico* based drug design techniques. Knowledge based drug discovery methods have been enduring in current times to understand theoretical predictions and to develop specific drug design strategy. To acquire favorable results, knowledge based CADD methods were followed for the current work, which are in two general categories: shape-based and energy-based drug design methods. As the primary objective of current work was to design novel, non-peptidic, ROCK-I and NOX2 dual inhibitors, CADD methodologies were employed to grab promising novel drug analogues from ASINEX database and BITS library.

5.1 Protein preparation and active site validation

Since our drug design strategy was based on structure-based approach, it was important to employ the 3D crystal structure of protein bound to the inhibitor. In this work we selected one co-crystal structure which was retrieved with most promising ligand, Fasudil reported from our previous work. Crystal coordinates were retrieved from the protein databank (PDB; http://www.rcsb.org/pdb) of ROCK-bound with Fasudil (2ESM) with a resolution of 3.30 Å (**Figure 5.1**). The crystal structure was imported into the protein preparation wizard of Schrodinger Software (Ver 9.4). The enzyme existed in dimeric form in the crystal. The

monomeric chain/pocket which had the active site to which the Fasudil ligand was bound was retained. Fasudil is a potent Rho-kinase inhibitor and vasodilator. Since it was discovered, it has been used for the treatment of cerebral vasospasm, which is often due to subarachnoid hemorrhage, as well as to improve the cognitive decline seen in stroke victims. It has been found to be effective for the treatment of pulmonary hypertension. It was demonstrated in February 2009 that Fasudil could also be used to enhance memory and improve the prognosis of Alzheimers patients. It was approved for use in Japan and China, but has not been approved by the United States Food and Drug Administration or by the European Medicines Agency. The crystal ligand Fasudil was found to show hydrogen bonding interactions with Glu154, Met156 and Asp202 (**Figure 5.1**). In order to validate the docking program utilized for e-pharmacophore and shape generation, the crystal ligand was prepared and redocked on to the grid of the active site. The docking score was found to be -9.649 kcal mol^{-1} .

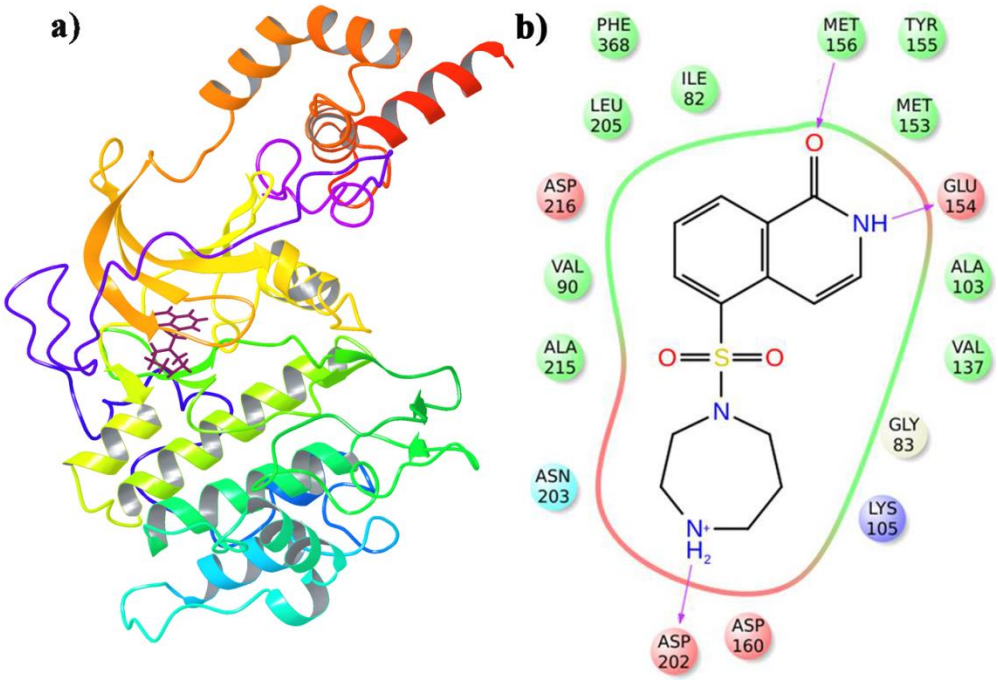

Figure 5.1 a) ROCK-I Crystal structure retrived from PDB (2ESM) with Fasudil (maroon color) in its active site pocket and b) ligand interaction picture generated in Maestro, pink solid arrow in the interaction picture is Hbond between backbone of the amino acid and the ligand.

In the same way crystal cooordinates from PDB were retrived for NOX2 (PDB id: 1OV3) which is a consisted of SH3 domain of $p47^{PHOX}$ bound to the proline rich region of $p22^{PHOX}$. As there were no inhibitor bound crystal structures available in PDB, we utilised 1OV3 as suitable crystal

structure to design NOX2 assembly inhibitors. Crystal coordinates of 1OV3 were retrieved from PDB with a resolution of 1.80 Å (**Figure 5.2**). The crystal structure was imported into the protein preparation wizard, and hydrogen atoms and water molecules were removed. As the crystal ligand was a 9 amino acid peptide due to the constraints in modeling we redocked into the active site virtually, to reproduce same binding pose and interactions using Glide methods. The spliced peptide which showed less RMSD was selected for the query generation for structure based methodologies. The 9 amino acid peptide (QSNPPPRPP) was subjected to splicing in intact crystal structure using the mutation residue option in Schrodinger, LLC. The aminoacid Q (Glu) was selected and deleted and subjected for the protein preparation wizard to minimize entire protein which is considered as peptide2. This peptide again subjected for split chain available in Schrodinger, the split peptide2 from crystal structure again subjected for the Ligprep to generate maximum possible conformations. The generated confiramations were redocked into the protein active site and checked for the RMSD to the crystal pose to docked pose.

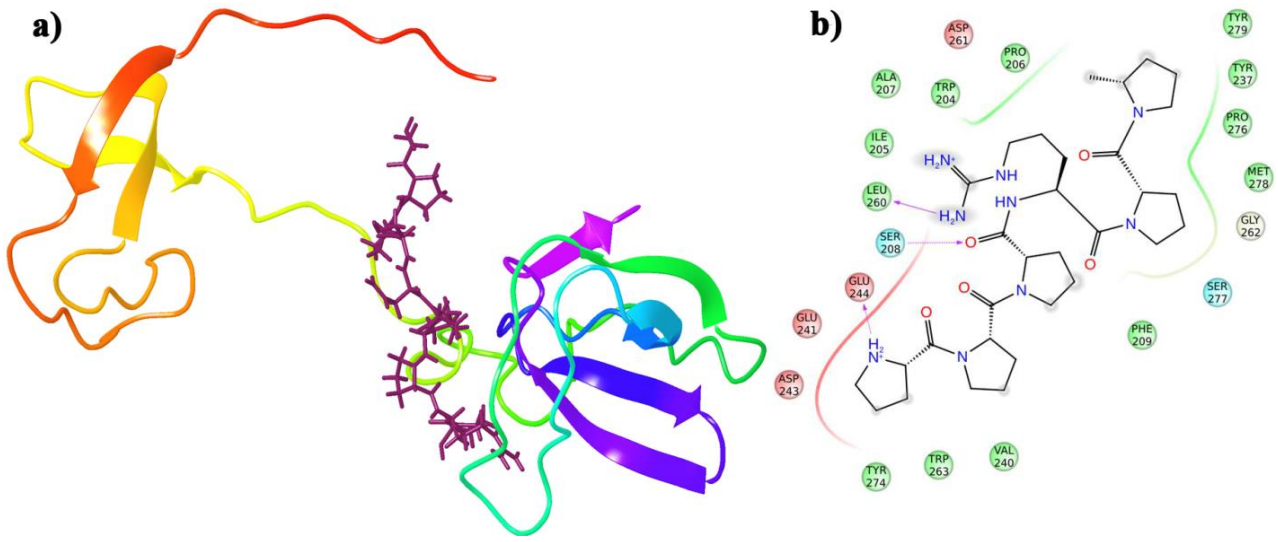

Figure 5.2 a) $p47^{PHOX}$ Crystal structure retrived from PDB (1OV3) with Peptide1 (maroon color) in its active site pocket and b) ligand interaction picture generated in Maestro for peptide5, pink solid arrow in the interaction picture is Hbond between backbone of the amino acid and the ligand.

Table 5.1 RMSD and docking scores of peptides of p47PHOX crystal structure.

Peptide		RMSD	Glide g Score
p22 PHOX	Peptide1	0.8915	-6.265
QSNPPPRPP	Peptide2	2.014	-5.231
SNPPPRPP	Peptide3	3.514	-6.14
NPPPRPP	Peptide4	2.621	-4.12
PPPRPP	Peptide5	0.6587	-7.593
PPPRP	Peptide6	0.826	-6.5

In the same way peptides 3, 4, 5 and 6 were generated and redocked into the protein active site and checked for RMSD and the docking scores were given in **Table 5.1**. As only PPPRPP were interacting with the loop present in SH3 domain it has produced good docking score and acceptable RMSD than other peptides. Peptide5 interacting with the Ser208, Glu244 and Leu260 which are also important aminoacids in SH3 domain of $p47^{PHOX}$ to bind to $p22^{PHOX}$. Thus peptide5 was taken forward to generate shape energy based queries to screen databases.

5.2 e-Pharmacophore generation for ROCK-I and NOX2

Energy-based drug design relies on the knowledge of the target protein structure to calculate interaction energies between the ligand molecule and the protein active site by utilizing high-resolution crystallized structural data. In current work, co-crystallized molecules in the active site were subjected to redocking with the protein active site virtually, to validate its original poses, with the help of docking based methods. Real time generation of energy descriptors while docking were utilized to recognize important interaction energies, which were important for binding interaction. Moreover, pharmacophore hypotheses generation based on important interaction energies was a fruitful strategy to attain novel chemical analogues with a property of protein active site favored interactions.

A co-crystal ligand (2ESM) with Fasudil, an isoquinoline moiety (**Figure 5.3**) was taken as reference ligand to generate e-pharmacophore, since it was known to be a potent inhibitor and is currently in phase III clinical trials of ROCK-I with a low IC_{50} value of 180-4300 nM [Jacobs M., *et al.*, 2006]. The hypothesis generated was with three pharmacophoric features consisting of one hydrogen bond acceptor (A-score-2.16), and two aromatic ring features (R5 and R6) (score -

2.98 and -0.99). Where the features A and R are most important interactions must needed for ROCK-I inhibition.

Template protein-ligand complex (1OV3) was energetically optimized and generated energetic terms computed by the Glide XP scoring function (Glide, version 5.8, Schr dinger, LLC, New York, NY, 2012) to rank the important pharmacophore features. For NOX2 design, co-crystal ligand (1OV3) with peptide 5 (**Figure 5.2**) was taken as reference ligand to generate e-Pharmacophore, since it showed better docking score and was found to exhibit six hydrogen bonding interactions. [Groemping Y., *et al.,* 2003]

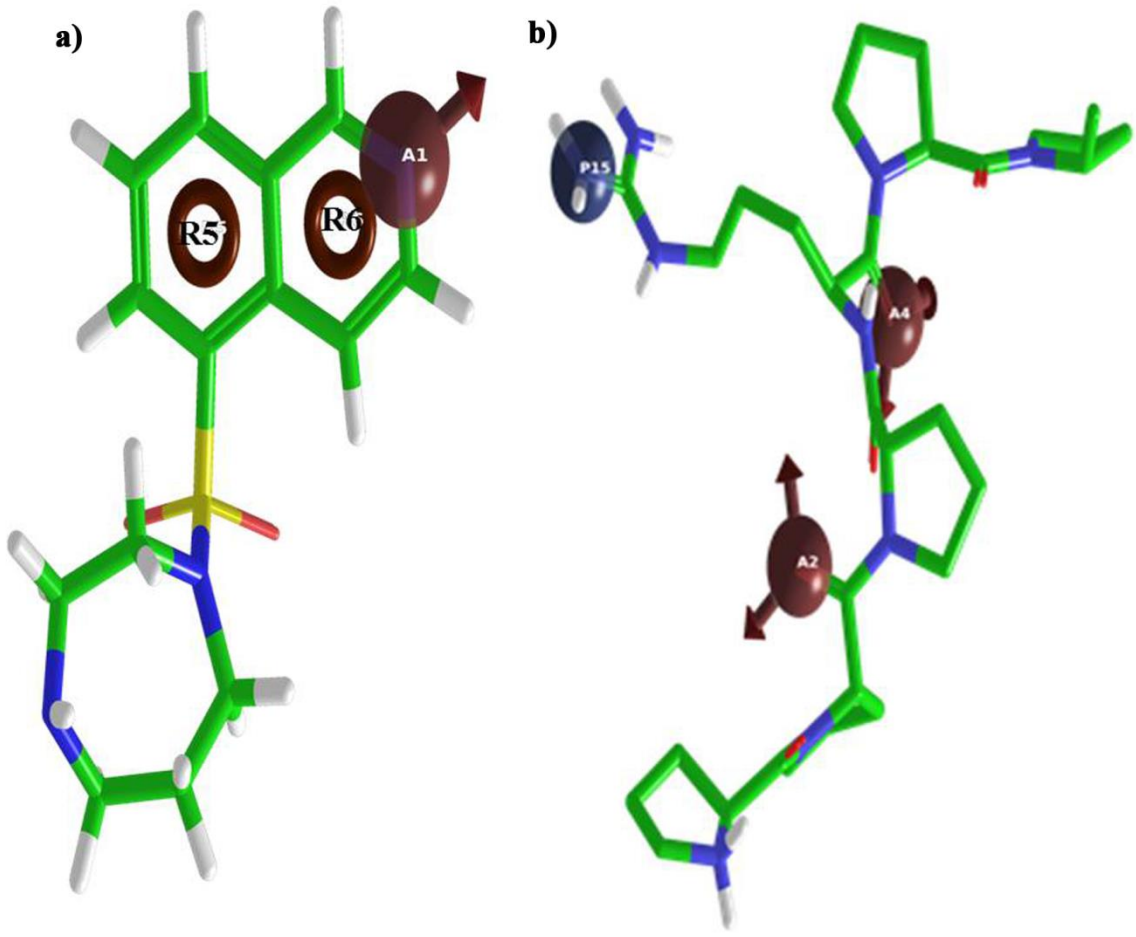

Figure 5.3 a) ROCK-I generated e-pharmacophore and b) Peptide5 generated e-pharmacophore, where R is Ring aromatic group, A is Acceptor feature and P is positive ionisable group.

Final hypothesis (**Figure 5.3**) generated with three pharmacophoric features consisted of two hydrogen bond acceptors (A-score-2.16 and -1.52), and one positive ionizable feature (P15) (score -0.99). The features A and P were required for NOX2 inhibition.

5.2.1 e-Pharmacophore validation

As there were no reported inhibitors for NOX2 assembly, the validation of the hypothesis was unfeasible. The ROCK-I hypotheses were taken and validation was performed using decoy set containing 1000 inactives along with 30 known active inhibitors of ROCK-I (http://www.brenda-enzymes.info). Ligand decoy sets were available for download as provided by Schrodinger (http://www.schrodinger.com/glide_decoy_set). Enrichment factor (EF) was employed for the fraction of known actives recovered when a fraction of database was screened. EF was defined as the ratio of number of actives retrieved relative to the number of database molecules tested. EF mainly gave the percentage of the database screened. The ROCK-I hypothesis thus generated was validated using decoy set containing 1000 inactive along with 30 reported known inhibitors [Uehata M., *et al.*, 1997; Uehata M., *et al.*, 1998; Iwakubo M., *et al.*, 2004; Gingras K., *et al.*, 2004; Lu M., *et al.*, 2004; Takanashi Y., *et al.*, 2001].

The enrichment results for the 3 feature pharmacophoric hypothesis for ROCK-I bound Fasudil were compared based on the enrichment factor, EF1%, EF and GH based on recovery rate of actives against the ranked decoy database and also capable of ranking actives better than the other two data fusion methods using the BEDROC, robust initial enhancement (RIE) and AUC metrics. By these methods, we obtained both good enrichment as well as diversity in our hits. The enrichment factor reflected the capability of a screening application to detect active ligands (true positives) compared to the random selection of molecules. Thus, its value was expected to be greater than 1 and higher the better enrichment performance of the virtual screening [Dror O., et al., 2009]. Hypothesis (**Figure 5.3**) displayed a good EF value of 10.256 and consistent GH value of 0.444. Enrichment in the top 1% of the decoys for hypothesis was 21. Further, the hypothesis also persisted in problem of "early recognition" by BEDROC (α=20) value of 0.778 and with good RIE value of 11.3 (**Table 5.2**). Although RIE and BEDROC produced different values, their distributions were identical in providing good "early recognition" of actives. With regard to NOX2 e-pharmaophore, validation was hindered due to non-availability of $p47^{PHOX}$ direct inhibitors.

Table 5.2 Pharmacophore enrichment validation of three combination hypothesis for ROCK-I.

Parameters	ROCK-I E-pharmacophore
EF	10.256
GH	0.444
EF 1%	21
BEDROC α=20	0.778
AUC	0.99
RIE	11.3

EF - Enrichment Factor (external validation using formula), GH - Goodness of fit score (external validation using formula), EF(1%) - The enrichment in the top 1% of the decoys, BEDROC (α=20) - Recovery rate of actives against the ranked decoy database, AUC – Area under curve, RIE Indicates good early recognition.

5.3 Shape hypotheses generation for ROCK-I and NOX2

Shape-based drug design exploits the knowledge of rapid similarity analysis of molecules. Thereby, the volume overlap of molecules could be assessed by gaussians, which were parameterized according to the hard sphere volume of heavy atoms. The use of gaussians allowed for fast calculation of overlaps between two atoms. In the first step, ROCS assessed the centers of mass of the query for the crystal ligand and the peptide-5 and subsequently started aligning their principal components of intertia. In the second step, the initial orientations of the above two molecules were optimized applying a solid-body optimization algorithm in order to maximize volume overlap. ROCS consider both shape and colour force fields for optimization of the overlap. Range of predictions to proceed further in generation of structure-activity relationships of novel molecules.

In order to obtain activity on a certain target, not only shape but also appropriate chemical functionality were crucial, which was why ROCS had implemented a color score to support the alignment process and evaluate chemical feature based similarity. The ROCS color force field was composed of SMARTS patterns [Grant JA *et al.,* 1996] for the characterization of chemical functions in combination with a rule set that describes how much functions interact.

Color score was the scoring function that quantified the matching of these chemical functionalities between the query compound and the molecule being screened. It was not independent from the query molecule; the query self-color represented the maximum color score value that could be obtained. Hence, the color score of the actual compound being screening

divided by color score of the query allowed for scaling score values between 0 and 1 which was referred to as "Scaling Color" score. In this way, ROCS is able to maximize both molecular shape overlay and chemical functionality overlap. The combo score function had exactly equal weights on its both components, the Shape Tanimoto and the Scaled color score. Both components obtain values between 1 and 0 and are summed up to combo score. Hence combo score, values ranged from 2 to 0, where 2 stand for the best possible overlap and 0 for no similarty. Overall, this screening and scoring approach was straightforward, based on a few basic assumptions, as also observed with related techniques like e.g.; pharmacophore modelling.

Once aligned in the same co-ordinate space, the co-crystalized ligand structures were clustered according to ROCK-I and $p47^{PHOX}$ crystal ligand fingerprints, and the obtained 3D alignment for each cluster was used to generate shape based query models using vROCS v3.1.2 (Open eye systemic software).

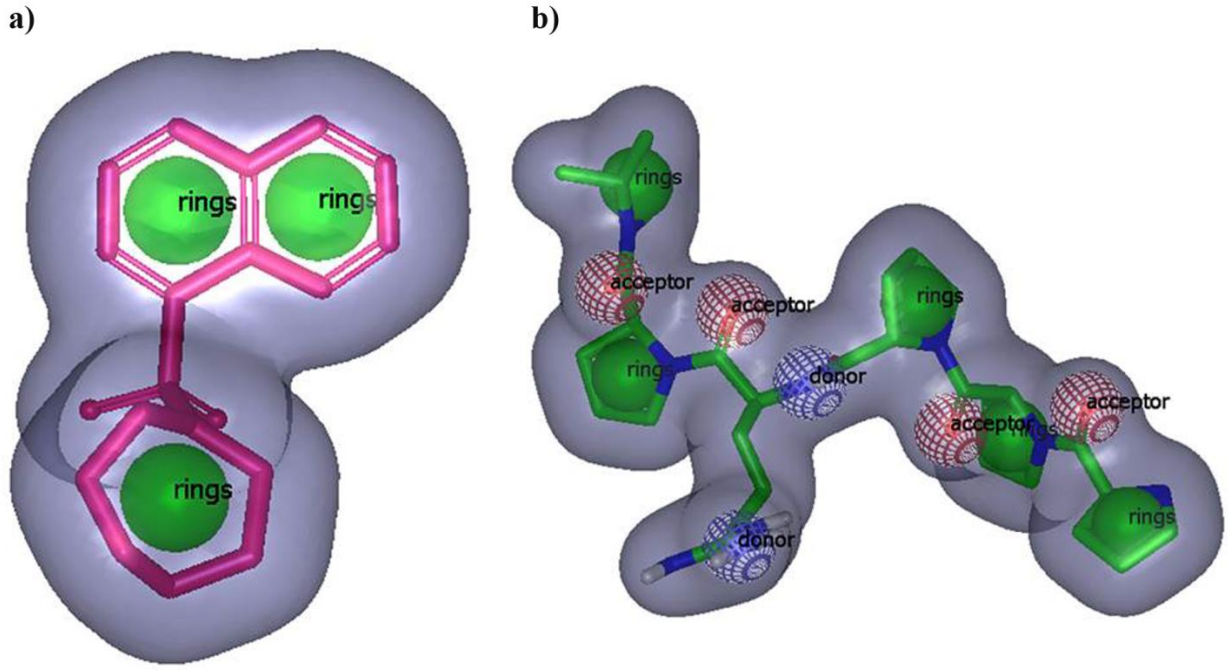

Figure 5.4 Shape generated for a)ROCK-I and b) $p47^{PHOX}$ crystal ligand. Blue mesh balls represents donor, red mesh balls represents acceptor and green balls represents ring features.

The shape query thus generated for ROCK-I bound with Fasudil and $p47^{PHOX}$ along with the designed peptide5 are presented in **Figure 5.4**. In comparison with e-pharmacophore and shape generated for Fasudil (2ESM), few similarities with regard to the features were observed. In e-pharmacophore model, R5 and R6 in the isoquinoline moiety was similar to the hydrophobic

groups in shape model. Whereas for the peptide5 (1OV3) e-pharmacophore representing side chain of Arg was identified as a positive ionisable group and in shape it was identified as donor group. In e-pharmacophore two acceptors on the proline aminoacids were similarly identified as acceptors as in shape hypothesis. Both hypotheses were similar but vROCS employed the guassian parameters whereas Schrodinger utilized the OPLS parameters to obtain diverse molecules.

5.3.1 Shape validation

ROCK-I hypothesis was validated according to the tanimoto combo score metric using a library of DUD (Directory of Useful Decoys) (http://dud.docking.org/) decoys and 30 known actives as utilized in the section 5.2.1. The validated model was retained and used as filter during docking procedure. The enrichment curve plotted the number of active compounds recovered *versus* the proportion of the database screened. The AUC (area under the curve of an ROC plot) was simply the probability that a randomly chosen active had a higher score than a randomly chosen inactive. As seen in **Table 5.3**, the area under the curve (AUC) of the probability obtained for the hypothesis was higher that 56% at ±95% confidence intervals, suggesting the hypothesis query could be considered moderately selective as most actives were ranked higher from the decoy molecules.

Table 5.3 Shape enrichment validation of hypothesis for ROCK-I.

Parameters	ROCK-I Shape
EF	5.231
GH	0.521
EF 1%	56.61
AUC	0.952

EF - Enrichment Factor (external validation using formula), GH - Goodness of fit score (external validation using formula), EF(1%) - The enrichment in the top 1% of the decoys, AUC – Area under curve.

With the knowledge of the drug design we selected these four hypotheses for both targets which were utilized to screen databases. These four hypotheses were used to screen Asinex database (Design I) and BITS library (Design II).

5.4 DESIGN I: IDENTIFICATION OF DUAL INHIBITORS FROM COMMERCIAL DATABASE (Asinex)

Asinex is a huge database contains natural product like pharmacophore rich compounds with experimentally controlled lipophilicity, solubility and chemical stability properties. This compound library has guaranteed 95% purity compounds which were confirmed by HPLC/MS and NMR data. Virtual screening of commercial database was performed as high-throughput screening of large database for lead identification. In this study, the hypotheses from e-pharmacophore and shape were used as queries to screen commercial database of 500,000 molecules (Asinex). Glide is unique in its reliance on the techniques of exhaustive systematic search, though approximations and truncations are required to achieve acceptable computational speed. Starting from the poses selected by the initial screening, the ligands were minimized in the field of the receptor using a standard molecular mechanics energy function with OPLS force field in conjunction with a distance-dependent dielectric model. Finally, three to six lowest-energy poses obtained in this fashion were subjected to a Monte Carlo procedure that examined nearby torsional minima. This procedure was needed in some cases to properly orient peripheral groups and occasionally to alter internal torsion angles. It was a modified and expanded version of the ChemScore scoring function, GlideScore, for use in predicting binding affinity and rank-ordering ligands in database screens. However, we utillised combination of GlideScore, the ligand receptor molecular mechanics interaction energy, and the ligand strain energy to select the correctly docked pose. The composite scoring function, Emodel, was much better at selecting the correct pose than was either the molecular mechanics energy or GlideScore alone.

5.4.1 Virtual screening for ROCK-I and NOX2

Virtual screening studies of the commercial database (Asinex) could retrieve novel active molecules for these two targets. Both energy-based and shape-based models of both targets operated for ligand find match database screening as depicted in **Figure 5.5**. The validated pharmacophore hypotheses from energy based (ARR) and shape based (RRR) for ROCK-I and energy based (ARP) and shape based (AAAADDRRRRR) for NOX2 were operated individually for ligand find match database screening of 5,00,000 compounds (Asinex database). Co-crystal ligand, isoquinoline compound from PDB id: 2ESM with IC_{50} value of 180-4300 nM and $p22^{PHOX}$ proline rich peptide from PDB id: 1OV3. [Jacobs M., *et al.,* 2006; Groemping, Y., *et al.,*

2003] was taken as reference ligand, since they were the source for e-pharmacophore and shape-based queries. Here we used multiple queries for both the targets so as to obtain diverse ligands. From both pharmacophore hypotheses, compounds with fitness more than 1.5 and tanimoto combo close to 1 were taken as initial cut-off to shortlist, hit compounds. The protocol was bit tedious as there were multiple queries employed for filtering the compounds. The protocol was bit tedious as there were multiple queries employed for filtering the compounds as depicted in **Figure 5.5**.

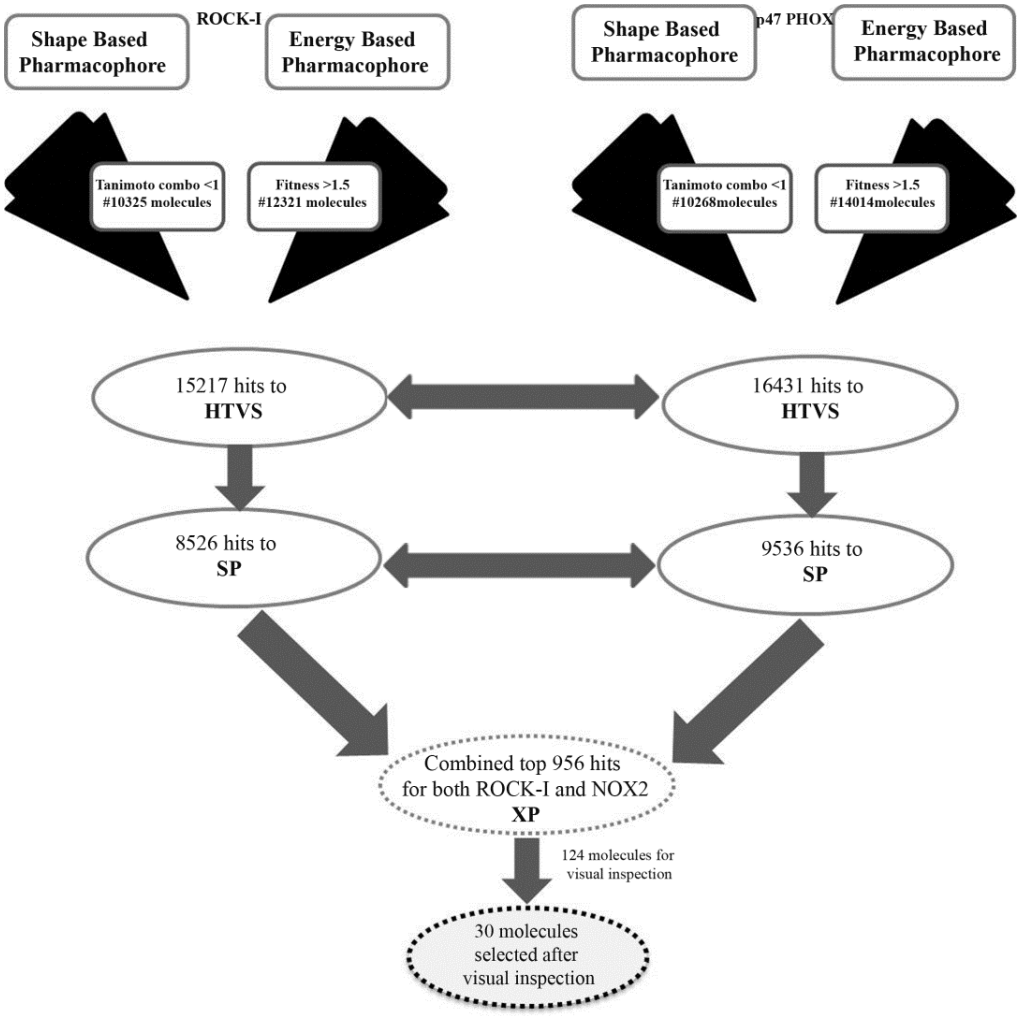

Figure 5.5 Virtual screening workflow followed for ROCK-I and NOX2.

From energy and shape-based pharmacophore, around 10325 hit molecules with good tanimoto combo (<1) and from e-pharmacophore, around 12321 hit molecules with good fitness (>1.5) were selected for further virtual screening (**Figure 5.6**) for ROCK-I. And for NOX2, around

10268 molecules from shape and 14014 molecules from epharmacophore were selected further for docking procedure. Molecules (around 15217 hits from ROCK-I and 16431 hits from NOX2) from both the pharmacophores were combined and made as a single database and taken for HTVS (High throughput virtual screening) as primary docking. 8526 from ROCK-I grid and 9536 from NOX2 from HTVS with a Glide score less than -6.0 were further refined using SP (standard precision) docking module and then 1035 ligand molecules were identified with good Glide score (< -6.0). The cut off value was taken as -6.0 as the reference crystal ligand of 2ESM Glide score were found to be -6.28, -4.5 in 1OV3. Cross docking among SP hits and only those which had good docking score were subjected to XP docking again in ROCK-I and NOX2. Where we acquired 956 compounds with good Glide score compared to crystal ligand (< -7.528 for ROCK-I and <-4.651 for NOX2). Though the docking score did not indicate the compound's binding affinity but it was helpful in prioritizing/ranking the ligands. Further, duplications of molecules were corrected from the hit molecules after XP docking, and were visually inspected for crucial amino acid residue involved in interaction within the active surface consisted in both ROCK-I and NOX2 active site.

Finally we prioritized 30 ligands with the parameters estimated for both the targets. The 2D structures of all 30 top hits are presented in **Figure 5.6** where it was clar that multiple hypotheses employing e-pharmacophore and shape based queries yielded diverse set of ligands. The ligands were coded **RA1**-**RA30** which were found to include various nucleus like phenyl, imidazolopyrimidine, piperazine, thiophene, oxadiazole, tetrahydrothiazole, tetrahydroquinoline, pyrimidine etc. The virtual screening and docking parameters of all the lead compounds are presented in **Table 5.3** and **5.4** for ROCK-I and NOX2 respectively.

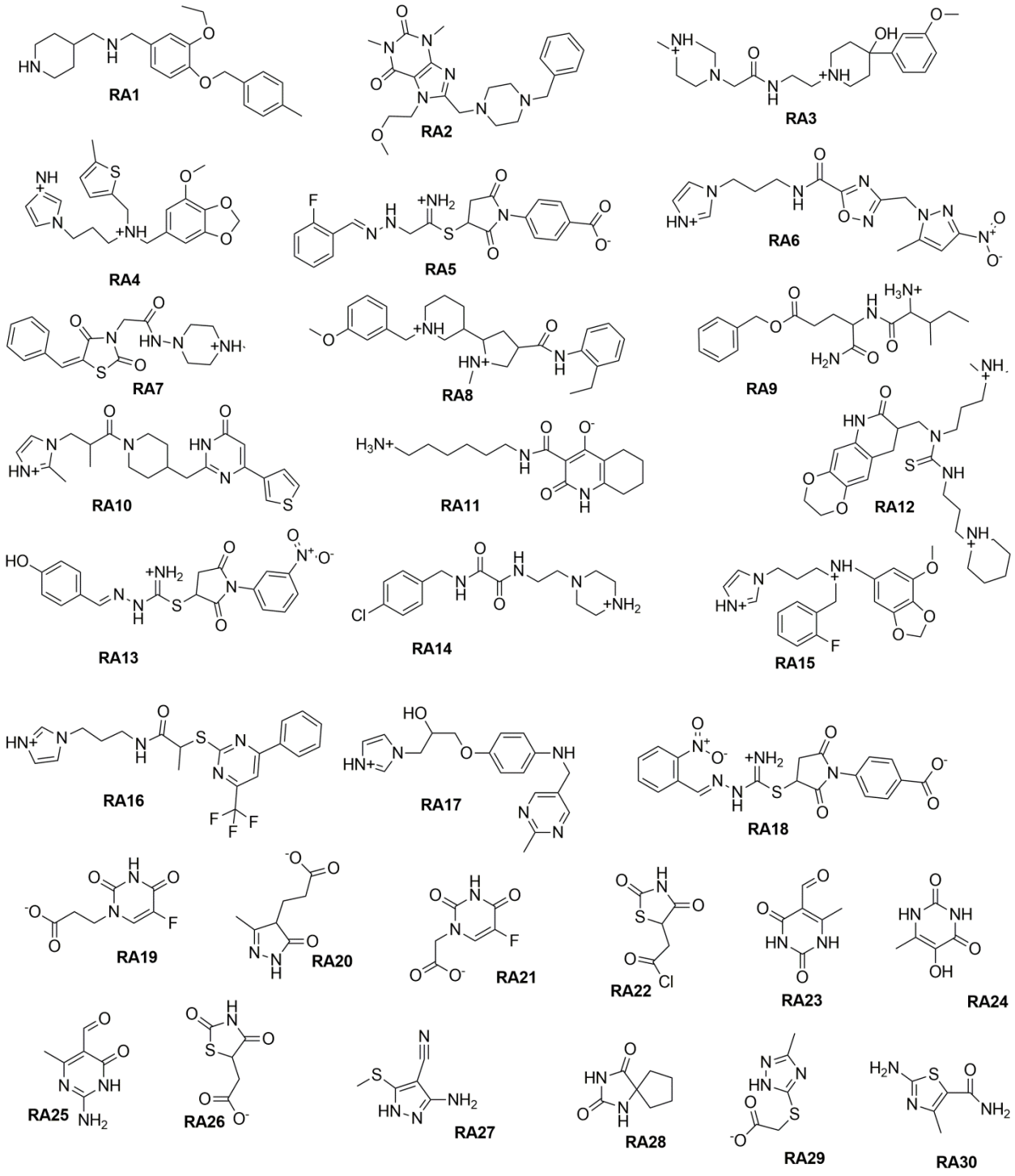

Figure 5.6 Structures of **RA1-RA30** shortlisted from ASINEX database.

Compounds **RA6**, **RA12**, **RA13**, **RA17** and **RA19-RA30** were found to show hydrogen bonding interaction with the Met156 and Glu154, which was crucial interaction necessary for compounds to fit into the hydrophobic cavity composed of Val137, Ala103 and Thr55. Remaining all

compounds showed hydrogen bonding with the another crucial aminoacid Asp160, Asp216, Asp198 and Asp202. All other compounds were found to interact with the hydrophobic pocket and were considered based on docking score and hydrogen bonding.

Table 5.4 Energy scores of 30 selected Asinex database compounds in ROCK-I

Sr.No	ROCK-I			
	H bond	Glide g score	Docking score	Interacting residues
RA1	3	-7.430	-7.430	Asn203, Asp216, Asp198
RA2	2	-6.456	-7.377	Phe87, Lys200
RA3	3	-5.654	-5.973	Asp202, Asp216, Lys200
RA4	1	-6.790	-7.047	Lys105, Asp369
RA5	9	-7.910	-9.421	Arg84, Phe87, Asp160
RA6	3	-9.026	-9.351	Met156, Asp160, Asp369
RA7	3	-6.111	-6.349	Lys105, Asp160, Asp202
RA8	0	-8.422	-8.490	Asp160
RA9	4	-7.396	-7.410	Asp160, Asp202
RA10	1	-8.014	-8.014	Lys105
RA11	1	-5.241	-5.241	Asp160
RA12	4	-8.013	-8.654	Met156, Phe87, Asp160, Asp202
RA13	6	-9.525	-9.590	Met156, Glu154, Lys105, Asp216
RA14	2	-6.280	-6.299	Lys105, Asp160
RA15	1	-7.057	-7.334	Lys105
RA16	0	-5.861	-6.171	Asp202
RA17	3	-7.824	-8.156	Met156, Asp216, Gly88
RA18	8	-10.164	-11.656	Arg84, Phe87, Asp160
RA19	3	-6.111	-6.111	Met156, Glu154, Lys105
RA20	3	-6.790	-6.456	Met156, Glu154
RA21	2	-7.430	-7.430	Met156, Glu154
RA22	1	-5.241	-6.111	Met156, Glu154
RA23	0	-6.111	-6.349	Met156, Glu154
RA24	3	-6.456	-6.790	Met156, Glu154
RA25	3	-6.111	-5.241	Met156, Glu154
RA26	5	-7.430	-7.430	Met156, Glu154
RA27	4	-5.241	-6.111	Met156, Glu154
RA28	3	-6.790	-6.456	Met156, Glu154
RA29	2	-6.111	-5.241	Met156, Glu154, Lys105
RA30	3	-6.111	-6.349	Met156, Glu154
Fasudil	3	-7.581	-7.581	Met156, Glu154, Asp202

Table 5.5 Energy scores of 30 selected Asinex database compounds in NOX2

Sr.No	NOX2			
	H bond	Glide g score	Docking score	Interacting aminoacids
RA1	4	-8.152	-8.152	Glu241, Asp243, Ser208
RA2	4	-5.147	-4.226	Ala207, Ser208, Trp263, Met278, Ser277
RA3	3	-6.639	-6.320	Asp221, Asp261
RA4	3	-9.319	-9.062	Glu241, Asp243, Trp263, Ser208
RA5	4	-11.614	-10.103	Glu244, Tyr279
RA6	5	-9.404	-9.079	Asp243, Ser208, Trp263
RA7	3	-7.828	-7.589	Trp263, Ser208
RA8	3	-7.687	-7.618	Asp221
RA9	6	-7.825	-7.812	Asp243, Glu244, Glu241, Trp263
RA10	1	-7.358	-7.358	Glu244, Ser208, Trp263
RA11	5	-8.180	-8.180	Asp261, Ser208, Glu241
RA12	2	-9.603	-8.962	Glu241, Asp261
RA13	5	-10.894	-10.829	Thr219, Asp261, Asp243
RA14	4	-7.431	-7.413	Asp261, Glu241, Asp243, Ser208
RA15	5	-9.029	-8.753	Ser208, Asp243, Trp263
RA16	2	-8.497	-8.187	Ser208, Trp263, Asp243
RA17	2	-8.923	-9.255	Ala207, Asp261, Glu241, Asp243
RA18	9	-8.738	-10.229	Asp261
RA19	3	-9.062	-9.319	Ser277, Met278, Trp263, Ser208
RA20	4	-6.639	-4.226	Ser277, Met278, Trp263
RA21	2	-9.319	-9.062	Ser277, Met278, Ala207
RA22	5	-9.062	-9.319	Met278
RA23	7	-5.147	-6.639	Ser277, Met278
RA24	3	-4.226	-7.413	Ser277, Met278
RA25	2	-5.147	-7.413	Glu220, Asp221
RA26	1	-6.639	-5.147	Ser277, Trp263
RA27	4	-6.639	-4.226	Ser277, Met278
RA28	6	-9.062	-9.319	Ser208, Asp261
RA29	2	-5.147	-6.639	Ser277, Met278, Asp261, Ala207
RA30	3	-4.226	-7.413	Asp261, Glu220
PPPRPP	3	-4.651	-4.214	Glu244, Ser208, Leu260

Similarly for NOX2, compounds **RA2**, **RA4**, **RA6**, **RA7**, **RA10**, **RA11**, **RA14**, **RA15**, **RA16** and **RA19** were found to show hydrogen bonding interaction with Ser208, which was important as observed with $p22^{PHOX}$ bound to $p47^{PHOX}$. Most of the compounds showed hydrogen bonding

with the two more crucial aminoacids Asp243 and Glu241. All the compounds were found interacting with peptide binding pocket as indicated by the aminoacids provided in **Table 5.5**.

5.4.2 ADME predictions for the selected 30 Asinex molecules

All the selected compounds were subjected to *in silico* ADME properties using QikProp module in Schrodinger. The compounds shortlisted were found to be in accordance with Lipinski's rule of five which was important for drug likeness. Various important properties like predicted octanol/water partition coefficient logP, predicted IC_{50} value for blockade of HERG K+ channels, predicted apparent Caco-2 cell permeability in nm/sec, predicted brain/blood partition coefficient, percent human oral absorption were predicted for the selected compounds and checked for any deviations (**Table 5.6**). The lead compounds **RA5**, **RA13** and **RA18** did not show good partition coefficient (QPlogP) values which were found violating. Factor QPlogCaco-2 were founnd in the unacceptable range for the lead compounds **RA3**, **RA5**, **RA9**, **RA12**, **RA13**, **RA14**, **RA18**, **RA19**, **RA21**, **RA26** and **RA27** indicating issues with intestinal permeability. This factor determines cell permeability in biological membranes and its metabolism. The critical factor governing drug access to cell membrane could be predicted through cell permeability. Some lead compounds (**RA1**, **RA5**, **RA7**, **RA8**, **RA13** and **RA30**) were predicted to be associated with HERG cardiotoxicity which could majorly restrict their further development as promising drug molecule. Also, many compounds (**RA5**, **RA9**, **RA13**, **RA19**, **RA23** and **RA26**) showed violation of Lipinski's rule of five mainly due to molecular weight (>500), hydrogen donor and acceptor. Predicted blood brain barrier and % human oral absorption were in the acceptable range for all the designed leads except **RA5**, **RA13** and **RA18**. This implied that oral bioavailability of the lead compounds was good.

Table 5.6 ADME prediction for the designed 30 compounds from Asinex database

Sr.No	QPlogPo/w[(a)]	QPlogHERG[(b)]	QPPCaco[(c)]	QPlogBB[(d)]	%HumanOral Absorption[(e)]	Rule of Five[(f)]
RA1	4.434	-4.512	304.617	0.463	68.5	0
RA2	1.268	-5.321	110.835	0.145	93.2	0
RA3	0.610	-5.698	12.019	-0.033	95	0
RA4	3.785	-5.214	1218.392	0.124	100	0
RA5	-6.953	-3.214	0.026	-3.718	91.5	3
RA6	0.731	-5.231	239.263	-2.556	99	0
RA7	1.448	-4.217	162.482	-0.405	98.5	2
RA8	3.896	-3.215	257.478	0.594	100	0
RA9	0.490	-6.214	23.317	-1.367	92.3	0
RA10	3.219	-5.932	279.608	-1.003	63.2	0
RA11	2.267	-6.529	31.373	-1.618	82.4	0
RA12	2.507	-6.793	120.183	0.006	85.4	0
RA13	-6.813	-3.573	0.040	-3.276	100	2
RA14	1.372	-7.681	26.042	-0.284	83.2	0
RA15	3.851	-5.601	1245.466	0.213	87.4	0
RA16	4.444	-5.794	1552.026	-0.223	94.2	0
RA17	2.589	-5.400	821.222	-1.117	36.5	0
RA18	-6.928	-6.773	0.027	-3.497	100	0
RA19	-0.114	-5.718	11.480	-1.532	45.2	3
RA20	-0.160	-7.031	25.590	-1.275	54.6	0
RA21	-0.304	-7.706	12.775	-1.360	98.4	0
RA22	-0.104	-6.713	252.932	-0.527	56.4	0
RA23	-0.380	-6.332	62.560	-1.291	78.2	1
RA24	-0.668	-5.654	91.333	-1.141	98.5	0
RA25	-0.398	-5.834	76.901	-1.288	100	0
RA26	-0.603	-5.890	7.717	-1.837	98.4	0
RA27	-0.297	-6.909	23.899	-0.927	97.5	1
RA28	-1.974	-5.104	33.341	-1.233	96.3	0
RA29	0.048	-6.567	165.155	-1.004	68.4	0
RA30	0.367	-5.632	30.163	-1.252	54.2	0
Fasudil	0.524	-6.254	148.54	-1.454	92.1	0

[a]Predicted octanol/water partition coefficient logP (acceptable range: −2.0 to 6.5); [b]Predicted IC_{50} value for blockage of HERG K+ channels.(below -5); [c]Predicted apparent Caco-2 cell permeability in nm/sec (<25 poor; >500 great); [d]Predicted brain/blood partition coefficient (-3.0 to 1.2); [e]Percent human oral absorption (<25% is poor and >80% is high); [f]Rule of 5 violation (mol_MW < 500, QPlogPo/w < 5, donorHB ≤5, accptHB≤10)

5.4.3 ROCK-I inhibition studies

5.4.3.1 Cloning, expression and purification studies of ROCK1

Human ROCK1was cloned as N-HIS_6-tagged protein using pET $21^{(+)}$ vector. ROCK1 (N-HIS6 tagged) protein was able to be expressed as soluble forms in *E.coli* BL21 (DE3) cells by induction with isopropyl-1-thio-b-D-galactopyranoside (IPTG, 0.1 mM). This was easily purified using Ni_2^+ -affinity chromatography. The expression level of soluble and active N-HIS6 tagged was relatively higher. About 3 mg of N-HIS_6 tagged protein was routinely obtained from the cell lysate of one litre *E.coli* cell culture. Sodium dodecylsulfate–polyacrylamide gel electrophoresis (SDS-PAGE) analysis indicated that one step Ni_2^+ -column purification was sufficient to provide pure ROCK-I. As expected from the calculated molecular weight of N-HIS_6 tagged ROCK1, the size of the protein from native SDS-PAGE was found about 158 kDa.

5.4.3.2 ROCK-I enzyme assay

Having identified the hit molecules from *in silico* screening approach, we attempted to prove the concept of designed compounds to inhibit ROCK1. To test this hypothesis, the compounds were screened for ROCK1 enzymatic activity at different concentrations from 100 µM -1 nM utilizing standard enzyme assay protocol and the relative inhibition of ROCK1 activity was evaluated for IC_{50} calculations. Initially range finding experiments were performed to check the concentration of enzyme which was found to be 25 pM. Further the substrate MBP was used at different concentrations to determne Km and Vmax using Michealis-Menton equation.

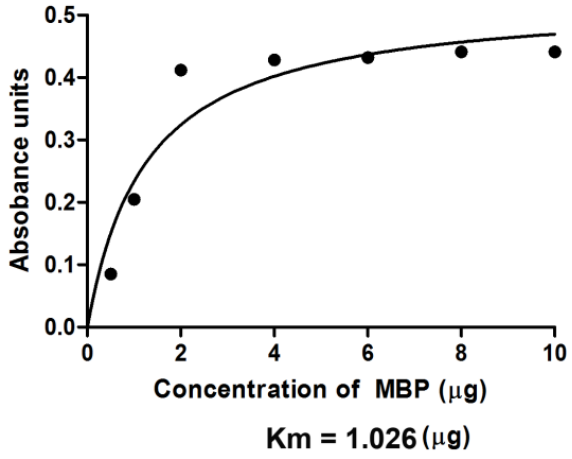

Figure 5.7 Kinetic parameters of MBP

The Km was calculated using Graphpad prism software and was found to be 1.026 µg. the kinetic parameters of the MBP were shown in the **Figure 5.7**.

Table 5.7 Biological data of ROCK-I for the selected Asinex molecules

Sr.No	ROCK $IC_{50}(\mu M)$[a]
RA1	0.002±0.001
RA2	≤0.001
RA3	≤0.001
RA4	≤0.001
RA5	0.002±0.001
RA6	≤0.001
RA7	0.002±0.001
RA8	0.003±0.001
RA9	0.004±0.001
RA10	0.009±0.001
RA11	0.015±0.010
RA12	0.008±0.001
RA13	≤0.001
RA14	0.021±0.010
RA15	0.017±0.010
RA16	0.009±0.001
RA17	0.007±0.001
RA18	0.007±0.001
RA19	18.141±2.342
RA20	0.162±0.121
RA21	0.044±0.015
RA22	4.312±1.542
RA23	5.367±2.474
RA24	1.568±0.526
RA25	1.048±0.262
RA26	5.859±1.363
RA27	0.746±0.020
RA28	44.711±3.212
RA29	0.227±0.052
RA30	15.430±3.452
Fasudil	5.240±3.458

[a]All data in triplicates was used for deriving and represented in Mean±SEM (n=3)

All the compounds except **RA19**, **RA28** and **RA30** exhibited ROCK-I enzyme inhibition with IC_{50} <6 µM (**Table 5.7**). Among these 27 compounds, 22 compounds were found to be in nanomolar range emerging as more potent hits when compared to Fasudil, the standard ROCK-I inhibitor. Compounds that showed potency at around <10 nM included **RA1**-**RA13** and **RA16**-**RA18**. Though all the 30 lead compounds exhibited *in silico* proof of concept, there were not much correlation to their docking scores. Among the promising lead compounds, it was noteworthy to compare their drug-likeliness properties. Though compounds **RA1**, **RA5**, **RA7**, **RA8** and **RA13** were found very effective, their HERG toxicity as predicted earlier (**Table 5.5**) could be a major hurdle in the development. As the major objective of our study was to develop the compounds for neurological disorders, it was crucial to consider blood brain barrier permeability of these hit compounds. Once again **RA5**, **RA13** and **RA18** stand very less chance for further development. Thus it appeared that except **RA1**, **RA3**, **RA5**, **RA7**-**RA9**, **RA13**, **RA18**, **RA19** and **RA26**, all other compounds could be useful as hit compounds that could be explored for further development.

5.4.4 NOX2 inhibition studies

5.4.4.1 X-ROS estimation

Due to non-availability of NOX clone, we explored alternate strategies to perform biological screening of the designed compounds. It appeared that X-ROS being a novel signaling pathway reported in most of the cells that arise when extracellular matter was triggered by membrane located NOX2. The human umbilical vein endothelial cell line (HUVEC), a type of macrophages, in which NOX2 was found to be overexpressed upon stimulation with lipopolysaccharide (LPS) attracted our attention to explore for bioassay. We performed experiments to confirm the overexpression of $p47^{PHOX}$ in both HUVEC and IMR32 and found that in HUVEC cells the expression was more (**Figure 5.8**) and hence for the present study we utilized these cell lines.

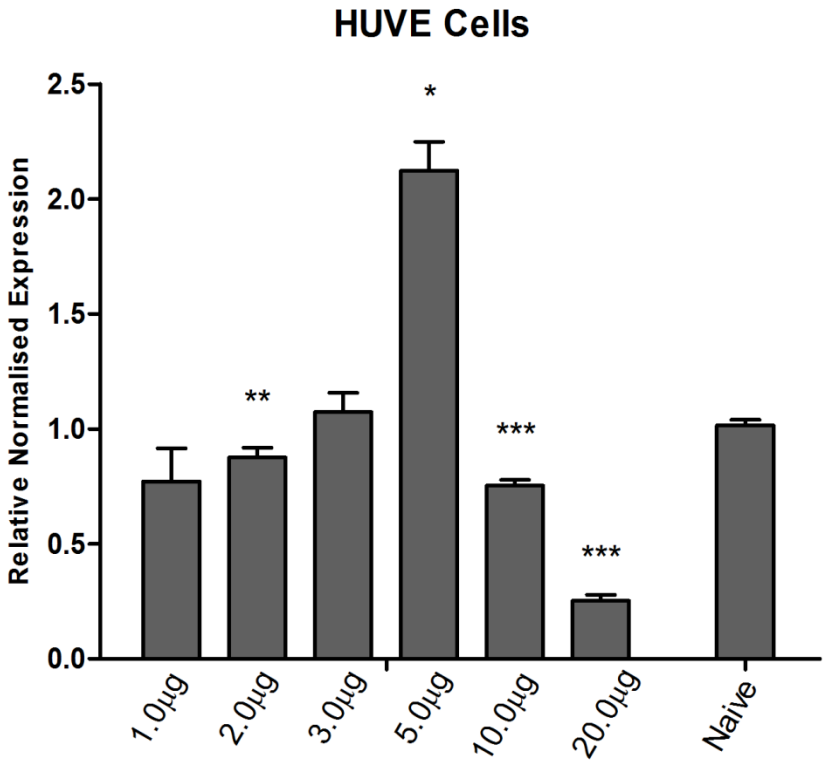

Figure 5.8 Relative normalized expression of p47PHOX in LPS induced HUVE cell lines.

The physiological generation of ROS could occur as a by-product of other biological reactions in mitochondria, peroxisomes, cytochrome P-450 and other cellular elements. However, the phagocyte NOX was the first identified example of a system that could generate ROS not as a by-product, but rather as the primary function of the enzyme system [Prosser B L *et.al* 2011]. Various endogenous or exogenous inflammatory signals that could alert the cells to nearby dangers were the most important biological factors that could trigger cellular NOX activation. One example was the bacterial endotoxin lipopolysaccharide (LPS), which not only activated leukocyte NOX, as expected but also showed significant effects on non-phagocytic NOX [Barth B M *et.al* 2010]. In the present study estimation of intracellular ROS was performed using DCFH-DA. The cells treated with 5 µg/µl of LPS (**Figure 5.8**) showed increased DCF fluorescence levels indicative of intracellular ROS production. However addition of test compounds revealed a dose-dependent increase in DCHF oxidation as measured at 3 h (**Table 5.8**).

From the **Table 5.8**, it was evident that about 12 compounds (**RA1**, **RA3**, **RA5**, **RA6**, **RA9**, **RA14**-**RA16**, **RA19**, **RA27**, **RA28** and **RA30**) were found promising with X-ROS IC_{50}s <10 µM. Among these, leads **RA5**, **RA9** and **RA16** were found to exhibit activity in nanomolar IC_{50}s of 0.08, 0.79, 0.77 µM respectively, but unfortunately these compounds were found to have ADME issues as detailed earlier (**Table 5.6**). Closer analyses of the next set of active leads, revealed that 7 compounds (**RA3**, **RA6**, **RA15**, **RA19**, **RA27**, **RA28** and **RA30**) were found to exhibit X-ROS IC_{50}s less than 5 µM, among which except for **RA3** and **RA19,** all other compounds were found within the drug-likeliness limit. It was gratifying to observe that **RA6**, **RA15** and **RA27** being the most effective NOX2 inhibitor also showed promising potential against ROCK-I. Also the proof of concept of our design strategies was thus successful in the identification of dual inhibitors of ROCK-I and NOX2. Fasudil was used as a control inhibitor in all the assays to understand the inhibition range. It is a small molecule and is currently the only ROCK inhibitor in clinical trial. Fasudil was not tested earlier for NOX2 inhibition, though its anti-inflammatory property was known. Pre-clinical studies have reported that Rho/ROCK signalling was involved in increased vasoconstriction, inflammation and remodeling in models of pulmonary hypertension. Furthermore, it was shown that inhibition of ROCK attenuated or reversed these effects. In our study Fasudil was found effective in inhibitiong NOX2 with IC_{50} of 2.98 µM. [Uehata M., *et.al* 1997].

5.4.5 Binding pattern analyses of designed compounds in ROCK-I and NOX2

Top active compounds **RA2**, **RA3**, **RA6**, **RA12** and **RA13** from enzyme inhibition data have shown activity around 1 nM against ROCK-I and **RA5**, **RA6**, **RA9**, **RA15**, **RA16**, **RA27** and **RA28** found to show inhibition below 3 µM. Based on the Qikprop prediction, only **RA6** among these did not show any violation of ADME properties. With the aim of getting insights into the structural basis for its activity, this compound was analyzed in more detail. The compound was found to display highest docking score among the other identified Asinex hits, with docking score of -9.351 kcal mol^{-1} for ROCK-I and -9.079 kcal mol^{-1} for NOX2. The lead compound was found to be associated with important hydrogen bonding interactions with relevant amino acid residues of the ROCK-I and NOX2 proteins (**Figure 5.9**). Oxygen atom of the nitro group was found to interact with Met156 which was analogous to the one observed with crystal ligand Fasudil (**Figure 5.1**).

Table 5.8 Biological data of NOX2 for the selected Asinex molecules

Sr.No	X-ROS IC_{50}(µM)[a]
RA1	8.836±2.311
RA2	13.923±1.253
RA3	3.304±0.524
RA4	18.195±3.546
RA5	0.077±0.027
RA6	2.853±0.148
RA7	10.759±2.191
RA8	10.454±0.012
RA9	0.792±0.163
RA10	10.254±3.875
RA11	12.036±2.987
RA12	14.458±3.979
RA13	18.211±4.522
RA14	8.794±0.983
RA15	1.037±0.244
RA16	0.773±0.054
RA17	>100
RA18	95.375±7.216
RA19	4.225±1.247
RA20	12.388±0.699
RA21	47.791±9.212
RA22	15.493±1.564
RA23	154.45±1.586
RA24	90.057±2.658
RA25	12.189±7.211
RA26	64.272±5.133
RA27	1.843±0.694
RA28	1.629±0.845
RA29	61.016±9.297
RA30	3.327±1.478
Fasudil	2.981±0.489

[a]All data in triplicates was used for deriving and represented in Mean±SEM (n=3)

The NH of carboxamide group attached to the oxadiazole end was found to be interacting with Asp160 and the NH atom on imidazole ring participated in hydrogen bonding with Asp369. In addition to hydrogen bonding interactions; **RA6** was found to be well placed in the hydrophobic

pocket consisting of Ile82, Val90, Met153, Val137, Ala103, Tyr155, Ala215, Leu205, Phe368 and Val162 in ROCK-I active site. The binding analysis for the lead molecule **RA6** is shown in **Figure 5.9**. On the other hand **RA6** in NOX2 active site was found to interact through NH group on imidazole ring with Asp243. NH group of pyrazole ring and NH group on oxaindazole were found to interact with the Trp263. Oxaindazole ring also revealed π-π interaction with Trp263. The carbonyl functional group of carboxamide group was found to render important hydrogen bonding with Ser208. **RA6** was found to be placed well in the hydrophobic cavity lined by Pro206, Ala207, Met278, Pro276, Trp263, Tyr274 and Phe209 in NOX2 active site.

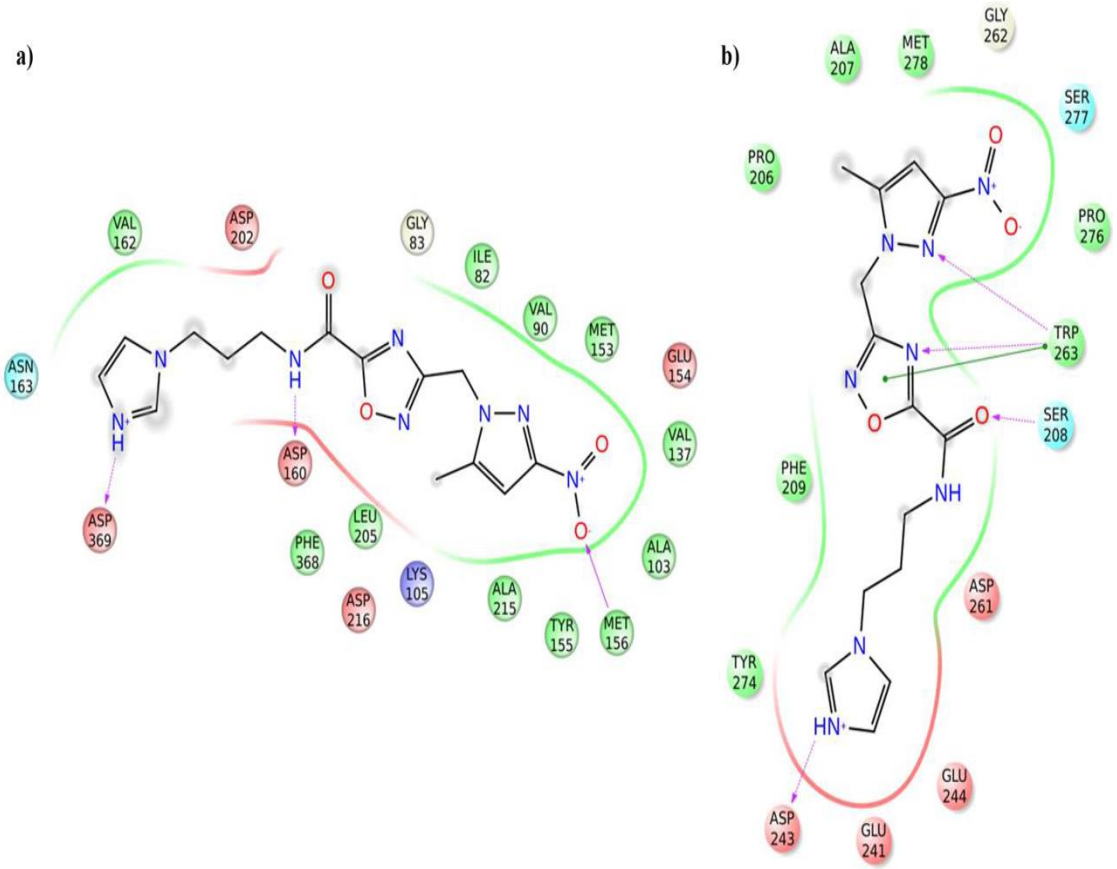

Figure 5.9 Ligand interaction pictures of **RA6** a) ROCK-I and b) $p47^{PHOX}$ active site, pink solid arrow in the interaction picture is Hbond between backbone of the amino acid and the ligand, pink dotted arrow in the interaction picture is Hbond between side chain of the amino acid and the ligand and green solid line indicates the π-π stacking interaction between amino acid and ligand.

The binding analyses of leads **RA2**, **RA3**, **RA12** and **RA13** were performed as these also showed similar range of activity against ROCK-I. The binding analysis of lead **RA2** revealed that Lys200 and Phe87 (**Figure 5.10**) in ROCK-I and in NOX2 Ser208, Ala207, Trp263, Met278

and Ser277 interacting similarly like **RA6** but compounds **RA3**, **RA12** and **RA13** failed to produce hydrogen bonding interaction of this kind. The leads **RA3**, **RA12** and **RA13** binding pattern in ROCK-I (**Figures 5.10** and **5.11**) revealed that, the amino group in these compounds shared the common interaction with one of the aspartic acid residue in the pocket as shown in **Figures 5.10**, and **5.11**, but all these compounds were found well fit into the hydrophobic cavity as expected.

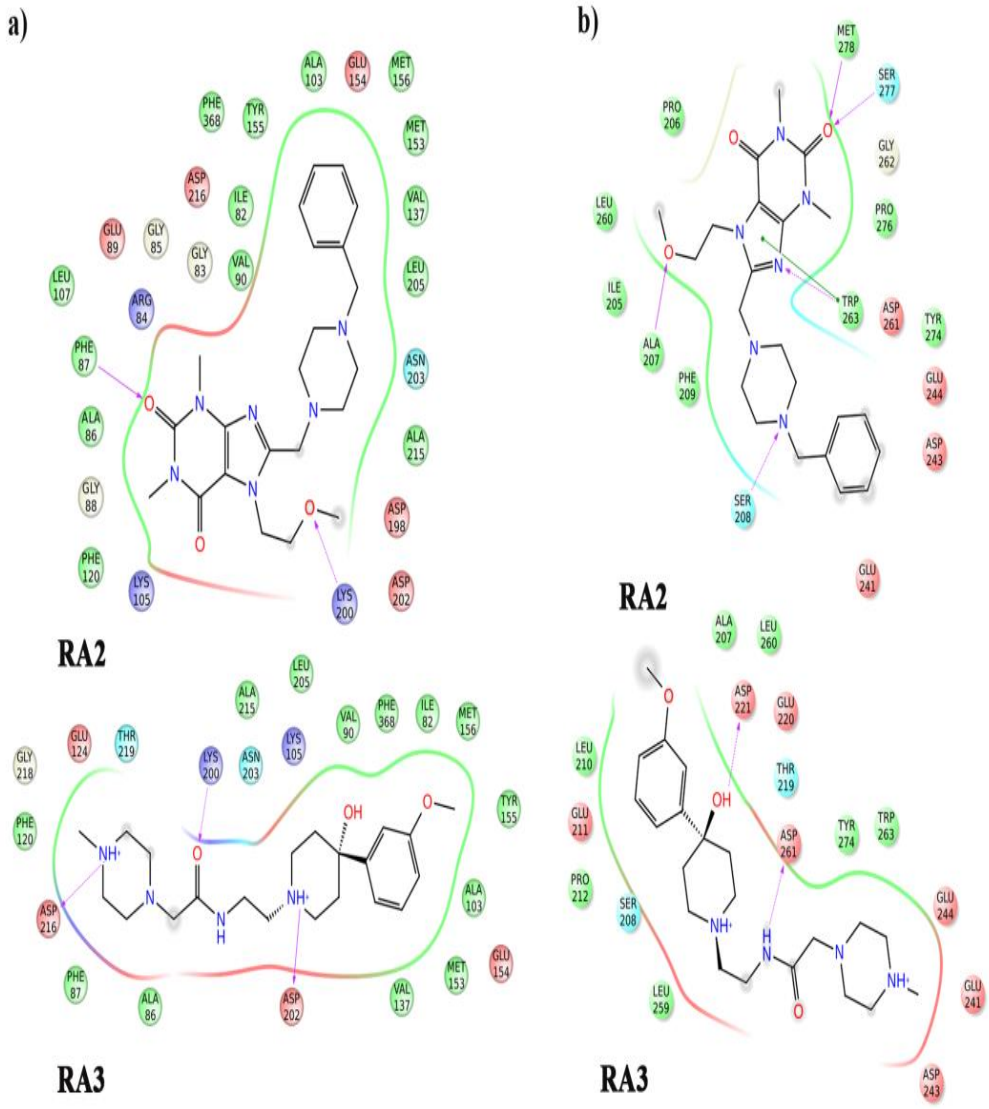

Figure 5.10 Interaction pictures of **RA2** and **RA3** in a) ROCK-I and b) $p47^{PHOX}$ active site, pink solid arrow in the interaction picture is Hbond between backbone of the amino acid and the ligand, pink dotted arrow in the interaction picture is Hbond between side chain of the amino acid and the ligand and green solid line indicates the π-π stacking interaction between amino acid and ligand.

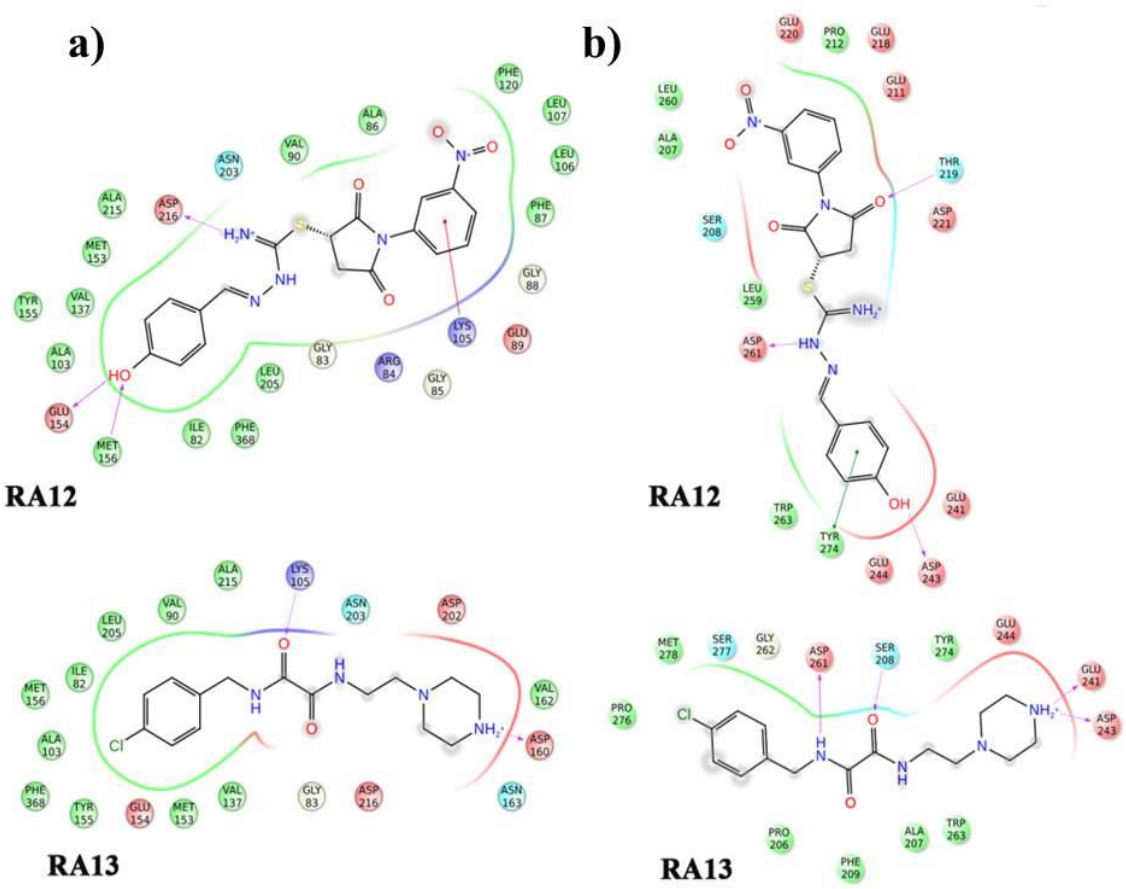

Figure 5.11 Interaction pictures of **RA12** and **RA13** in a) ROCK-I and b) $p47^{PHOX}$ active site, pink solid arrow in the interaction picture is Hbond between backbone of the amino acid and the ligand, pink dotted arrow in the interaction picture is Hbond between side chain of the amino acid and the ligand and green solid line indicates the π-π stacking interaction between amino acid and ligand.

5.4.6 Thermofluor assay for ROCK -I

Thermal shift assays have many biophysical attributes that satisfy the requirements of a general cross target drug discovery assay. Ligand induced conformational stabilization of protein is a well understood phenomenon in which substrates, inhibitors, cofactors, metal ions, synthetic analogues of natural ligands and even other proteins provide enhanced stability to proteins on binding. This phenomenon is based on the energetic coupling of the ligand binding and receptor melting reactions. This energetic linkage results in ligand-dependent changes in the midpoint for thermally induced melting curves for the ligand receptor complex relative to the uncomplexed receptor (ΔTm).

The results from the miniaturized thermal shift assay were found to correlate with the results obtained through the enzymatic assay by the reasonable fit to the slope for temperature *vs* RFU (10^3). Data analysis for this experiment was simplified using CFX manager V3.0 software displayed the computed Tm determinations for experiments. The results for the (from **Figure 5.12**a) blank (red peak) which was only enzyme with the dye showed a Tm of 40.20 ^{0}C, whereas **RA6** (blue peak) with enzyme showed Tm of 43.30 ^{0}C. Usually the Tm shift more than 1 considered as strong binding to the receptor as shown in **Figure 5.12**. Thus **RA6** showed Tm shift of +3.30^{0}C at 1 µM concentration whereas Fasudil at 1 µM showed Tm shift of 0.5 ^{0}C. From **Figure 5.12**b the Tm of native protein was found to be 49.6 ^{0}C and Tm of enzyme and Fasudil complex found to be 43.6 ^{0}C.

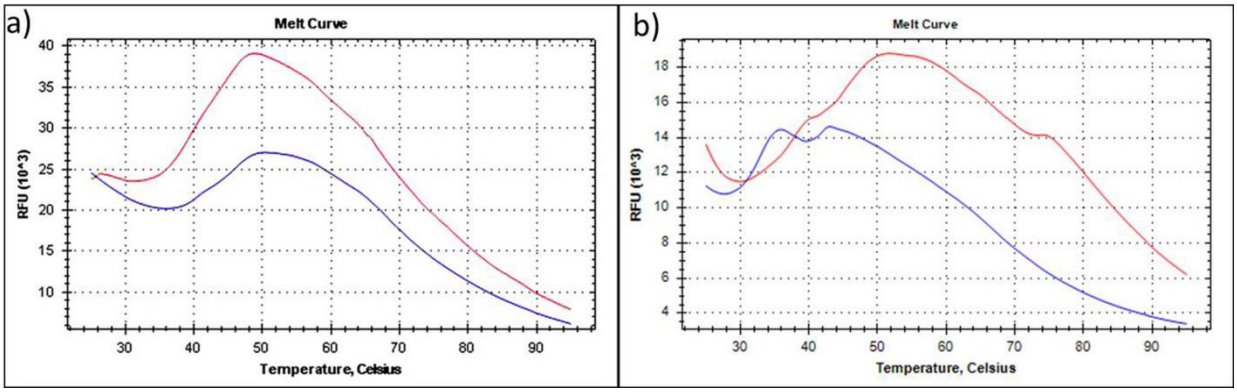

Figure 5.12 Thermofluor assay results for ROCK-I. The data were obtained for a) ROCK-I in the presence (Blue peak) and absence (Red peak) of **RA6**, b) ROCK-I in the presence (Blue peak) and absence (Red peak) of Fasudil.

5.5 DESIGN II: IDENTIFICATION OF DUAL INHIBITORS FROM *IN HOUSE* LIBRARY (BITS)

As we had successfully demonstrated lead identification based on the structure based protocol using high throughput screening of Asinex database. In the design II, we attempted to identify lead compounds as dual inhibitors of ROCK-I and NOX2 from our *in house* library (BITS-Hyderabad). This library consisted of diverse set of molecules available readily in our lab. As these library molecules were not explored for the neuroinflammation or neurological disorders, we utilised this library to find hits which could be taken forward for proof of concept. Also compared to Asinex, *in house* library was advantageous due to availability of compounds readily as compared to cost of purchase of Asinex library of compounds.

5.5.1 Virtual screening for ROCK-I and NOX2

Virtual screening of *in house* library to filter out novel active compounds for the dual inhibition of ROCK-I and NOX2 was attempted similar to that followed for Asinex library as depicted on **Figure 5.5**. Both energy and shape based strategies were used for ligand searching from *in house* library. For both the targets around 11417 hit molecules from shape and 13321 from e-phamacophore for ROCK-I and 14789 hit molecules and 13256 hit molecules for NOX2 shape and e-pharmacophore respectively were retrieved with similar filters applied as in design I strategy *i.e* close to 1 tanimoto combo and >1.5 for the fitness. Total number of molecules from initial filtering was about 19847 for ROCK-I and 19521 for NOX2 and these were combined and subjected for HTVS docking protocol. As a second filter that glide score <-6.0 was applied for 10121 molecules from ROCK-I grid and 9984 molecules from NOX2 retrieved from HTVS step. These molecules were subjected for SP docking module in both the grids utilising cross docking. The cut off value was taken as -6.0 as the reference crystal ligand of 2ESM Glide score were found to be -7.581, and -7.593 for peptide-5 in 1OV3. Cross docking among SP hits and only those which had good docking score were subjected to XP docking again in ROCK-I and NOX2. Thus, we acquired 1034 compounds with good Glide score compared to crystal ligand (<-7.581 for ROCK-I and -6.265for NOX2). Finally 37 molecules (**Figures 5.13** and **5.14**) were identified as promising hits for both targets. Though the docking score did not indicate the compound's binding affinity, it was helpful in prioritizing/ranking the ligands. Further, duplication of molecules due to multiple conformations were corrected from the list after XP docking, and were

visually inspected for crucial amino acid residue binding within the surface of ROCK-I and NOX2 active sites.

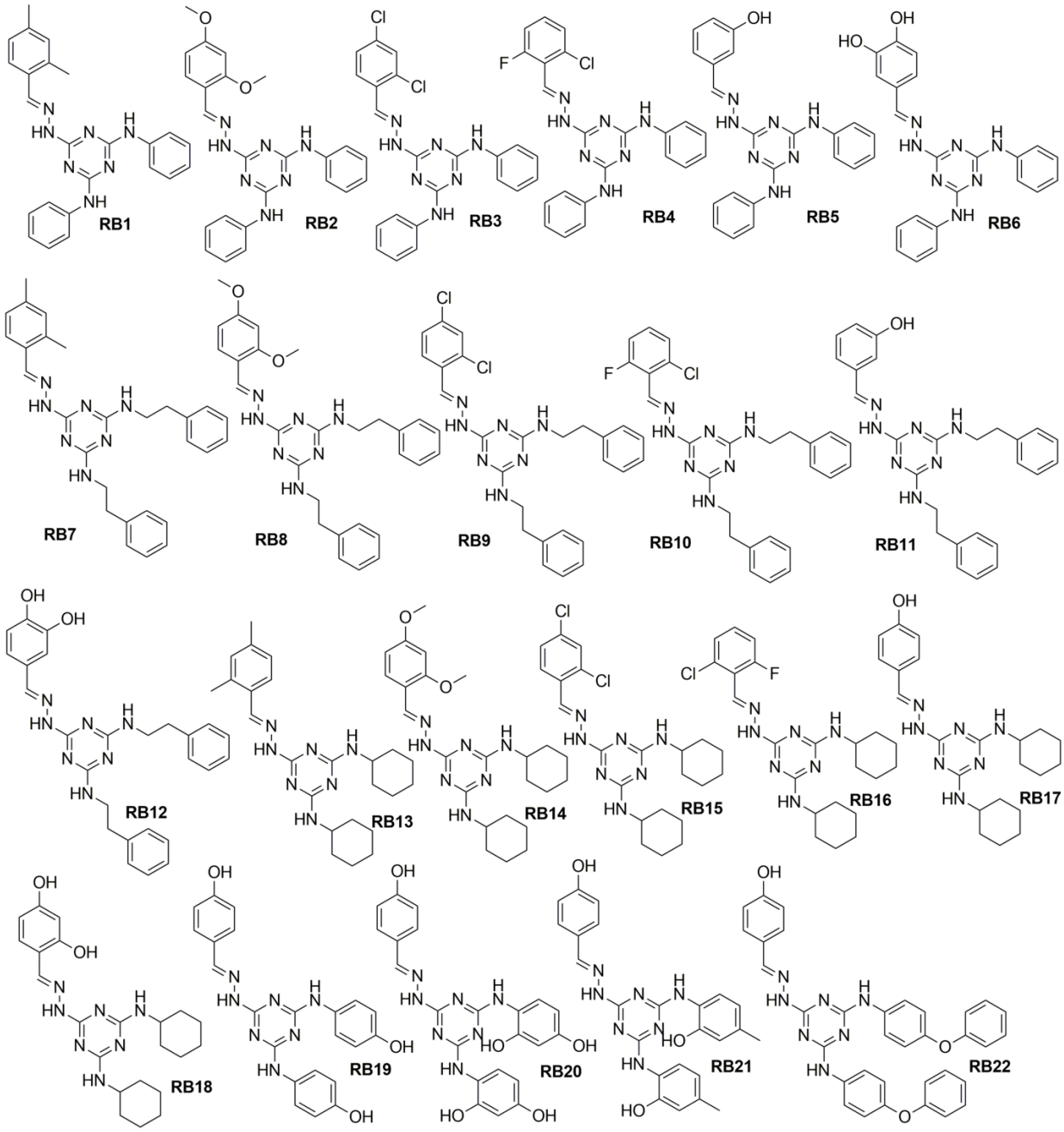

Figure 5.13 Structures of **RB1-RB22** screened from BITS library.

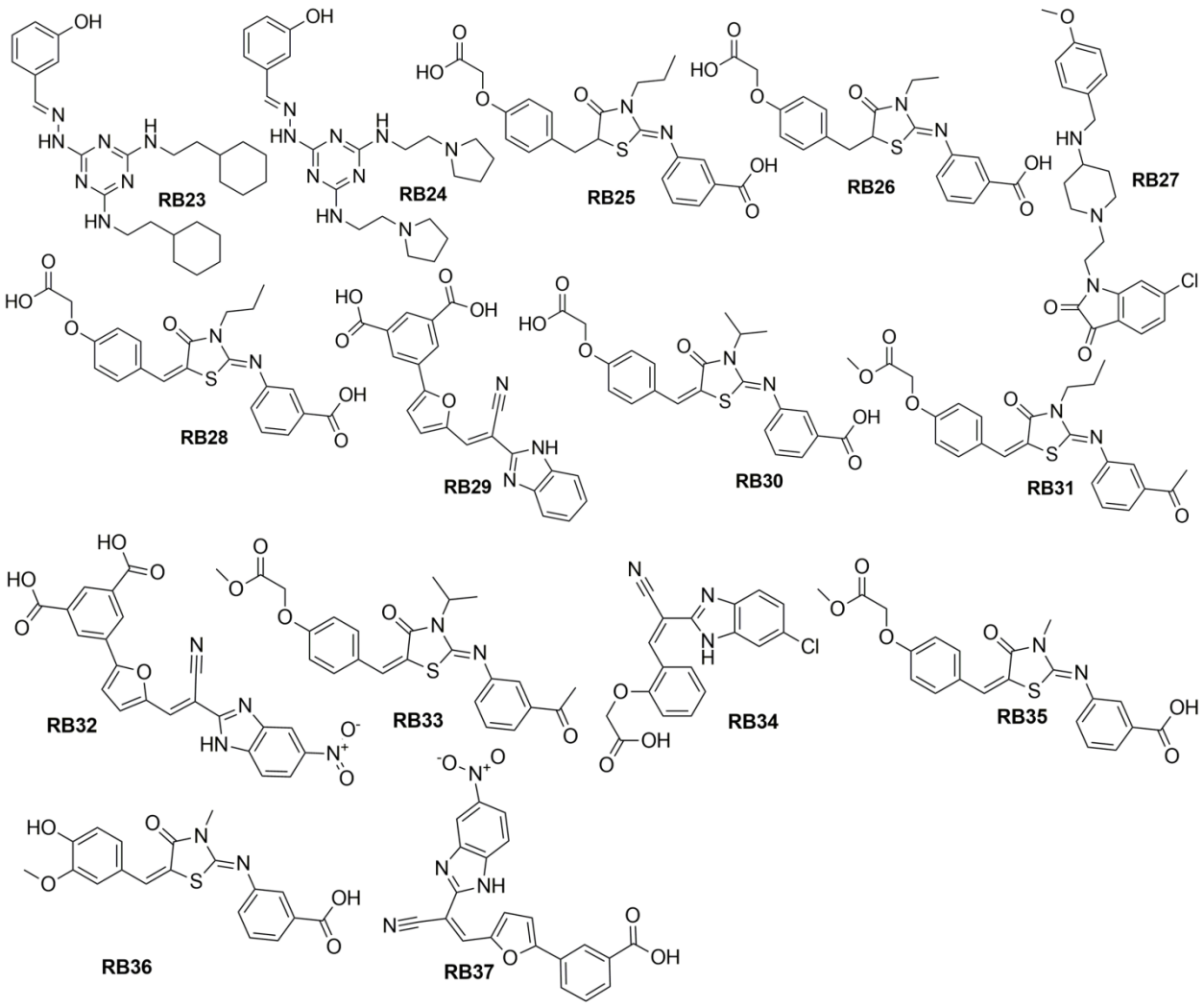

Figure 5.14 Structures of **RB23-RB37** screened from BITS library.

The 2D structures of all 37 compounds are presented in **Figure 5.13** and **5.14**. Most of the compounds were found to be from triazine scaffold (**RB1**-**RB24**) and some were found to be with thiazolidine nucleus (**RB25**, **RB26**, **RB30**, **RB31**, **RB33**, **RB35** and **RB36**) and other scaffolds included isatin (**RB27**) and benzimidazoles (**RB29**, **RB32**, **RB34**, and **RB37**). The docking parameters for ROCK-I and NOX2 for these 37 leads are tabulated in **Table 5.9** and **5.10**.

Table 5.9 Energy scores of 37 selected BITS library compounds in ROCK-I

Sr.No	H bond	Glide g score	Docking score	Interacting aminoacids
RB1	2	-6.152	-6.152	Gly88
RB2	3	-5.014	-5.014	Asp202, Asp216
RB3	2	-6.734	-6.734	Asp160
RB4	1	-6.747	-6.747	Ile82
RB5	2	-3.806	-3.806	Lys105, Glu154
RB6	4	-8.465	-8.465	Met156, Glu154, Lys105
RB7	2	-7.290	-7.290	Arg84
RB8	3	-7.489	-7.489	Arg84, Gly88, Lys105
RB9	4	-7.951	-7.951	Asp216, Lys105
RB10	2	-9.058	-9.058	Asp160, Lys105
RB11	5	-9.251	-9.251	Asp160, Met156, Glu154, Lys105
RB12	3	-7.143	-7.143	Met156, Glu154
RB13	1	-5.471	-5.471	Ile82
RB14	2	-5.372	-5.372	Asp216
RB15	1	-5.467	-5.467	Asp216
RB16	2	-6.701	-6.701	Asp202, Asp216
RB17	3	-5.987	-5.987	Asp202, Asp216, Glu154
RB18	3	-8.663	-8.663	Met156, Glu154
RB19	3	-6.325	-6.325	Met156, Glu154, Ile82, Asp202
RB20	5	-6.969	-6.969	Met156, Glu154, Lys200, Asp202, Asp216
RB21	4	-7.684	-7.684	Met156, Gly88, Asp160
RB22	3	-7.597	-7.597	Phe120, Asp160
RB23	6	-7.560	-7.560	Glu154, Asp160
RB24	3	-8.071	-8.071	Met156, Glu154, Lys105
RB25	4	-7.396	-7.396	Met156, Glu154, Lys105, Asp216
RB26	1	-8.014	-8.014	Lys105, Asp216, Glu124
RB27	1	-5.241	-5.241	Met156
RB28	4	-8.013	-8.013	Met156 Asp216, Lys105
RB29	6	-9.525	-9.525	Glu154, Asp216, Glu124, Lys105, Arg84
RB30	1	-5.023	-5.023	Glu154, Lys105, Asp216
RB31	5	-6.734	-6.734	Lys105, Phe87
RB32	4	-7.597	-7.597	Met156, Glu154, Lys105
RB33	3	-6.541	-6.541	Met156, Lys105
RB34	2	-7.156	-7.156	Lys105, Asp216, Glu124
RB35	5	-5.023	-5.023	Met156, Asp216, Lys105
RB36	4	-6.454	-6.454	Asp216, Lys105
RB37	1	-7.629	-7.629	Glu154

Table 5.10 Energy scores of 37 selected BITS library compounds in NOX2

Sr.No	H bond	Glide g score	Docking score	Interacting aminoacids
RB1	1	-1.501	-1.501	Asp261, Trp263, Phe209
RB2	3	-2.798	-2.798	Asp261, Trp263, Phe209
RB3	2	-5.110	-5.110	Glu244, Trp263, Tyr237
RB4	1	-4.641	-4.641	Asp261, Trp263, Phe209
RB5	2	-4.314	-4.314	Asp261, Trp263, Phe209
RB6	2	-2.118	-2.118	Trp263, Glu244
RB7	1	-3.817	-3.817	Ser208, Asp261, Trp263
RB8	1	-4.337	-4.337	Ser208, Asp261, Trp263
RB9	1	-4.700	-4.700	Ser208, Asp261, Trp263
RB10	1	-4.500	-4.500	Asp261, Trp263
RB11	2	-3.319	-3.319	Ser208, Asp261, Trp263, Glu241
RB12	2	-4.346	-4.346	Asp261, Trp263, Trp204, Tyr279
RB13	1	-2.583	-2.583	Ser277, Gly262
RB14	2	-2.135	-2.135	Ser208, Tyr279
RB15	1	-2.082	-2.082	Ser208, Trp263
RB16	2	-3.254	-3.254	Ser208, Trp263
RB17	2	-3.119	-3.119	Ile205, Tyr279
RB18	0	-3.174	-3.174	Ser208, Trp263, Glu241
RB19	2	-3.761	-3.761	Phe209, Asp261, Thr219, Asp221
RB20	2	-4.171	-4.171	Asp243, Glu244, Ser208, Asp261, Tyr279, Tyr237, Trp263
RB21	2	-3.684	-3.684	Trp263, Asp261
RB22	2	-3.603	-3.603	Glu244, Trp263
RB23	3	-3.720	-3.720	Asp243, Tyr274, Glu244, Trp263
RB24	2	-4.336	-4.336	Asp261, Ser208, Trp263
RB25	2	-2.356	-2.356	Ile205, Trp204, Met278, Ser277, Asp261
RB26	4	-2.952	-2.952	Ser277, Met278, Ser208
RB27	3	-5.320	-5.320	Asp261, Asp243
RB28	2	-3.237	-3.237	Asp261, Ser277, Met278, Trp263, Tyr279, Tyr237
RB29	1	-3.812	-3.812	Met278, Gly262, Ser277, Glu244, Trp263
RB30	1	-3.892	-3.892	Tyr279, Met278, Ser277
RB31	3	-2.650	-2.650	Ser208, Asp261, Met278, Tyr279
RB32	3	-3.514	-3.514	Ser277, Met278, Tyr279
RB33	2	-3.820	-3.820	Ser208, Trp263, Tyr279
RB34	1	-4.542	-4.542	Ser208, Ala207, Trp263, Asp261
RB35	3	-2.841	-2.841	Tyr279, Ser277, Met278
RB36	1	-2.112	-2.112	Glu244, Asp261, Tyr274, Ser208, Trp263
RB37	2	-3.592	-3.592	Asp261, Ser208, Asp243, Trp263, Tyr274

Compounds **RB6**, **RB11**, **RB12**, **RB18**, **RB19**, **RB20**, **RB21**, **RB23**, **RB24**, **RB25**, **RB27**, **RB28**, **RB32** and **RB35** showed hydrogen bonding interaction with Met156, which was crucial. All other compounds showed hydrogen bonding with one or more aminoacid Asp160, Asp216, Asp198 and Asp202.

Similarly in NOX2, (**Table 5.10**) compounds **RB7**, **RB8**, **RB9**, **RB11**, **RB14**, **RB15**, **RB16**, **RB18**, **RB20**, **RB24**, **RB26**, **RB31**, **RB33**, **RB34**, **RB36** and **RB37** were found to show hydrogen bonding interaction with Ser208, which was important as discussed earlier. Remaining all other compounds was found to reveal hydrogen bonding with another Asp243, Glu244 and Glu241.

5.5.2 ADME predictions for the selected *in house* lead compounds

ADME predictions would help in identifying the pharmaceutical relevance of the candidate drugs, all the selected designed compounds were subjected to *in silico* ADME properties using QikProp module in Schrodinger (**Table 5.11**). The compounds **RB3**, **RB4**, **RB8**, **RB10**, **RB19**, **RB23**, **RB29**, **RB30**, **RB34**, and **RB35** shortlisted were found to violate the Lipinski's rule of five. Various other important properties like predicted octanol/water partition coefficient logP, predicted IC_{50} value for blockage of HERG K^+ channels, predicted apparent Caco-2 cell permeability in nm/sec, predicted brain/blood partition coefficient, percent human oral absorption were determined for the selected compounds and checked for any deviations. Predicted logP values for the hits were in the acceptable range for all the compounds. Predicted Caco-2 cell permeability property was in the expected range for **RB2**, **RB31**, **RB32**, **RB36** and **RB37**. About 14 compounds (**RB4**, **RB8**-**RB10**, **RB13**, **RB16**, **RB18**-**RB19**, **RB23**-**RB25**, **RB29**, **RB31** and **RB37**) were found to be predicted to have cardiotoxicity as their QPlogHERG parameter was out of the acceptable range. This was important to know the future perspective of the leads. Whereas predicted blood brain barrier and % human oral absorption were also found in the range for all compounds unlike the hits derived from Asinex database. Moreover, these predictions of ADME properties could be useful in further modifications of active molecules after preliminary enzymatic screening.

Table 5.11 ADME prediction for the designed 37 compounds from *in house* library

S.No	QPlogPo/w [a]	QPlogHERG [b]	QPPCaco [c]	QPlogBB [d]	Human Oral Absorption [e]	Rule of Five [f]
RB1	2.549	-5.932	132.116	-2.174	65.2	0
RB2	0.787	-6.529	12.548	-3.261	45.2	0
RB3	2.821	-6.793	101.453	-1.985	98.5	3
RB4	2.666	-3.573	144.566	-2.131	100.0	1
RB5	3.860	-7.682	294.606	-1.930	100.0	0
RB6	4.762	-5.601	1255.394	-0.642	100.0	0
RB7	4.484	-7.681	1297.172	-0.895	95.6	0
RB8	5.471	-4.123	1756.065	-0.853	78.2	3
RB9	4.088	-3.120	1176.384	-1.042	98.4	0
RB10	4.262	-2.104	1405.651	-0.640	65.3	2
RB11	4.774	-6.141	1340.434	-0.772	74.3	0
RB12	-1.782	-7.412	133.579	-2.987	100.0	0
RB13	3.656	-4.125	579.603	-1.495	92.1	0
RB14	5.359	-5.132	1181.455	-1.190	96.3	1
RB15	4.729	-6.147	2062.027	-0.678	68.2	0
RB16	2.983	-3.456	117.647	-2.238	98.4	0
RB17	5.017	-5.214	1451.878	-0.535	74.2	0
RB18	3.199	-3.102	142.150	-2.103	56.2	0
RB19	3.404	-4.201	390.092	-1.618	58.7	3
RB20	4.306	-5.912	1461.866	-0.964	79.4	0
RB21	3.414	-5.631	671.369	-1.196	98.5	0
RB22	5.412	-5.214	1530.494	-1.241	96.2	0
RB23	5.680	-4.201	1244.946	-0.956	78.4	4
RB24	2.543	-4.321	126.239	-2.223	84.1	0
RB25	0.266	-4.621	583.765	-0.346	100.0	0
RB26	0.328	-5.210	42.689	-1.079	95.6	0
RB27	-1.093	-5.963	76.054	-1.298	78.2	0
RB28	-0.687	-5.971	168.465	-0.885	74.1	1
RB29	-0.620	-3.176	25.566	-1.258	98.3	2
RB30	1.810	-6.214	1832.655	-0.373	95.4	0
RB31	0.082	-4.321	21.755	-1.403	96.2	3
RB32	-1.449	-7.258	18.695	-1.540	87.4	0
RB33	-0.375	-6.414	28.715	-1.202	94.5	0
RB34	-0.541	-5.213	91.790	-1.495	97.6	1
RB35	-1.293	-5.214	239.017	-0.822	89.2	1
RB36	-0.944	-6.314	4.924	-1.855	63.1	0
RB37	-0.798	-4.127	11.730	-1.361	54.3	0

[a]Predicted octanol/water partition coefficient logP (accep**Table** range: −2.0 to 6.5); [b]Predicted IC50 value for blockage of HERG K+ channels.(below -5); [c]Predicted apparent Caco-2 cell permeability in nm/sec (<25 poor; >500 great); [d]Predicted brain/blood partition coefficient (-3.0 to 1.2); [e]Percent human oral absorption (<25% is poor and >80% is high); [f]Rule of 5 violation (mol_MW < 500, QPlogPo/w < 5, donorHB ≤5, accptHB≤10)

5.5.3 ROCK-I inhibition studies

The hit molecules obtained from *in silico* screening of our *in house* library were tested for ROCK-I enzymatic activity. As described, ROCK-I enzyme was purified according to section 5.4.3.1, which was later at 20 pM concentration incubated with the test compounds at different concentrations from 100 µM-1 nM. The enzyme inhibitor mixture pH was equilibrated in 100 mM HEPES buffer. Standard protocol for the mentioned inhibition assay was followed and the % inhibitions were calculated using graphpad prism software. Out of the 37 compounds investigated, 27 compounds were found to be inhibiting ROCK-I enzyme effectively with IC_{50}s <10 µM (**Table 5.12**). Among the promising hits, 19 compounds were found to exhibit activity (IC_{50}) <1 µM which was very much encouraging. It was found that 12 compounds (**RB3**, **RB6**, **RB7**, **RB9**, **RB10**, **RB14**-**RB16**, **RB18**, **RB19**, **RB21** and **RB24**) emerged as most promising exhibiting IC_{50}s in the submicromolar range (<0.1 µM). Among these compounds RB3, RB9, RB10, RB16, RB18, RB19 and RB24 were predicted with HERG toxicity, hence it was worth to keep in mind while developing them further. Compound **RB13** was found ineffective in the assay.Among the other compounds, **RB2**, **RB4**, **RB5**, **RB8**, **RB11** and **RB12** showed comparatively moderate inhibition of ROCK displaying 321, 101, 427, 101.2, 460.6 and 357 nM respectively (**Table 5.12**). Among them **RB2** and **RB12** did not violate any of the ADME properties. Whereas, compounds **RB1**, **RB13**, **RB17** and **RB25-37** showed weak inhibition of ROCK displaying 11.86, 212.6, 4.2, 8.93, 6.24, 5.21, 2.56, 1.03, 72.2, 68.6, 47.8, 48.2, 18.33, 36.98, 43.82 and 28.36 µM respectively.

Table 5.12 Biological data of ROCK-I for the selected BITS molecules

Sr.No	ROCK $IC_{50}(\mu M)$[a]
RB1	11.862±1.243
RB2	0.321±0.012
RB3	0.005±0.001
RB4	0.101±0.012
RB5	0.427±0.013
RB6	0.012±0.010
RB7	0.028±0.015
RB8	0.101±0.016
RB9	0.012±0.007
RB10	0.006±0.001
RB11	0.461±0.018
RB12	0.357±0.019
RB13	>100
RB14	0.009±0.001
RB15	0.009±0.001
RB16	≤0.001
RB17	4.212±2.123
RB18	0.096±0.014
RB19	0.005±0.001
RB20	0.322±0.015
RB21	0.079±0.016
RB22	6.235±0.624
RB23	2.001±0.526
RB24	0.094±0.010
RB25	8.937±2.698
RB26	6.249±1.451
RB27	5.212±2.144
RB28	2.565±0.781
RB29	1.032±0.233
RB30	72.241±3.125
RB31	68.611±6.312
RB32	47.847±5.781
RB33	48.224±3.873
RB34	18.337±1.542
RB35	36.987±6.418
RB36	43.829±3.541
RB37	28.364±3.765
Fasudil	5.240±3.458

[a] All data in triplicates was used for deriving and represented in Mean±SEM (n=3).

5.5.4 NOX2 inhibition assay

As LPS treatment to HUVE cell lines were found to over express $p47^{PHOX}$, we used this model to study indirectly the effect of test compounds on NOX2 using DCFH-DA fluorescent dye. Activation of NOX2 subunits upon LPS treatment lead to the generation of free radicals and DCFH-DA probe react with the free radicals and emit fluorescent signal which was measured. The cells were treated with the 5 μg/ml of LPS and test compounds were tested at different concentrations from 100 μM-10 nM. The percentage inhibitions for all compounds at different concentrations were used to generate IC_{50} which is presented in **Table 5.13**. All the 37 compounds except **RB1** showed NOX2 inhibition as indicated by their X-ROS IC_{50}s. About 23 compounds were found to be more effective with IC_{50}s <10 μM among which 10 lead compounds (**RB5**-**RB7**, **RB11**-**RB14**, **RB16**, **RB29** and **RB33**) were found promising against NOX2 exhibiting potential inhibition in nanomolar range. Lead compounds **RB7**, **RB14**, **RB16** and **RB29** were found to inhibit X-ROS at submicromolar concentration (<0.1 μM), however as indicated by the ADME predicition, compounds **RB16** and **RB29** could be cardiotoxic as their predicted logHERG IC_{50} was >-5. Further structural insights as discussed in next section could be useful in proceeding further with these compounds.

5.5.5 Binding pattern analyses of active compounds from *in house* library

To evaluate the difference in the potency of these compounds, docking orientations were compared with the crystal ligands for both the targets of ROCK-I and NOX2, lead compounds revealed important hydrogen bonding interactions with Met156, Glu154 and Asp202 in ROCK-I and Ser208, Glu244 and Leu260 in NOX2. The main aim was to get structural insights of the most promising molecule. The compound **RB12** was shown to have highest docking score and fruitful hydrogen bonding interactions in both ROCK-I and NOX2 and in the enzymatic assays, it was found to inhibit ROCK-I with IC_{50} of 357 nM and NOX2 with X-ROS IC_{50} of 817 nM.

Table 5.13 Biological data of NOX2 for the selected BITS molecules

Sr.No	X-ROS IC_{50}(µM) [a]
RB1	>100
RB2	43.530±6.210
RB3	1.671±0.640
RB4	6.120±1.470
RB5	0.254±0.010
RB6	0.200±0.010
RB7	0.038±0.010
RB8	9.641±2.310
RB9	2.765±1.540
RB10	3.637±1.980
RB11	0.599±0.010
RB12	0.817±0.010
RB13	0.333±0.010
RB14	0.012±0.001
RB15	1.792±0.233
RB16	0.006±0.001
RB17	6.963±1.324
RB18	3.438±1.535
RB19	20.176±6.321
RB20	56.752±1.243
RB21	7.256±2.314
RB22	1.198±0.565
RB23	25.046±2.314
RB24	18.414±3.655
RB25	8.836±1.546
RB26	13.937±0.548
RB27	3.304±1.549
RB28	18.197±2.368
RB29	0.077±0.011
RB30	2.853±0.982
RB31	10.753±1.544
RB32	4.454±1.655
RB33	0.792±0.016
RB34	10.251±4.212
RB35	12.031±2.323
RB36	14.454±6.315
RB37	18.216±2.101

[a] All data in triplicates was used for derivingand represented in Mean±SEM.

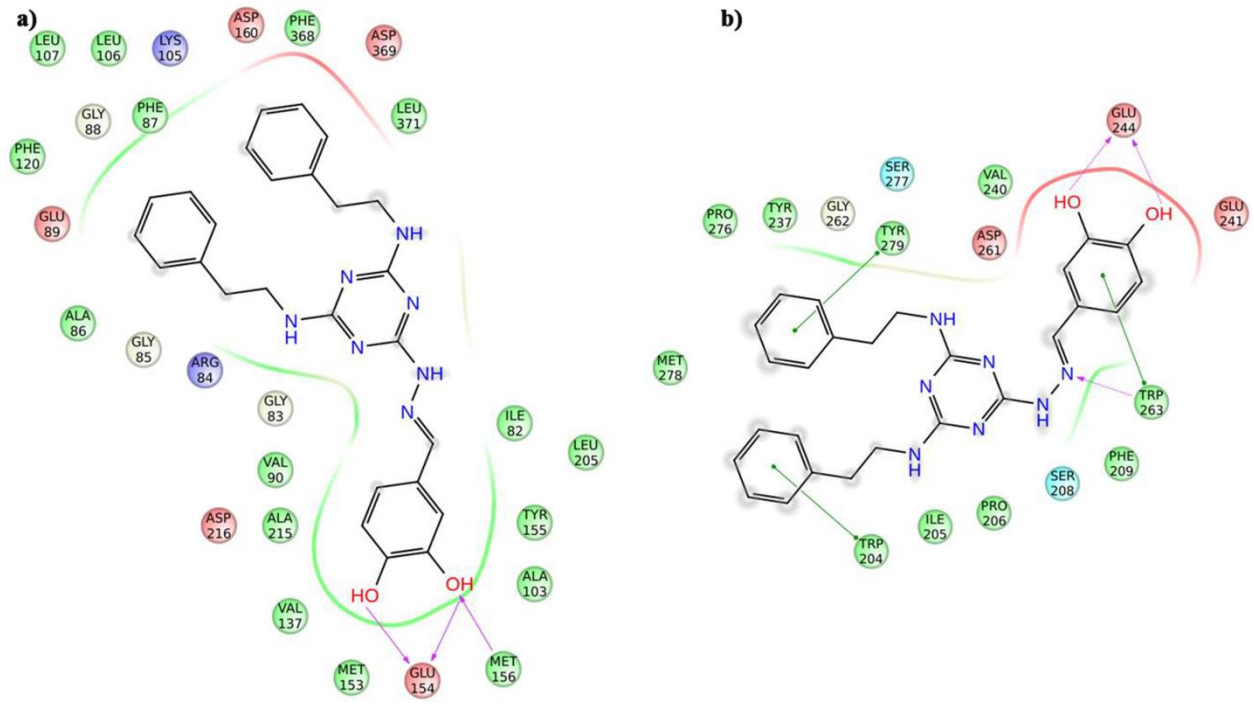

Figure 5.15 Ligand interaction pictures of **RB12** a) ROCK-I and b) $p47^{PHOX}$ active site, pink solid arrow in the interaction picture is Hbond between backbone of the amino acid and the ligand, pink dotted arrow in the interaction picture is Hbond between side chain of the amino acid and the ligand and green solid line indicates the π-π stacking interaction between amino acid and ligand.

Compound **RB12** was found to display docking score of -7.143 kcal mol^{-1} for ROCK-I and -4.346 kcal mol^{-1} for NOX2. **RB12** occupied the hydrophobic pocket in both ROCK-I and NOX2. In ROCK-I two hydroxyl groups on the phenyl ring showed interactions with the Met156 and Glu154. The hydrophobic pocket of ROCK-I around **RB12** consist of Met153, Ala103, Tyr155, Ile82, Leu205, Leu371, Phe87, Phe120, Ala86, Val90 and Ala215, and showed polar contacts with asp216, Glu89, Lys105, Asp160 and Asp369. Whereas, in NOX2 two hydroxyl groups was found to interact with the Glu244. The imino nitrogen atom located in between catechol and triazine ring interacted with Trp263. The two phenyl rings on the other hand showed π-π interactions with Tyr279 and Trp204. These interactions could have stabilised the complex and hence a good docking score was obtained. The benzene ring also showed π-π interaction with Trp263. The hydrophobic pocket of NOX2 was small consisting of Ile205, Pro206, Phe209, Val240, Tyr237 and Pro276 and **RB12** also showed polar contacts with Asp261, Ser277 and Ser208. The 2D ligand **RB12** docking poses are depicted in **Figure 5.15**.

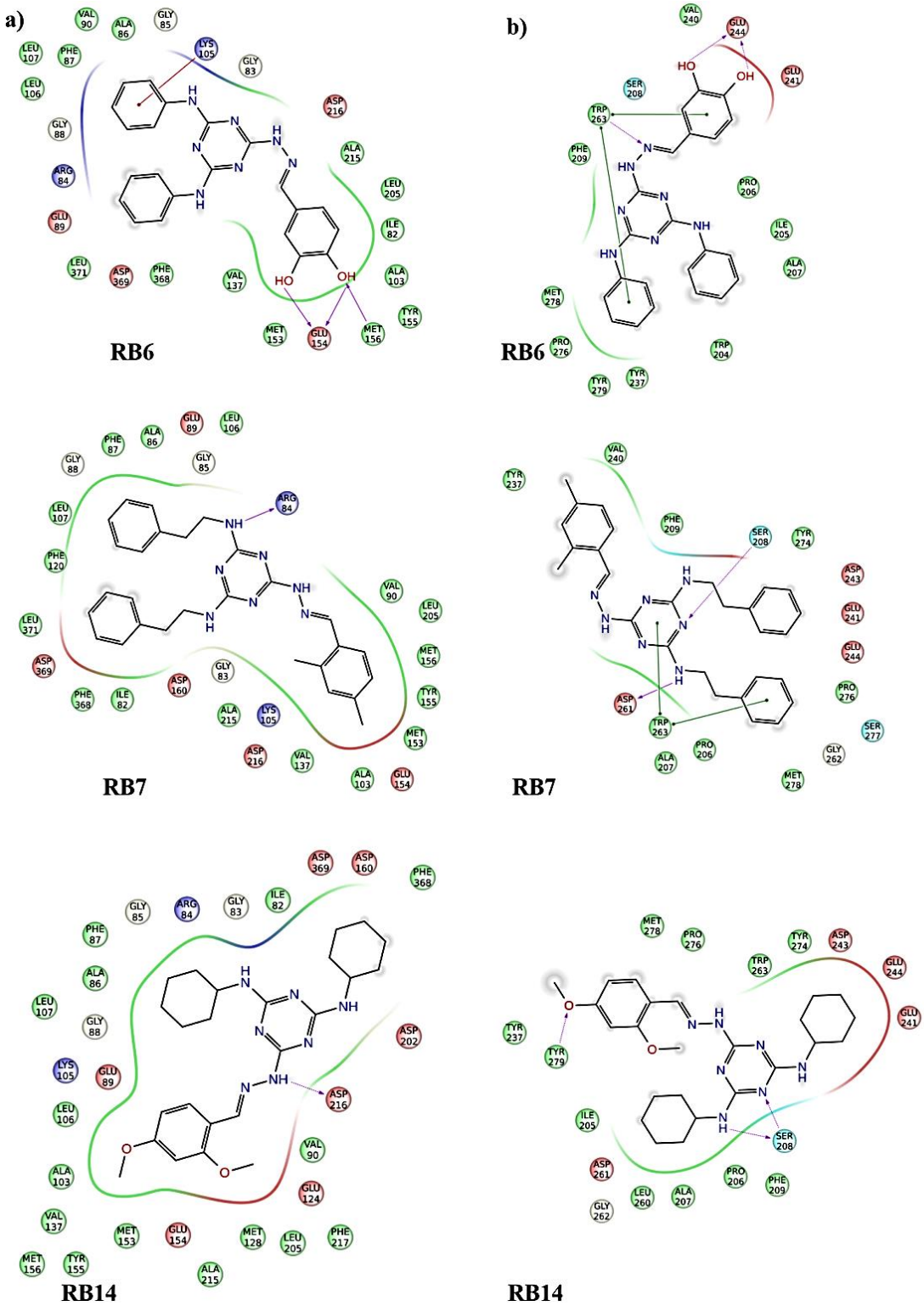

Figure 5.16 Interaction pictures of **RB6**, **RB7** and **RB14** in a) ROCK-I and b) $p47^{PHOX}$ active site, pink solid arrow in the interaction picture is Hbond between backbone of the amino acid and the ligand, pink dotted arrow in the interaction picture is Hbond between side chain of the amino acid and the ligand and green solid line indicates the π-π stacking interaction between amino acid and ligand.

As shown in **Figure 5.16**, binding analyses of other top active compounds like **RB6**, **RB7** and **RB14** showed similar range of activity in ROCK-I. **RB6** showed interactions with Met156, Glu154 and σ-π interaction with Lys105 in ROCK-I and Glu244 and Trp263 and also π-π interaction with Trp263 in NOX2. While **RB7**, through NH and N atom on triazine ring interacted with Arg84 in ROCK-I and Ser208, Asp261 in NOX2. Finally **RB14**, showed amino groups of triazene ring interacting with the Asp216 in ROCK-I and Ser208 and Tyr279 in NOX2.

5.5.6 Thermofluor analysis of ROCK-I

The stabilization effect of ROCK protein in complex with ligand **RB12** was evaluated by measuring the fluorescence of native protein and ligand-protein complex when exposed to hydrophobic residues of the protein. A positive shift in ΔTm of protein-ligand complexes compared with native protein signified better stabilization of protein by the ligand binding. The representative potent compound **RB12** showed a good positive shift when complexed to ROCK-I protein.

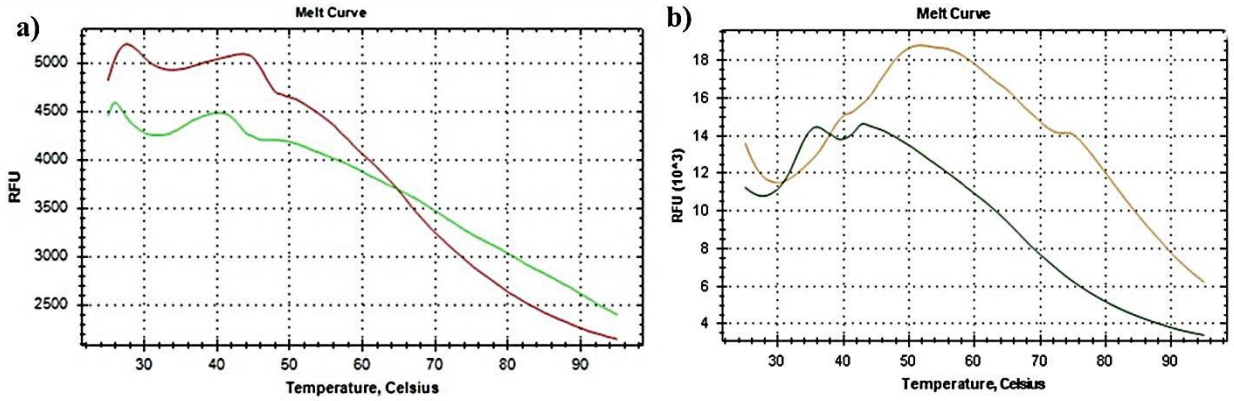

Figure 5.17 Thermofluor assay results for ROCK-I. The data were obtained for a) ROCK-I in the presence (Red peak) and absence (green peak) of **RB12**, b) ROCK-I in the presence (orange peak) and absence (green peak) of Fasudil..

Data analysis for this experiment was simplified using CFX manager V3.0 software that displayed the computed Tm in wells. The native protein showed a Tm of 37.50 ^{0}C, as seen in in **Figure 5.17** shown in red peak whereas protein with **RB12** showed Tm of 42.50 ^{0}C presented as green peak. Usually a Tm shift more than 1 was considered as stabilization effect. Hence **RB12**

with ΔTm shift of $+5^0$C at 1 μM concentration was considered promising. Compared to Fasudil, **RB12** was more effective.

5.6 Conclusion

We utilized computational tools of structure based drug design involving both energy and shape based strategies. E-pharmacophore based approach relied on the knowledge of interaction energies between the ligand and the protein active site, whereas shape based approach relied on the crystal conformation of the bound ligand to generate guassian based shape of the molecule. This chapter demonstrated two design phases for lead identification as dual inhibitiors of ROCK-I and NOX2 and the summary of observation are thus given below.

In design-I, structure based e-pharmacophore and shape modeling was employed to identify structurally diverse, small molecule dual inhibitors for ROCK-I and NOX2 from commercial (Asinex) library. About 30 compounds from different structural classes were identified and all of them except few exhibited dual inhibition of ROCK-I and NOX2. Based on cross evaluation of ADME and toxicity, compound **RA6** was found promising compared to other lead compounds.

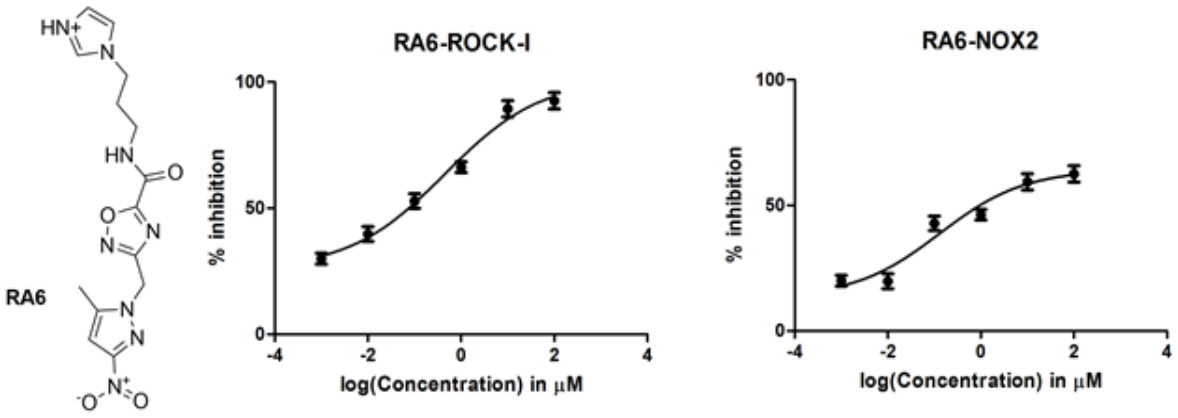

Figure 5.18 Structure of **RA6** and its dose response curve (DRC) drawn for ROCK-I IC_{50} and NOX2 $IC_{50.}$

In design II, we successfully demonstrated that the filters used for design-I was efficient in identifying lead from *in house* library. Top 37 active compounds from four different structural classes were identified as dual inhibitors of ROCK-I and NOX2. **RB12** was found to show good enzyme inhibition and correlated well with docking score and good interaction profile. **RB12** was found to have good ADME and no cardiotoxicity as predicted by Qikprop.

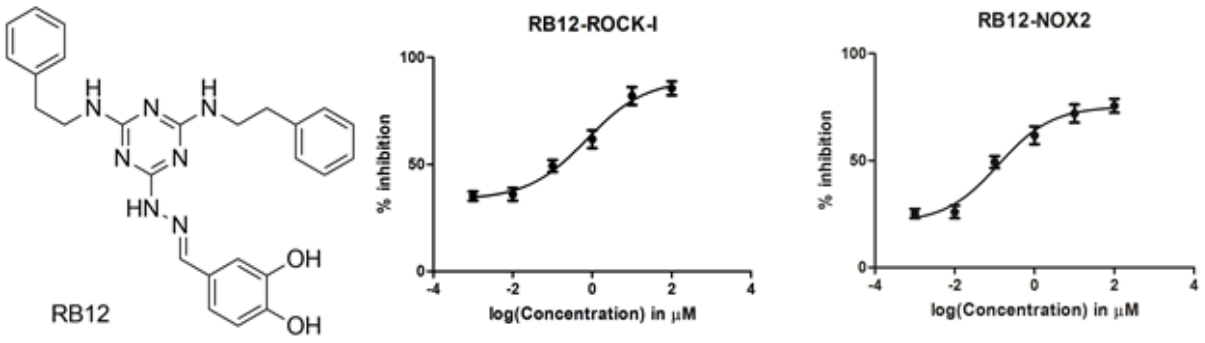

Figure 5.19 Structure of **RB12** and its dose response curve (DRC) drawn for ROCK-I IC_{50} and NOX2 IC_{50}.

Chapter6

Results and discussion: Neuropharmcological screening in Cell based and Animal models

In an ideal situation a structural series of compounds will have unlimited cell permeability, and one can therefore correlate between rank-order enzyme affinity (IC_{50}), and the EC_{50} (effective concentration) in cellular assays which could be equivalent to *in vitro* IC_{50}; where EC_{50} was the concentration of compound that elicit a 50% effect in the cellular or organismal experiment. In practice, however this was rarely a case. Different compounds within a structural series may demonstrate significantly different cell permeability; hence many compounds with good enzyme inhibition may not be good in *in vitro* and may not elicit a cellular effect because they could fail to enter the cell. Likewise compounds could enter the cell freely may be effluxed out of the cell by a variety of active transport mechanisms (e.g multi drug resistant transporter) so that the net effect could be limited to the intracellular concentration of compound. Thus, a lack of correlation between enzymatic inhibition and the cellular effect cannot be viewed as evidence that target enzyme inhibition was not the cause of the observed cellular effects. To overcome this situation, desired protein was overexpressed with a specific induction to get desired results. Importantly, *ex vivo* systems permit direct treatment with pharmacological agents modulating these responses and thus provide as a surrogate therapeutic screening system without recourse to whole animal studies. Also, the whole animal which could overexpress desired proteins in a specific disease models could be used to know the therapeutic efficacy of the compound. In this chapter, section 6.1 and 6.2 describes about cellular studies, 6.3 and 6.4 for *ex vivo* brain slice models and 6.5 reports *in vivo* pharmacological studies.

6.1 *In vitro* cellular assays for ROCK- I and NOX2 dual inhibitors

6.1.1 ROCK-I cellular studies in MeHg induced IMR-32 cell lines

The ROCK signalling pathway has previously been reported to increase cell viability in few cell types, while enhancing apoptotic pathways in other cell lines. The mechanism behind this noticeable ambiguity was largely unknown. To undestand the role of ROCK signalling pathway in cell survival, [Catharine AS., *et al*.,2010] treated various neuroblastoma cell lines with cisplatin, UV, hydrogen peroxide and with novel ROCK inhibitor Y27632 and measured the cell survival 72 h post treatment. The results showed that pharmacological inhibition of ROCK led to significant increase in cell survival in all the treatments. Thus, we employed IMR-32 and re-estimated the expression levels of ROCK-I under MeHg treatment. We found that at 10 μM, there was a >10 times overexpression (**Figure 6.1**) of ROCK-I and hence utilized this system for high throughput screening. We also examined the inhibitory activity of compounds on the *in vitro* growth of MeHg induced human neuroblastoma cell lines (IMR32) for evaluating the effect of lead compounds (**RA1-RA30** and **RB1-RB37**) in cell-based model.

6.1.1.1 ROCK-I cell viabilbity studies

Addition of MeHg at different concentrations elevated ROCK-I gene expression determined using RT-PCR on IMR-32 cell lines (**Figure 6.1**). At 10 μM concentration ROCK-I was over expressed up to 10 fold in comparison to naïve and it showed 50% of the growth (**Figure 6.2**). Dose dependent MeHg effect on survival of IMR-32 cell lines was performed with MTT assay and presented in **Figure 6.2**.

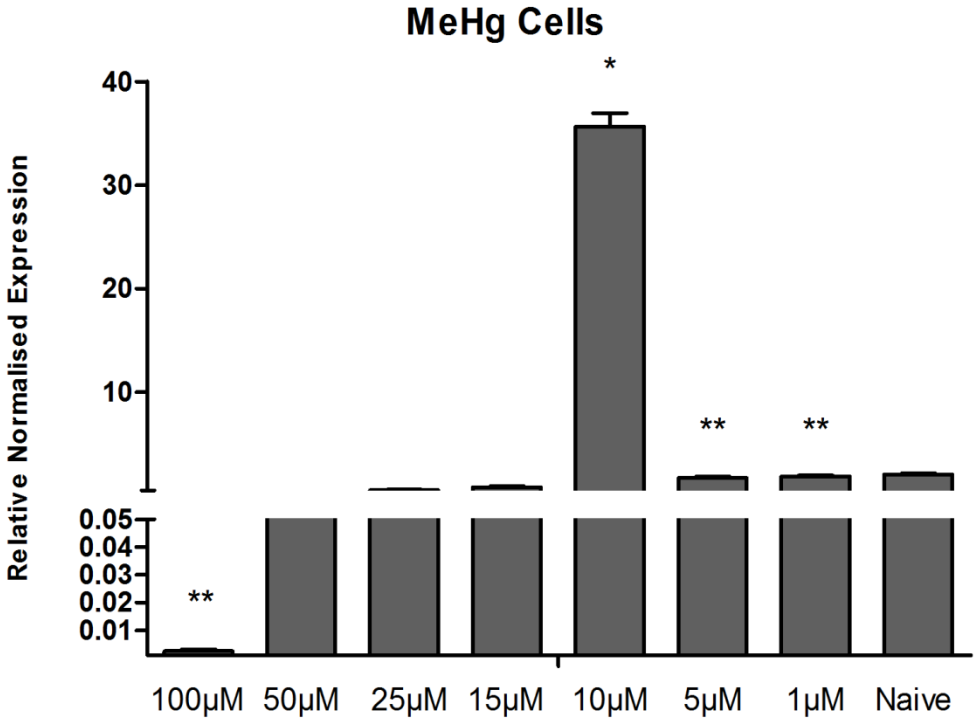

Figure 6.1 Relative normalized expression of ROCK-I in MeHg induced IMR-32 cell lines.

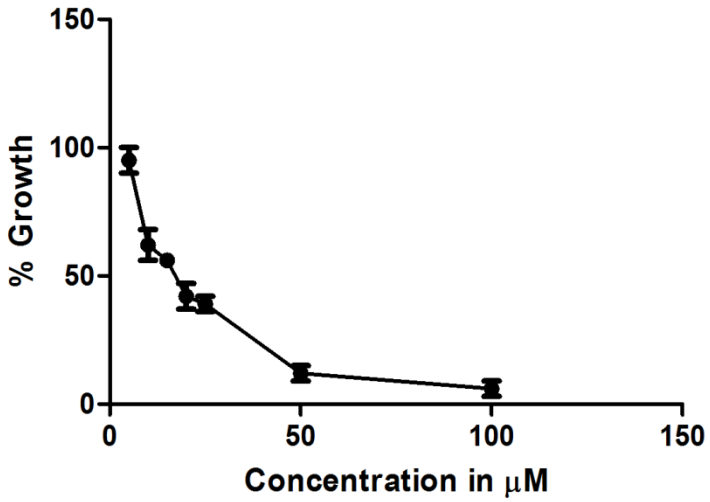

Figure 6.2 Graph represents the % growth of IMR-32 cell lines at different concentrations of MeHg using MTT assay.

Thus IMR-32 cells induced with MeHg were utilized for high-throughput screening of all the designed lead compounds from both Asinex (**RA1**-**RA30**) and *in house* (**RB1**-**RB37**) libraries.

The results of the assays done in triplicates are presented as EC_{50} values in **Table**s **6.1** and **6.2**. Among the Asinex hits (**RA1**-**RA30**), all the compounds except **RA24** exhibited activity in the ROCK-I specific cell system. Compared to Fasudil, a standard ROCK-I inhibitor, four compounds (**RA2**, **RA6**, **RA11** and **RA25**) showed more effectiveness. Lead **RA6** emerged as the most active compound with an EC_{50} of 3 nM compared to all other hit compounds including Fasudil whose EC_{50} was 23 nM. When compared to ROCK-I IC_{50} and cell based EC_{50}, most of the potent ROCK-I inhibitors exhibited good cellular activity except **RA1**, **RA4** and **RA13**.

On the other hand, the *in house* library had compounds (**RB1**-**RB37**) when evaluated in ROCK-I specific cellular assay, all except **RB5** and **RB15** were found effective in inhibiting MeHg induced IMR-32 cells. Compounds with EC_{50} in nanomolar range included **RB1**-**RB4**, **RB8**, **RB9**, **RB12**, **RB13**, **RB16**, **RB19**, **RB20**, **RB22**-**RB24**, **RB29**-**RB32** and **RB36**. It was surprising to note that **RB13** which was inactive in ROCK-I inhibition showed promising activity in cellular assay. This could be due to the involvement of a different mechanism other than ROCK-I.

6.1.1.2 Cytotoxicity assay on HEK293 cells

It was important to perform cytotoxicity evaluation of lead compounds to indicate their specificity towards diseased conditions. HEK293 cells were human embryonic kidney cells, usually employed for assessing cytotoxicity. All the 67 compounds (**RA1**-**RA30** and **RB1**-**RB37**) were estimated for possible cytotoxicity utilizing MTT assay at similar range of concentrations (100 μM- 1 nM) to derive CC_{50}s. The results are presented in **Table**s **6.1** and **6.2**. In the Asinex list of leads, 13 compounds that were found to be cytotoxic included **RA1**, **RA4**, **RA8**, **RA10**, **RA12**, **RA13**, **RA16**-**RA18**, **RA24**, **RA26**, **RA28** and **RA29**. Compound **RA6** was found to be non- cytotoxic upto the highest concentration tested (100 μM). Among the *in house* library leads, only eight compounds were cytotoxic that included **RB4**-**RB7**, **RB11**, **RB13**, **RB15** and **RB18**. It was found that **RB22** was not cytotoxic until 100 μM.

Table 6.1 Biological data of ROCK-I for the selected Asinex molecules

Sr.No	$CC_{50}(\mu M)^a$	$EC_{50}(\mu M)^b$	SI (CC_{50}/EC_{50})
RA1	0.056±0.012	59.650±3.661	0.001
RA2	0.047±0.002	0.018±0.001	2.612
RA3	0.547±0.013	0.197±0.052	2.762
RA4	1.151±0.562	33.470±3.211	0.034
RA5	64.460±8.748	2.232±1.402	28.878
RA6	>100	0.003±0.001	>100
RA7	20.410±5.969	0.720±0.061	28.344
RA8	0.012±0.001	0.198±0.092	0.062
RA9	1.359±0.636	0.165±0.037	8.211
RA10	0.052±0.001	0.101±0.073	0.516
RA11	0.075±0.001	0.005±0.003	14.264
RA12	0.044±0.001	0.057±0.001	0.778
RA13	0.066±0.001	35.420±5.122	0.001
RA14	16.020±3.145	1.374±0.051	11.659
RA15	41.780±4.611	16.970±2.69	2.467
RA16	0.012±0.001	5.092±1.413	0.002
RA17	0.061±0.001	0.859±0.055	0.078
RA18	0.004±0.001	2.073±1.056	0.002
RA19	47.680±8.742	0.099±0.010	>100
RA20	14.440±4.353	5.039±0.621	2.872
RA21	1.616±0.618	0.092±0.060	17.493
RA22	80.510±7.639	2.113±0.629	38.107
RA23	10.390±2.564	0.384±0.069	27.028
RA24	0.801±0.015	>100	0.007
RA25	0.005±0.001	0.002±0.001	1.861
RA26	0.091±0.001	0.093±0.001	0.976
RA27	57.760±6.316	0.034±0.001	>100
RA28	0.117±0.001	6.402±1.745	0.012
RA29	0.074±0.001	2.365±0.541	0.033
RA30	72.160±6.877	0.796±0.075	90.654
Fasudil	1.616±0.542	0.023±0.011	68.765

[a]- Cell cytotoxicity of compounds on HEK-293 cell lines, [b]- effective concentration of compounds on MeHg induced IMR-32 cell lines; All data presented as Mean±SEM (n=3).

Table 6.2 Biological data of ROCK-I for the selected BITS molecules

Sr.No	$CC_{50}(\mu M)^a$	$EC_{50}(\mu M)^b$	SI (CC_{50}/EC_{50})
RB1	8.116±0.540	0.257±0.010	31.555
RB2	0.075±0.010	0.004±0.001	18.101
RB3	0.750±0.010	0.432±0.010	1.738
RB4	0.016±0.010	0.219±0.010	0.075
RB5	0.047±0.010	>100	0.0001
RB6	1.758±0.560	41.270±6.350	0.042
RB7	0.076±0.010	2.392±0.560	0.031
RB8	0.067±0.010	0.032±0.010	2.112
RB9	0.139±0.010	0.032±0.010	4.408
RB10	3.569±0.987	1.873±0.560	1.905
RB11	0.091±0.010	9.705±2.350	0.009
RB12	30.570±5.840	0.094±0.001	323.561
RB13	0.116±0.010	0.139±0.010	0.834
RB14	10.330±3.140	2.590±0.980	3.986
RB15	0.922±0.010	>100	0.006
RB16	0.027±0.010	0.004±0.001	6.854
RB17	7.885±1.690	6.780±0.610	1.163
RB18	0.446±0.010	15.100±1.230	0.029
RB19	4.904±1.350	0.852±0.010	5.758
RB20	11.200±3.280	0.630±0.010	17.766
RB21	2.322±1.100	1.624±0.140	1.429
RB22	>100	0.751±0.010	>100
RB23	4.429±2.140	0.018±0.010	242.419
RB24	40.990±5.980	0.665±0.010	61.676
RB25	50.200±5.470	13.490±2.650	3.721
RB26	56.570±2.430	11.360±1.540	4.979
RB27	55.490±12.560	22.230±3.540	2.496
RB28	49.930±6.310	34.030±6.320	1.467
RB29	41.860±5.420	0.887±0.010	47.216
RB30	55.320±3.540	0.701±0.010	78.955
RB31	62.210±4.650	0.197±0.010	316.282
RB32	35.640±5.210	0.268±0.010	132.738
RB33	37.160±6.310	27.670±6.540	1.343
RB34	43.580±2.350	12.880±3.250	3.383
RB35	62.230±1.470	13.480±3.120	4.616
RB36	57.370±5.780	0.778±0.010	73.711
RB37	51.910±8.460	6.792±0.110	7.643

[a]- Cell cytotoxicity of compounds on HEK-293 cell lines, [b]- effective concentration of compounds on MeHg induced IMR-32 cell lines; All data presented as Mean±SEM (n=3).

6.1.1.3 Selectivity index analyses

In this ROCK-I based cell system, compounds were able to reduce the cell proliferation in a dose -dependent manner and their EC_{50} values ranged from 3 nM to 33 µM for the 30 molecules selected from the Asinex database. The dose-dependent suppressive effect of compounds on cell proliferation was accompanied by a marked inhibition of ROCK1. In HEK 293 cells compounds displayed no cytotoxicity and it ranged from 1.15 µM to 428.2 µM. The selectivity index ($SI=CC_{50}/EC_{50}$) was a comparison of the amount of the therapeutic agent that cause the biological effect to the amount that cause toxicity to understand specificity. As shown in **Figure 6.3**, the SI of **RA2**, **RA3**, **RA5**, **RA6**, **RA7**, **RA9**, **RA11**, **RA14**, **RA15**, **RA19**, **RA20**, **RA21**, **RA22**, **RA23**, **RA25**, **RA27** and **RA30** were found >1. (**Figure 6.3**) Among these **RA6**, **RA19**, **RA27** and **RA30** SIs were higher because of their less toxicity and more therapeutic capacity. For remaining compounds the SI ranged from 2.4 to 480.1. **RA6** emerged as a good ROCK-I inhibitor with IC_{50} <1 nM and EC_{50} of 3 nM in cell based study.

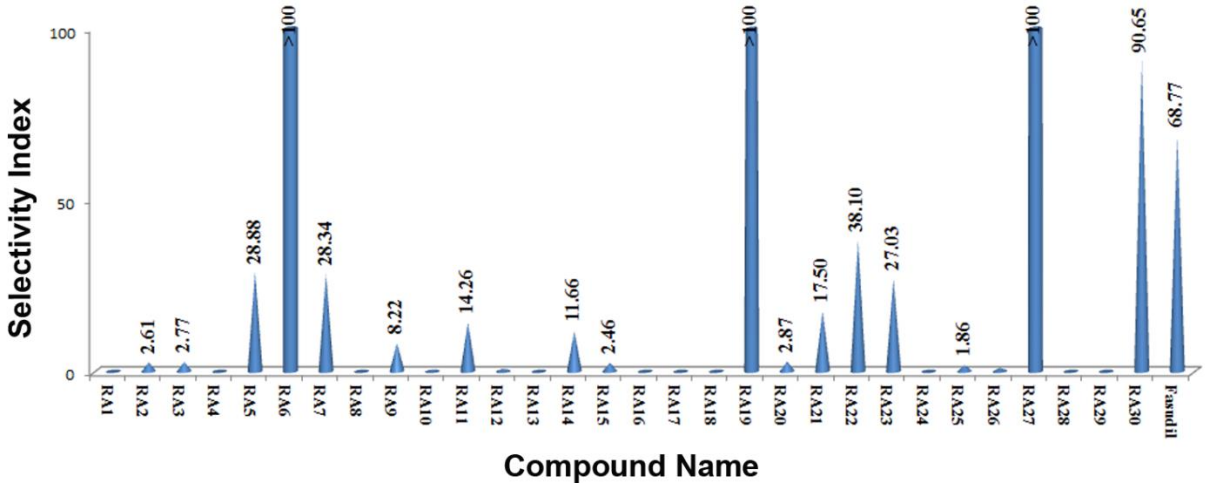

Figure 6.3 Graph represents SI which is a ratio drawn from CC_{50}/EC_{50} for ROCK-I Asinex molecules.

For the 37 *in house* molecules EC_{50} values ranged from 4 nM to 59 µM. In HEK 293 system compounds displayed no cytotoxicity and CC_{50} ranged from 16.5 nM to >100 µM. As shown in **Figure 6.4**, SI of **RB12**, **RB22**, **RB23**, **RB31** and **RB32** were >100, which were high because of less toxicity and more therapeutic capacity. For remaining compounds the SI ranged lower. **RB12** showed good ROCK-I inhibition at IC_{50} of 357 nM, EC_{50} of 94 nM. **RB6** was more effective than **RB12.** The most active molecules **RA6** and **RB12** in *in vitro* enzymatic and

cellular assay were further taken up for additional assays to evaluate their neuropharmacological effect.

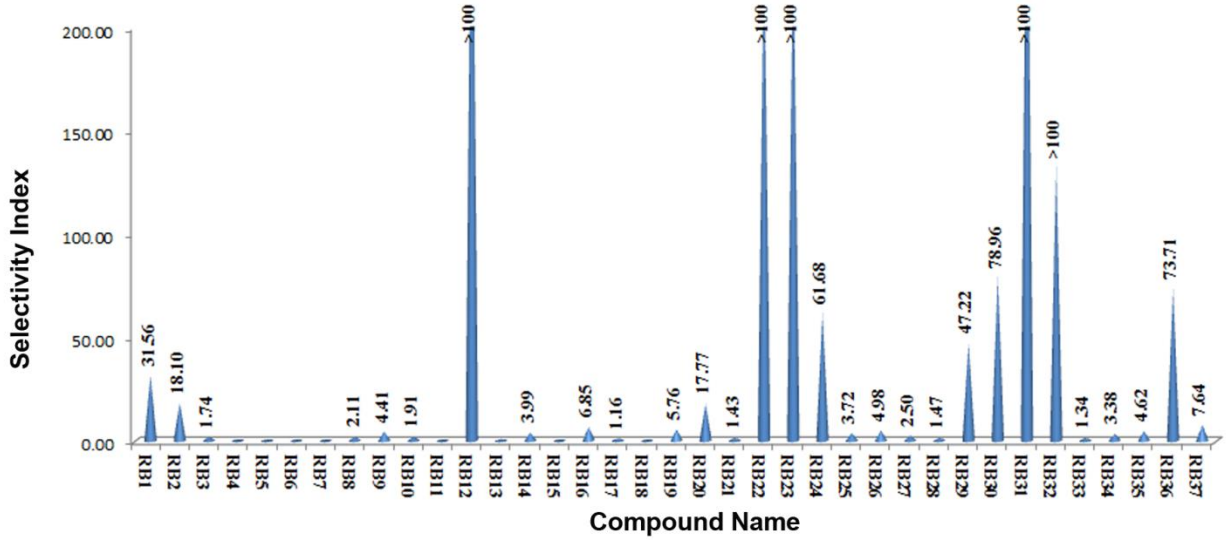

Figure 6.4 Graph represents the SI which is a ratio drawn from CC_{50}/EC_{50} for ROCK-I BITS molecules.

6.1.1.4 Clonogenic assay

The compounds (**RA6**, **RA27**, **RB12** and **RB31**) which exhibited good selectivity index were taken up further to evaluate in clonogenic assay. Clonogenic assay was an effective method for the determination of single cell proliferation capacity, thereby retaining its reproductive ability to form a large colony or clone (**Figure 6.5**). We found that IMR32 cells were able to form colonies in response to exposure to compounds compared to those without any treatment. In this assay, **RA6** (SF= 8.836) made more significant number of colonies compared to Fasudil (SF= 3.136) and **RA27** (SF= 2.916) treated systems. Whereas, **RB12** and **RB31** (SF= 9.801 and 2.1) made more significant number of colonies compared to Fasudil (SF= 3.136) treated systems. This assay confirmed that **RA6** and **RB12** found to ameliorate the toxic conditions in cells than Fasudil. **RA27** and **RB31** found to show good proliferative capacity which was supported by clonogenic assay and proliferative studies, but have not shown good enzymatic inhibition. **RA6** and **RB12** found to survive MeHg toxicity up to 88.3% and 98% respectively in comparison with **RA27** and **RB31** by inhibiting cellular ROCK-I which primarily involves in the cell proliferation and mitotic spindle fiber formation in the cell.

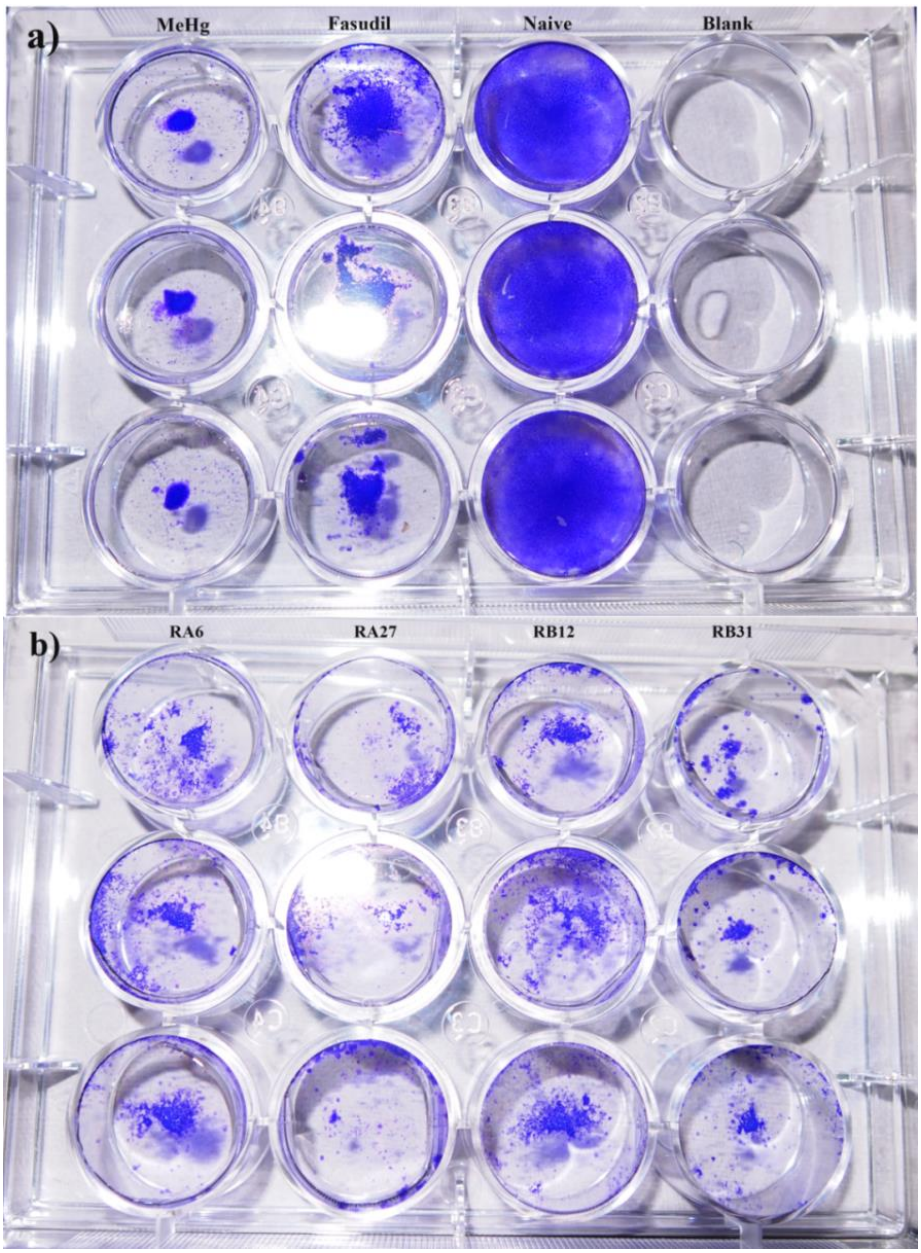

Figure 6.5 Clonogenic assay of the compounds at 1μM after treatment with MeHg at 10 μM.

6.1.1.5 Cell motility studies

Cell migration is a complex phenomenon that requires coordination of numerous cellular processes. As shown in **Figure 6.6**, Rho kinase mainly promotes myosin II activity by inhibiting the myosin light chain (MLC) phosphatase and phosphorylating the myosin light chain. This in turn favors the assembly of actin myosin filaments that generate the tensile strength underlying the RhoA-ROCK associated dynamic events in numerous cell types. Administration of ROCK-I

inhibitors like Fasudil was reported to induce the relaxation of these cells by suppressing MLC phosphorylation and promote the cellular motility. The overexpression of ROCK-I or activation of ROCKI function by expression of constitutively active RhoA could promote MLC phosphorylation in cortical bundles.

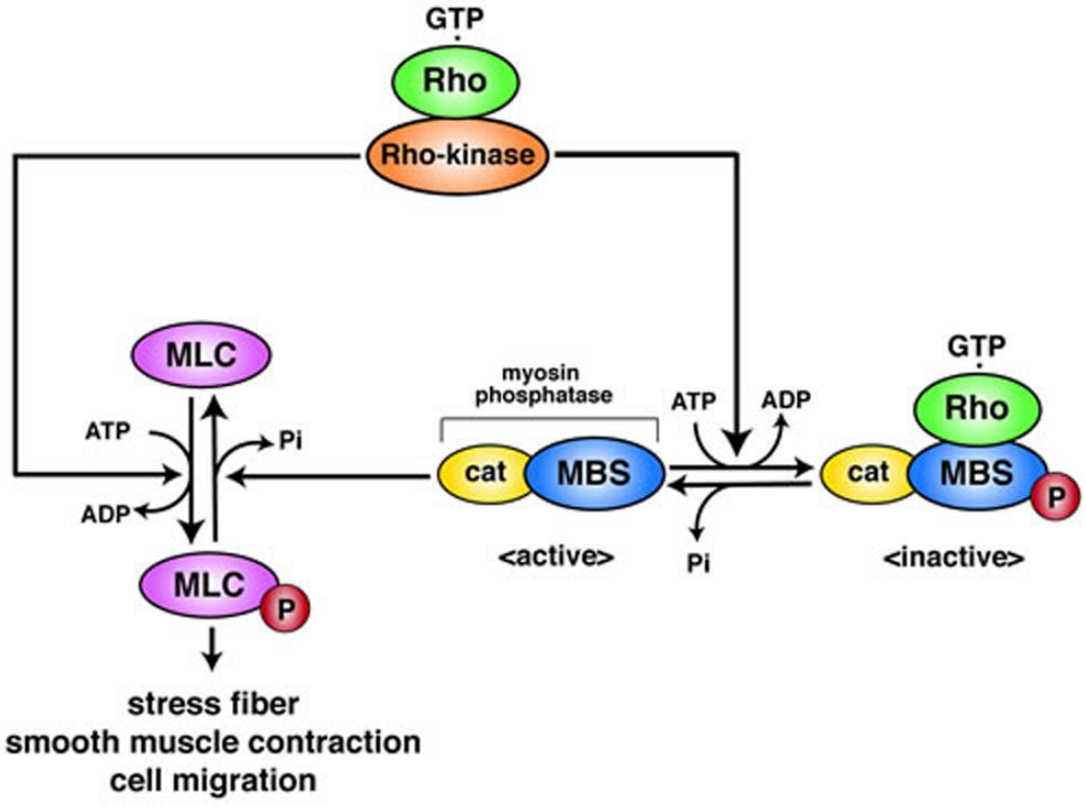

Figure 6.6 Model for regulation of MLC phosphorylation by Rho, Rho-kinase, and myosin phosphatase. MLC, myosin light chain; cat, catalytic subunit; MBS, myosin-binding subunit [Ren, X. D *et al.*, 1999].

In the present study, phosphorylation of MLC by ROCK-I led to invasion or cellular motility in IMR32 cells and this effect was reversed by blockade of ROCK-I function with Fasudil and **RA6** and **RB12** as shown in **Figure 6.7**. We concluded that the motility of neuroblastoma cells was due to activation of ROCK-I function which altered the organization of MLC, as many other coordinated changes in the actin machinery were needed to drive cell motility (**Figure 6.7**). This further reascertained that the designed leads were affecting ROCK-I pathway.

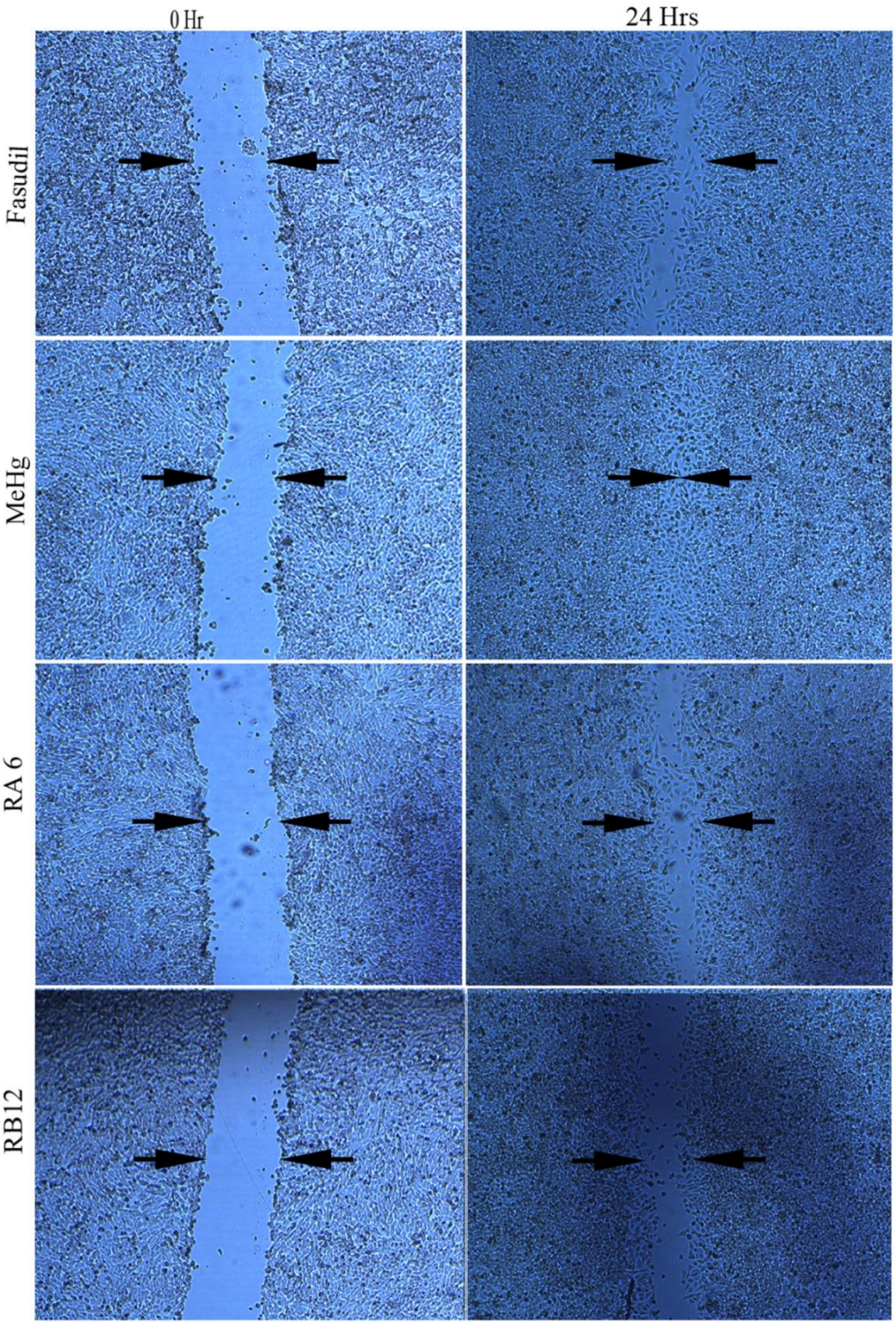

Figure 6.7 Cell motility assay for MeHg induced IMR-32 cell lines. Migration of cells was assessed after 24h.

6.1.1.6 Gene expression analyses in MeHg induced IMR-32 cell lines

The systematic study of simultaneous changes in gene expression for several pro-inflammatory cytokines in MeHg induced IMR-32 was performed using RT gene expression studies.

Comparing the MeHg induced and untreated cells, IL-6, IL1-β and TNF-α expression showed a statistically significant upregulation. **RA6** and **RB12** at 1 μM concentration when compared with Fasudil also at 1 μM were able to reduce significantly the expressions of IL-6, IL-1β, NFκB, and TNF-α. However, neutralization of pro-inflammatory cytokines, especially TNF-α, was a clear indication of the translocation of $p47^{PHOX}$ and $p67^{PHOX}$ from cytosol. On the other hand, over expression of TNF-α and other pro inflammatory cytokines were also found to be induced by the RhoA-ROCK mediated pathway. The decrease in expression of inflammatory mediators by **RA6** and **RB12** and Fasudil treated cells could be concluded to be due to the inhibition of ROCK-I and $p47^{PHOX}$ in MeHg induced cells as shown in **Figure 6.8**.

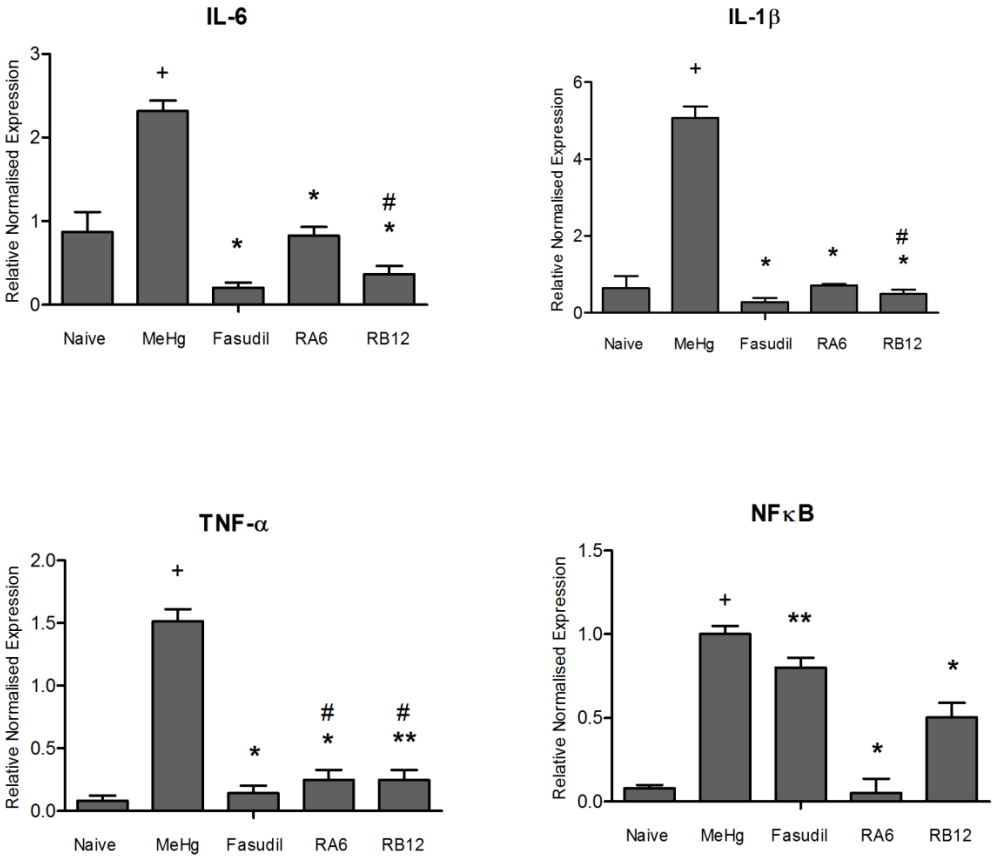

Figure 6.8 Normalised gene expression levels of proinflammatory cytokines in MeHg induced IMR32 cell lines (n=3). The mRNA expression values were given as mean±SD normalised to GAPDH levels in each sample. Y-axis values represent the number of mRNA copies relative to the number of GAPDH copies in the sample. A significant reduction of IL-6, IL-1β and NFκB (*P<0.05), TNF-α (**P<0.01) in Fasudil treated cells compared to **RA6** and **RB12**, + represents the significance of MeHg in comaparison with the naive. # represents the significance in comparison with the Fasudil to **RA6** and **RB12** at 95% confidence intervals.

6.1.2 NOX2 specific studies in LPS induced HUVE cell lines

6.1.2.1 NOX2 overexpression in LPS induced HUVE cell lines

The NOX2 signaling pathway has previously been reported to be the source for ROS involved in the cell death and astrocyte survival. The mechanism behind this noticeable ambiguity was largely unknown. To conclude the role of ROCK signaling pathway in cell survival, and the ROS production in HUVE cells with LPS treatment at different concentrations and when measured the cell survival and $p47^{PHOX}$ gene expression analyses 3 h post treatment confirmed that $p47^{PHOX}$ was overexpressed when induced with LPS (shown in **Figure 5.7**, Chapter 5). Thus we examined the inhibitory activity of designed compounds on the *in vitro* growth of LPS induced human umbilical vein endothelial cell lines (HUVEC) to assess the cellular activity of NOX2 inhibitors.

Addition of LPS at different concentrations elevated NOX2 gene expression determined using RT-PCR on HUVE cell lines. At 5 µg/ml concentration NOX2 was overexpressed up to 10 fold in comparison to naïve and it showed about 50% of the growth (**Figure 6.9**). Dose-dependent LPS effect on survival of HUVE cell lines was performed with MTT assay. Hence a protocol was designed to test the designed compounds in LPS induced HUVEC.

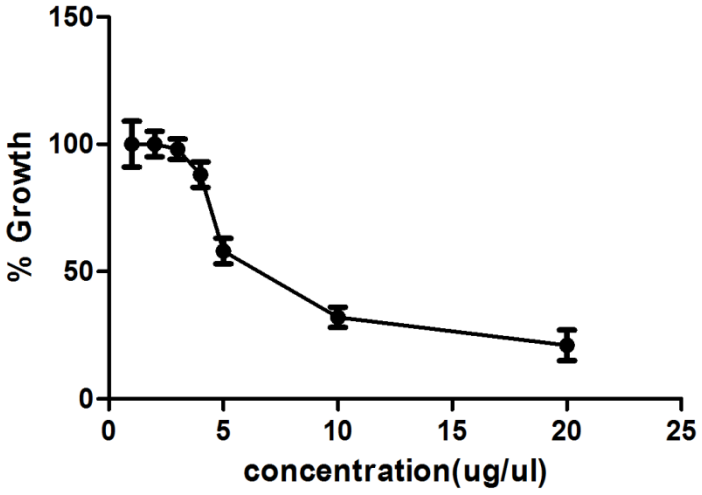

Figure 6.9 Graph represents the % growth of HUVE cell lines at different concentrations of LPS using MTT assay.

6.1.2.2 NOX2 cell viabilbity studies

The designed lead compounds from Asinex (**RA1**-**RA30**) and *in house* (**RB1**-**RB37**) libraries were evaluated in the NOX2/$p47^{PHOX}$ specific cellular system at concentrations from 100 μM-1 nM. The results are presented as quantified EC_{50} values (**Table 6.3**). Among the 30 designed leads from Asinex database except **RA24**, all the compounds to be effective. About 26 compounds exhibited EC_{50}s <10 μM out of which 17 compounds revealed potential at nanomolar concentration. Fasudil was also found promising in this assay with EC_{50} of 18 nM and none of the Asinex leads were as effective as Fasudil. Comparing the results with X-ROS activity discussed earlier (section 5.4.4.1), compounds **RA5**, **RA9** and **RA16** that showed nanomolar X-ROS activity, were found to exhibit EC_{50}s in micromolar concentration except **RA9** whose EC_{50} was 165 nM. Compounds **RA3**, **RA6**, **RA19**, **RA27** and **RA30** were found better in the cellular activity than X-ROS inhibition, while compounds **RA14-RA15** and **RA28** were better inhibitor of X-ROS than cellular activity. Two compounds **RA17** and **RA23** which were ineffective in X-ROS assay were found promising in the cellular activity with EC_{50} of 859 nM and 384 nM respectively (**Table 6.3**). Thus, it was worth investigating the lead compounds in the LPS-induced HUVEC system for both X-ROS and cellular activity to understand the usefulness of the designed compounds.

Table 6.3 Biological data of NOX2 for the selected Asinex molecules

Sr.No	$EC_{50}(\mu M)$ [a]	$SI(CC_{50}$ [b]$/EC_{50})$
RA1	9.650±1.214	0.006
RA2	0.483±0.011	0.099
RA3	0.198±0.054	2.767
RA4	33.472±5.477	0.034
RA5	2.232±1.198	28.881
RA6	0.303±0.021	>100
RA7	0.727±0.212	3.347
RA8	0.199±0.044	0.063
RA9	0.165±0.017	8.216
RA10	0.102±0.054	0.516
RA11	0.531±0.024	1.426
RA12	0.057±0.003	0.771
RA13	35.426±6.545	0.002
RA14	3.374±1.354	0.302
RA15	16.974±5.367	2.462
RA16	5.092±2.587	0.002
RA17	0.859±0.041	0.071
RA18	2.073±1.022	0.002
RA19	0.099±0.003	47.125
RA20	5.034±1.022	2.871
RA21	0.092±0.021	17.497
RA22	2.113±1.034	38.102
RA23	0.384±0.054	27.029
RA24	>100	0.008
RA25	0.028±0.017	18.642
RA26	0.094±0.010	0.977
RA27	0.347±0.145	>100
RA28	6.402±1.656	0.018
RA29	2.365±1.027	0.032
RA30	0.796±0.019	90.653
Fasudil	0.018±0.017	91.247

[a] Effective concentration of compounds on LPS induced HUVE cell lines presented as Mean±SEM (n=3), [b] CC_{50} values were obtained from Table 6.1.

Similar studies on the 37 leads designed from *in house* library was also performed and analysed as presented in **Table 6.4**. All the 37 compounds except **RB5** and **RB15** were found to be

effective in this assay. About 25 compounds were found to be effective with EC_{50} <10 μM, out of which 15 compounds were active in nanomolar range EC_{50} ranging from 18 nM-857 nM. Compunds **RB4**, **RB8**, **RB9**, **RB12**, **RB16** and **RB23** were found to be effective in with EC_{50} <100 nM. Among these except **RB12** all others were predicted to be cardiotoxic. Comparing these results with X-ROS activity, we found that **RB5** and **RB15** were inactive in this test were promising in X-ROS inhibition with IC_{50}s of 254 nM and 1.79 μM respectively, while **RB1** which was ineffective in X-ROS inhibition showed EC_{50} of 2.59 μM in this assay. Activity of compounds **RB12**, **RB13**, **RB16** and **RB29** were consistent in both X-ROS assay and the cellular effectiveness, but compounds **RB6**, **RB7**, **RB11** and **RB14** were better effective in X-ROS inhibition than celluar activity. Thus, **RB12** with no implication on cardiotoxicity and having passed the drug-likeliness properties emerged as the promising lead in the assay consistent with its effectiveness against X-ROS production.

6.1.2.3 Selectivity index analyses

In this NOX2 specific cell system compounds were able to reduce the cell proliferation in a dose-dependent manner and their EC_{50} values were found torange from 92 nM to 35 μM for 30 Asinex molecules. The dose-dependent suppressive effect of compounds on cell proliferation could be due to marked inhibition of NOX2. Cytotoxicity results as reported in **Table 6.1** was utilized to calculate selectivity index ($SI=CC_{50}/EC_{50}$) for knowing selectivity towards therapeutic effect and toxicity. As shown in **Figure 6.10** the SIs of **RA6**, **RA19**, **RA27** and **RA30** were found very high because of its less toxicity and more therapeutic capacity. **RA6** showed good NOX2 X-ROS inhibition at IC_{50} of 2.853 μM, EC_{50} of 303 nM and SI of 753 and emerged as the most potential lead from Asinex set.

Table 6.4 Biological data of NOX2 for the selected BITS molecules

Sr.No	$EC_{50}(\mu M)^{a}$	SI ($CC_{50}{}^{b}/EC_{50}$)
RB1	2.591±0.989	19.376
RB2	1.624±0.647	34.835
RB3	15.100±2.314	3.675
RB4	0.091±0.018	0.182
RB5	>100	<0.001
RB6	41.277±5.852	0.043
RB7	2.392±0.634	0.032
RB8	0.031±0.017	2.112
RB9	0.031±0.019	4.408
RB10	1.873±0.955	1.905
RB11	9.705±0.114	0.009
RB12	0.088±0.016	>100
RB13	0.139±0.014	0.478
RB14	2.591±0.981	0.054
RB15	>100	0.021
RB16	0.004±0.001	23.179
RB17	6.780±0.564	1.163
RB18	15.100±5.325	0.029
RB19	0.852±0.011	5.759
RB20	0.630±0.014	0.106
RB21	1.624±0.312	0.085
RB22	0.751±0.013	>100
RB23	0.018±0.011	4.961
RB24	0.665±0.012	61.676
RB25	13.491±2.353	1.498
RB26	11.364±6.144	2.339
RB27	22.237±1.125	1.597
RB28	34.038±7.856	1.174
RB29	0.887±0.017	24.661
RB30	0.701±0.012	21.869
RB31	0.197±0.011	163.765
RB32	0.268±0.014	58.251
RB33	27.671±5.415	1.343
RB34	2.392±0.986	18.219
RB35	13.494±3.227	4.613
RB36	11.367±2.318	5.051
RB37	1.873±0.599	27.719

[a]- Effective concentration of compounds on LPS induced HUVE cell lines and all data in Mean±SEM (n=3), [b] CC_{50} values were obtained from Table 6.1.

On closer look of **RA6** we found the compound inhibiting NOX2 as predicted in the *in silico* approach. LPS over expressed $p47^{PHOX}$ at gene level which was the main subunit to activate NOX2 complex. This led to generation of free radicals and further cell death. When induced cells were treated with LPS and **RA6**, they ameliorated LPS damage to the cells. Hence **RA6** was found to protect the cells from toxin induced cell damage.

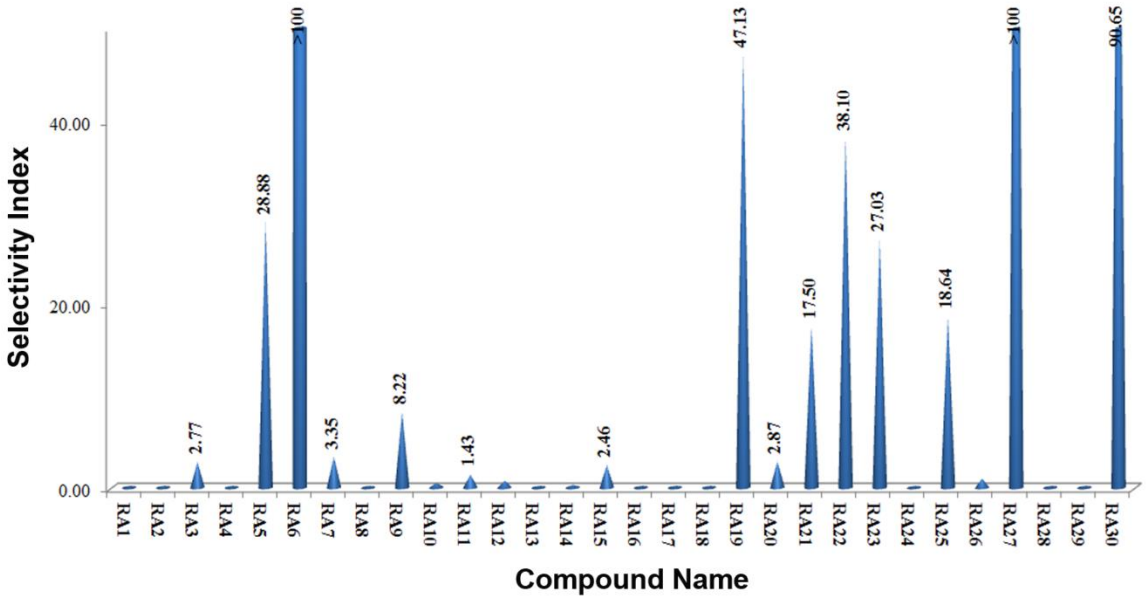

Figure 6.10 Graph represents the SI which is a ratio drawn from CC_{50}/EC_{50} for NOX2 Asinex molecules.

With regard to 37 *in house* molecules, EC_{50} values ranges from 4 nM to 41 µM better than Asinex hits. In HEK293 system, compounds displayed no cytotoxicity and it ranged from 16 nM to 62 µM. As shown in **Figure 6.11**, **RB12** and **RB31** SIs were high as 429.40, and 163.76 because of less toxicity and more therapeutic capacity. Based on the selectivity of the leads, **RB12** seemed to be better than **RB31** due to its greater potency in X-ROS inhibition (357 nM), better EC_{50} of 88 nM, no cytotoxicity and cardiotoxicity implications were observed.

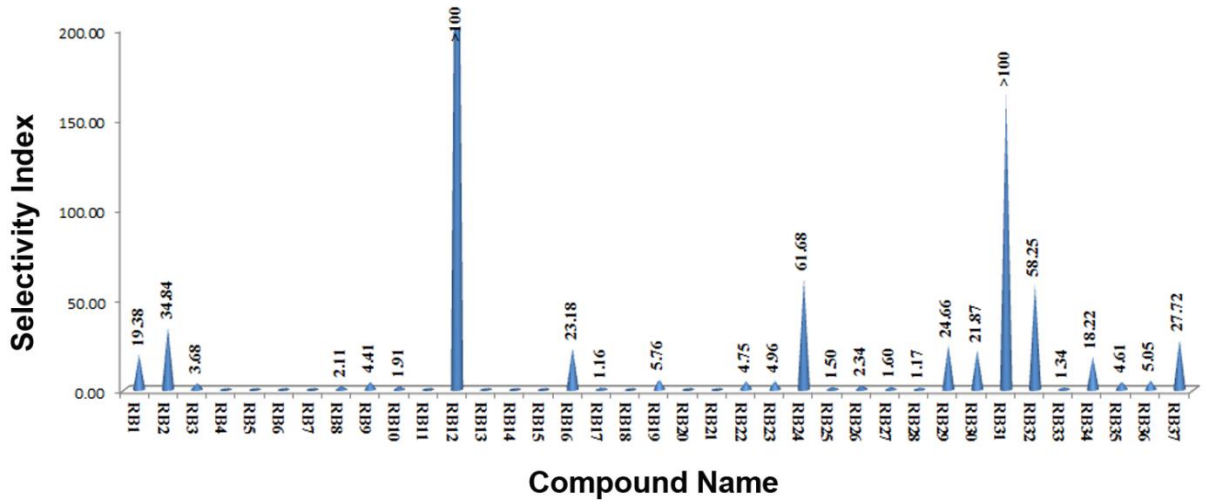

Figure 6.11 Graph represents the SI which is a ratio drawn from CC_{50}/EC_{50} in NOX2 for BITS molecules.

6.1.2.4 Gene expression analyses in LPS induced HUVE cell lines

LPS induced HUVE cells overexpressed ROCK-I and $p47^{PHOX}$, and when treatment with **RA6** and **RB12** was found to inhibit the proinflammatory gene expressions significantly compared to LPS induced cells. The proinflammatory cytokines IL-6, IL1β and TNF-α, and NFκB expression were analysed by real time PCR studies. Comparing LPS induced cells to the naïve cells, the cytokine expressions were found upregulated with statistical significance (**Figure 6.12**). **RA6, RB12** and Fasudil were able to reduce significantly the expressions of IL-6, IL-1β and TNF-α. The inhibition of proinflammatory cytokine TNF-α, was a clear indication of the translocation of $p47^{PHOX}$ and $p67^{PHOX}$ from cytosol. On the other hand, over expression of TNF-α and other pro inflammatory cytokines were also found to be induced by the RhoA-ROCK mediated pathway. As shown in **Figure 6.12**, the decrease in expression of inflammatory mediators by **RA6**, **RB12** and Fasudil treated cells could be concluded to be due to the possible inhibition of ROCK-I and p47 PHOX also in LPS induced cells. This was in consistent to the results with MeHg induced IMR-32 cells.

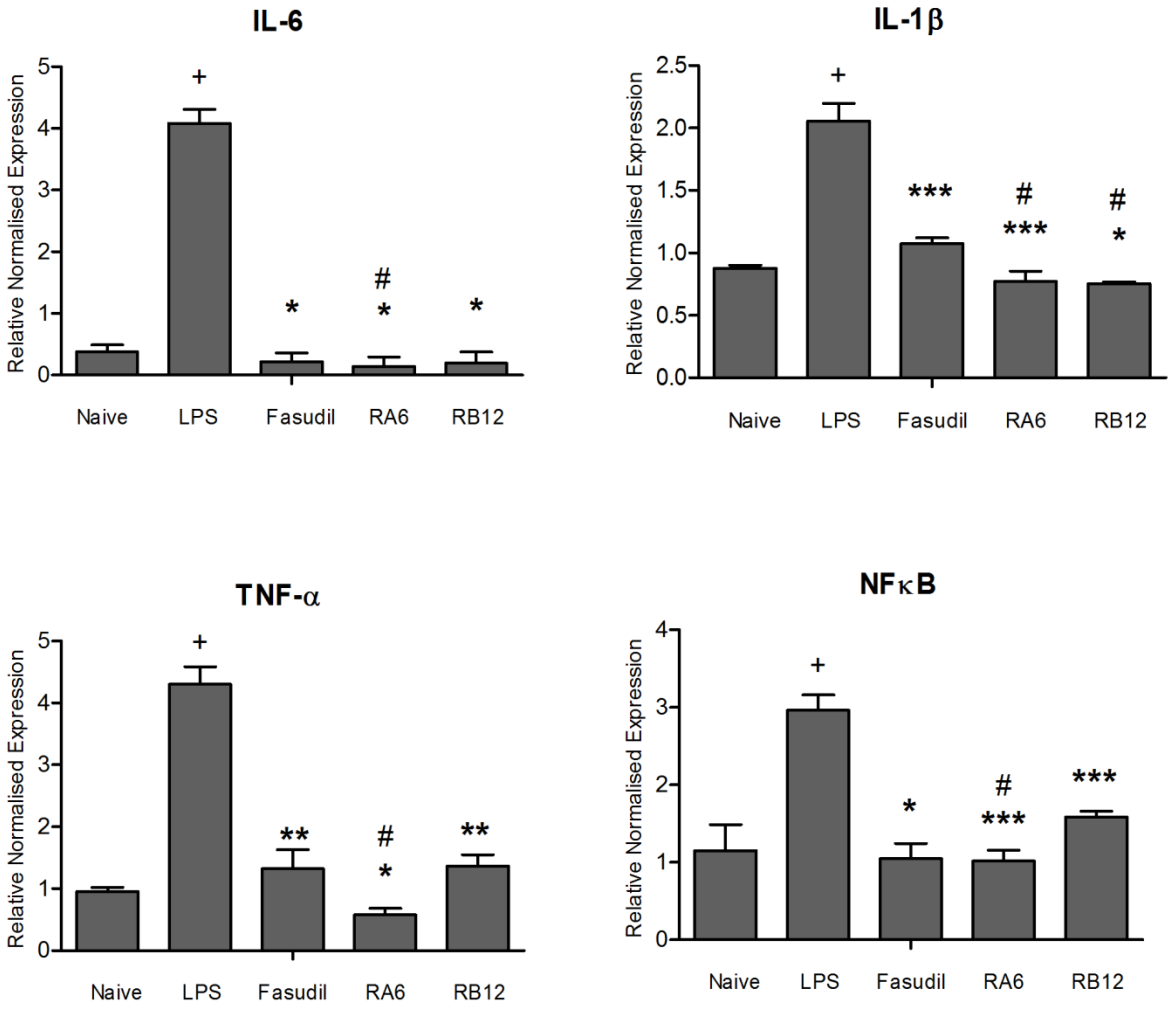

Figure 6.12 Normalised gene expression levels of pro inflammatory cytokines in LPS induced HUVE cell lines (n=3). The mRNA expression values are given as mean±SD normalised to GAPDH levels in each sample. Y-axis values represent the number of mRNA copies relative to the number of GAPDH copies in the sample. A significant reduction of IL-6 (*P<0.05), TNF-α (*P<0.05) IL-1β and NFκB (**P<0.01), TNF-α (***P<0.001) in Fasudil treated cells compared to **RA6** and **RB12**, + represents the significance of LPS in comaparison with the naive. # represents the significance in comparison with the Fasudil to **RA6** and **RB12** at 95% confidence intervals.

6.2 Combination studies of RA6 and RB12 with Fasudil

6.2.1 Synergistic effect of RA6 with Fasudil

6.2.1.1 Cell motility studies

Upon MeHg treatment, profound abnormalities were observed and one of it was increase in the cell motility rate. IMR-32 cells when treated with **RA6**, and Fasudil in combination, their synergistic effect was found to show increased blockade of cellular motility (**Figure 6.13**). Thus the motility of neuroblastoma cells were due to the activation of ROCK-I function which altered the organization of MLC. **RA6** in combination with Fasudil ceased cell migration more effectively compared with that of **RA6** alone**,** showing synergistic effect with Fasudil (**Figure 6.13**).

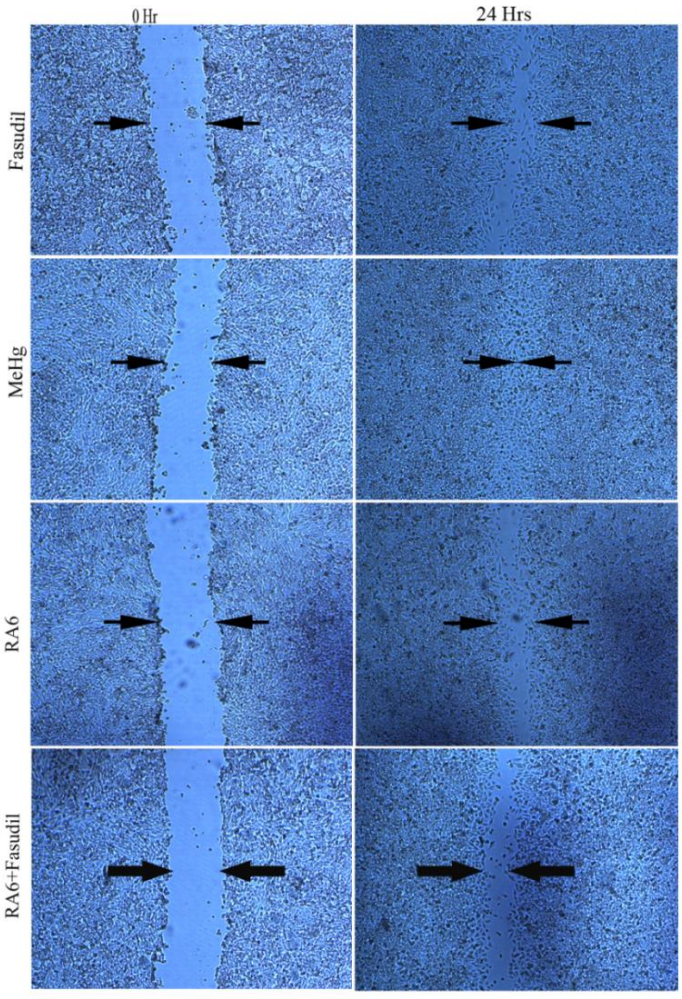

Figure 6.13 Cell motility studies of **RA6** in combination with the Fasudil in MeHg induced IMR-32 cell lines.

6.2.1.2 Gene expression analyses of MeHg and RA6+ Fasudil treated cells

Synergistic drug combinations should permit increased control of such complex biology, but there was a common concern that therapeutic synergy would generally be mirrored by synergic side-effects. Here we demonstrated **RA6** in combination with Fasudil showed synergistic effect on proinflammatory cytokine production at trascript level which was measured using real time PCR studies. Comparing the MeHg induced and untreated cells, IL-6, IL1-β, NFκB and TNF-α expression showed a statistically significant up regulation. (**Figure 6.14**)

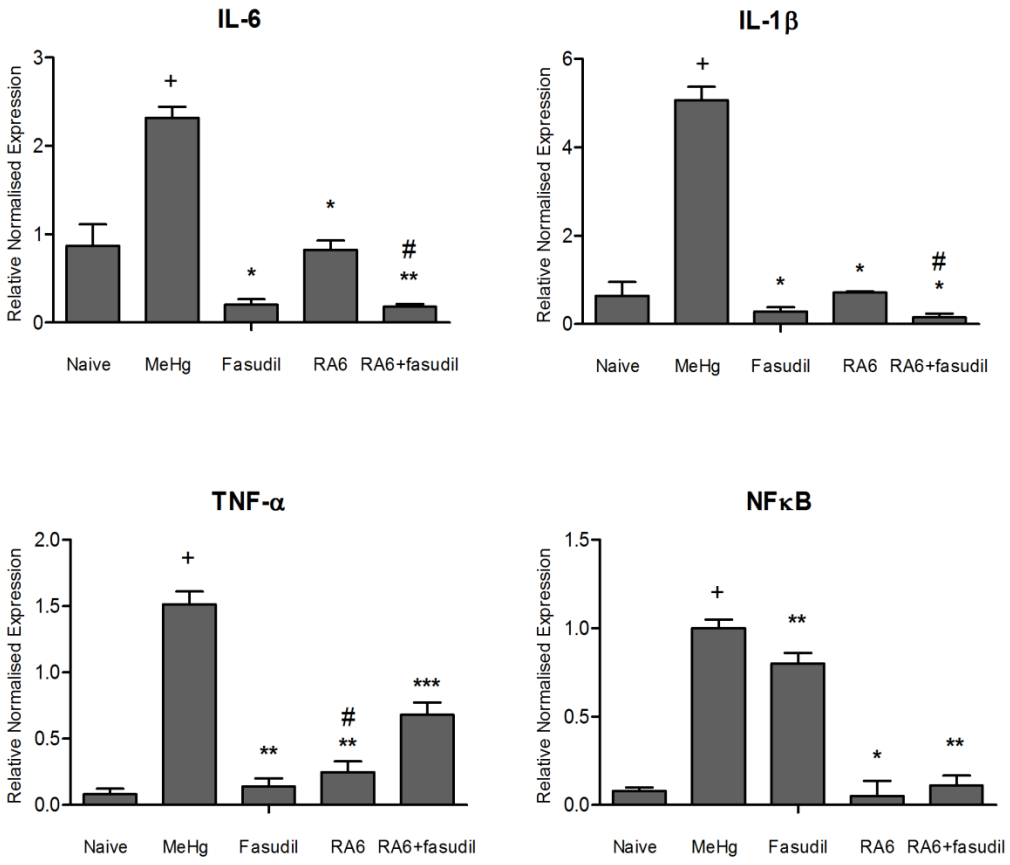

Figure 6.14 Normalised gene expression levels of pro inflammatory cytokines in MeHg induced IMR32 cell lines with the **RA6** and Fasudil combination (n=3). The mRNA expression values are given as mean±SD normalised to GAPDH levels in each sample. Y-axis values represent the number of mRNA copies relative to the number of GAPDH copies in the sample. A significant reduction of IL-6, IL-1β (*P<0.05) and TNF-α (***P<0.001, **P<0.01) in Fasudil treated cells compared to **RA6**. # represents the significance in comparison with the Fasudil to **RA6** and **RB12** at 95% confidence intervals.

RA6 when compared with Fasudil was able to reduce significantly the expressions of IL-6, IL-1β and TNF-α. However, neutralization of pro-inflammatory cytokines, especially TNFα, was a clear indication of the translocation of p47 PHOX and p67 PHOX from cytosol. In combination with Fasudil, **RA6** showed significant decrease in IL-6 and IL-1β better than single treatment. Though there is no reduction in TNF- α gene expression, **RA6**+Fasudil combination was found to be effective against other inflammatory mediators.

6.2.1.3 Gene expression analyses of LPS and RA6+ Fasudil treated cells

Many drugs have been reported in combition therapy for inflammatory diseases. LPS induced HUVE cells were found to show increased expression of proinflammatory cytokines responsible for eliciting inflammatory damage in brain. Comparing the LPS induced and untreated cells; there was a statistically significant upregulation of all mediators. In **Figure 6.15**, **RA6** when compared with Fasudil was able to reduce significantly the expressions of IL-6, IL-1β and TNF-α. However, nullification of pro-inflammatory cytokines, especially TNF-α, was a clear indication of the translocation of $p47^{PHOX}$ and $p67^{PHOX}$ from cytosol. In combination with Fasudil, **RA6** exhibited significant decrease in IL-1β, TNF-α and NFκB better than single treatments.

6.2.2 Synergistic effect of RB12 with Fasudil

6.2.2.1 Cell motility studies

Achieving therapeutic selectivity has been a major obstacle in drug discovery, leading to disappointing returns despite a surge in research and development spending. In precise, target modulation could be thwarted by the compensatory mechanisms available to complex biological systems. Here we demonstrated that **RB12** which not only reduced proinflammatory cytokine expression but also the cellular events like motility and proliferation. In short, Rho kinase with pleotropic functions including the regulation of cellular contraction, motility, morphology, polarity, cell division, and gene expression, once activated, ROCK-I alters the cell contraction by regulating MLC phosphorylation of myosin II, mediated by Ca^{2+} dependent MLC kinase and MLC phosphatase.

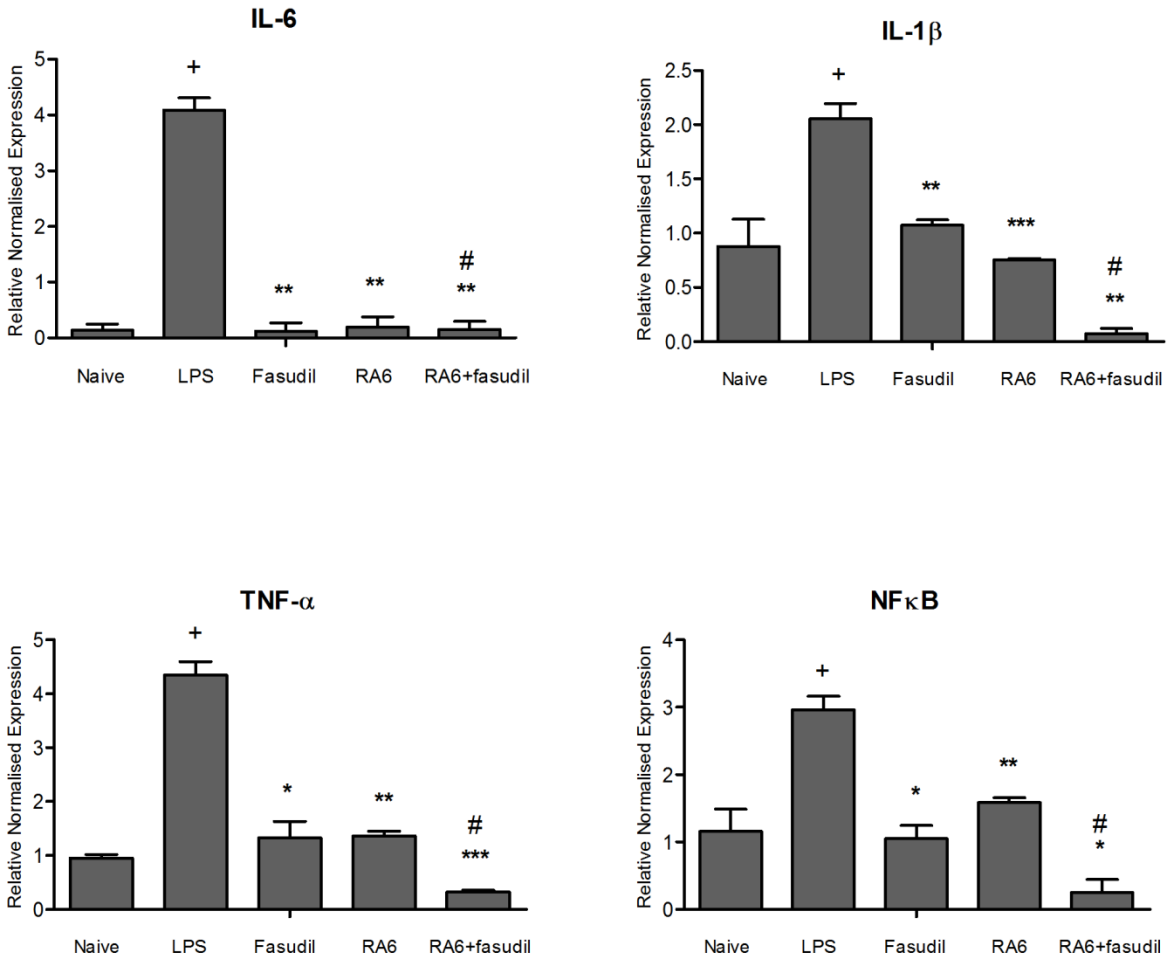

Figure 6.15 Normalised gene expression levels of pro inflammatory cytokines in LPS induced HUVE cell lines with the **RA6** and Fasudil combination (n=3). The mRNA expression values are given as mean±SD normalised to GAPDH levels in each sample. Y-axis values represent the number of mRNA copies relative to the number of GAPDH copies in the sample. A significant reduction of IL-1β (*P<0.05) in LPS induced cells compared to **RA6**+Fasudil. (**P<0.01 and ***p<0.001). # represents the significance in comparison with the Fasudil to **RA6** and **RB12** at 95% confidence intervals.

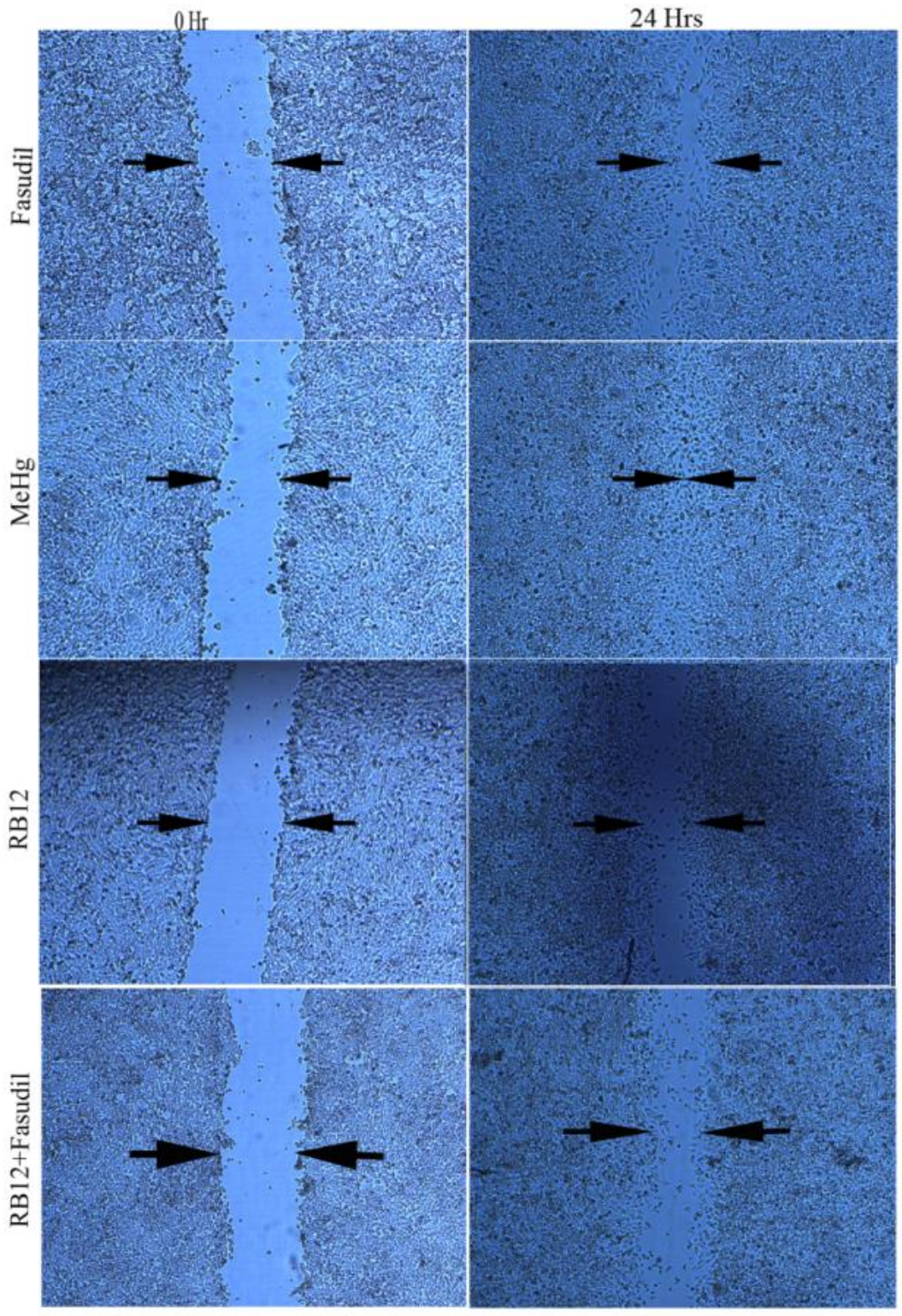

Figure 6.16 Cell motility studies of **RB12** in combination with Fasudil in MeHg induced IMR-32 cell lines.

Several studies using permiablised smooth muscle cells and selective inhibitors like Fasudil were found to show the modulated ROCK activity. Here we demonstrated that upon MeHg induction, increased motility was observed in IMR-32 cells. This could be concluded that MeHg induction led to overexpression of ROCK-I. The motility of neuroblastoma cells were due to the activation of ROCK-I function which altered the organization of MLC. **RB12** in combination with Fasudil ceased cell migration better than single treatment with the **RB12** and Fasudil (**Figure 6.16**).

6.2.2.2 Gene expression analyses of MeHg and RB12+Fasudil treated cells

The cytokines that appeared to play a fundamental role in neuroblastoma cells were IL-6, IL1-β and TNF-α. Comparing the MeHg induced and untreated cells, IL-6, IL-1β, NFκB, and TNF-α expression showed a statistically significant up regulation. (**Figure 6.17**). **RB12** when compared with Fasudil was able to reduce significantly the expressions of IL-6, IL-1β and TNF-α. TNF-α is an important proinflammatory mediator that caused the stimulation to produce other inflammatory cytokines. In combination with Fasudil, **RB12** exhibited significant decrease in IL-6 and IL-1β, but not very promising with TNF-α and NFκB expressions when compared to single treatments.

6.2.2.3 Gene expression analyses of LPS and RB12+Fasudil treated cells

Interleukin-6 is an interleukin that acts as both proinflammatory cytokine and anti-inflammatory myokine. It is secreted by T-cells, macrophages and endothelial cells to stimulate immune response. So here we had chosen umbilical vein endothelial cells to study the cytokine production upon LPS induction and their modulation with the **RB12**, Fasudil and their synergistic combination. The transcript levels of the IL-6, IL-1β, NFκB and TNF-α were measured using real time PCR studies. Comparing the MeHg induced and untreated cells, IL-6, IL-1β, NFκB and TNF-α expression showed a statistically significant upregulation (**Figure 6.18**) **RB12** when compared with Fasudil was able to reduce significantly the expressions of IL-6, IL-1β, NFκB,and TNF-α. However, neutralization of pro-inflammatory cytokines, especially TNF-α, was a clear indication of the translocation of $p47^{PHOX}$ and $p67^{PHOX}$ from cytosol. In combination with Fasudil, **RB12**+Fasudil exhibited better suppression of IL-6, IL-1β, TNF-α and NFκB revealing their synergism.

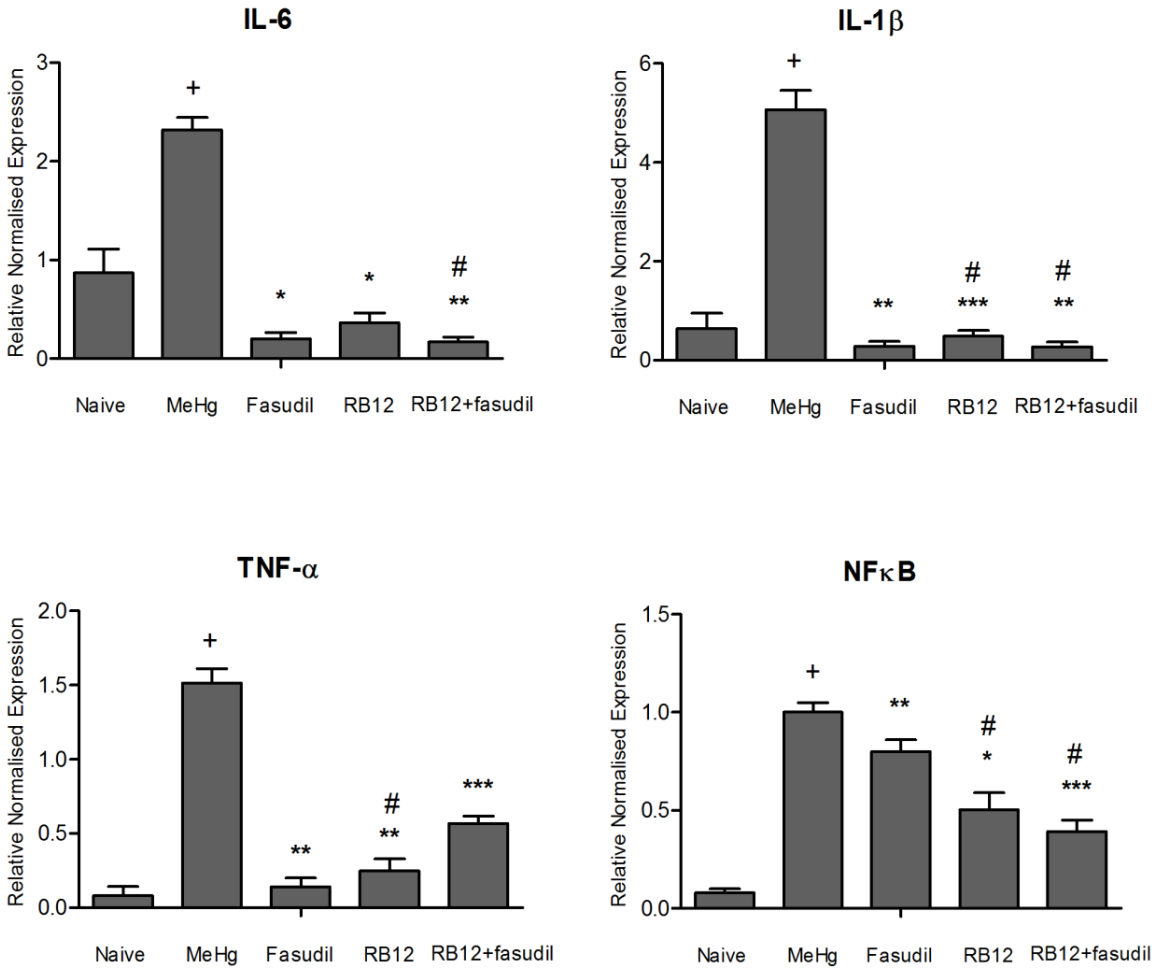

Figure 6.17 Normalised gene expression levels of pro inflammatory cytokines in MeHg induced IMR-32 with **RB12**+Fasudil combination (n=3). The mRNA expression values in MeHg IMR-32 cells given as mean±SD normalised to GAPDH levels in each sample. Y-axis values represent the number of mRNA copies relative to the number of GAPDH copies in the sample. A significant reduction of IL-6, IL-1β (*P<0.05) and TNF-α (**P<0.01) and NFκB (***P<0.001) in Fasudil treated cells compared to **RB12**. # represents the significance in comparison with the Fasudil to **RA6** and **RB12** at 95% confidence intervals.

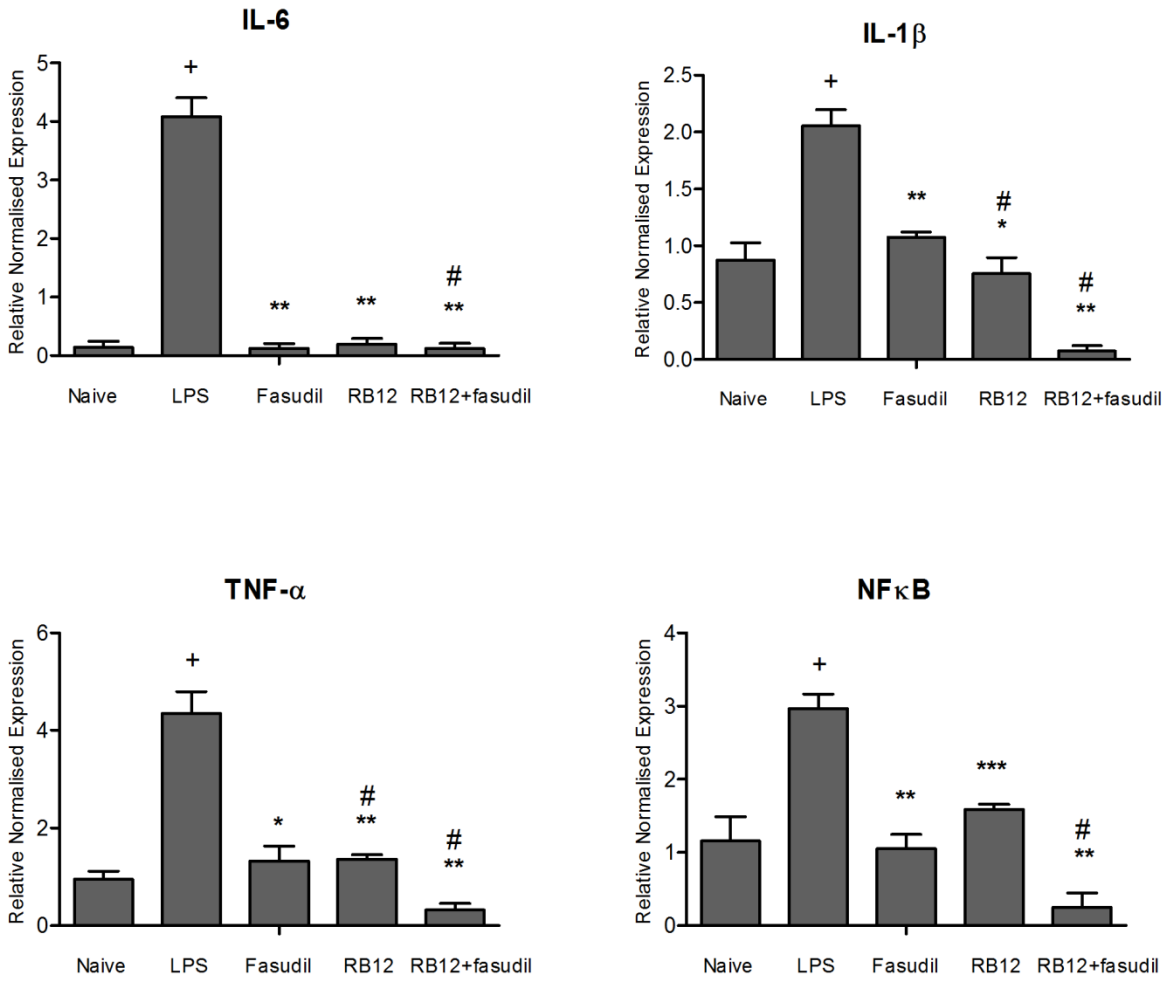

Figure 6.18 Normalised gene expression levels of pro inflammatory cytokines in LPS induced HUVEC with **RB12**+Fasudil combination (n=3). The mRNA expression values in LPS induced HUVE cells given as mean±SD normalised to GAPDH levels in each sample. Y-axis values represent the number of mRNA copies relative to the number of GAPDH copies in the sample. A significant reduction of IL-1β (**P<0.01) in LPS induced cells compared to **RB12**+Fasudil (*P<0.05, ***P<0.001). # represents the significance in comparison with the Fasudil to **RA6** and **RB12** at 95% confidence intervals.

6.3 *Ex vivo* assays for ROCK- I and NOX2 dual inhibitors

Brain slice models offer unique advantages over other *in vitro* platforms in that they replicate many aspects of the *in vivo* context. Slices largely preserved the tissue architecture of the brain regions that they originated from and maintained neuronal activities with intact functional local synaptic circuitry. With no need for lengthy animal surgery to model neuropathology of brain injury or laborious monitoring of multiple physiological parameters following *in vivo* manipulation, the usefulness of brain slices in basic research, as well as in the drug discovery process, has been increasing in recent years [Nimmerjahn A., *et al*., 2005]. A number of pharmacological and genetic manipulations that affect the neurochemical behaviors of the brain *in vivo* have been shown to be reproduced in brain slices. As slice-based assay systems provide good experimental access and allowed precise control of extracellular environments, it facilitated research establishing clear correlations between molecular changes with neuropathological outcomes. In addition, it was possible to adopt these *ex vivo* models for the screening of therapeutic molecules or novel genes. With development of disease-relevant slice models that simulate essential features of *in vivo* neurodegenerative pathologies, a larger panel of treatments could be efficiently evaluated in living tissues in a normal or injured brain tissue context without complication from brain penetration or metabolic stability.

6.3.1 ROCK-I *ex vivo* inhibition

6.3.1.2 Gene expression analyses of inflammatory mediators in MeHg induced brain slices.

Methyl mercury (MeHg), an environmental pollutant found to damage peripheral and central nervous system on long time exposure, induce inflammation in *in vivo, ex vivo* and *in vitro* and was reported to cause progressive neuronal death over time. In the current study, estimation of pro inflammatory cytokines like IL-6, IL-1β, TNF-α and NFκB gene expressions were analyzed using real time PCR studies in MeHg induced brain slices. mRNA expression was found to be high in MeHg induced brain slices and conversely, significant decrease of mediators was observed when treated with Fasudil and **RB12** (**Figure 6.19**). **RA6** and **RB12** (1 µM) were found to significantly reduce ($p<0.05$) TNF-α, while **RA6** was not significant in NFκB. In case of TNF-α, **RB12** showed remarkable decrease in expression when compared to Fasudil. IL-6, IL-1β mRNA expressions were reduced noticeably by Fasudil in comparison with naïve. Therefore, from this study we could infer that **RB12** was successful in down regulating the inflammatory

mediators especially IL-6, TNF-α and NFκB more significantly than Fasudil and **RA6**. This was in concordance to the previous observations *in vitro*.

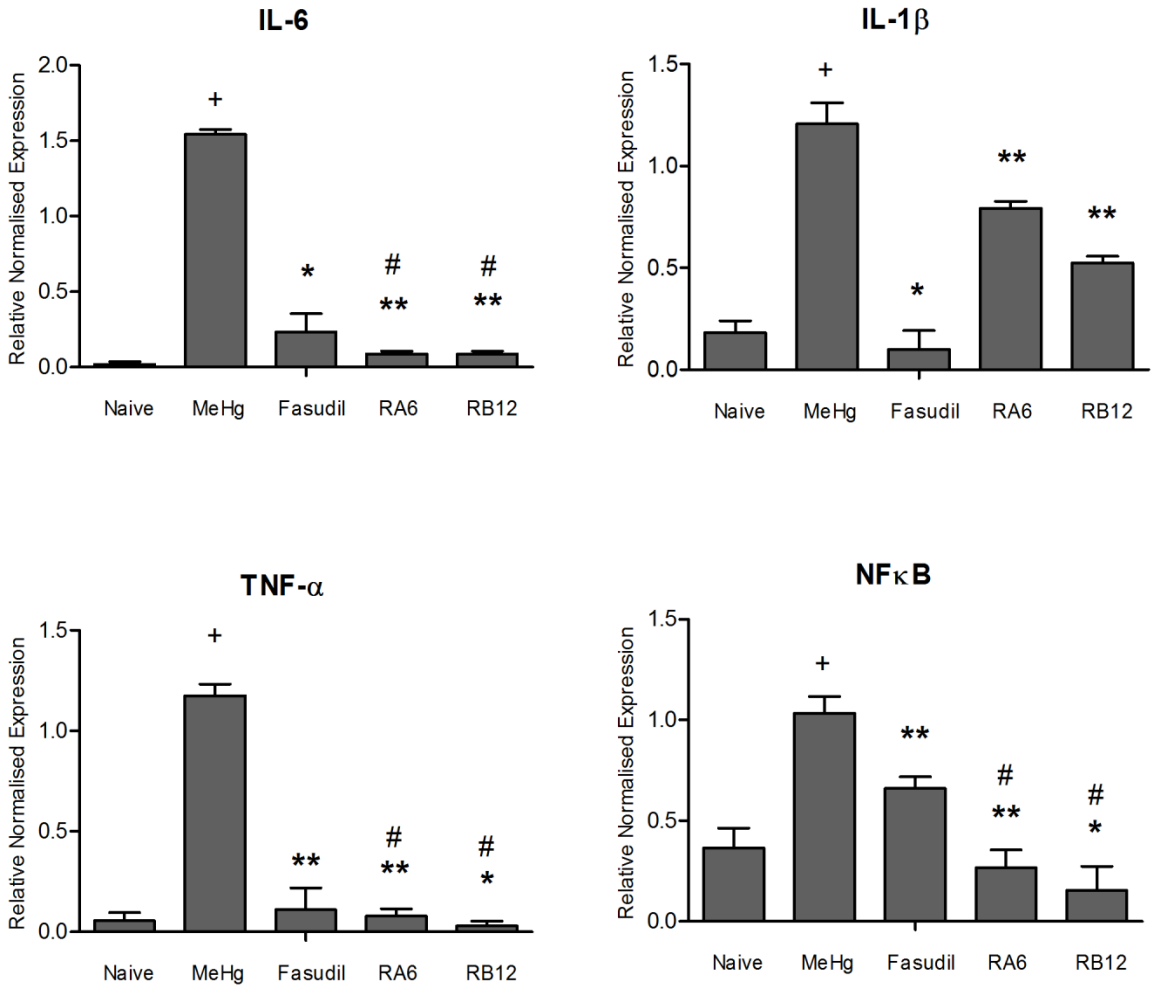

Figure 6.19 Normalised gene expression levels of pro inflammatory cytokines in MeHg induced rat brain slices (n=3). The mRNA expression values are given as mean±SD normalised to GAPDH levels in each sample. Y-axis values represent the number of mRNA copies relative to the number of GAPDH copies in the sample. A significant (***P<0.001) reduction of IL-6 and TNF-α (**P<0.01), IL-1β (*P<0.05) in Fasudil treated cells compared to **RA6** and **RB12**. + represents the significance of MeHg in comaparison with the naive. # represents the significance in comparison with the Fasudil to **RA6** and **RB12** at 95% confidence intervals.

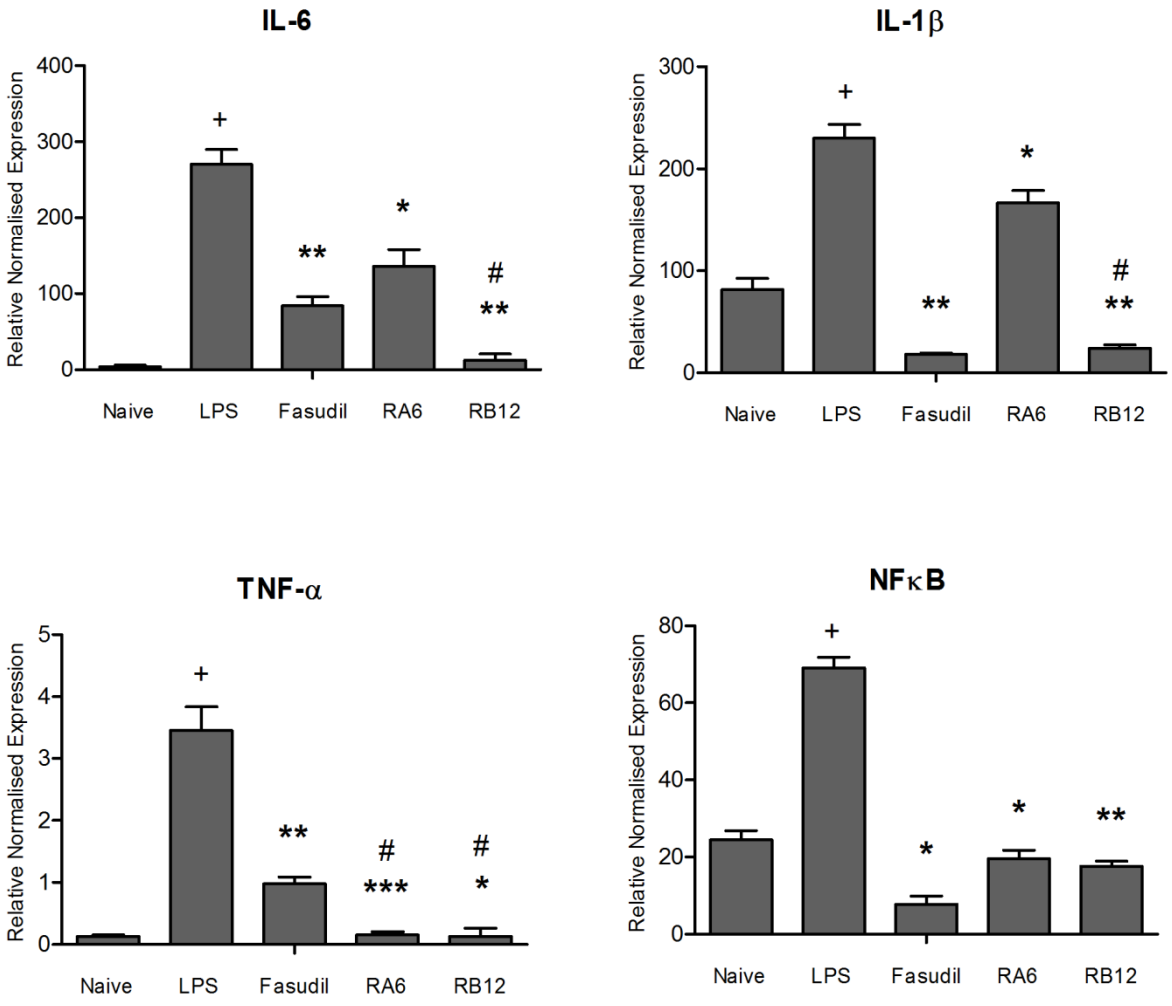

Figure 6.20 Normalised gene expression levels of pro inflammatory cytokines in LPS induced rat brain slices (n=3). The mRNA expression values are given as mean±SD normalised to GAPDH levels in each sample. Y-axis values represent the number of mRNA copies relative to the number of GAPDH copies in the sample. + represents the significance of MeHg in comaparison with the naive. (*P<0.05, **P<0.01, ***P<0.001). # represents the significance in comparison with the Fasudil to **RA6** and **RB12** at 95% confidence intervals.

6.3.2 NOX2 *ex vivo* inhibition

Lipopolysaccharide (LPS), an endotoxin derived from gram-negative bacteria was found to damage peripheral and central nervous system. LPS also induced inflammation in both *in vivo*, *ex vivo* and *in vitro* and was reported to cause progressive neuronal death over time. Hence was found to be toxic to the neighboring neurons, and further caused microglial activation and self-thrusting progressive cycle of inflammation and neuronal damage. Proinflammatory cytokines released in response to LPS treatment, IL-6, IL-1β, TNF-α, and NFκB gene expressions were analyzed using real time PCR studies in LPS induced brain slices. mRNA expression of cytokines were found to be high in LPS induced brain slices and contrariwise, significant decrease of mediators was observed when treated with Fasudil and **RA6** (**Figure 6.20**). **RA6**, and **RB12** were found to significantly reduce ($p<0.05$) IL-6, TNF-α and NFκB. In case of TNF-α, **RA6** and **RB12** showed remarkable decrease in expression when compared to Fasudil. **RB12** was found to suppress IL-6, IL-1β, TNF-α and NFκB mRNA expressions better than Fasudil and comparable with naïve. Therefore, from this study we could infer that **RB12** was successful in down regulating the inflammatory mediators more significantly than Fasudil and **RA6**.

6.4 Combination studies of RA6 and RB12 with Fasudil

6.4.1 Synergistic effect of RA6 with Fasudil

6.4.1.1 Gene expression analyses of MeHg and RA6+ Fasudil treated brain slice

To estimate the efficacy of **RA6** with Fasudil further in inflammatory conditions, we also attempted in *ex vivo* model for inflammation for their synergistic effect. Synergistic effect of **RA6** in the tissue architecture *i.e ex vivo* gave an idea over the *in vivo* animal models. In the current study, estimation of pro inflammatory cytokines (IL-6, IL-1β, TNF-α, and NFκB) gene expressions were analyzed using real time PCR studies in MeHg induced tissues. mRNA expression was found to be high in MeHg induced brain slices and conversely, significant decrease of mediators was observed when treated with Fasudil in combination of **RA6** (**Figure 6.21**).

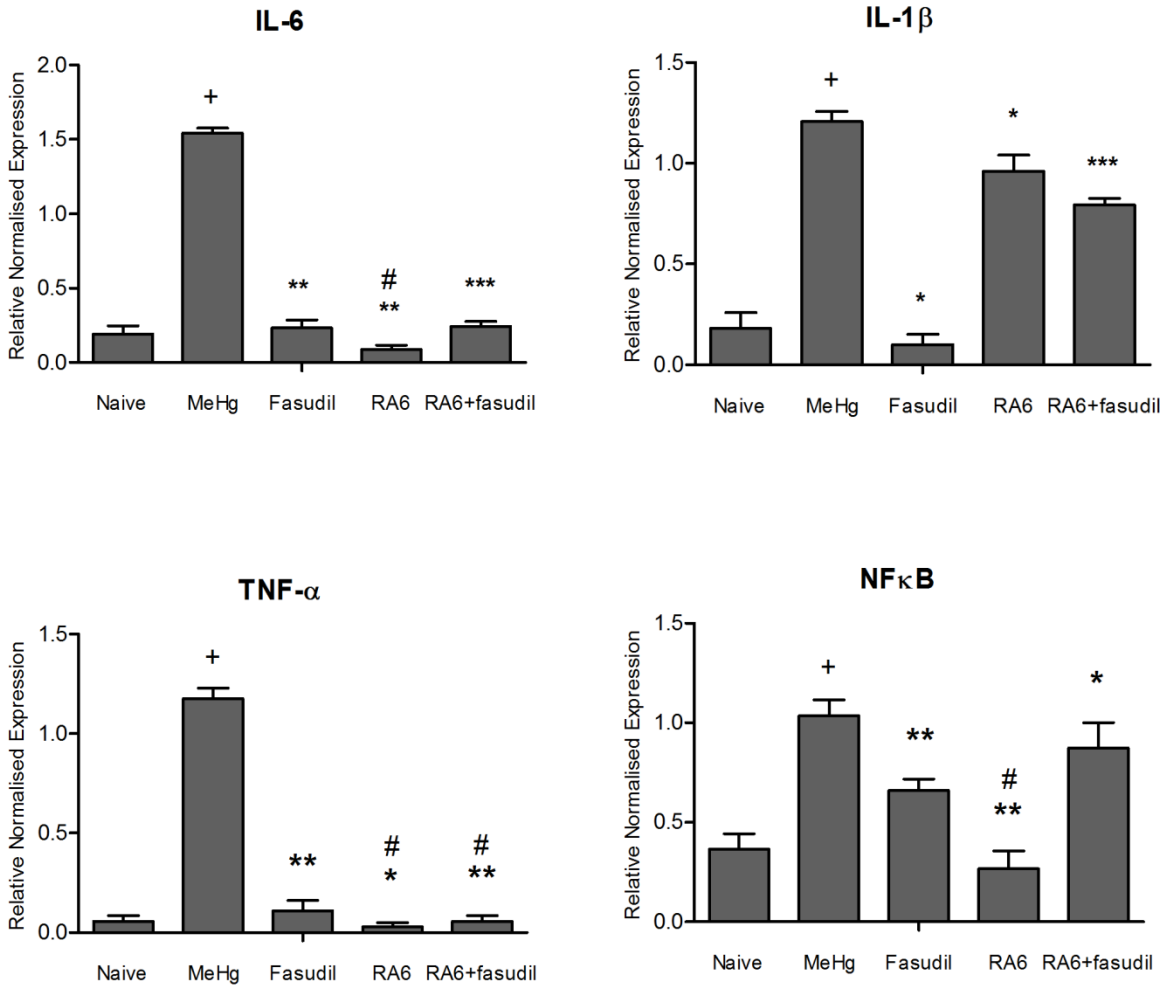

Figure 6.21 Normalized gene expression levels of pro inflammatory cytokines, in MeHg induced *versus* normal brain slice models **RA6** in combination with Fasudil (n=3). The mRNA expression values are given as mean±SD normalized to GAPDH levels in each sample. Y-axis values represent the number of mRNA copies relative to the number of GAPDH copies in the sample. (*P<0.05, **P<0.01, ***P<0.001). # represents the significance in comparison with the Fasudil to **RA6** and **RB12** at 95% confidence intervals.

The combination effect was not better when compared to single treatments with regard to IL-6, IL-1β, and NFκB, but little difference was observed with TNF-α experiment. These results were in contrast to that observed in *in vitro* synergestic effects as depicted in **Figure 6.14**.

6.4.1.2 Gene expression analyses of LPS and RA6+ Fasudil treated brain slice

The synergistic effects of the drugs were used for the multi-targeted therapy. Here we demonstrated that dual inhibitor **RA6** for ROCK-I and NOX2 in treating neuroinflammatory

diseases with decrease in proinflammatory cytokine expression. To estimate the efficacy of **RA6** further in inflammatory conditions, we also attempted in *ex vivo* model for inflammation. In the current study, estimation of pro-inflammatory cytokines (IL-6, IL-1β, TNF-α, and NFκB) gene expressions were analyzed using real time PCR studies in LPS induced brain slices. mRNA expression was found to be significantly high in LPS induced brain slices in comparison with the naïve model. Conversely, significant decrease of mediators was observed when treated in combination with Fasudil and **RA6** (**Figure 6.22**). **RA6** was found to significantly reduce ($p<0.05$) TNF-α and NFκB. In case of TNF-α. In combination with **RA6** Fasudil exhibited better reduction of IL-6 expression and IL-1β, better than single treatments.

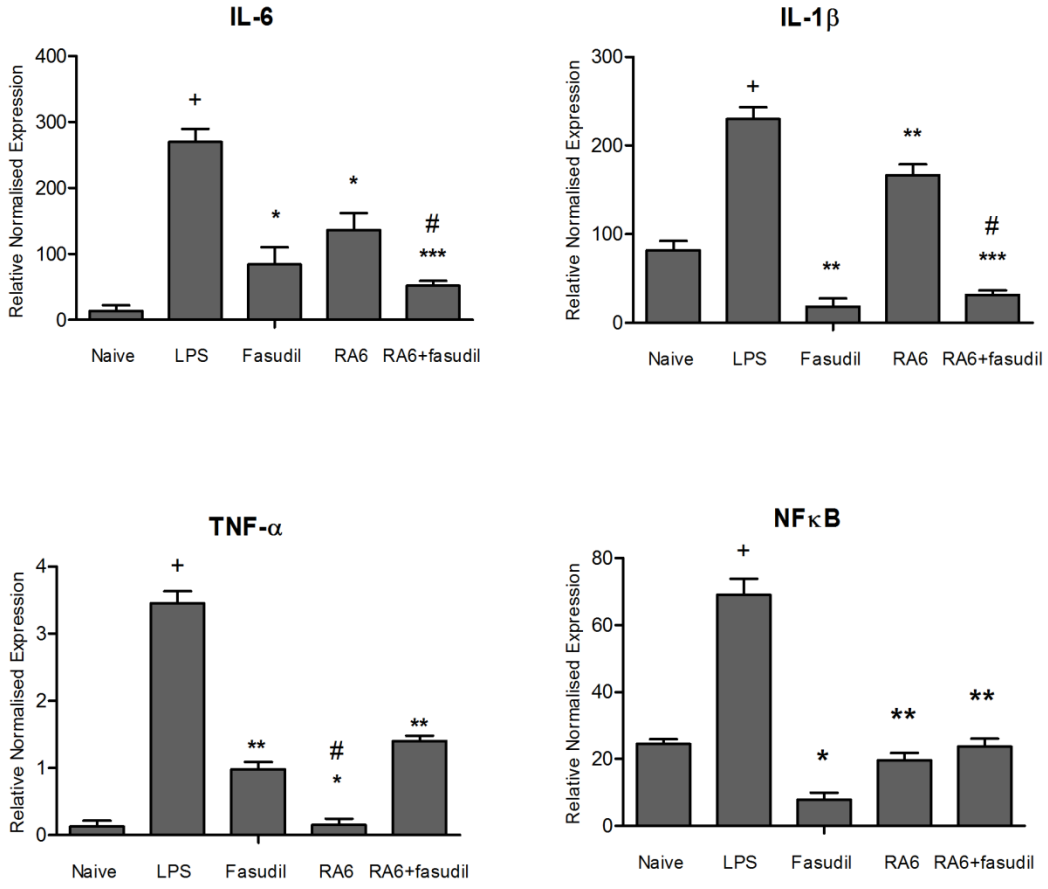

Figure 6.22 Normalized gene expression levels of pro inflammatory cytokines, in LPS induced versus normal brain slice models **RA6** in combination with Fasudil (n=3). The mRNA expression values are given as mean±SD normalized to GAPDH levels in each sample. Y-axis values represent the number of mRNA copies relative to the number of GAPDH copies in the sample. (*P<0.05, **P<0.01, ***P<0.001). # represents the significance in comparison with the Fasudil to **RA6** and **RB12** at 95% confidence intervals.

6.4.2 Synergistic effect of RB12 with Fasudil

6.4.2.1 Gene expression analyses of MeHg and RB12+Fasudil treated brain slice

To estimate the efficacy of **RB12** with Fasudil further in combination, we also attempted in *ex vivo* model for inflammation. In the current study, estimation of pro inflammatory cytokines (IL-6, IL-1β, TNF-α, and NFκB) gene expressions were analyzed using real time PCR studies in MeHg induced tissues in combination of **RB12** with Fasudil (**Figure 6.23**).

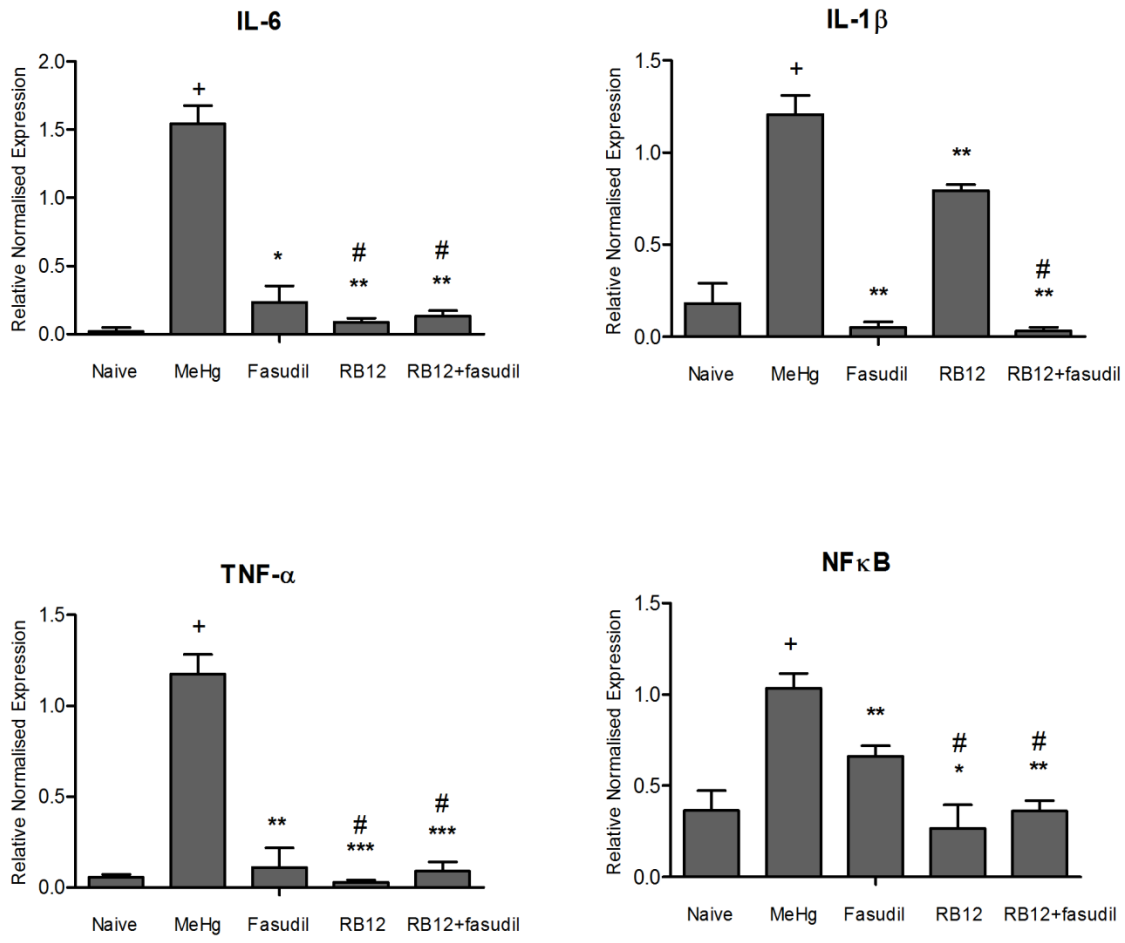

Figure 6.23 Normalized gene expression levels of pro inflammatory cytokines, in MeHg induced versus normal brain slice models in combination with **RB12**+Fasudil (n=3). The mRNA expression values are given as mean±SD normalized to GAPDH levels in each sample. Y-axis values represent the number of mRNA copies relative to the number of GAPDH copies in the sample. A significant reduction of IL-6 and NFκB (**P<0.01), TNF-α (***P<0.001) in Fasudil treated brain slices compared to **RB12** Fasudil combination. (*P<0.05, **P<0.01, ***P<0.001). # represents the significance in comparison with the Fasudil to **RA6** and **RB12** at 95% confidence intervals.

RB12 in combination with Fasudil exhibited significant synergestic effect in suppressing all the pro-inflammatory cytokines better than observed in *in vitro* assay. Therefore, from this study we could infer that **RB12** was successful in down regulating the inflammatory mediators especially TNF-α more significantly than Fasudil. In combination with Fasudil and **RB12**, IL-6, IL-1β, TNF-α and NFκB were significantly reduced.

6.4.2.2 Gene expression analyses of LPS and RB12+Fasudil treated brain slice

To estimate the efficacy of **RB12** with Fasudil further in inflammatory conditions, we also attempted in *ex vivo* model for inflammation. In the current study, estimation of pro-inflammatory cytokines (IL-6, IL-1β, TNF-α, and NFκB) gene expressions were analyzed using real time PCR studies in LPS induced tissues.

Under some circumstances the initial inflammatory response could become uncontrolled and ultimately lead to other deleterious effects including prolonged inflammation and cytokine release known to contribute to CNS dysfunction, chronic depressive disorders and neurological disorders. Although CNS actions of cytokines have been implicated in LPS induced neurotoxicity or the septic shock, in the current study, estimation of pro inflammatory cytokines (IL-6, IL-1β, TNF-α, NFκB) gene expressions were analyzed using real time PCR studies in LPS induced brain slices to miniaturize the *in vivo* animal model. mRNA expression was found to be high in LPS induced brain slices and conversely, significant decrease of mediators was observed when treated with Fasudil and **RB12** (**Figure 6.24**). **RB12** was found to significantly reduce ($p<0.05$) TNF-α and NFκB. In combination with **RB12** and Fasudil, marked decrease in IL-6 ($*P<0.05$) and comparable reduction of IL-1β, TNF-α and NFκB was onserved.

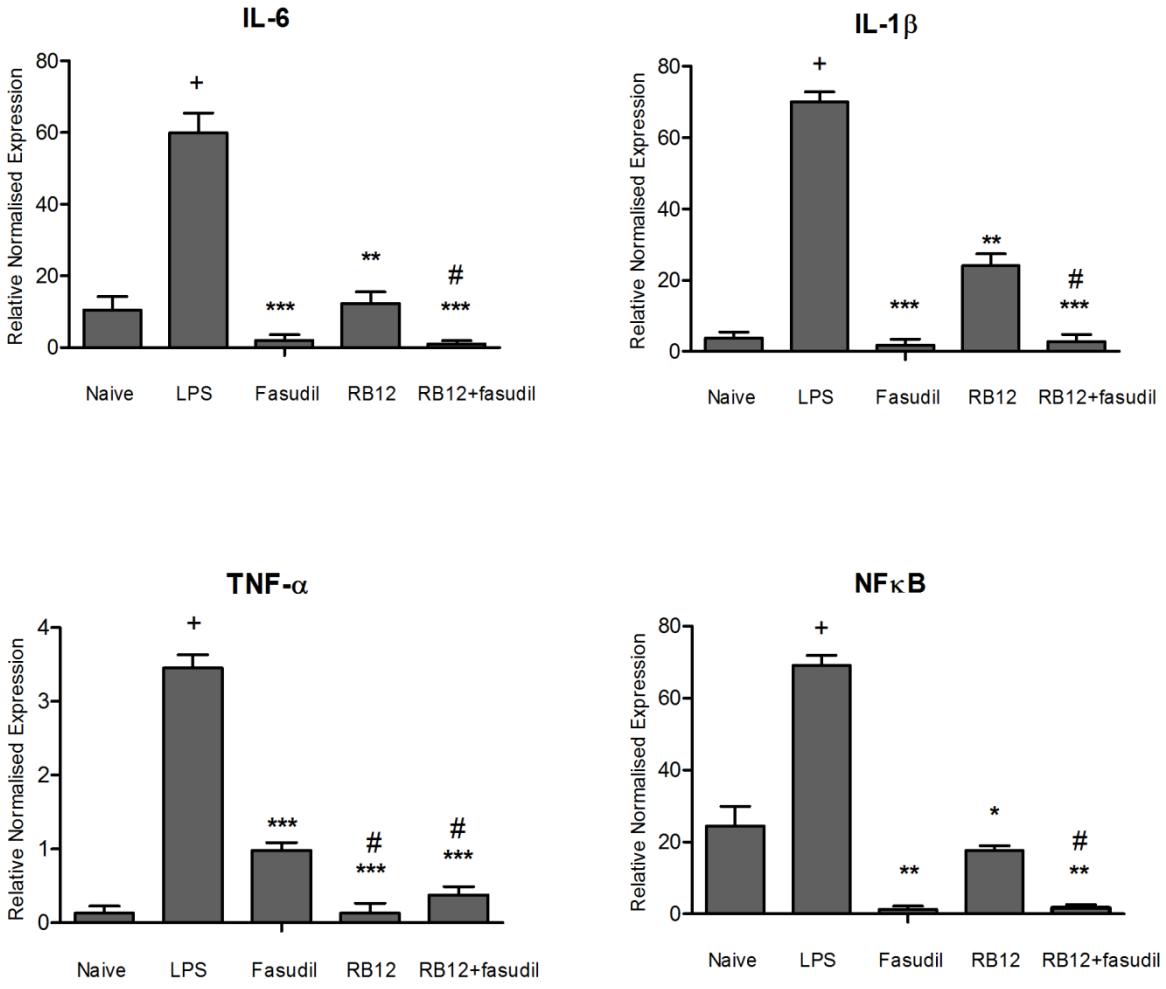

Figure 6.24 Normalized gene expression levels of pro inflammatory cytokines, in LPS induced versus normal brain slice models in combination with **RB12**+Fasudil (n=3). The mRNA expression values are given as mean±SD normalized to GAPDH levels in each sample. Y-axis values represent the number of mRNA copies relative to the number of GAPDH copies in the sample. A significant reduction of TNF-α (***P<0.001) and NFκB (*P<0.05) in Fasudil treated brain slices compared to **RB12**. (*P<0.05, **P<0.01, ***P<0.001). # represents the significance in comparison with the Fasudil to **RA6** and **RB12** at 95% confidence intervals.

Summary of the assays conducted are depicted in the flow chart in **Figure 6.25**. These results were encouraging to take forward the most promising lead to the next level of *in vivo* assessment.

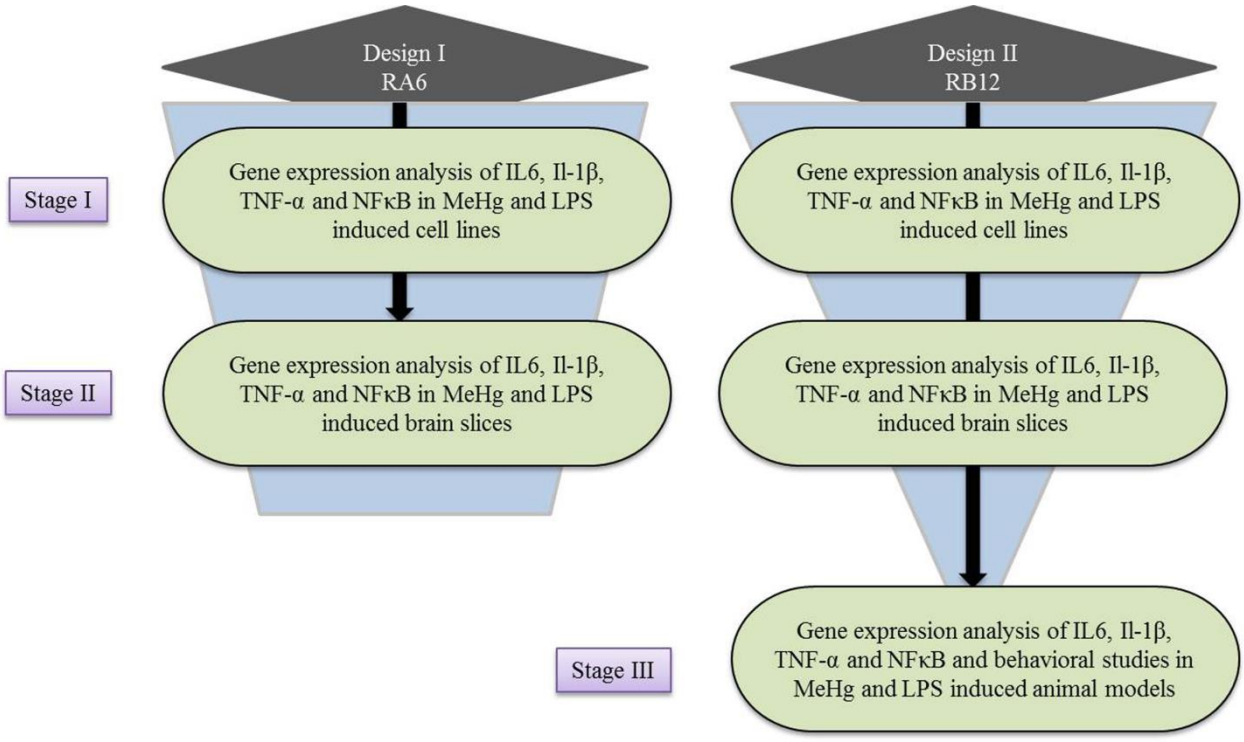

Figure 6.25 Flowchart for cellular, exvivo and invivo assays for the selected **RA6** and **RB12** compounds.

When compared to **RA6**, **RB12** (**Figure 6.26**) was found more promising as dual inhibitors of ROCK-I and NOX2 with nanomolar activity and also found to better stabilize ROCK protein as indicated by its higher ΔTm of +5°C and better *in vitro* activity. Though both **RA6** and **RB12** had good predicted ADME and lesser cytotoxicity, **RB12** had a lower cardiotoxicity potential the **RB12** has -7.412 of HERG cytotoxicity and **RA6** showed -5.231 which is in the border line for the HERG activity. Also due to the availability in our lab in high quantity **RB12** was selected further for *in vivo* assays.

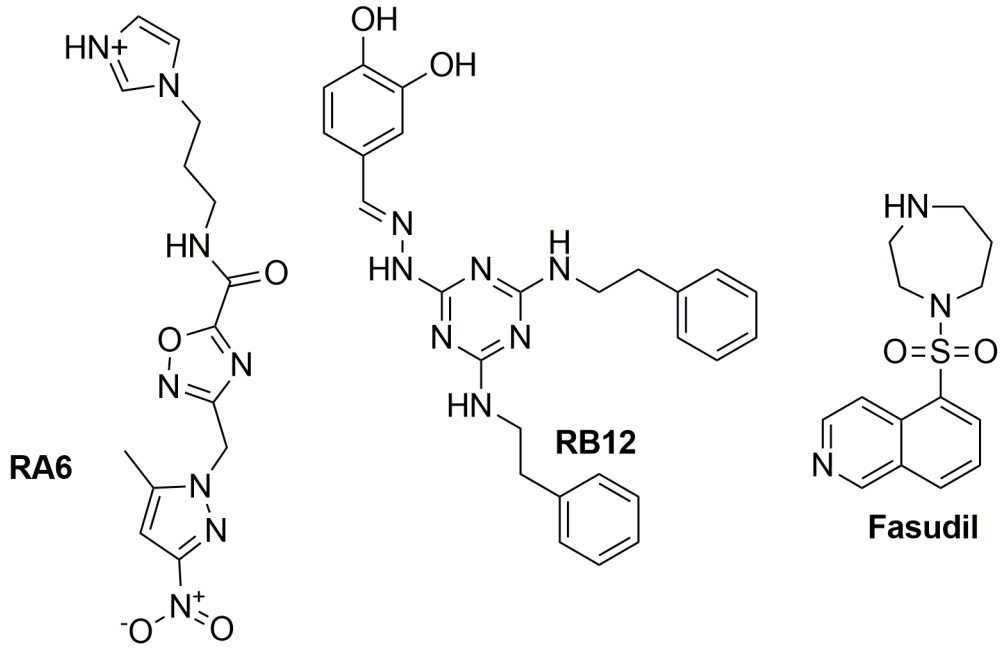

	RA6	**RB12**	**Fasudil**
IC_{50}	<1 nM	357 nM	5.24 μM
X-ROS IC_{50}	2.85 μM	817 nM	2.98 μM
ΔTm shift	3.1 °C	5 °C	0.5 °C
EC_{50} (MeHg)	3 nM	94 nM	230 nM
SI (MeHg)	>100	>100	68.76
EC_{50} (LPS)	303 nM	88 nM	180 nM
SI (LPS)	>100	>100	91.24

Figure 6.26 Structures and biological parameters of **RA6**, **RB12** and Fasudil compounds.

6.5 *In vivo* pharmacological screening of RB12

The effect of lead molecules from Asinex and BITS database were identified using extensive drug design strategies followed by a battery of *in vitro* and *ex vivo* experimentation. **RA6** and **RB12** emerged as promising leads from the enzyme inhibition and also based on the selectivity towards the disease models compared to normal cells. To select a better compound to be used for animal studies, we applied different stages of filters to select most promising compound to evaluate neuroinflammatory conditions in *in vivo*. From cellular studies **RB12** was found to inhibit more potently than **RA6** in cell motility assays and cytokine transcript expression. Though there were no profound difference between two compounds, we employed in *ex vivo* inhibition of the cytokine production. **RB12** was found to decrease all cytokines significantly compared to **RA6**. One more filter we applied was the synergistic effect of compounds with Fasudil. Fasudil being a potent inhibitor and vasodilator, discovered, it has been in use for the treatment of inflammatory disorders especially, cerebral vasospasm, subarachnoid hemorrhage and cognitive deficits [Shimokawa H., *et al*., 2002] . So, combining Fasudil with the **RA6** and **RB12,** we found more significant effects with the **RB12** than with **RA6**. The synergistic effect of **RB12** with Fasudil increased the therapeutic potential of the compound, so we selected **RB12** further to check the neuroprotective activity in *in vivo* animal models.

6.5.1 Animal model-I: MeHg induced neurodegenerative model

Methyl mercury (MeHg) is an environmental toxicant that poses serious health risks in humans and especially children, whose brains are still developing and are therefore particularly vulnerable to exogenous toxicants. MeHg exposure results primarily from the consumption of contaminated food [Rocha JB., *et al*., 1993]. MeHg is easily absorbed from the diet into the bloodstream and distributes to all tissues including the brain. Indeed, MeHg exhibits high mobility in the body, due to its ability to form thiol complexes with small molecules such as the amino acid cysteine. The kinetics of MeHg accumulation in the brain differs from that of peripheral organs, such as liver or kidney, raising the possibility that therapeutic interventions could be organ-specific. In the central nervous system, MeHg interferes with developmental processes, such as neurogenesis and cell survival, as demonstrated in both humans and animal models [Farina M., *et al*., 2011]. In humans, it is difficult to estimate the level of exposure in the fetus and in children in affected areas, and effective treatments for brain toxicity have yet to be

defined. The cellular mechanisms underlying mercury neurotoxicity are not fully understood, although several studies now indicated that ROS production play a central role.

6.5.1.1 Neurotoxicity assessment

Neurotoxicty of **RB12** was essential for drug development process in treatment for neurological disorders. The side effects of a test compound on the central nervous system could be studied through neurotoxicity studies. The peripheral nervous system is further divided into the somatic and autonomic nervous systems. Neurotoxic studies may be employed to evaluate the specific histopathological and behavioral neurotoxicity of a compound and could be used to characterize neurotoxic responses such as loss of memory, sensory deficits and learning and memory dysfuntions. Neurotoxicological studies were performed in adult rodents. The neurotoxicity of the **RB12** after intraperitoneal administration (300 mg/kg) showed minimal effect on neurotoxicity as observed as 22.6% at 1 h and 27.9% for 2 h. Hence **RB12** nontoxic dose at 30 mg/kg was considered for further neuropharmacological studies.

6.5.1.2 Behavioral assessment on MeHg induced animal model

6.5.1.2.1 Spontaneous locomotor activity

High dose of MeHg intoxication was known to cause damage to the cerebellum. Even though the present study was performed by exposing the rats to a minimal dose of MeHg, we decided to use a test for cerebellar functions to exclude the presence of prominent alteration. An evaluation of total spontaneous locomotor activity to obtain a general pattern of motor deficit in treated and untreated groups was conducted. The present study was undertaken to investigate the precursory effects of MeHg poisoning by measuring the locomotor activity of rats. MeHg was administered to rats by oral gavage daily for 32 days. The motor acivity of rats was recorded over 5 min period following injection of test compound, Fasudil and methyl mercury. Treatment with **RB12** increased spontaneous locomotor activity, *i.e* motility and locomotion. A significant decrease ($p<0.05$) of neurotoxicity was observed in **RB12** treated animals in comparison with MeHg induced rats from Day 7 to Day 32. **Figure 6.27** shows the mean % neurotoxicity for all animals in all groups for 32 days. The two co-exposed groups showed similar neurotoxicity compared to untreated group. This test was performed using actophotometer.

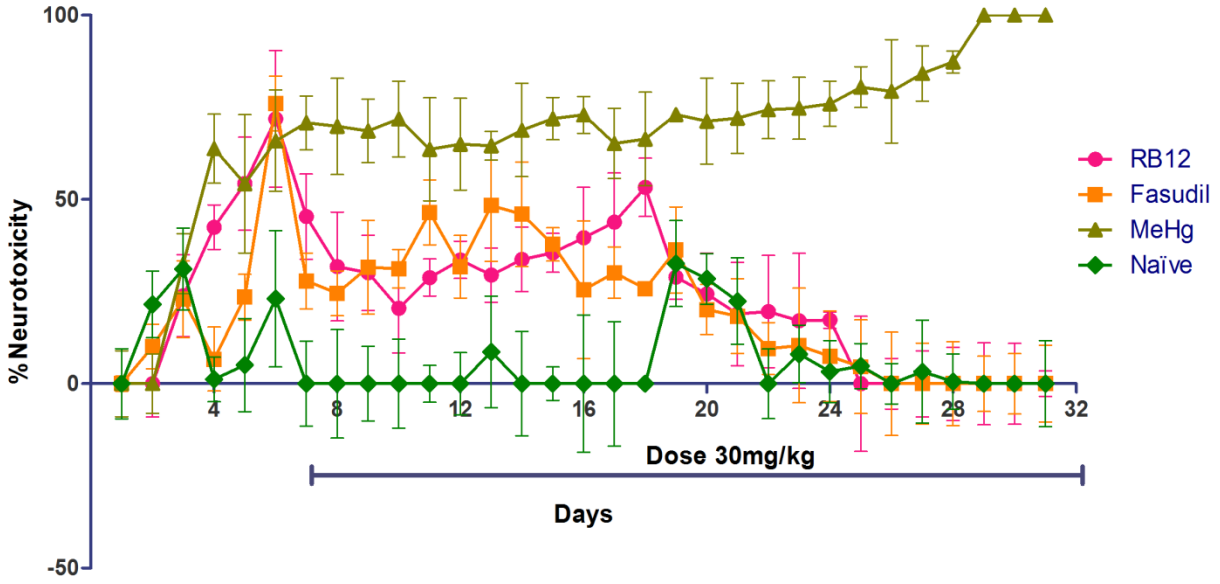

Figure 6.27 Graph represents the % neurotoxicity of MeHg on all groups. As Day7 has shown significant increase in all groups, the same day **RB12** dosage was started to observe the neuroprotective activity on MeHg chronic dosing. The data represented as mean±SEM (n=5).

6.5.1.2.2 Body weight and clasping analyses

To investigate, if the body weight of the treated and untreated groups in rats differed, we analysed body weight of the rats from Day 0 to Day 7 and Day 7 to Day 32. The body weights were similar from Day 0 to Day 7 in all the groups (**Figure 6.28**). Then it lowered for the MeHg induced groups and was found increased for the Fasudil and **RB12** treated rats significantly ($p<0.01$). The body weight of the naive group increased through out the entire experiment. Just before euthanasia (Day 32), MeHg+Fasudil co-exposed, and MeHg+**RB12** co-exposed groups gained body weights significantly ($p<0.05$) when compared to that of MeHg exposed group (Control). However, Fasudil (30 mg/kg) exposed group showed significantly higher weight gain than the **RB12** (30 mg/kg) exposed group (**Figure 6.28**).

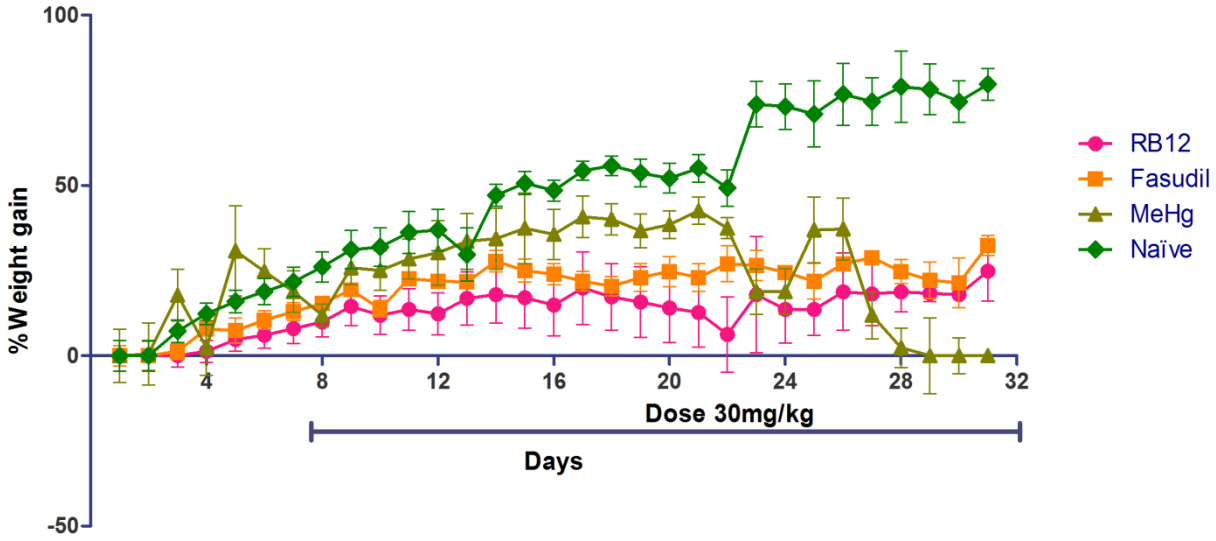

Figure 6.28 Graph represents the weight gain of animals on all groups for 32 days. The data represented as mean±SEM (n=5).

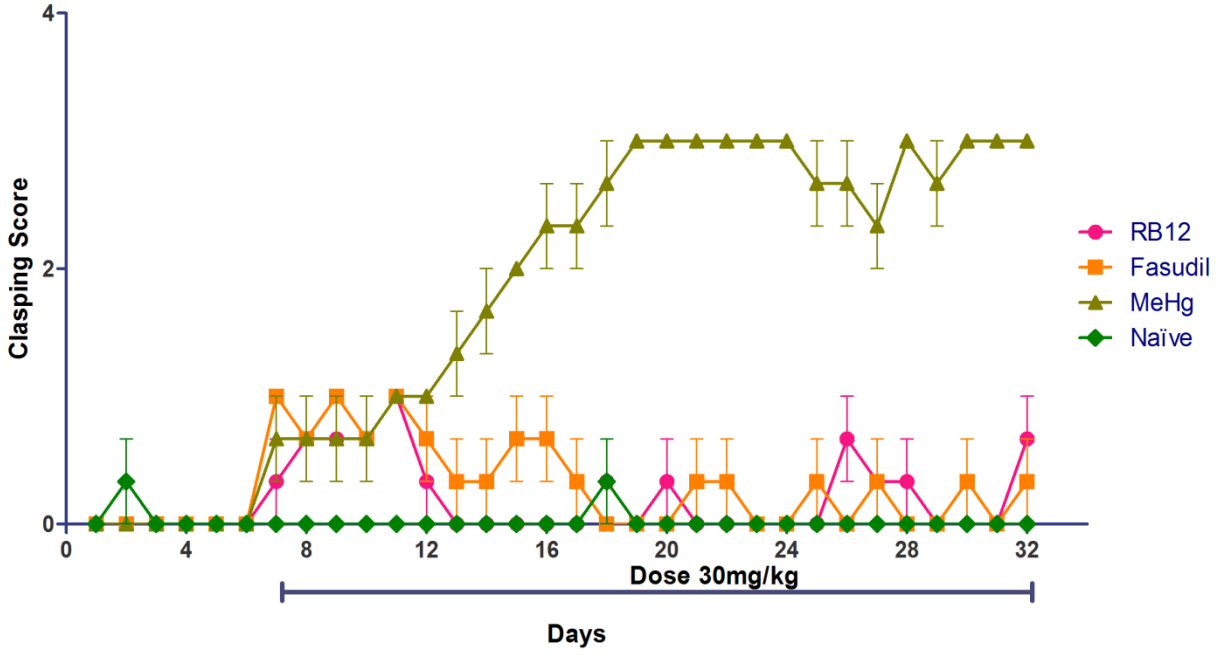

Figure 6.29 Graph represents the clasping score of animals on all groups for 32days. The data represented as mean±SEM (n=5).

The 20 ppm dose of MeHg used in this study was sufficient enough to produce a fast-onset motor impairment within 7 days in all groups. Mortality was not observed till day 32. Hind limb clasping was a marker of disease progression in a number of rodent models of neurodegeneration. We describe here a protocol for the rapid and sensitive quantification of

disease severity in mouse models of cerebellar ataxia and other neurodegenrative diseases. Hind limb clasping was shown to occur in various neurodegenrative models. For this test, rats were suspended by the base of the tail and kept for 10-15 seconds. Hind limb clasping was rated from 0 to 3 based on severity. 0= hindlimbs splayed outward and away from the abdomen, 1= one hind limb retracted inwards towards the abdomen for atleast 50% of the observation period, 2= both hind limbs partially retracted inwards towards abdomen for 100% of the observation time, 3= both hind limbs completely retracted inwards towards the abdomen for atleast 80% of the observation period. Partial scores of 0.5 were utilised when appropriate. Hind limb clasping scores were added together for the three seperate groups for 32 days. As shown in **Figure 6.29**, there was a significant difference between the MeHg induced groups and naive group ($p<0.05$).

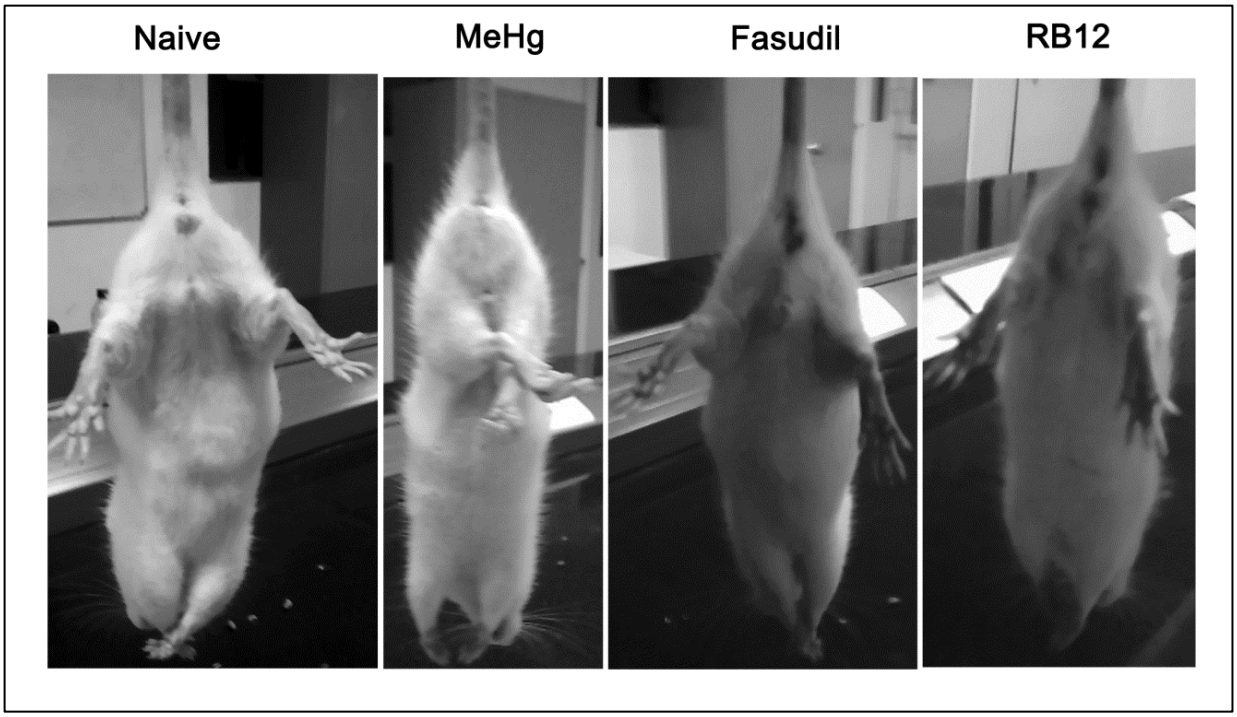

Figure 6.30 Hind limb clasping shown by representative animal from each group on Day 32.

To achieve dyskinetic posture, rats were suspended by holding tail as shown in **Figure 6.30**, presenting clasping behaviour of representative animals from each groups and the graph (**Figure 6.29**) represents the mean of clasping of all animals in all groups. MeHg induced group was found to show severe hind limb clasping behaviour compared to other groups. Drug co-exposed groups were found to exhibit less scores and was significantly lesser ($p<0.05$) when compared to MeHg exposed group on day 32. **RB12** and Fasudil groups did not differ much from each other

in their clasping scores. This shows the severity of the disease with MeHg intoxication and could effectively be treated with our test compound **RB12**.

6.5.1.2.3 Gait analysis

Foot placement could be a sensitive measure of coordination in rodents. In this test, it was possible to observe the pattern of progressive motor decreased activity based on stride length, stance length and sway length which were all indications of decreased coordination. **RB12** treated animals exhibited significant increase in stride and stance length similar to normal rats when compared to MeHg exposed rats (**Figure 6.31**).

Whereas sway length was found to be reduced significantly compared to MeHg exposed group. The decrease in the stride, sway and stance lengths clearly implicated that MeHg induces loss of motor coordination. **RB12** was found to be better than Fasudil as depicted in **Figure 6.30b**.

The quantitative gait analyses (**Figure 6.30b**) used in the present study, the catwalk method, provided both static gait parameters as well as time-based information and a pressure parameter, in contrast to conventional gait analysis test, such as the analysis of the footprints obtained by allowing rodents to walk with the inked paws along a sheet of paper, which provided information about static gait. We used the catwalk method to quantify disturbances in gait analysis in rats with MeHg induced animals compared to untreated group (Naïve). There was a significant difference in the usage of contralateral *vs* ipsilateral hind limbs. This was expressed by stride, sway and stance lengths. All these parameters showed that MeHg induced animals put a higher pressure on the ipsilateral paw just to drag the hindlimbs. This imbalance was likely due to compensation of the animal to spare the MeHg induced group. The effect on stride length during continuous locomotion was decresed in the MeHg induced groups compared to other groups. The reduced gait stance showed that the decreased nerve impulse was decreased in comparison to other groups. **RB12** treated group showed improved stance or stride lengths significantly.

6.5.1.2.4 Demyelination studies

Studies had shown that Rho/Rho kinase signaling pathway played a role in neurodegeneration. Therefore, over-activity of Rho/Rho kinase signaling pathway might inhibit nerve conduction. The rat caudal nerve revealed good characteristics for studying nerve conduction using non-invasive techniques.

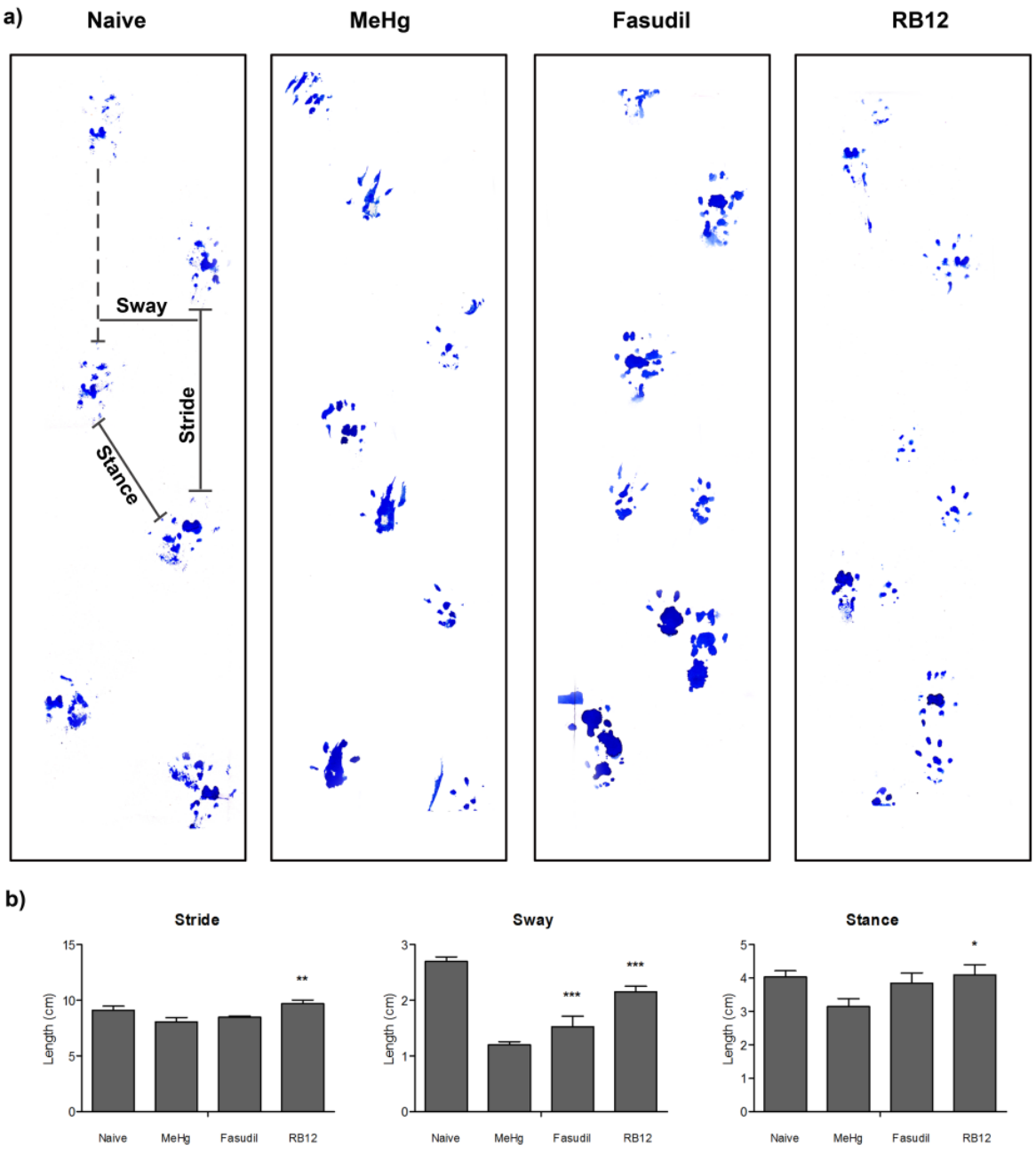

Figure 6.31 a) Gait analysis shown by representative animal from each groups on day 32, b) Quantitative gait analyses of all animals. (*P<0.05, **P<0.01, ***P<0.001)

Its superficial trajectory allowed easy stimulation and recording of potentials with surface electrodes and its 10 cm trajectory allowed accurate measurement of distances. Slower conduction velocity could probably due to an abnormal development of myelin sheath of demyelinated nerves. In **Figure 6.32** we could observe that the nerve conduction velocity (NCV) was increased significantly with drug treatments (**RB12** and Fasudil) when compared to MeHg

exposed animals. **Figure 6.33** shows the histopathological analysis of brain samples from representative animal from each groups. More demyelination was observed with MeHg induction, and Fasudil exhibited little demyelination in comparison to naïve and **RB12**. Naïve and **RB12** treated samples did not show any kind of demyelination indicating the neuroprotective effect of **RB12**. MeHg animal tissue was observed as holow tissue which might be due to demyelination of nerve fibers as implicated in neurodegeneration.

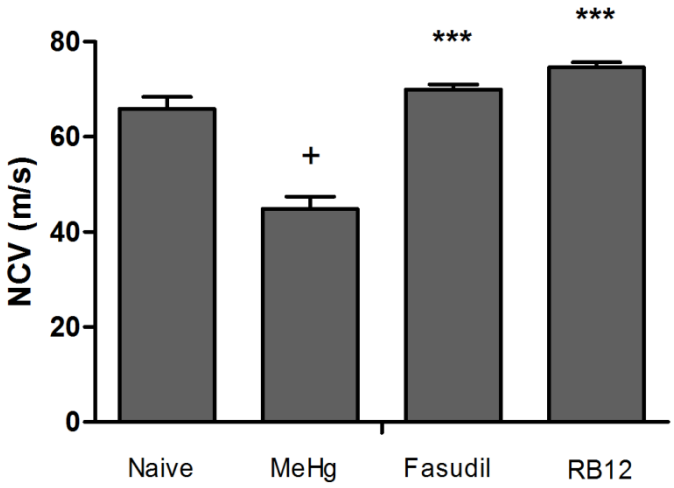

Figure 6.32 Nerve conduction velocity analysis of animals from all groups on day 32. (*P<0.05, **P<0.01, ***P<0.001) n=5.

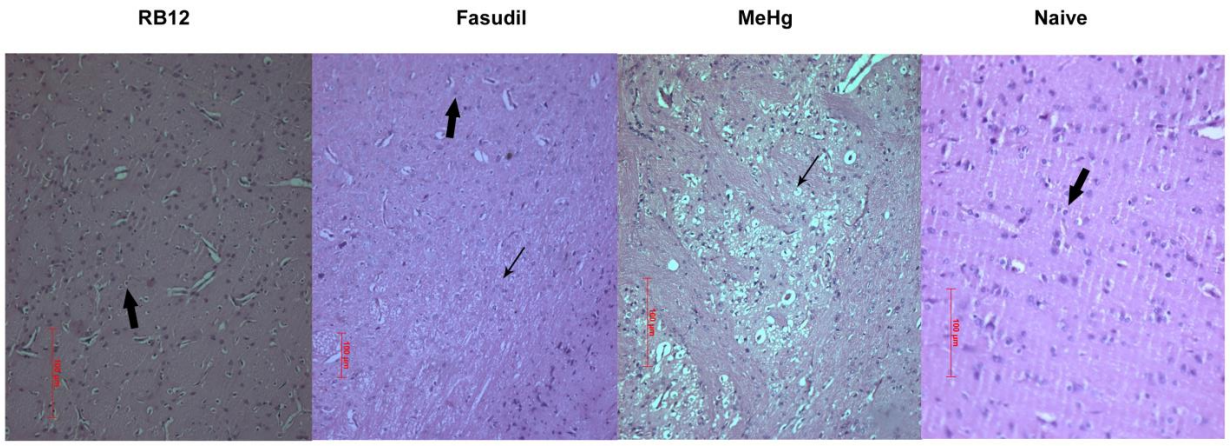

Figure 6.33 Histopathological analysis of brain tissue of the representative animal from each group on Day 32. Big arrow represents the healthy myelinated tissue and small arrow represents the demyelinated portion of the tissue sample.

There were small focal areas of degeneration and necrosis of neurons in the cortex. No consistent distribution could be established as small foci were located at levels throughout the cortex. Most prominent feature of the MeHg induced animal brain section showed deepening of the basophilia of the cells. These changes were most pronounced in the rats that had disability in movements. The extent of degeneration, as a mild demyelination was observed in Fasudil treated animal brain section (**Figure 6.33**). The affected nerve fibers showed swollen myelin sheaths with small clear globular to oval shapes. In MeHg induced rats, severe demyelination was observed as the nerve fibers were disrupted, and macrophages, fibroblasts and collagen were also present in the affected area.

It has been well established that MeHg intoxication exhibit slow nerve conduction. The slow nerve conduction velocity due to demyelination and loss of large myelinated fibers, cause a decrease in nerve action potentials owing to loss of axons. Since ROCK inhibitors could regulate neuronal extension and cell growth, we evaluated the effect of these compounds on the nerve conduction velocity. Apparently, the nerve conduction velocity was significantly decreased by the Day 32 in MeHg induced rats (**Figure 6.32**), when compared to normal control rats. Compound **RB12** showed significant improvement in nerve conduction velocity and brought it to the level of naïve animals. Fasudil also showed statistically significant improvements in the nerve condution velocity.

6.5.1.2.5 Gene expression analyses of inflammatory mediators in MeHg induced animal whole brain smaples

In order to understand the effect of **RB12** *in vivo*, we attempted for gene expression pattern on day 32. *In vivo* administered brain samples were pelleted or collected and treated with TRIzol reagent according to manufacture‘s instruction. Microglia seemed to be the primary source of pro-inflammatory cytokine, TNF-α which disrupted hippocampal neuronal functions such as long term potentiation and working memory consolidation. Gene expression of four inflammatory mediators were normalized using the house keeping gene GAPDH. The oligonucleotide primer sequence of all the inflammatory mediators are provided in methods section in **Table 4.2** from Chapter 4. TNF-α being the primary pro-inflammatory mediator to cross blood brain barrier and induce inflammation in brain, it was determined in our study. TNF-α expression was found to be increased significantly in animal brains treated with MeHg,

(**Figure 6.34**). IL-6, IL-1β and NFκB *in vivo* was also increased significantly in MeHg exposed animals. **RB12** treated group exhibited a remarkable reduction in all the cytokines expression complementing that observed in *in vitro* and *ex vivo* assays.

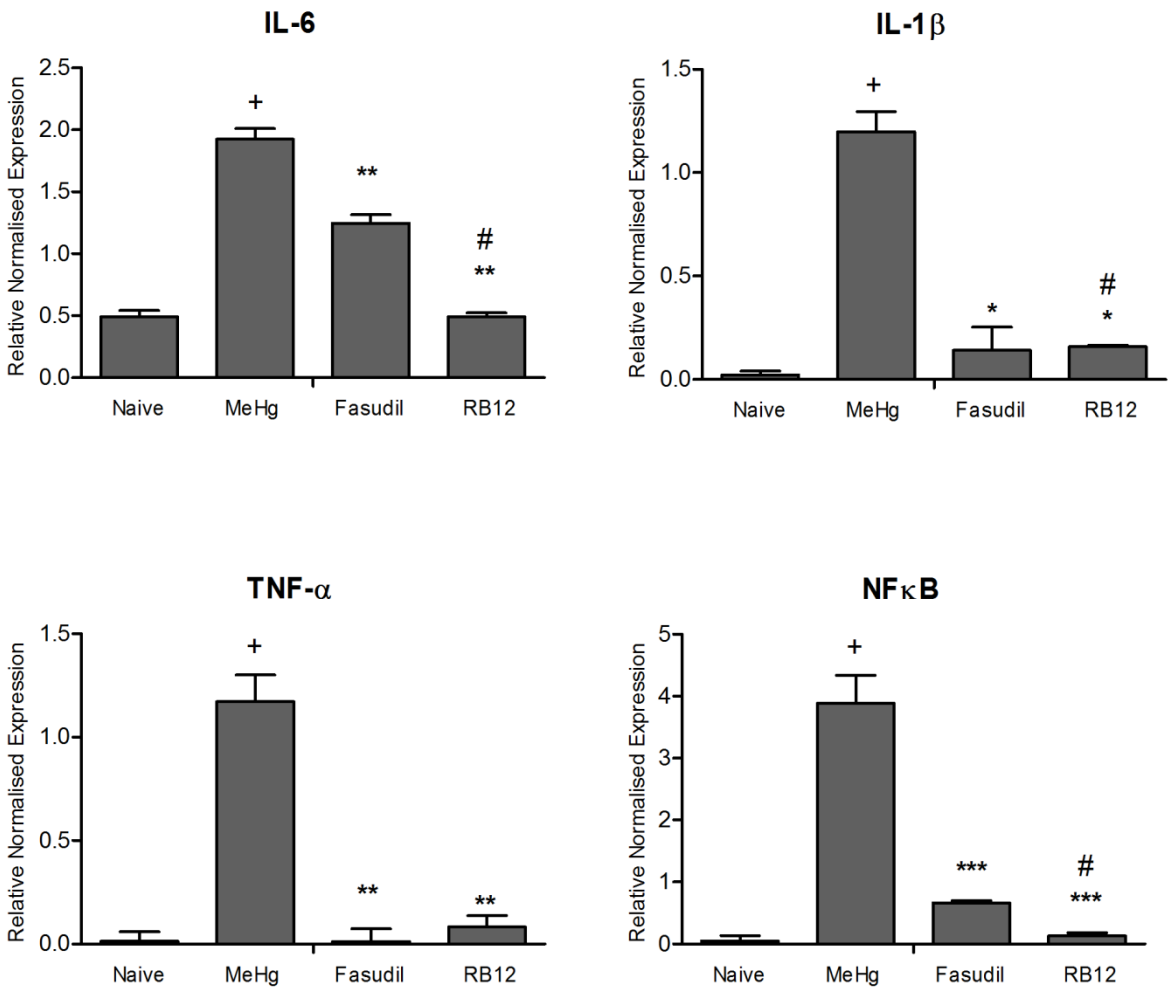

Figure 6.34 Normalized gene expression levels of pro inflammatory cytokines, in MeHg induced *versus* normal brain *in vivo* animal models (n=5). The mRNA expression values are given as mean±SD normalized to GAPDH levels in each sample. Y-axis values represent the number of mRNA copies relative to the number of GAPDH copies in the sample. A significant reduction of IL-6 and TNF-α (**P<0.01) and NFκB (***<0.001), IL-1β (*P<0.05) in Fasudil treated animals compared to **RB12**. + represents the significant difference in the MeHg induced brain samples in comparison with the naïve. # represents the significance in comparison with the Fasudil to **RA6** and **RB12** at 95% confidence intervals.

6.5.2 Animal model-II: LPS induced neuroinflammatory model

Inflammation is implicated in progressive nature in several neurodegenerative and neurological disroders, but mechanism is poorly understood. A single systemic injection of LPS (50 mg/kg) was administered [Qin,L., *et.al*., 2007]. Systemic LPS administration resulted in rapid brain TNF-α increase that remain eliminated for several months, while peripheral TNF-α subside within hours. While microglial activation was necessary and critical for host defence, over activation of microglia could be neurotoxic. At this time, the mechanism initiating deleterious neuroinflammation in neurodegenerative disease are poorly understood. LPS damages DA neurons only in the presence of microglia. Further, LPS activation of microglia both *in vivo* and *in vitro* causes the preogressive and cumulative loss of DA neurons over time. Brain samples showed an increase in TNF-α mRNA and protein levels that both peaked at 60 min [Li,G., *et.al*., 2005]. A single intraperitoneal LPS injection resulted in TNFα production in the periphery, which initiated brain TNF-α production (mRNA and protein) in the brain that continued for months after the systemic source of TNF-α has been abated. However, we speculated that the initial entry of the pro-inflammatory factors, such as TNF-α in brain could cause the activation of microglia to produce more inflammatory factors, which might lead to neuronal death. Upon exposure to TNF-α, microglia were well known to synthesize and secrete TNF-α. Thus, this initial damage may then result in reactive microgliosis, causing the release of additional pro-inflammatory factors to begin a self-propelling and a vicious cycle of neuronal damage. Thus reactive microgliosis may underlie the progressive and long-lasting neuroinflammation and neurodegeneration of numerous neurodegenerative diseases. In the present study, we performed evaluation of **RB12** in LPS induced animal model and the results are discussed in further sections.

6.5.2.1 Assessment of peripheral nerve damage

6.5.2.1.1 Hot plate test

Acute heat nociceptive thresholds for the hot plate test were converted to percent maximum possible effect (%MPE) according to the formula, as follows

$$\%MPE = \frac{(\text{post treatment value}) - (\text{pretreatment value})}{(\text{cutoff value}) - (\text{pretreatment value})} X100$$

MPE was defined as the lack of a nociceptive response during 120 s (cutoff time) of exposure to the heat stimulus. The animals were tested prior to drug and LPS administration and after 2 h. %MPE was calculted using the above formula. **Figure 6.35** represents the acute heat antinociceptive effect of animlas. There was significant neuroprotective effect observed with both **RB12** and Fasudil treatment groups.

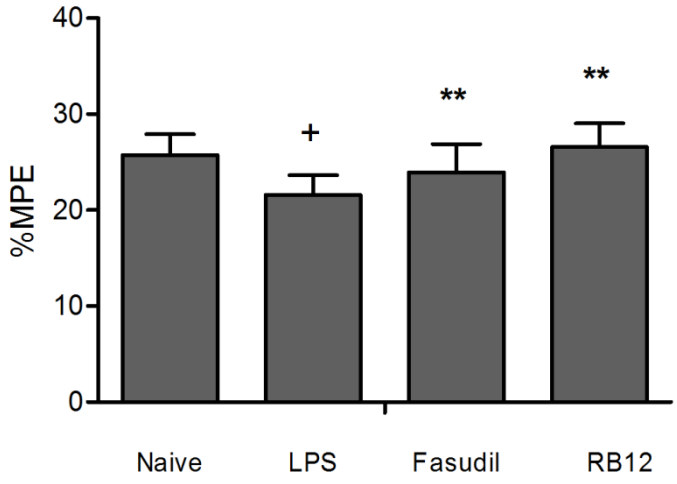

Figure 6.35 Anti nociceptive effect of **RB12** (30 mg/kg) and Fasudil (30 mg/kg) in LPS (50 mg/kg) induced thermal pain evaluated as %MPE in the hot plate test, (**P<0.01) (***<0.001) and (*P<0.05). + represents the significant difference in LPS induced animals compared to naïve.

6.5.2.1.2 Tail flick test

The tail is the most important thermoregulatory organ in rodents. Heat dissipation is regulated by an on-off regulation of blood flow in the tail. Rapid variations in skin temparature occur as a result of this regulation of flow. The veins and arteries are situated in bundles along the tail; the arterial supply runs mainly along the ventral aspect and the veins are located laterally. Therefore, the temperature may vary between the dorsal, ventral or lateral surfaces. Due to heat loss, the temperature also varies considerably between the proximal and distal parts of the tail. The amount and duration of vasodilation is partly dependent on the relationship between the ambient temperature and the temperature at which the mice were acclimatized. In mice at rest, the ambient temperature where vasodilation occurs was lower after acclimatization to cold than after acclimatization to a warmer environment. Mice restrained in tubes for a short time showed a considerable increase in the temperature of the tail probably due to vasodilation. If there was any

damage in the peripheral nerves the latency of flicking would increase. Based on these principles, tail flick test was performed.

It has been described that tail-flick occur when temperature at the level of nociceptors in the skin reach a critical value. %MPE was calculated for the mice with LPS induction and drug treatment. **Figure 6.36** shows %MPEs of all the test groups. It was clear that Fasudil and **RB12** were neuroprotective as indicated by their significant increase in %MPE similar to naive animals.

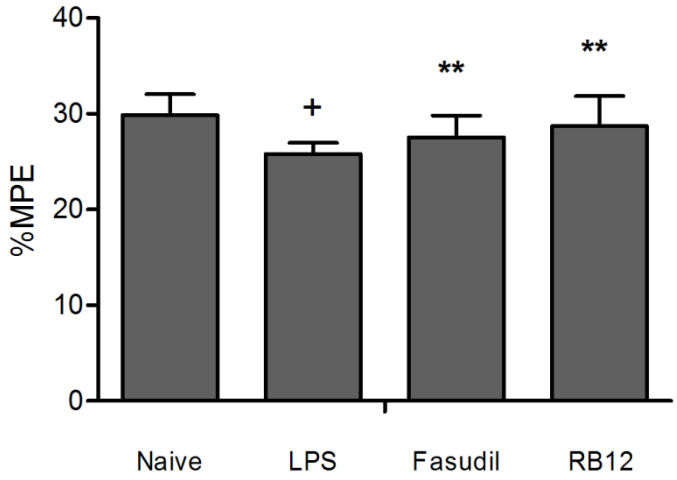

Figure 6.36 Anti nociceptive effect of **RB12** (30 mg/kg) and Fasudil (30 mg/kg) in LPS (50 mg/kg) induced thermal pain evaluated as %MPE in the tail flick test (**P<0.01) (***<0.001) and (*P<0.05). + represents the significant difference in LPS induced animals compared to naïve.

6.5.2.1.3 Clasping assay

After 3 h of LPS injection, mice were tested for the manifestation of hind limb clasping phenomenon. Hind limb clasping as described earlier was a dyskinetic posture whereby mice clasped their hind limbs tightly into their abdomen when suspended by their tail indicating neurotoxic effect. The mean of the hind limb score in all animals were plotted as a graph (**Figure** 6.37). Over the past two decades, many attempts have been made to generate animal models of neurodegenerative diseases. In an excellent review by [Whishaw IQ., *et al.*, 1985], the authors had not only listed various tests but also had highlighted the most appropriate test(s) for a particular experimental program or application. Apart from other activity oriented tests, various observational techniques were indicated as stand-alone assessments of mouse behavior. Some of these tests included rating scale assessments of general motor behavior like gait abnormalities,

abnormal limb displacements during walking and running as there were some specific abnormalities like clasping being reported. Clasping observation at the same day 3 h post-treatment for each group is shown in **Figure 6.37**. Naïve group exhibited no clasping whereas LPS group showed severe clasping. Interestingly, **RB12** and Fasudil treated animals reversed the sign of clasping significantly. From this observation, it was clear of LPS dependent effect on the functional parameter of mice, and **RB12** and Fasudil were able to reverse the septic shock or the inflammatory shock of LPS exposure only to some extent significantly.

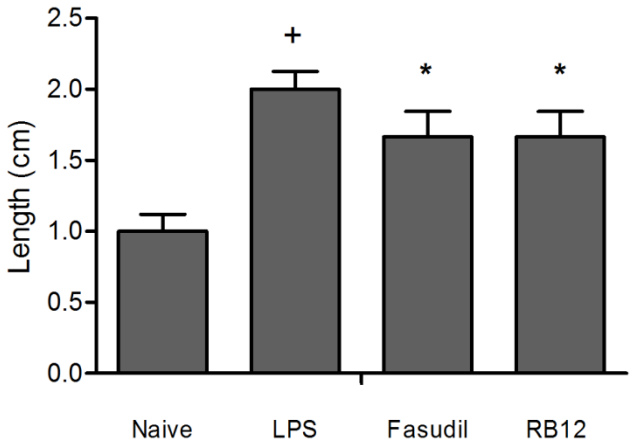

Figure 6.37 Clasping behaviour of **RB12** (30 mg/kg) and Fasudil (30 mg/kg) in LPS (50 mg/kg) induced clasping assay. + represents the significant difference in LPS induced animals compared to naïve.

6.5.2.1.4 Gene expression analysis of inflammatory mediators in LPS induced animal whole brain smaples

In order to understand the effect of **RB12** we attempted for gene expression pattern. After 3 h *in vivo* administered brain samples were pelleted or collected and treated with TRIzol reagent according to manufacture‘s instruction. Though there were no significant effect of LPS on peripheral damage but inflammatory gene expressions were found altered (**Figure 6.38**). Gene expression of four inflammatory mediators were normalized using the house keeping gene GAPDH. The oligonucleotide primer sequence of all the inflammatory mediators are provided in **Table 4.3** in methods section. TNF-α being the primary pro-inflammatory mediator to cross blood brain barrier and induce inflammation in brain, it was also determined in our study. Treatment groups (**RB12** and Fasudil) were effective in attenuating LPS induced inflammatory signals by suppressive expression of IL-6, IL-1β, TNF-α and NFκB. This was in concurrence

with our observationss in *in vitro* and *ex vivo* studies. Thus the effectiveness of the designed lead compound was accomplished till preclinical proof of concept.

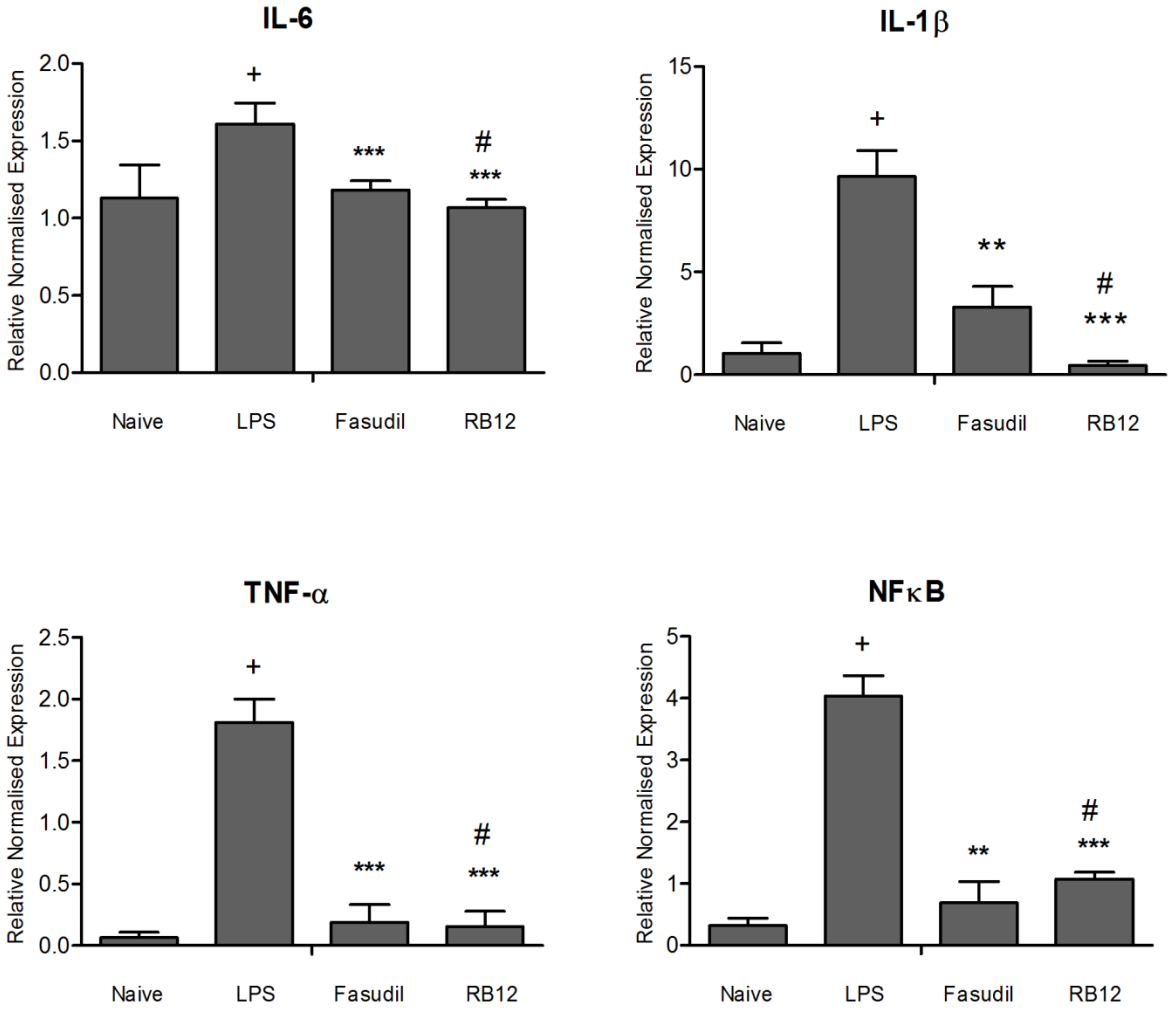

Figure 6.38 Normalized gene expression levels of pro inflammatory cytokines, in LPS induced versus normal brain *in vivo* animal models (n=5). The mRNA expression values were given as mean±SD normalized to GAPDH levels in each sample. Y-axis values represent the number of mRNA copies relative to the number of GAPDH copies in the sample. A significant reduction of (*P<0.05) IL-6 and TNF-α (***P<0.001) and IL-1β (**P<0.01) in Fasudil treated animals compared to **RB12**. # represents the significance in comparison with the Fasudil to **RA6** and **RB12** at 95% confidence intervals.

6.6 Conlusions

Lead molecules obtained from the structure based drug design strategies using energy based and shape based drug design methods, were experimentally evaluated *in vitro*, *ex vivo* and *in vivo* testing, where, the most active lead compounds were found to be **RA6** from Asinex database and **RB12** from BITS library with IC_{50} of 1nM and 357 nM respectively. However, compounds, which displayed good enzyme inhibition and MeHg/ LPS induced IMR-32/ HUVEC cell viability with low cytotoxicity, were considered for *ex vivo* assays. After cytotoxicity analysis (MTT assays) **RA6** and **RB12** were found to be non-cytotoxic compound, and its selectivity index towards cancer cells were >100 for both the compounds. To select a better compound to be utilized for animal studies, we applied different stages of filters to select most promising compound to treat neuroinflammatory conditions in neurological disorders. From cellular studies **RB12** was found more potent than **RA6** in cell motility assays and cytokine transcript expression. Though there were no profound differences between two compounds, we studied both in *ex vivo* inhibition of the cytokine production. **RB12** was found to decrease all cytokines significantly compared to **RA6**. One more filter we applied was the synergistic effect of compounds with the Fasudil. So, combining Fasudil with the **RA6** and **RB12,** revealed more significant effects with **RB12**. The synergistic effect of **RB12** with Fasudil increased the therapeutic effect of the compound, so we selected **RB12** for the neuroprotective activity in *in vivo* animal models. Therefore, compound **RB12** was selected as final lead molecule. Thus we could conclude that **RB12** was found promising to be further developed as drug candidate.

Chapter7

Recapitulation and Future perspectives

With the intention of developing novel ROCK-I and NOX2 dual inhibitors to attenuate neuroinflmmation in neurological disorders, we explored the structure based inhibitor design of two most important targets in neuroinflmmatory pathway: ROCK-I and NOX2. We employed a series of computer aided drug design based approaches and various *in vitro, ex vivo* and *in vivo* interventions to identify potential inhibitors of these two proteins.

- To identify potential hits as dual inhibitors for ROCK-I and NOX2, we retrieved both crystal structures from PDB for 2ESM and 1OV3 respectively.
- A combination of e-pharmacophore and shape based design approach was appled to identify potential hits Asinex database
- For e-pharmacophore and shape approachesw, hypotheses were generated and validated using external and internal parameters. For NOX2, till date there were no repoted inhibitors for the assembly.
- Validated hypothesis were utilized as template to screen Asinex database. The virtual screening protocol was applied, with hypotheses matching to get similar featured and shaped molecules. The hits were clubbed for ROCK-I and NOX2 seperately and docked into their respective grid using HTVS option.
- Then cross docking was performed at SP, the molecules from ROCK-I docked to NOX2 grid and *vice versa*. All molecules were again clubbed together and docked into respective grids simultaneously. Finally 30 compounds were shortlisted by visual inspection and docking parameters.

- We performed ROCK-I enzymatic assay with a conventional method, and for NOX2 indirect cell based assays were performed to draw IC_{50}s ufor all compounds. The most potent compound identified from Asinex databased based on enzymatic activity was **RA6** with the IC_{50} around 1 nM. Notably DSF analyses revealed that ROCK protein complexed with **RA6** improved stability relative to Fasudil.
- Most of the compounds were found promising dual inhibitros of both ROCK-I and NOX2. However some compounds were predicted to show violations of drug-likeliness properties or showed potential cardiotoxicity.
- Similar virtual screening protocol was applied, using hypotheses matching to get similar featured and shaped molecules from our *in house* library.
- Finally, 37 molecules were shortlisted based on docking score as visual inspection from our library.
- IC_{50}s were obtained for the selected 37 molecules for both ROCK-I and NOX2. The most potent compound identified from BITS database based on enzymatic activity was **RB12** with the IC_{50} of 357 nM. Notably DSF analysis revealed that ROCK protein complexed with **RB12** enhanced stability relative to Fasudil.
- The structures of both **RA6** and **RB12** are presented below.

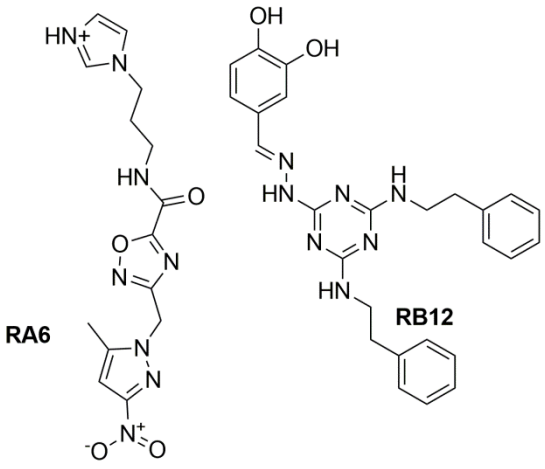

- Compounds, which displayed good enzyme inhibition and cell based MeHg/LPS induced IMR-32/HUVEC cell viability with low cytotoxicity, were analysed. After cytotoxicity analyses (MTT assays) **RA6** and **RB12** were found to be promising and non-cytotoxic and their selectivity indices were found to be higher.

- From cellular studies **RB12** was found to inhibit more efficiently than **RA6** in cell motility assays and cytokine transcript expression.
- The synergistic effect of compounds with Fasudil was also explored. Combining Fasudil with **RA6** or **RB12** revealed more significant effects observed with **RB12** on gene expression of proinflammatory mediators.
- Furthermore, we studied the effect of **RB12** in two animal models: Chronic dosing of MeHg induced neurodegenerative model and LPS induced neuroinflammatory model.
- **RB12** was found effective in treating neuroinflammatory conditions in neurological disorders with suppression of gene expression of cytokines in brain sample from treated animals.
- In LPS induced animal model, peripheral nerve damage was protected upon **RB12** treatment.

8.3 Achievements of the study

This study represents a systematic drug discovery process starting from target crystal structure modelling hypotheses, used for screening of a large database of structures. Virtual docking of the ligands into the receptor identified a set of dual inhibitors, which were tested in a series of assays including *in vitro* enzymatic screening, thermoflour assay, cellular assays, gene expression analysis, *ex vivo* brain slice models and *in vivo* animal models for the neurodegenerative and neuroinflammatory models. This study was unique in a sense of inhibition of multiple targets involved in neuroinflammatory pathway. Identified hits were found novel in inhibiting the two enzymes and their pathway, thereby emerging as prototypical lead for further development.

Future perspectives

- Structural modification of lead compounds **RA6** and **RB12**, could be useful for further molecular development with improved bioactivity.
- Protein expression studies using western blotting, immunofluorescence and immuno histopathological studies on *in vitro*, *ex vivo* and *in vivo* could be performed further to image and understand the allied expressions of particular molecular targets (ROCK-I, NOX2 and ROS generating pathway).
- Studies are still required to confirm the chronic pharmacodynamic and pharmacokinetic profile of the active molecules including safety profile.
- Profound molecular pharmacological studies on specific molecular targets (ex: ROCK-I and NOX2) that causes other neuro degenerative diseases and concomitantly inducing inflammation, need to be studied further.
- Advancement of the candidate compounds presented in this thesis along a drug development path would require a significant investment in medicinal chemistry, preclinical and clinical studies.

References

Abeti, R., Abramov, A. Y., & Duchen, M. R. (2011). Beta-amyloid activates PARP causing astrocytic metabolic failure and neuronal death. *Brain : A Journal of Neurology, 134*(Pt 6), 1658-1672.

Ahmed, Z., Walker, P. S., & Fellows, R. E. (1983). Properties of neurons from dissociated fetal rat brain in serum-free culture. *The Journal of Neuroscience : The Official Journal of the Society for Neuroscience, 3*(12), 2448-2462.

Aimone, J. B., Leasure, J. L., Perreau, V. M., Thallmair, M., & Christopher Reeve Paralysis Foundation Research Consortium. (2004). Spatial and temporal gene expression profiling of the contused rat spinal cord. *Experimental Neurology, 189*(2), 204-221.

Akhter, H., Katre, A., Li, L., Liu, X., & Liu, R. (2011). Therapeutic potential and anti-amyloidosis mechanisms of tert-butylhydroquinone for Alzheimer's disease. *Journal of Alzheimer's Disease, 26*(4), 767-778.

Akiyama, H., Barger, S., Barnum, S., Bradt, B., Bauer, J., Cole, G. M., et al. (2000). Inflammation and Alzheimer's disease. *Neurobiology of Aging, 21*(3), 383-421.

Allen, L. A., DeLeo, F. R., Gallois, A., Toyoshima, S., Suzuki, K., & Nauseef, W. M. (1999). Transient association of the nicotinamide adenine dinucleotide phosphate oxidase subunits p47PHOX and p67PHOX with phagosomes in neutrophils from patients with X-linked chronic granulomatous disease. *Blood, 93*(10), 3521-3530.

Aloe, L., & Fiore, M. (1997). TNF-α expressed in the brain of transgenic mice lowers central tyroxine hydroxylase immunoreactivity and alters grooming behavior. *Neuroscience Letters, 238*(1), 65-68.

Amano, M., Chihara, K., Nakamura, N., Kaneko, T., Matsuura, Y., & Kaibuchi, K. (1999). The COOH terminus of Rho-kinase negatively regulates rho-kinase activity. *The Journal of Biological Chemistry, 274*(45), 32418-32424.

Amano, M., Fukata, Y., & Kaibuchi, K. (2000). Regulation and functions of Rho-associated kinase. *Experimental Cell Research, 261*(1), 44-51.

Amano, M., Kaneko, T., Maeda, A., Nakayama, M., Ito, M., Yamauchi, T., *et al.* (2003). Identification of tau and MAP2 as novel substrates of Rho-kinase and myosin phosphatase. *Journal of Neurochemistry, 87*(3), 780-790.

Andersson, K. E., & Hedlund, P. (2002). New directions for erectile dysfunction therapies. *International Journal of Impotence Research, 14 Suppl 1*, S82-92.

Arai, K., Matsuki, N., Ikegaya, Y., & Nishiyama, N. (2001). Deterioration of spatial learning performances in lipopolysaccharide-treated mice. *The Japanese Journal of Pharmacology, 87*(3), 195-201.

Arbiser, J. L. (2014). Fulvene and fulvalene analogs and their use in treating cancers. U.S. Patent 8,841,276, issued September 23, 2014.

Arimoto, T., & Bing, G. (2003). Up-regulation of inducible nitric oxide synthase in the substantia nigra by lipopolysaccharide causes microglial activation and neurodegeneration. *Neurobiology of Disease, 12*(1), 35-45.

Arimura, N., Inagaki, N., Chihara, K., Menager, C., Nakamura, N., Amano, M., et al. (2000). Phosphorylation of collapsin response mediator protein-2 by Rho-kinase. evidence for two separate signaling pathways for growth cone collapse. *The Journal of Biological Chemistry, 275*(31), 23973-23980.

Asakura, W., Matsumoto, K., Ohta, H., & Watanabe, H. (1993). Effect of α_2-adrenergic drugs on REM sleep deprivation-induced increase in swimming activity. *Pharmacology Biochemistry and Behavior, 46*(1), 111-115.

Aschner, M., & Syversen, T. (2005). Methylmercury: Recent advances in the understanding of its neurotoxicity. *Therapeutic Drug Monitoring, 27*(3), 278-283.

Ashkenazi, A., & Dixit, V. M. (1998). Death receptors: Signaling and modulation. *Science (New York, N.Y.), 281*(5381), 1305-1308.

Aznar, S., Fernández-Valerón, P., Espina, C., & Lacal, J. C. (2004). Rho GTPases: Potential candidates for anticancer therapy. *Cancer Letters, 206*(2), 181-191.

Babior, B. M. (1999). NOX: An update. *Blood, 93*(5), 1464-1476.

Banati, R. B., Daniel, S. E., & Blunt, S. B. (1998). Glial pathology but absence of apoptotic nigral neurons in long-standing parkinson's disease. *Movement Disorders, 13*(2), 221-227.

Barrocas, A. M., Cochrane, D. E., Carraway, R. E., & Feldberg, R. S. (1999). Neurotensin stimulation of mast cell secretion is receptor-mediated, pertussis-toxin sensitive and requires activation of phospholipase C. *Immunopharmacology, 41*(2), 131-137.

Barth, B. M., Gustafson, S. J., Young, M. M., Fox, T. E., Shanmugavelandy, S. S., Kaiser, J. M., (2010). Inhibition of NOX by glucosylceramide confers chemoresistance. *Cancer Biology & Therapy, 10*(11), 1126-1136.

Bastos, G., Moriya, T., Inui, F., Katura, T., & Nakahata, N. (2008). Involvement of cyclooxygenase-2 in lipopolysaccharide-induced impairment of the newborn cell survival in the adult mouse dentate gyrus. *Neuroscience, 155*(2), 454-462.

Baune, B. T., Wiede, F., Braun, A., Golledge, J., Arolt, V., & Koerner, H. (2008). Cognitive dysfunction in mice deficient for TNF-α and its receptors. *American Journal of Medical Genetics Part B: Neuropsychiatric Genetics, 147*(7), 1056-1064.

Bažil, V., Baudyš, M., Hilgert, I., Štefanová, I., Low, M. G., Zbrožek, J. (1989). Structural relationship between the soluble and membrane-bound forms of human monocyte surface glycoprotein CD 14. *Molecular Immunology, 26*(7), 657-662.

Bedard, K., & Krause, K. H. (2007). The NOX family of ROS-generating NOXs: Physiology and pathophysiology. *Physiological Reviews, 87*(1), 245-313.

Beers, D. R., Henkel, J. S., Xiao, Q., Zhao, W., Wang, J., Yen, A. A., et al. (2006). Wild-type microglia extend survival in PU.1 knockout mice with familial amyotrophic lateral sclerosis. *Proceedings of the National Academy of Sciences of the United States of America, 103*(43), 16021-16026.

Belletti, S., Orlandini, G., Vettori, M. V., Mutti, A., Uggeri, J., Scandroglio, R. (2002). Time course assessment of methylmercury effects on C6 glioma cells: Submicromolar concentrations induce oxidative DNA damage and apoptosis. *Journal of Neuroscience Research, 70*(5), 703-711.

Bertoni, A., Giuliano, P., Galgani, M., Rotoli, D., Ulianich, L., Adornetto, A. (2011). Early and late events induced by polyQ-expanded proteins: Identification of a common pathogenic property of polYQ-expanded proteins. *The Journal of Biological Chemistry, 286*(6), 4727-4741.

Bishop, A., & Hall, A. (2000). Rho GTPases and their effector proteins. *Biochem.J, 348*, 241-255.

Bjorkqvist, M., Wild, E. J., Thiele, J., Silvestroni, A., Andre, R., Lahiri, N. (2008). A novel pathogenic pathway of immune activation detec**Table** before clinical onset in huntington's disease. *The Journal of Experimental Medicine, 205*(8), 1869-1877.

Block, M. L., Zecca, L., & Hong, J. (2007). Microglia-mediated neurotoxicity: Uncovering the molecular mechanisms. *Nature Reviews Neuroscience, 8*(1), 57-69.

Block, M. L., & Calderón-Garcidueñas, L. (2009). Air pollution: Mechanisms of neuroinflammation and CNS disease. *Trends in Neurosciences, 32*(9), 506-516.

Boillee, S., Yamanaka, K., Lobsiger, C. S., Copeland, N. G., Jenkins, N. A., Kassiotis, G. (2006). Onset and progression in inherited ALS determined by motor neurons and microglia. *Science (New York), 312*(5778), 1389-1392.

Boka, G., Anglade, P., Wallach, D., Javoy-Agid, F., Agid, Y., & Hirsch, E. (1994). Immunocytochemical analysis of tumor necrosis factor and its receptors in parkinson's disease. *Neuroscience Letters, 172*(1), 151-154.

Boku, S., Nakagawa, S., Masuda, T., Nishikawa, H., Kato, A., & Kitaichi, Y. (2009): Glucocorticoids and lithium reciprocally regulate the proliferation of adult dentate gyrus-derived neural precursor cells through GSK-3beta and beta-catenin/TCF pathway. *Neuropsychopharmacology, 34*, 805-815.

Borisoff, J. F., Chan, C. C., Hiebert, G. W., Oschipok, L., Robertson, G. S., Zamboni, R. (2003). Suppression of Rho-kinase activity promotes axonal growth on inhibitory CNS substrates. *Molecular and Cellular Neuroscience, 22*(3), 405-416.

Bourne, K. Z., Ferrari, D. C., Lange-Dohna, C., Roßner, S., Wood, T. G., & Perez-Polo, J. R. (2007). Differential regulation of BACE1 promoter activity by nuclear factor-κB in neurons and glia upon exposure to β-amyloid peptides. *Journal of Neuroscience Research, 85*(6), 1194-1204.

Bourne, H. R., Sanders, D. A., & McCormick, F. (1990). The GTPase superfamily: A conserved switch for diverse cell functions. *Nature, 348*(6297), 125-132.

Brabeck, C., Beschorner, R., Conrad, S., Mittelbronn, M., Bekure, K., Meyermann, R., et al. (2004). Lesional expression of RhoA and RhoB following traumatic brain injury in humans. *Journal of Neurotrauma, 21*(6), 697-706.

Breitenlechner, C., Gaßel, M., Hidaka, H., Kinzel, V., Huber, R., Engh, R. A., et al. (2003). Protein kinase A in complex with rho-kinase inhibitors Y-27632, Fasudil, and H-1152P: Structural basis of selectivity. *Structure, 11*(12), 1595-1607.

Bridges, C. C., & Zalups, R. K. (2010). Transport of inorganic mercury and methylmercury in target tissues and organs. *Journal of Toxicology and Environmental Health, Part B, 13*(5), 385-410.

Brown, R. C., Lockwood, A. H., & Sonawane, B. R. (2005). Neurodegenerative diseases: An overview of environmental risk factors. *Environmental Health Perspectives, ,* 1250-1256.

Bruce-Keller, A. J., Gupta, S., Parrino, T. E., Knight, A. G., Ebenezer, P. J., Weidner, A. M. (2010). NOX activity is increased in mild cognitive impairment. *Antioxidants & Redox Signaling, 12*(12), 1371-1382.

Burridge, K., & Wennerberg, K. (2004). Rho and rac take center stage. *Cell, 116*(2), 167-179.

Bush, E. W., Helmke, S. M., Birnbaum, R. A., & Perryman, M. B. (2000). Myotonic dystrophy protein kinase domains mediate localization, oligomerization, novel catalytic activity, and autoinhibition. *Biochemistry, 39*(29), 8480-8490.

Buttke, T. M., McCubrey, J. A., & Owen, T. C. (1993). Use of an aqueous soluble tetrazolium/formazan assay to measure viability and proliferation of lymphokine-dependent cell lines. *Journal of Immunological Methods, 157*(1), 233-240.

Cacci, E., Ajmone-Cat, M. A., Anelli, T., Biagioni, S., & Minghetti, L. (2008). In-vitro neuronal and glial differentiation from embryonic or adult neural precursor cells are differently affected by chronic or acute activation of microglia. *Glia, 56*(4), 412-425.

Caroff, M., Karibian, D., Cavaillon, J., & Haeffner-Cavaillon, N. (2002). Structural and functional analyses of bacterial lipopolysaccharides. *Microbes and Infection, 4*(9), 915-926.

Carraway, R., & Leeman, S. E. (1973). The isolation of a new hypotensive peptide, neurotensin, from bovine hypothalami. *The Journal of Biological Chemistry, 248*(19), 6854-6861.

Carraway, R. E., Singer, E. A., Ferris, C. F., & Mitra, S. P. (1986). Generation of immunoreactive neurotensin(s) and enkephalin(s) by pepsin-treatment of plasma. *Advances in Experimental Medicine and Biology, 198*, 169-179.

Carvey, P., Chen, E., Lipton, J., Tong, C., Chang, Q., & Ling, Z. (2005). Intra-parenchymal injection of tumor necrosis factor-α and interleukin 1-β produces dopamine neuron loss in the rat. *Journal of Neural Transmission, 112*(5), 601-612.

Catharine, A. S., Alissa, A. R., Carrie, S., Ashley L. P., Katherine, M., Alexander, H., John M. E., Dennstedt., & Brad, A. B. (2010). Pharmacological inhibition of Rho-kinase (ROCK) signaling enhances cisplatin resistance in neuroblastoma cells. *International Journal of Oncology*, 37(5), 1297-1305.

Chan, E. C., Jiang, F., Peshavariya, H. M., & Dusting, G. J. (2009). Regulation of cell proliferation by NOX-mediated signaling: Potential roles in tissue repair, regenerative medicine and tissue engineering. *Pharmacology & Therapeutics, 122*(2), 97-108.

Chance, B., Sies, H., & Boveris, A. (1979). Hydroperoxide metabolism in mammalian organs. *Physiological Reviews, 59*(3), 527-605.

Chang, J. Y. (2007). Methylmercury causes glial IL-6 release. *Neuroscience Letters, 416*(3), 217-220.

Chomczynski, P. (1993). A reagent for the single-step simultaneous isolation of RNA, DNA and proteins from cell and tissue samples. *Biotechniques, 15*(3), 532-4.

Clement, A. M., Nguyen, M. D., Roberts, E. A., Garcia, M. L., Boillee, S., Rule, M. (2003). Wild-type non-neuronal cells extend survival of SOD1 mutant motor neurons in ALS mice. *Science (New York, N.Y.), 302*(5642), 113-117.

Cleren, C., Calingasan, N. Y., Chen, J., & Beal, M. F. (2005). Celastrol protects against MPTP- and 3-nitropropionic acid-induced neurotoxicity. *Journal of Neurochemistry, 94*(4), 995-1004.

Coleman, M. L., Sahai, E. A., Yeo, M., Bosch, M., Dewar, A., & Olson, M. F. (2001). Membrane blebbing during apoptosis results from caspase-mediated activation of ROCK I. *Nature Cell Biology, 3*(4), 339-345.

Dalrymple, A., Wild, E. J., Joubert, R., Sathasivam, K., Björkqvist, M., Petersén, Å. (2007). Proteomic profiling of plasma in huntington's disease reveals neuroinflammatory activation and biomarker candidates. *Journal of Proteome Research, 6*(7), 2833-2840.

Das, S., Rao, B. N., & Rao, B. S. (2011). Mangiferin attenuates methylmercury induced cytotoxicity against IMR-32, human neuroblastoma cells by the inhibition of oxidative stress and free radical scavenging potential. *Chemico-Biological Interactions, 193*(2), 129-140.

Das, A. K., Cohen, P. W., & Barford, D. (1998). The structure of the tetratricopeptide repeats of protein phosphatase 5: Implications for TPR-mediated protein-protein interactions. *The EMBO Journal, 17*(5), 1192-1199.

De Luca, G., Russo, M. T., Degan, P., Tiveron, C., Zijno, A., Meccia, E. (2008). A role for oxidized DNA precursors in huntington's Disease–Like striatal neurodegeneration. *PLoS Genetics, 4*(11), e1000266.

De Mendez, I., Homayounpour, N., & Leto, T. L. (1997). Specificity of p47PHOX SH3 domain interactions in NOX assembly and activation. *Molecular and Cellular Biology, 17*(4), 2177-2185.

Dean, E. (2008). Apoptosis in neurodegeneration: Programmed cell death and its role in Alzheimer's and Huntington's diseases. *Eukaryon*, 4, 42-48.

Del Bigio, M. R. (2010). Ependymal cells: Biology and pathology. *Acta Neuropathologica, 119*(1), 55-73.

Dergham, P., Ellezam, B., Essagian, C., Avedissian, H., Lubell, W. D., & McKerracher, L. (2002). Rho signaling pathway targeted to promote spinal cord repair. *The Journal of Neuroscience : The Official Journal of the Society for Neuroscience, 22*(15), 6570-6577.

Dewil, M., Lambrechts, D., Sciot, R., Shaw, P., Ince, P., Robberecht, W. (2007). Vascular endothelial growth factor counteracts the loss of phospho-Akt preceding motor neurone degeneration in amyotrophic lateral sclerosis. *Neuropathology and Applied Neurobiology, 33*(5), 499-509.

Dinauer, M. C. (2003). Regulation of neutrophil function by rac GTPases. *Current Opinion in Hematology, 10*(1), 8-15.

Dixon, S. L., Smondyrev, A. M., Knoll, E. H., Rao, S. N., Shaw, D. E., & Friesner, R. A. (2006). PHASE: a new engine for pharmacophore perception, 3D QSAR model development, and 3D database screening: 1. Methodology and preliminary results. *Journal of computer-aided molecular design*, 20(10), 647-671.

Dobrovolskaia, M. A., Medvedev, A. E., Thomas, K. E., Cuesta, N., Toshchakov, V., Ren, T. (2003). Induction of in vitro reprogramming by toll-like receptor (TLR)2 and TLR4 agonists in murine macrophages: Effects of TLR "homotolerance" versus "heterotolerance" on NF-κ B signaling pathway components. *Journal of Immunology (Baltimore, Md.: 1950), 170*(1), 508-519.

Dolga, A. M., Nijholt, I. M., Ostroveanu, A., Ten Bosch, Q., Luiten, P. G., & Eisel, U. L. (2008). Lovastatin induces neuroprotection through tumor necrosis factor receptor 2 signaling pathways. *Journal of Alzheimer's Disease, 13*(2), 111-122.

Doran, J., Liu, X., Taslimi, P., Saadat, A., & Fox, T. (2004). New insights into the structure-function relationships of rho-associated kinase: A thermodynamic and hydrodynamic study of the dimer-to-monomer transition and its kinetic implications. *Biochem.J,* 384, 255-262.

Doussiere, J., Brandolin, G., Derrien, V., & Vignais, P. V. (1993). Critical assessment of the presence of an NADPH binding site on neutrophil cytochrome b558 by photoaffinity and immunochemical labeling. *Biochemistry, 32*(34), 8880-8887.

Doran, J. D., & Jacobs, M. D. (2008). ROCK enzymatic assay. *Wnt signaling* (pp. 197-205) Springer.

Dröge, W., & Schipper, H. M. (2007). Oxidative stress and aberrant signaling in aging and cognitive decline. *Aging Cell, 6*(3), 361-370.

Dubreuil, C. I., Winton, M. J., & McKerracher, L. (2003). Rho activation patterns after spinal cord injury and the role of activated rho in apoptosis in the central nervous system. *The Journal of Cell Biology, 162*(2), 233-243.

Duffy, E. M., & Jorgensen, W. L. (2000). Prediction of properties from simulations: free energies of solvation in hexadecane, octanol, and water. *Journal of the American chemical society,* 122(12), 2878-2888.

Duman, E. N., Kesim, M., Kadioglu, M., Ulku, C., Kalyoncu, N. I., & Yaris, E. (2006). Effect of gender on antinociceptive effect of paroxetine in hot plate test in mice. *Progress in Neuro-Psychopharmacology and Biological Psychiatry*, 30(2), 292-296.

Dvorsky, R., Blumenstein, L., Vetter, I. R., & Ahmadian, M. R. (2004). Structural insights into the interaction of ROCKI with the switch regions of RhoA. *The Journal of Biological Chemistry, 279*(8), 7098-7104.

Eldridge, M. D., Murray, C. W., Auton, T. R., Paolini, G. V., & Mee, R. P. (1997). Empirical scoring functions: I. the development of a fast empirical scoring function to estimate the binding affinity of ligands in receptor complexes. *Journal of Computer-Aided Molecular Design, 11*(5), 425-445.

Elliott, J. L. (2001). Cytokine upregulation in a murine model of familial amyotrophic lateral sclerosis. *Molecular Brain Research, 95*(1), 172-178.

Engelhardt, J. F., Sen, C. K., & Oberley, L. (2001). Redox-modulating gene therapies for human diseases. *Antioxidants and Redox Signaling, 3*(3), 341-346.

Eriksen, J. L., Sagi, S. A., Smith, T. E., Weggen, S., Das, P., McLendon, D. C. (2003). NSAIDs and enantiomers of flurbiprofen target gamma-secretase and lower abeta 42 in vivo. *The Journal of Clinical Investigation, 112*(3), 440-449.

Eskes, C., Honegger, P., Juillerat-Jeanneret, L., & Monnet-Tschudi, F. (2002). Microglial reaction induced by noncytotoxic methylmercury treatment leads to neuroprotection via interactions with astrocytes and IL-6 release. *Glia, 37*(1), 43-52.

Fancy, S. P., Kotter, M. R., Harrington, E. P., Huang, J. K., Zhao, C., Rowitch, D. H. (2010). Overcoming remyelination failure in multiple sclerosis and other myelin disorders. *Experimental Neurology, 225*(1), 18-23.

Farina, M., Aschner, M., & Rocha, J. B. (2011). Oxidative stress in MeHg-induced neurotoxicity. *Toxicology and Applied Pharmacology, 256*(3), 405-417.

Ferger, B., Leng, A., Mura, A., Hengerer, B., & Feldon, J. (2004). Genetic ablation of tumor necrosis factor-alpha (TNF-α) and pharmacological inhibition of TNF-synthesis attenuates MPTP toxicity in mouse striatum. *Journal of Neurochemistry, 89*(4), 822-833.

Ferri, A., Nencini, M., Battistini, S., Giannini, F., Siciliano, G., Casali, C. (2004). Activity of protein phosphatase calcineurin is decreased in sporadic and familial amyotrophic lateral sclerosispatients. *Journal of Neurochemistry, 90*(5), 1237-1242.

Fillit, H., Ding, W., Buee, L., Kalman, J., Altstiel, L., Lawlor, B. (1991). Elevated circulating tumor necrosis factor levels in alzheimer's disease. *Neuroscience Letters, 129*(2), 318-320.

Fournier, A. E., Takizawa, B. T., & Strittmatter, S. M. (2003). Rho kinase inhibition enhances axonal regeneration in the injured CNS. *The Journal of Neuroscience : The Official Journal of the Society for Neuroscience, 23*(4), 1416-1423.

Friesner, R. A., Murphy, R. B., Repasky, M. P., Frye, L. L., Greenwood, J. R., Halgren, T. A., & Mainz, D. T. (2006). Extra precision glide: docking and scoring incorporating a model of hydrophobic enclosure for protein-ligand complexes. *Journal of medicinal chemistry,* 49(21), 6177-6196.

Fujimoto, T., Yamazaki, S., Eto-Kimura, A., Takeshige, K., & Muta, T. (2004). The amino-terminal region of toll-like receptor 4 is essential for binding to MD-2 and receptor translocation to the cell surface. *The Journal of Biological Chemistry, 279*(46), 47431-47437.

Gallagher, M., Landfield, P. W., McEwen, B., Meaney, M. J., Rapp, P. R., Sapolsky, R. (1996). Hippocampal neurodegeneration in aging. *Science (New York), 274*(5287), 484-485.

Gao, H., & Hong, J. (2008). Why neurodegenerative diseases are progressive: Uncontrolled inflammation drives disease progression. *Trends in Immunology, 29*(8), 357-365.

Garcia-Ovejero, D., Azcoitia, I., DonCarlos, L. L., Melcangi, R. C., & Garcia-Segura, L. M. (2005). Glia-neuron crosstalk in the neuroprotective mechanisms of sex steroid hormones. *Brain Research Reviews, 48*(2), 273-286.

Gerhard, A., Pavese, N., Hotton, G., Turkheimer, F., Es, M., Hammers, A. (2006). In-vivo imaging of microglial activation with [11 C](R)-PK11195 PET in idiopathic parkinson's disease. *Neurobiology of Disease, 21*(2), 404-412.

Genkyo Tex, S. A. (2010). Tetrahydroindole derivatives as NOX inhibitors. USPTO20100120749

Gibertini, M., Newton, C., Friedman, H., & Klein, T. W. (1995). Spatial learning impairment in mice infected with legionella pneumophila or administered exogenous interleukin-1-β. *Brain Behavior and Immunity, 9*(2), 113-128.

Girirajan, S., Patel, N., Slager, R. E., Tokarz, M. E., Bucan, M., Wiley, J. L. (2008). How much is too much? phenotypic consequences of Rai1 overexpression in mice. *European Journal of Human Genetics, 16*(8), 941-954.

Goines, P. E., & Ashwood, P. (2013). Cytokine dysregulation in autism spectrum disorders (ASD): Possible role of the environment. *Neurotoxicology and Teratology, 36,* 67-81.

Goto, H., Kosako, H., Tanabe, K., Yanagida, M., Sakurai, M., Amano, M. (1998). Phosphorylation of vimentin by rho-associated kinase at a unique amino-terminal site that is specifically phosphorylated during cytokinesis. *The Journal of Biological Chemistry, 273*(19), 11728-11736.

Gourie-Devi, M. (2014). Epidemiology of neurological disorders in India: Review of background, prevalence and incidence of epilepsy, stroke, Parkinson's disease and tremors. *Neurology India*, 62(6), 588.

Gralewicz, S., Wiaderna, D., Lutz, P., & Sitarek, K. (2009). Neurobehavioural functions in adult progeny of rat mothers exposed to methylmercury or 2, 2', 4, 4', 5, 5'-hexachlorobiphenyl (PCB 153) alone or their combination during gestation and lactation. *International Journal of Occupational Medicine and Environmental Health, 22*(3), 277-291.

Grant, J. A., Gallardo, M. A., & Pickup, B. T. (1996). A fast method of molecular shape comparison: A simple application of a Gaussian description of molecular shape. *Journal of computational chemistry*, 17(14), 1653-1666.

Greenwood, J., Walters, C. E., Pryce, G., Kanuga, N., Beraud, E., Baker, D. (2003). Lovastatin inhibits brain endothelial cell rho-mediated lymphocyte migration and attenuates experimental autoimmune encephalomyelitis. *FASEB Journal : Official Publication of the Federation of American Societies for Experimental Biology, 17*(8), 905-907.

Greenwood, J. R., Calkins, D., Sullivan, A. P., & Shelley, J. C. (2010). Towards the comprehensive, rapid, and accurate prediction of the favorable tautomeric states of drug-like molecules in aqueous solution. *Journal of computer-aided molecular design*, 24(6-7), 591-604.

Groemping, Y., Lapouge, K., Smerdon, S. J., & Rittinger, K. (2003). Molecular basis of phosphorylation-induced activation of the NOX. *Cell*, *113*(3), 343-355.

Gu, Y., Jia, B., Yang, F. C., D'Souza, M., Harris, C. E., Derrow, C. W. (2001). Biochemical and biological characterization of a human Rac2 GTPase mutant associated with phagocytic immunodeficiency. *The Journal of Biological Chemistry, 276*(19), 15929-15938.

Guerreiro, R. J., Santana, I., Bras, J. M., Santiago, B., Paiva, A., & Oliveira, C. (2007). Peripheral inflammatory cytokines as biomarkers in alzheimer's disease and mild cognitive impairment. *Neuro-Degenerative Diseases, 4*(6), 406-412.

Hagberg, H., Gressens, P., & Mallard, C. (2012). Inflammation during fetal and neonatal life: Implications for neurologic and neuropsychiatric disease in children and adults. *Annals of Neurology*, *71*(4), 444-457.

Hagiwara, N., Ikeda, K., Higashida, H., Tomita, K., & Yokoyama, S. (2005). Induction of tumor necrosis factor-α in schwann cells after gradual elongation of rat sciatic nerve. *Journal of Orthopaedic Science*, *10*(6), 614-621.

Håkansson, A., Westberg, L., Nilsson, S., Buervenich, S., Carmine, A., Holmberg, B., *et.al*. (2005a). Interaction of polymorphisms in the genes encoding interleukin-6 and estrogen receptor beta on the susceptibility to parkinson's disease. *American Journal of Medical Genetics Part B: Neuropsychiatric Genetics, 133*(1), 88-92.

Håkansson, A., Westberg, L., Nilsson, S., Buervenich, S., Carmine, A., Holmberg, B. (2005b). Investigation of genes coding for inflammatory components in parkinson's disease. *Movement Disorders, 20*(5), 569-573.

Halgren, T. A., Murphy, R. B., Friesner, R. A., Beard, H. S., Frye, L. L., Pollard, W. T., & Banks, J. L. (2004). Glide: a new approach for rapid, accurate docking and scoring. 2. Enrichment factors in database screening. *Journal of medicinal chemistry*, 47(7), 1750-1759.

Hara, M., Takayasu, M., Watanabe, K., Noda, A., Takagi, T., Suzuki, Y. (2000). Protein kinase inhibition by Fasudil hydrochloride promotes neurological recovery after spinal cord injury in rats. *Journal of Neurosurgery: Spine, 93*(1), 94-101.

Hardy, J., & Orr, H. (2006). The genetics of neurodegenerative diseases. *Journal of Neurochemistry, 97*(6), 1690-1699.

Harman, D. (1955). Aging: A theory based on free radical and radiation chemistry. *Science's SAGE KE,* 2002(37), 14.

Hashimoto, R., Nakamura, Y., Goto, H., Wada, Y., Sakoda, S., Kaibuchi, K. (1998). Domain- and site-specific phosphorylation of bovine NF-L by rho-associated kinase. *Biochemical and Biophysical Research Communications, 245*(2), 407-411.

Hashimoto, R., Nakamura, Y., Kosako, H., Amano, M., Kaibuchi, K., Inagaki, M. (1999). Distribution of rho-kinase in the bovine brain. *Biochemical and Biophysical Research Communications, 263*(2), 575-579.

Hauss-Wegrzyniak, B., Dobrzanski, P., Stoehr, J. D., & Wenk, G. L. (1998). Chronic neuroinflammation in rats reproduces components of the neurobiology of alzheimer's disease. *Brain Research, 780*(2), 294-303.

Hauwel, M., Furon, E., Canova, C., Griffiths, M., Neal, J., & Gasque, P. (2005). Innate (inherent) control of brain infection, brain inflammation and brain repair: The role of microglia, astrocytes,"protective" glial stem cells and stromal ependymal cells. *Brain Research Reviews, 48*(2), 220-233.

Hayamizu, T. F., Chan, P. T., & Johanson, C. E. (2001). FGF-2 immunoreactivity in adult rat ependyma and choroid plexus: Responses to global forebrain ischemia and intraventricular FGF-2. *Neurological Research, 23*(4), 353-358.

He, Z., & Koprivica, V. (2004). The nogo signaling pathway for regeneration block. *Annual Reviews Neuroscience, 27,* 341-368.

He, P., Zhong, Z., Lindholm, K., Berning, L., Lee, W., Lemere, C. (2007). Deletion of tumor necrosis factor death receptor inhibits amyloid beta generation and prevents learning and memory deficits in alzheimer's mice. *The Journal of Cell Biology, 178*(5), 829-841.

Head, R. J., McLennan, P. L., Raederstorff, D., Muggli, R., Burnard, S. L., & McMurchie, E. J. (2000). Prevention of nerve conduction deficit in diabetic rats by polyunsaturated fatty acids. *The American Journal of Clinical Nutrition, 71*(1 Suppl), 386S-92S.

Hendriks, J. J., Alblas, J., van der Pol, S. M., van Tol, E. A., Dijkstra, C. D., & de Vries, H. E. (2004). Flavonoids influence monocytic GTPase activity and are protective in experimental allergic encephalitis. *The Journal of Experimental Medicine, 200*(12), 1667-1672.

Henkel, J. S., Engelhardt, J. I., Siklós, L., Simpson, E. P., Kim, S. H., Pan, T. (2004). Presence of dendritic cells, MCP-1, and activated microglia/macrophages in amyotrophic lateral sclerosis spinal cord tissue. *Annals of Neurology, 55*(2), 221-235.

Henkel, J. S., Beers, D. R., Siklós, L., & Appel, S. H. (2006). The chemokine MCP-1 and the dendritic and myeloid cells it attracts are increased in the mSOD1 mouse model of ALS. *Molecular and Cellular Neuroscience, 31*(3), 427-437.

Heyworth, P. G., Knaus, U. G., Settleman, J., Curnutte, J. T., & Bokoch, G. M. (1993). Regulation of NOX activity by rac GTPase activating protein(s). *Molecular Biology of the Cell, 4*(11), 1217-1223.

Heyworth, P. G., Cross, A. R., & Curnutte, J. T. (2003). Chronic granulomatous disease. *Current Opinion in Immunology, 15*(5), 578-584.

Hidaka, H., Matsuura, A., & Matsuzaki, T. (2000). *Isoquinoline Derivatives and Drugs, U.S. Patent No.* 6,153,608. Washington, DC.

Hirooka, Y., & Shimokawa, H. (2005). Therapeutic potential of Rho-kinase inhibitors in cardiovascular diseases. *American Journal of Cardiovascular Drugs, 5*(1), 31-39.

Hodges, A., Strand, A. D., Aragaki, A. K., Kuhn, A., Sengstag, T., Hughes, G. (2006). Regional and cellular gene expression changes in human huntington's disease brain. *Human Molecular Genetics, 15*(6), 965-977.

Hoffman, G. R., Nassar, N., & Cerione, R. A. (2000). Structure of the rho family GTP-binding protein Cdc42 in complex with the multifunctional regulator RhoGDI. *Cell, 100*(3), 345-356.

Holmes, C., Cunningham, C., Zotova, E., Woolford, J., Dean, C., Kerr, S. (2009). Systemic inflammation and disease progression in alzheimer disease. *Neurology, 73*(10), 768-774.

Honing, H., van den Berg, T. K., van der Pol, S. M., Dijkstra, C. D., van der Kammen, R. A., Collard, J. G. (2004). RhoA activation promotes transendothelial migration of monocytes via ROCK. *Journal of Leukocyte Biology, 75*(3), 523-528.

Hu, X. (2003). Proteolytic signaling by TNF-α: Caspase activation and IκB degradation. *Cytokine, 21*(6), 286-294.

Hu, E., & Lee, D. (2003). Rho kinase inhibitors as potential therapeutic agents for cardiovascular diseases. *Current Opinion in Investigational Drugs (London, England : 2000), 4*(9), 1065-1075.

Huang, Y., Lu, Y., Zhang, L., Yan, J., Jiang, J., & Jiang, H. (2014). Perineural dexmedetomidine attenuates inflammation in rat sciatic nerve via the NF-κB pathway. *International Journal of Molecular Sciences, 15*(3), 4049-4059.

Huh, S. H., Chung, Y. C., Piao, Y., Jin, M. Y., Son, H. J., Yoon, N. S. (2011). Ethyl pyruvate rescues nigrostriatal dopaminergic neurons by regulating glial activation in a mouse model of parkinson's disease. *Journal of Immunology (Baltimore, Md.: 1950), 187*(2), 960-969.

Ikenoya, M., Hidaka, H., Hosoya, T., Suzuki, M., Yamamoto, N., & Sasaki, Y. (2002). Inhibition of Rho-kinase-induced myristoylated alanine-rich C kinase substrate (MARCKS) phosphorylation in human neuronal cells by H-1152, a novel and specific Rho-kinase inhibitor. *Journal of Neurochemistry, 81*(1), 9-16.

Ingalls, R. R., & Golenbock, D. T. (1995). CD11c/CD18, a transmembrane signaling receptor for lipopolysaccharide. *The Journal of Experimental Medicine, 181*(4), 1473-1479.

Inoue, M., Rashid, M. H., Fujita, R., Contos, J. J., Chun, J., & Ueda, H. (2004). Initiation of neuropathic pain requires lysophosphatidic acid receptor signaling. *Nature Medicine, 10*(7), 712-718.

Ishida, T., Takanashi, Y., Doi, H., Yamamoto, I., & Kiwada, H. (2002). Encapsulation of an antivasospastic drug, Fasudil, into liposomes, and in vitro stability of the Fasudil-loaded liposomes. *International Journal of Pharmaceutics, 232*(1), 59-67.

Ishizaki, T., Maekawa, M., Fujisawa, K., Okawa, K., Iwamatsu, A., Fujita, A. (1996). The small GTP-binding protein rho binds to and activates a 160 kDa Ser/Thr protein kinase homologous to myotonic dystrophy kinase. *The EMBO Journal, 15*(8), 1885-1893.

Ito, T., Matsui, Y., Ago, T., Ota, K., & Sumimoto, H. (2001). Novel modular domain PB1 recognizes PC motif to mediate functional protein–protein interactions. *The EMBO Journal, 20*(15), 3938-3946.

Jacobs, M., Hayakawa, K., Swenson, L., Bellon, S., Fleming, M., Taslimi, P. (2006). The structure of dimeric ROCK I reveals the mechanism for ligand selectivity. *The Journal of Biological Chemistry, 281*(1), 260-268.

Ji, R. R., & Strichartz, G. (2004). Cell signaling and the genesis of neuropathic pain. *Science's STKE : Signal Transduction Knowledge Environment, 2004*(252), reE14.

Jin, X., Lok, E., Bondy, G., Caldwell, D., Mueller, R., Kapal, K. (2007). Modulating effects of dietary fats on methylmercury toxicity and distribution in rats. *Toxicology, 230*(1), 22-44.

Jacobson, M. P., Pincus, D. L., Rapp, C. S., Day, T. J., Honig, B., Shaw, D. E., & Friesner, R. A. (2004). A hierarchical approach to all-atom protein loop prediction. *Proteins: Structure, Function, and Bioinformatics*, 55(2), 351-367.

Johnson, C. P., Myers, S. M., & American Academy of Pediatrics Council on Children With Disabilities. (2007). Identification and evaluation of children with autism spectrum disorders. *Pediatrics, 120*(5), 1183-1215.

Jorgensen, W. L., Maxwell, D. S., & Tirado-Rives, J. (1996). Development and testing of the OPLS all-atom force field on conformational energetics and properties of organic liquids. *Journal of the American Chemical Society, 118*(45), 11225-11236.

Kahles, T., Luedike, P., Endres, M., Galla, H. J., Steinmetz, H., Busse, R. (2007). NOX plays a central role in blood-brain barrier damage in experimental stroke. *Stroke; a Journal of Cerebral Circulation, 38*(11), 3000-3006.

Kakulas, B. A. (1999). A review of the neuropathology of human spinal cord injury with emphasis on special features. *The Journal of Spinal Cord Medicine, 22*(2), 119-124.

Kami, K., Takeya, R., Sumimoto, H., & Kohda, D. (2002). Diverse recognition of non-PxxP peptide ligands by the SH3 domains from p67PHOX, Grb2 and Pex13p. *The EMBO Journal, 21*(16), 4268-4276.

Kanai, F., Liu, H., Field, S. J., Akbary, H., Matsuo, T., Brown, G. E. (2001). The PX domains of p47PHOX and p40PHOX bind to lipid products of PI (3) K. *Nature Cell Biology, 3*(7), 675-678.

Kang, S. H., Li, Y., Fukaya, M., Lorenzini, I., Cleveland, D. W., Ostrow, L. W. (2013). Degeneration and impaired regeneration of gray matter oligodendrocytes in amyotrophic lateral sclerosis. *Nature Neuroscience, 16*(5), 571-579.

Kawamata, T., Akiyama, H., Yamada, T., & McGeer, P. L. (1992). Immunologic reactions in amyotrophic lateral sclerosis brain and spinal cord tissue. *The American Journal of Pathology, 140*(3), 691-707.

Keizman, D., Rogowski, O., Berliner, S., Ish-Shalom, M., Maimon, N., Nefussy, B. (2009). Low-grade systemic inflammation in patients with amyotrophic lateral sclerosis. *Acta Neurologica Scandinavica, 119*(6), 383-389.

Kim, S., Lee, J., Cho, W., Cho, K., Sakong, J., Kim, J. (2010). Role of NOX-2 in lipopolysaccharide-induced matrix metalloproteinase expression and cell migration. *Immunology and Cell Biology, 88*(2), 197-204.

Kim, C., Marchal, C. C., Penninger, J., & Dinauer, M. C. (2003). The hemopoietic Rho/Rac guanine nucleotide exchange factor Vav1 regulates N-formyl-methionyl-leucyl-phenylalanine-activated neutrophil functions. *Journal of Immunology (Baltimore, Md.: 1950), 171*(8), 4425-4430.

Kimura, K., Ito, M., Amano, M., Chihara, K., Fukata, Y., Nakafuku, M. (1996). Regulation of myosin phosphatase by rho and rho-associated kinase (rho-kinase). *Science (New York, N.Y.), 273*(5272), 245-248.

Kitaoka, Y., Kitaoka, Y., Kumai, T., Lam, T. T., Kuribayashi, K., Isenoumi, K., et al. (2004). Involvement of RhoA and possible neuroprotective effect of Fasudil, a Rho kinase inhibitor, in NMDA-induced neurotoxicity in the rat retina. *Brain Research, 1018*(1), 111-118.

Kobayashi, T., Tsunawaki, S., & Seguchi, H. (2001). Evaluation of the process for superoxide production by NOX in human neutrophils: Evidence for cytoplasmic origin of superoxide. *Redox Report, 6*(1), 27-36.

Kohama, I., Lankford, K. L., Preiningerova, J., White, F. A., Vollmer, T. L., & Kocsis, J. D. (2001). Transplantation of cryopreserved adult human schwann cells enhances axonal conduction in demyelinated spinal cord. *The Journal of Neuroscience : The Official Journal of the Society for Neuroscience, 21*(3), 944-950.

Komagome, r., kimura, K., & Saito, M. (2000). Postnatal changes in rho and rho-related proteins in the mouse brain. *Japanese Journal of Veterinary Research, 47*(3-4), 127-133.

Kosako, H., Amano, M., Yanagida, M., Tanabe, K., Nishi, Y., Kaibuchi, K. (1997). Phosphorylation of glial fibrillary acidic protein at the same sites by cleavage furrow kinase and rho-associated kinase. *The Journal of Biological Chemistry, 272*(16), 10333-10336.

Koshkin, V., Lotan, O., & Pick, E. (1996). The cytosolic component p47PHOX is not a sine qua non participant in the activation of NOX but is required for optimal superoxide production. *Journal of Biological Chemistry, 271*(48), 30326-30329.

Krause, K. (2007). Aging: A revisited theory based on free radicals generated by NOX family NOXs. *Experimental Gerontology, 42*(4), 256-262.

Kreutzberg, G. W. (1995). Microglia, the first line of defence in brain pathologies. *Arzneimittel-Forschung, 45*(3A), 357-360.

Krüger, R., Hardt, C., Tschentscher, F., Jäckel, S., Kuhn, W., Müller, T. (2000). Genetic analysis of immunomodulating factors in sporadic parkinson's disease. *Journal of Neural Transmission, 107*(5), 553-562.

Kuhle, J., Lindberg, R., Regeniter, A., Mehling, M., Steck, A., Kappos, L. (2009). Increased levels of inflammatory chemokines in amyotrophic lateral sclerosis. *European Journal of Neurology, 16*(6), 771-774.

Kullander, K., Butt, S. J., Lebret, J. M., Lundfald, L., Restrepo, C. E., Rydstrom, A. (2003). Role of EphA4 and EphrinB3 in local neuronal circuits that control walking. *Science (New York,.), 299*(5614), 1889-1892.

Lavigne, M. C., Malech, H. L., Holland, S. M., & Leto, T. L. (2001). Genetic requirement of p47PHOX for superoxide production by murine microglia. *FASEB Journal : Official Publication of the Federation of American Societies for Experimental Biology, 15*(2), 285-287.

Lee, J. K., Kim, J. E., Sivula, M., & Strittmatter, S. M. (2004). Nogo receptor antagonism promotes stroke recovery by enhancing axonal plasticity. *The Journal of Neuroscience : The Official Journal of the Society for Neuroscience, 24*(27), 6209-6217.

Leto, T. L., Adams, A. G., & de Mendez, I. (1994). Assembly of the phagocyte NOX: Binding of src homology 3 domains to proline-rich targets. *Proceedings of the National Academy of Sciences of the United States of America, 91*(22), 10650-10654.

Leung, T., Manser, E., Tan, L., & Lim, L. (1995). A novel serine/threonine kinase binding the ras-related RhoA GTPase which translocates the kinase to peripheral membranes. *The Journal of Biological Chemistry, 270*(49), 29051-29054.

Leung, T., Chen, X. Q., Manser, E., & Lim, L. (1996). The p160 RhoA-binding kinase ROK alpha is a member of a kinase family and is involved in the reorganization of the cytoskeleton. *Molecular and Cellular Biology, 16*(10), 5313-5327.

Leusen, J. H., de Boer, M., Bolscher, B. G., Hilarius, P. M., Weening, R. S., Ochs, H. D (1994). A point mutation in gp91-PHOX of cytochrome b558 of the human NOX leading to defective translocation of the cytosolic proteins p47-PHOX and p67-PHOX. *The Journal of Clinical Investigation, 93*(5), 2120-2126.

Li, G., Liu, Y., Tzeng, N., Cui, G., Block, M. L., Wilson, B. (2005). Protective effect of dextromethorphan against endotoxic shock in mice. *Biochemical Pharmacology, 69*(2), 233-240.

Liang, C., Park, A. Y., & Guan, J. (2007). In-vitro scratch assay: A convenient and inexpensive method for analysis of cell migration in vitro. *Nature Protocols, 2*(2), 329-333.

Liao, J. K., Seto, M., & Noma, K. (2007). Rho kinase (ROCK) inhibitors. *Journal of Cardiovascular Pharmacology, 50*(1), 17-24.

Lieberman, A. P., Pitha, P. M., Shin, H. S., & Shin, M. L. (1989). Production of tumor necrosis factor and other cytokines by astrocytes stimulated with lipopolysaccharide or a neurotropic virus. *Proceedings of the National Academy of Sciences of the United States of America, 86*(16), 6348-6352.

Lino, M. M., Schneider, C., & Caroni, P. (2002). Accumulation of SOD1 mutants in postnatal motoneurons does not cause motoneuron pathology or motoneuron disease. *The Journal of Neuroscience : The Official Journal of the Society for Neuroscience, 22*(12), 4825-4832.

Litvan, I., Halliday, G., Hallett, M., Goetz, C. G., Rocca, W., Duyckaerts, C. (2007). The etiopathogenesis of parkinson disease and suggestions for future research. part I. *Journal of Neuropathology and Experimental Neurology, 66*(4), 251-257.

Liu, Y., Lin, H., & Tzeng, S. (2005). Tumor necrosis factor-α and interleukin-18 modulate neuronal cell fate in embryonic neural progenitor culture. *Brain Research, 1054*(2), 152-158.

Liu, J., Qu, W., Saavedra, J. E., & Waalkes, M. P. (2004). The nitric oxide donor, O2-vinyl 1-(pyrrolidin-1-yl)diazen-1-ium-1,2-diolate (V-PYRRO/NO), protects against cadmium-induced hepatotoxicity in mice. *The Journal of Pharmacology and Experimental Therapeutics, 310*(1), 18-24.

Liu, J., Cheng, M. L., Shi, J. Z., Yang, Q., Wu, J., Li, C. X. (2006). Differential effects between maotai and ethanol on hepatic gene expression in mice: Possible role of metallothionein and heme oxygenase-1 induction by maotai. *Experimental Biology and Medicine (Maywood, N.J.), 231*(9), 1535-1541.

Liu, M., & Bing, G. (2011). Lipopolysaccharide animal models for parkinson's disease. *Parkinson's Disease, 2011*, 327089.

Lobanov, A. V., Hatfield, D. L., & Gladyshev, V. N. (2009). Eukaryotic selenoproteins and selenoproteomes. *Biochimica Et Biophysica Acta (BBA)-General Subjects, 1790*(11), 1424-1428.

MacDonald, M. E., Ambrose, C. M., Duyao, M. P., Myers, R. H., Lin, C., Srinidhi, L. (1993). A novel gene containing a trinucleotide repeat that is expanded and unstable on huntington's disease chromosomes. *Cell, 72*(6), 971-983.

Madura, T., Yamashita, T., Kubo, T., Fujitani, M., Hosokawa, K., & Tohyama, M. (2004). Activation of Rho in the injured axons following spinal cord injury. *EMBO Reports, 5*(4), 412-417.

Magaki, S., Mueller, C., Dickson, C., & Kirsch, W. (2007). Increased production of inflammatory cytokines in mild cognitive impairment. *Experimental Gerontology, 42*(3), 233-240.

Maragakis, N. J., & Rothstein, J. D. (2006). Mechanisms of disease: Astrocytes in neurodegenerative disease. *Nature Clinical Practice Neurology, 2*(12), 679-689.

Martin, S., Vincent, J. P., & Mazella, J. (2003). Involvement of the neurotensin receptor-3 in the neurotensin-induced migration of human microglia. *The Journal of Neuroscience : The Official Journal of the Society for Neuroscience, 23*(4), 1198-1205.

Masek, B. B., Merchant, A., & Matthew, J. B. (1993). Molecular shape comparison of angiotensin II receptor antagonists. *Journal of Medicinal Chemistry, 36*(9), 1230-1238.

Matsui, T., Amano, M., Yamamoto, T., Chihara, K., Nakafuku, M., Ito, M. (1996). Rho-associated kinase, a novel serine/threonine kinase, as a putative target for small GTP binding protein rho. *The EMBO Journal, 15*(9), 2208-2216.

McCoy, M. K., Ruhn, K. A., Martinez, T. N., McAlpine, F. E., Blesch, A., & Tansey, M. G. (2008). Intranigral lentiviral delivery of dominant-negative TNF attenuates neurodegeneration and behavioral deficits in hemiparkinsonian rats. *Molecular Therapy, 16*(9), 1572-1579.

McGeer, P. L., Itagaki, S., Boyes, B. E., & McGeer, E. G. (1988). Reactive microglia are positive for HLA-DR in the substantia nigra of parkinson's and alzheimer's disease brains. *Neurology, 38*(8), 1285-1291.

Mcmanus, C. M., Liu, J. S., Hahn, M. T., Hua, L. L., Brosnan, C. F., Berman, J. W. (2000). Differential induction of chemokines in human microglia by type I and II interferons. *Glia, 29*(3), 273-280.

Melendez-Vasquez, C. V., Einheber, S., & Salzer, J. L. (2004). Rho kinase regulates schwann cell myelination and formation of associated axonal domains. *The Journal of Neuroscience : The Official Journal of the Society for Neuroscience, 24*(16), 3953-3963.

Min, K., Pyo, H., Yang, M., Ji, K., Jou, I., & Joe, E. (2004). Gangliosides activate microglia via protein kinase C and NOX. *Glia, 48*(3), 197-206.

Minagar, A., Toledo, E. G., Alexander, J. S., & Kelley, R. E. (2004). Pathogenesis of brain and spinal cord atrophy in multiple sclerosis. *Journal of Neuroimaging, 14*(s3), 5S-10S.

Monje, M. L., Toda, H., & Palmer, T. D. (2003). Inflammatory blockade restores adult hippocampal neurogenesis. *Science (New York,.), 302*(5651), 1760-1765.

Monnier, P. P., Sierra, A., Schwab, J. M., Henke-Fahle, S., & Mueller, B. K. (2003). The Rho/ROCK pathway mediates neurite growth-inhibitory activity associated with the chondroitin sulfate proteoglycans of the CNS glial scar. *Molecular and Cellular Neuroscience, 22*(3), 319-330.

Moreau-Fauvarque, C., Kumanogoh, A., Camand, E., Jaillard, C., Barbin, G., Boquet, I. (2003). The transmembrane semaphorin Sema4D/CD100, an inhibitor of axonal growth, is expressed on oligodendrocytes and upregulated after CNS lesion. *The Journal of Neuroscience : The Official Journal of the Society for Neuroscience, 23*(27), 9229-9239.

Moynagh, P. N. (2005). The interleukin-1 signalling pathway in astrocytes: A key contributor to inflammation in the brain. *Journal of Anatomy, 207*(3), 265-269.

Mudò, G., Mäkelä, J., Di Liberto, V., Tselykh, T. V., Olivieri, M., Piepponen, P. (2012). Transgenic expression and activation of PGC-1α protect dopaminergic neurons in the MPTP mouse model of Parkinson's disease. *Cellular and Molecular Life Sciences, 69*(7), 1153-1165.

Münch, G., Gasic-Milenkovic, J., Dukic-Stefanovic, S., Kuhla, B., Heinrich, K., Riederer, P. (2003). Microglial activation induces cell death, inhibits neurite outgrowth and causes neurite retraction of differentiated neuroblastoma cells. *Experimental Brain Research, 150*(1), 1-8.

Nadeau, S., & Rivest, S. (1999). Effects of circulating tumor necrosis factor on the neuronal activity and expression of the genes encoding the tumor necrosis factor receptors (p55 and p75) in the rat brain: A view from the blood–brain barrier. *Neuroscience, 93*(4), 1449-1464.

Nagatsu, T., & Sawada, M. (2006). Cellular and molecular mechanisms of Parkinson's disease: Neurotoxins, causative genes, and inflammatory cytokines. *Cellular and Molecular Neurobiology, 26*(4-6), 779-800.

Nakagawa, O., Fujisawa, K., Ishizaki, T., Saito, Y., Nakao, K., & Narumiya, S. (1996). ROCK-I and ROCK-II, two isoforms of rho-associated coiled-coil forming protein serine/threonine kinase in mice. *FEBS Letters, 392*(2), 189-193.

Nave, K. (2010). Myelination and support of axonal integrity by glia. *Nature, 468*(7321), 244-252.

Neuhaus, O., Stüve, O., Zarnvil, S. S., & Hartung, H. (2004). Are statins a treatment option for multiple sclerosis? *The Lancet Neurology, 3*(6), 369-371.

Neumann, H., Schweigreiter, R., Yamashita, T., Rosenkranz, K., Wekerle, H., & Barde, Y. A. (2002). Tumor necrosis factor inhibits neurite outgrowth and branching of hippocampal neurons by a rho-dependent mechanism. *The Journal of Neuroscience : The Official Journal of the Society for Neuroscience, 22*(3), 854-862.

Ni, M., Li, X., Yin, Z., Jiang, H., Sidoryk-Wegrzynowicz, M., Milatovic, D. (2010). Methylmercury induces acute oxidative stress, altering Nrf2 protein level in primary microglial cells. *Toxicological Sciences : An Official Journal of the Society of Toxicology, 116*(2), 590-603.

Nichols, N. R. (1999). Glial responses to steroids as markers of brain aging. *Journal of Neurobiology, 40*(4), 585-601.

Niederost, B., Oertle, T., Fritsche, J., McKinney, R. A., & Bandtlow, C. E. (2002). Nogo-A and myelin-associated glycoprotein mediate neurite growth inhibition by antagonistic regulation of RhoA and Rac1. *The Journal of Neuroscience : The Official Journal of the Society for Neuroscience, 22*(23), 10368-10376.

Niesen, F. H., Berglund, H., & Vedadi, M. (2007). The use of differential scanning fluorimetry to detect ligand interactions that promote protein stability. *Nature Protocols, 2*(9), 2212-2221.

Nimmerjahn A, Kirchhoff F, Helmchen F (2005). Resting microglial cells are highly dynamic surveillants of brain parenchyma in vivo. Sci 308: 1314-1318.

Nishimura, M., Mizuta, I., Mizuta, E., Yamasaki, S., Ohta, M., Kaji, R. (2001). Tumor necrosis factor gene polymorphisms in patients with sporadic parkinson's disease. *Neuroscience Letters, 311*(1), 1-4.

Nishimura, M., Kuno, S., Kaji, R., Yasuno, K., & Kawakami, H. (2005). Glutathione-S-transferase-1 and interleukin-1β gene polymorphisms in japanese patients with parkinson's disease. *Movement Disorders, 20*(7), 901-902.

Nisimoto, Y., Freeman, J. L., Motalebi, S. A., Hirshberg, M., & Lambeth, J. D. (1997). Rac binding to p67 phox structural basis for interactions of the rac1 effector region and insert

region with components of the respiratory burst oxidase. *Journal of Biological Chemistry, 272*(30), 18834-18841.

Nita, D. A., Nita, V., Spulber, S., Moldovan, M., Popa, D. P., Zagrean, A. (2001). Oxidative damage following cerebral ischemia depends on reperfusion-a biochemical study in rat. *Journal of Cellular and Molecular Medicine, 5*(2), 163-170.

Norflus, F., Nanje, A., Gutekunst, C., Shi, G., Cohen, J., Bejarano, M. (2004). Anti-inflammatory treatment with acetylsalicylate or rofecoxib is not neuroprotective in huntington's disease transgenic mice. *Neurobiology of Disease, 17*(2), 319-325.

O'Donnell, E., Vereker, E., & Lynch, M. (2000). Age-related impairment in LTP is accompanied by enhanced activity of stress-activated protein kinases: Analysis of underlying mechanisms. *European Journal of Neuroscience, 12*(1), 345-352.

Ogata, S., Morishige, K., Sawada, K., Hashimoto, K., Mabuchi, S., Kawase, C. (2009). Fasudil inhibits lysophosphatidic acid-induced invasiveness of human ovarian cancer cells. *International Journal of Gynecological Cancer : Official Journal of the International Gynecological Cancer Society, 19*(9), 1473-1480.

Ohashi, K., Nagata, K., Maekawa, M., Ishizaki, T., Narumiya, S., & Mizuno, K. (2000). Rho-associated kinase ROCK activates LIM-kinase 1 by phosphorylation at threonine 508 within the activation loop. *The Journal of Biological Chemistry, 275*(5), 3577-3582.

Oitzl, M. S., Van Oers, H., Schöbitz, B., & de Kloet, E. R. (1993). Interleukin-1β, but not interleukin-6, impairs spatial navigation learning. *Brain Research, 613*(1), 160-163.

Onyido, I., Norris, A. R., & Buncel, E. (2004). Biomolecule-mercury interactions: Modalities of DNA base-mercury binding mechanisms. remediation strategies. *Chemical Reviews, 104*(12), 5911-5930.

Page, P., Orchard, M., Laleu, B., & Gaggini, F. (2013). "Pyrazolo pyridine derivatives as NOX inhibitors." U.S. Patent 8,455,485, issued June 4, 2013.

Park, E., Gao, X., Chung, J. M., & Chung, K. (2006). Levels of mitochondrial reactive oxygen species increase in rat neuropathic spinal dorsal horn neurons. *Neuroscience Letters, 391*(3), 108-111.

Pavese, N., Gerhard, A., Tai, Y. F., Ho, A. K., Turkheimer, F., Barker, R. A. (2006). Microglial activation correlates with severity in huntington disease: A clinical and PET study. *Neurology, 66*(11), 1638-1643.

Pearson, R. G., & Songstad, J. (1967). Application of the principle of hard and soft acids and bases to organic chemistry. *Journal of the American Chemical Society, 89*(8), 1827-1836.

Pedrini, S., Carter, T. L., Prendergast, G., Petanceska, S., Ehrlich, M. E., & Gandy, S. (2005). Modulation of statin-activated shedding of alzheimer APP ectodomain by ROCK. *PLoS Medicine, 2*(1), e18.

Perry, R. T., Collins, J. S., Wiener, H., Acton, R., & Go, R. C. (2001). The role of TNF and its receptors in Alzheimer's disease. *Neurobiology of Aging, 22*(6), 873-883.

Pichery, M., Mirey, E., Mercier, P., Lefrancais, E., Dujardin, A., Ortega, N. (2012). Endogenous IL-33 is highly expressed in mouse epithelial barrier tissues, lymphoid organs, brain, embryos, and inflamed tissues: In situ analysis using a novel il-33-LacZ gene trap reporter strain. *Journal of Immunology (Baltimore, Md.: 1950), 188*(7), 3488-3495.

Pickering, M., & O'Connor, J. J. (2007). Pro-inflammatory cytokines and their effects in the dentate gyrus. *Progress in Brain Research, 163*, 339-354.

Poloni, M., Facchetti, D., Mai, R., Micheli, A., Agnoletti, L., Francolini, G. (2000). Circulating levels of tumour necrosis factor-α and its soluble receptors are increased in the blood of patients with amyotrophic lateral sclerosis. *Neuroscience Letters, 287*(3), 211-214.

Poltorak, A., He, X., Smirnova, I., Liu, M. Y., Van Huffel, C., Du, X. (1998). Defective LPS signaling in C3H/HeJ and C57BL/10ScCr mice: Mutations in Tlr4 gene. *Science (New York,), 282*(5396), 2085-2088.

Ponting, C. P. (1996). Novel domains in NOX subunits, sorting nexins, and PtdIns 3-kinases: Binding partners of SH3 domains? *Protein Science, 5*(11), 2353-2357.

Pramatarova, A., Laganiere, J., Roussel, J., Brisebois, K., & Rouleau, G. A. (2001). Neuron-specific expression of mutant superoxide dismutase 1 in transgenic mice does not lead to motor impairment. *The Journal of Neuroscience : The Official Journal of the Society for Neuroscience, 21*(10), 3369-3374.

Price, M. O., Atkinson, S. J., Knaus, U. G., & Dinauer, M. C. (2002). Rac activation induces NOX activity in transgenic COSPHOX cells, and the level of superoxide production is exchange factor-dependent. *The Journal of Biological Chemistry, 277*(21), 19220-19228.

Prosser, B. L., Ward, C. W., & Lederer, W. J. (2011). X-ROS signaling: Rapid mechano-chemo transduction in heart. *Science (New York, N.Y.), 333*(6048), 1440-1445.

Puck, T. T., & Marcus, P. I. (1955). A rapid method for viable cell titration and clone production with hela cells in tissue culture: The use of X-irradiated cells to supply conditioning factors. *Proceedings of the National Academy of Sciences of the United States of America, 41*(7), 432-437.

Pugh, C. R., Kumagawa, K., Fleshner, M., Watkins, L. R., Maier, S. F., & Rudy, J. W. (1998). Selective effects of peripheral lipopolysaccharide administration on contextual and auditory-cue fear conditioning. *Brain, Behavior, and Immunity, 12*(3), 212-229.

Qin, B., Cartier, L., Dubois-Dauphin, M., Li, B., Serrander, L., & Krause, K. (2006). A key role for the microglial NOX in APP-dependent killing of neurons. *Neurobiology of Aging, 27*(11), 1577-1587.

Qin, L., Wu, X., Block, M. L., Liu, Y., Breese, G. R., Hong, J. (2007). Systemic LPS causes chronic neuroinflammation and progressive neurodegeneration. *Glia, 55*(5), 453-462.

Qnais, E. (2011). The analgesic effect of the ethanolic extract of Matricaria aurea. Turkish *Journal of Biology*, 35(3), 347-352.

Quinn, M. T., & Gauss, K. A. (2004). Structure and regulation of the neutrophil respiratory burst oxidase: Comparison with nonphagocyte oxidases. *Journal of Leukocyte Biology, 76*(4), 760-781.

Quark Pharmaceuticals. (2008). Small interfering RNAs for inhibiting NADPH oxidase-related gene expression. WO152636

Ramer, L. M., Borisoff, J. F., & Ramer, M. S. (2004). Rho-kinase inhibition enhances axonal plasticity and attenuates cold hyperalgesia after dorsal rhizotomy. *The Journal of Neuroscience : The Official Journal of the Society for Neuroscience, 24*(48), 10796-10805.

Rantamäki, T., Kemppainen, S., Autio, H., Staven, S., Koivisto, H., Kojima, M. (2013). The impact of bdnf gene deficiency to the memory impairment and brain pathology of APPswe/PS1dE9 mouse model of Alzheimer's disease. *PloS One, 8*(7), e68722.

Regier, D. S., Greene, D. G., Sergeant, S., Jesaitis, A. J., & McPhail, L. C. (2000). Phosphorylation of p22PHOX is mediated by phospholipase D-dependent and -independent mechanisms. correlation of NOX activity and p22PHOX phosphorylation. *The Journal of Biological Chemistry, 275*(37), 28406-28412.

Reiter, R. J., Manchester, L. C., & Tan, D. X. (2010). Neurotoxins: Free radical mechanisms and melatonin protection. *Current Neuropharmacology, 8*(3), 194-210.

Ren, X. D., Kiosses, W. B., & Schwartz, M. A. (1999). Regulation of the small GTP-binding protein Rho by cell adhesion and the cytoskeleton. *The EMBO journal*, 18(3), 578-585.

Ridley, A. J. (2001). Rho GTPases and cell migration. *Journal of Cell Science, 114*(Pt 15), 2713-2722.

Riekenberg, S., Farhat, K., Debarry, J., Heine, H., Jung, G., Wiesmüller, K. (2009). Regulators of G-protein signalling are modulated by bacterial lipopeptides and lipopolysaccharide. *FEBS Journal, 276*(3), 649-659.

Riento, K., & Ridley, A. J. (2003). Rocks: Multifunctional kinases in cell behaviour. *Nature Reviews Molecular Cell Biology, 4*(6), 446-456.

Rocha, J. B., Freitas, A. J., Marques, M. B., Pereira, M. E., Emanuelli, T., & Souza, D. O. (1993). Effects of methylmercury exposure during the second stage of rapid postnatal brain growth on negative geotaxis and on delta-aminolevulinate dehydratase of suckling rats. *Brazilian Journal of Medical and Biological Research = Revista Brasileira De Pesquisas Medicas e Biologicas / Sociedade Brasileira De Biofisica 26*(10), 1077-1083.

Roos, D., Seeger, R., Puntel, R., & Vargas Barbosa, N. (2012). Role of calcium and mitochondria in MeHg-mediated cytotoxicity. *BioMed Research International, 2012*

Rosen, D. R., Siddique, T., Patterson, D., Figlewicz, D. A., Sapp, P., Hentati, A. (1993). Mutations in Cu/Zn superoxide dismutase gene are associated with familial amyotrophic lateral sclerosis. *Nature,* 362(6415):59-62.

Rosi, S., Vazdarjanova, A., Ramirez-Amaya, V., Worley, P., Barnes, C., & Wenk, G. (2006). Memantine protects against LPS-induced neuroinflammation, restores behaviorally-induced gene expression and spatial learning in the rat. *Neuroscience, 142*(4), 1303-1315.

Rossman, K. L., Der, C. J., & Sondek, J. (2005). GEF means go: Turning on RHO GTPases with guanine nucleotide-exchange factors. *Nature Reviews Molecular Cell Biology, 6*(2), 167-180.

Sakaguchi, H. (2004). Amide compounds and use thereof. U.S. Patent 6,762,321, issued July 13, 2004

Sapp, E., Kegel, K., Aronin, N., Hashikawa, T., Uchiyama, Y., Tohyama, K. (2001). Early and progressive accumulation of reactive microglia in the huntington disease brain. *Journal of Neuropathology & Experimental Neurology, 60*(2), 161-172.

Sargsyan, S. A., Monk, P. N., & Shaw, P. J. (2005). Microglia as potential contributors to motor neuron injury in amyotrophic lateral sclerosis. *Glia, 51*(4), 241-253.

Sathyamoorthy, M., de Mendez, I., Adams, A. G., & Leto, T. L. (1997). p40(PHOX) down-regulates NOX activity through interactions with its SH3 domain. *The Journal of Biological Chemistry, 272*(14), 9141-9146.

Satoh, S., Utsunomiya, T., Tsurui, K., Kobayashi, T., Ikegaki, I., Sasaki, Y. (2001). Pharmacological profile of hydroxy Fasudil as a selective rho kinase inhibitor on ischemic brain damage. *Life Sciences, 69*(12), 1441-1453.

Sawamoto, K., Wichterle, H., Gonzalez-Perez, O., Cholfin, J. A., Yamada, M., Spassky, N. (2006). New neurons follow the flow of cerebrospinal fluid in the adult brain. *Science (New York, N.Y.), 311*(5761), 629-632.

Schnädelbach, O., Özen, Í., Blaschuk, O. W., Gour, B. J., Meyer, R. L., & Fawcett, J. W. (2001). N-cadherin is involved in axon-oligodendrocyte contact and myelination. *Molecular and Cellular Neuroscience, 17*(6), 1084-1093.

Schwab, J. M., Conrad, S., Monnier, P. P., Julien, S., Mueller, B. K., & Schluesener, H. J. (2005a). Spinal cord injury-induced lesional expression of the repulsive guidance molecule (RGM). *European Journal of Neuroscience, 21*(6), 1569-1576.

Schwab, J. M., Monnier, P. P., Schluesener, H. J., Conrad, S., Beschorner, R., Chen, L. (2005b). Central nervous system injury–induced repulsive guidance molecule expression in the adult human brain. *Archives of Neurology, 62*(10), 1561-1568.

Schweigreiter, R., Walmsley, A. R., Niederöst, B., Zimmermann, D. R., Oertle, T., Casademunt, E. (2004). Versican V2 and the central inhibitory domain of nogo-A inhibit neurite growth via p75 NTR/NgR-independent pathways that converge at RhoA. *Molecular and Cellular Neuroscience, 27*(2), 163-174.

Seal, R. P., & Edwards, R. H. (2006). Functional implications of neurotransmitter co-release: Glutamate and GABA share the load. *Current Opinion in Pharmacology, 6*(1), 114-119.

Sebbagh, M., Renvoizé, C., Hamelin, J., Riché, N., Bertoglio, J., & Bréard, J. (2001). Caspase-3-mediated cleavage of ROCK I induces MLC phosphorylation and apoptotic membrane blebbing. *Nature Cell Biology, 3*(4), 346-352.

Seifert, R., Burde, R., & Schultz, G. (1989). Activation of NOX by purine and pyrimidine nucleotides involves G proteins and is potentiated by chemotactic peptides. *Biochem.J, 259*, 813-819.

Seno, K., Nishi, K., Matsuo, Y., & Fujishita, T. (2010). *Pyrazolo [1, 5-a] Pyrimidine Derivative and Nad (p) h Oxidase Inhibitor Containing the Same,* U.S. Patent 7,662,826, issued February 16, 2010.

Setoguchi, S., Hirooka, Y., Eshima, K., Shimokawa, H., & Takeshita, A. (2002). Tetrahydrobiopterin improves impaired endothelium-dependent forearm vasodilation in patients with heart failure. *Journal of Cardiovascular Pharmacology, 39*(3), 363-368.

Shamah, S. M., Lin, M. Z., Goldberg, J. L., Estrach, S., Sahin, M., Hu, L. (2001). EphA receptors regulate growth cone dynamics through the novel guanine nucleotide exchange factor ephexin. *Cell, 105*(2), 233-244.

Shanker, G., Aschner, J. L., Syversen, T., & Aschner, M. (2004). Free radical formation in cerebral cortical astrocytes in culture induced by methylmercury. *Molecular Brain Research, 128*(1), 48-57.

Sharpe, C. C., & Hendry, B. M. (2003). Signaling: Focus on Rho in renal disease. *Journal of the American Society of Nephrology : JASN, 14*(1), 261-264.

Shibuya, M., Suzuki, Y., Sugita, K., Saito, I., Sasaki, T., Takakura, K. (1992). Effect of AT877 on cerebral vasospasm after aneurysmal subarachnoid hemorrhage: Results of a prospective placebo-controlled double-blind trial. *Journal of Neurosurgery, 76*(4), 571-577.

Shimazu, R., Akashi, S., Ogata, H., Nagai, Y., Fukudome, K., Miyake, K. (1999). MD-2, a molecule that confers lipopolysaccharide responsiveness on toll-like receptor 4. *The Journal of Experimental Medicine, 189*(11), 1777-1782.

Shimizu, T., Ihara, K., Maesaki, R., Amano, M., Kaibuchi, K., & Hakoshima, T. (2003). Parallel coiled-coil association of the RhoA-binding domain in rho-kinase. *The Journal of Biological Chemistry, 278*(46), 46046-46051.

Shimizu, Y., Thumkeo, D., Keel, J., Ishizaki, T., Oshima, H., Oshima, M. (2005). ROCK-I regulates closure of the eyelids and ventral body wall by inducing assembly of actomyosin bundles. *The Journal of Cell Biology, 168*(6), 941-953.

Shimokawa, H., Hiramori, K., Iinuma, H., Hosoda, S., Kishida, H., Osada, H. (2002). Anti-anginal effect of Fasudil, a rho-kinase inhibitor, in patients with stable effort angina: A multicenter study. *Journal of Cardiovascular Pharmacology, 40*(5), 751-761.

Shirao, S., Kashiwagi, S., Sato, M., Miwa, S., Nakao, F., Kurokawa, T. (2002). Sphingosylphosphorylcholine is a novel messenger for rho-kinase-mediated Ca2+

sensitization in the bovine cerebral artery: Unimportant role for protein kinase C. *Circulation Research, 91*(2), 112-119.

Shivakumar, D., Williams, J., Wu, Y., Damm, W., Shelley, J., Sherman, W. Prediction of Absolute Solvation Free Energies using Molecular Dynamics Free Energy Perturbation and the OPLS Force Field. *J Chem Theory Comput.* 2010, 6: 1509–19.

Singh, A., & Jiang, Y. (2004). How does peripheral lipopolysaccharide induce gene expression in the brain of rats? *Toxicology, 201*(1), 197-207.

Singhrao, S., Neal, J., Morgan, B., & Gasque, P. (1999). Increased complement biosynthesis by microglia and complement activation on neurons in huntington's disease. *Experimental Neurology, 159*(2), 362-376.

Somlyo, A. P., & Somlyo, A. V. (2000). Signal transduction by G-proteins, Rho-kinase and protein phosphatase to smooth muscle and non-muscle myosin II. *The Journal of Physiology, 522*(2), 177-185.

Somlyo, A. P., & Somlyo, A. V. (2003). Ca2+ sensitivity of smooth muscle and nonmuscle myosin II: Modulated by G proteins, kinases, and myosin phosphatase. *Physiological Reviews, 83*(4), 1325-1358.

Soto, C. (2003). Unfolding the role of protein misfolding in neurodegenerative diseases. *Nature Reviews Neuroscience, 4*(1), 49-60.

Sprang, S. R. (1997). G protein mechanisms: Insights from structural analysis. *Annual Review of Biochemistry, 66*(1), 639-678.

Stack, E. C., Smith, K. M., Ryu, H., Cormier, K., Chen, M., Hagerty, S. W. (2006). Combination therapy using minocycline and coenzyme Q 10 in R6/2 transgenic huntington's disease mice. *Biochimica Et Biophysica Acta (BBA)-Molecular Basis of Disease, 1762*(3), 373-380.

Stewart, W. F., Kawas, C., Corrada, M., & Metter, E. J. (1997). Risk of alzheimer's disease and duration of NSAID use. *Neurology, 48*(3), 626-632.

Stringari, J., Meotti, F. C., Souza, D. O., Santos, A. R., & Farina, M. (2006). Postnatal methylmercury exposure induces hyperlocomotor activity and cerebellar oxidative stress in mice: Dependence on the neurodevelopmental period. *Neurochemical Research, 31*(4), 563-569.

Sumi, T., Matsumoto, K., & Nakamura, T. (2001). Specific activation of LIM kinase 2 via phosphorylation of threonine 505 by ROCK, a rho-dependent protein kinase. *The Journal of Biological Chemistry, 276*(1), 670-676.

Sumimoto, H., Sakamoto, N., Nozaki, M., Sakaki, Y., Takeshige, K., & Minakami, S. (1992). Cytochrome b 558, a component of the phagocyte NOX, is a flavoprotein. *Biochemical and Biophysical Research Communications, 186*(3), 1368-1375.

Sung, J., Miao, L., Calvert, J. W., Huang, L., Harkey, H. L., & Zhang, J. H. (2003). A possible role of RhoA/Rho-kinase in experimental spinal cord injury in rat. *Brain Research, 959*(1), 29-38.

Supinski, G., Stofan, D., Nethery, D., Szweda, L., & DiMarco, A. (1999). Apocynin improves diaphragmatic function after endotoxin administration. *Journal of Applied Physiology (Bethesda, Md.: 1985), 87*(2), 776-782.

Swiercz, J. M., Kuner, R., Behrens, J., & Offermanns, S. (2002). Plexin-B1 directly interacts with PDZ-RhoGEF/LARG to regulate RhoA and growth cone morphology. *Neuron, 35*(1), 51-63.

Sylvester, J. T. (2004). The tone of pulmonary smooth muscle: ROK and rho music? *American Journal of Physiology.Lung Cellular and Molecular Physiology, 287*(4), L624-30.

Tai, Y. F., Pavese, N., Gerhard, A., Tabrizi, S. J., Barker, R. A., Brooks, D. J. (2007). Microglial activation in presymptomatic huntington's disease gene carriers. *Brain : A Journal of Neurology, 130*(Pt 7), 1759-1766.

Takami, A., Iijima, H., Iwakubo, M., & Okada, Y. (2007). *Nitrogen-Containing Compounds having Kinase Inhibitory Activity and Drugs Containing the Same, U.S. Patent No. 7,217,722*. Washington, DC.

Takanashi, Y., Ishida, T., Meguro, T., Kiwada, H., Zhang, J. H., & Yamamoto, I. (2001). Efficacy of intrathecal liposomal Fasudil for experimental cerebral vasospasm after subarachnoid hemorrhage. *Neurosurgery, 48*(4), 894-901.

Takeda, K., & Akira, S. (2004). TLR signaling pathways. *Seminars in Immunology* 16. (1) pp. 3-9.

Tan, I., Seow, K. T., Lim, L., & Leung, T. (2001). Intermolecular and intramolecular interactions regulate catalytic activity of myotonic dystrophy kinase-related Cdc42-binding kinase alpha. *Molecular and Cellular Biology, 21*(8), 2767-2778.

Tanaka, H., Yamashita, T., Yachi, K., Fujiwara, T., Yoshikawa, H., & Tohyama, M. (2004). Cytoplasmic p21 Cip1/WAF1 enhances axonal regeneration and functional recovery after spinal cord injury in rats. *Neuroscience, 127*(1), 155-164.

Taoufik, E., Valable, S., Muller, G. J., Roberts, M. L., Divoux, D., Tinel, A. (2007). FLIP(L) protects neurons against in vivo ischemia and in vitro glucose deprivation-induced cell death. *The Journal of Neuroscience: The Official Journal of the Society for Neuroscience, 27*(25), 6633-6646.

Tartaglia, L. A., Rothe, M., Hu, Y., & Goeddel, D. V. (1993). Tumor necrosis factor's cytotoxic activity is signaled by the p55 TNF receptor. *Cell, 73*(2), 213-216.

Tatsumi, S., Mabuchi, T., Katano, T., Matsumura, S., Abe, T., Hidaka, H. (2005). Involvement of rho-kinase in inflammatory and neuropathic pain through phosphorylation of myristoylated alanine-rich C-kinase substrate (MARCKS). *Neuroscience, 131*(2), 491-498.

Taylor, W. R., Jones, D. T., & Segal, A. W. (1993). A structural model for the nucleotide binding domains of the flavocytochrome b–245 β-chain. *Protein Science, 2*(10), 1675-1685.

Tegtmeier, F., Walter, U., Schinzel, R., Wingler, K., Scheurer, P., & Schmidt, H. (2005). *Compounds Containing a N-Heteroaryl Moiety Linked to Fused Ring Moieties for the Inhibition of NAD (P) H Oxidases and Platelet Activation,* U.S. Patent Application 11/579,999, filed May 13, 2005

Theoharides, T. C., & Doyle, R. (2008). Autism, gut-blood-brain barrier, and mast cells. *Journal of Clinical Psychopharmacology, 28*(5), 479-483.

Thumkeo, D., Keel, J., Ishizaki, T., Hirose, M., Nonomura, K., Oshima, H. (2003). Targeted disruption of the mouse rho-associated kinase 2 gene results in intrauterine growth retardation and fetal death. *Molecular and Cellular Biology, 23*(14), 5043-5055.

Tony V, Alain R, Patricia S.M, Marie-Odile V, Marie-Francoise B, Michel W. (2006) Diosmetin derivatives for the treatment and prevention of thrombotic pathologies. WO2006092490

Toshima, Y., Satoh, S., Ikegaki, I., & Asano, T. (2000). A new model of cerebral microthrombosis in rats and the neuroprotective effect of a rho-kinase inhibitor. *Stroke; a Journal of Cerebral Circulation, 31*(9), 2245-2250.

Tsujita, Y., Muraski, J., Shiraishi, I., Kato, T., Kajstura, J., Anversa, P. (2006). Nuclear targeting of akt antagonizes aspects of cardiomyocyte hypertrophy. *Proceedings of the National Academy of Sciences of the United States of America, 103*(32), 11946-11951.

Tuppo, E. E., & Arias, H. R. (2005). The role of inflammation in Alzheimer's disease. *The International Journal of Biochemistry & Cell Biology, 37*(2), 289-305.

Turner, M. S., Trauger, J. W., Stephens, J., & LoGrasso, P. (2002). Characterization and purification of truncated human rho-kinase II expressed in sf-21 cells. *Archives of Biochemistry and Biophysics, 405*(1), 13-20.

Turner, M., Cagnin, A., Turkheimer, F., Miller, C., Shaw, C., Brooks, D. (2004). Evidence of widespread cerebral microglial activation in amyotrophic lateral sclerosis: An [11 C](R)-PK11195 positron emission tomography study. *Neurobiology of Disease, 15*(3), 601-609.

Uehata, M., Ishizaki, T., Satoh, H., Ono, T., Kawahara, T., Morishita, T. (1997). Calcium sensitization of smooth muscle mediated by a rho-associated protein kinase in hypertension. *Nature, 389*(6654), 990-994.

Uehata, M., Ono, T., Satoh, H., Yamagami, K., & Kawahara, T. (2001). *Medicines Comprising Rho Kinase Inhibitor, INCOMPLETE*

Ulevitch, R., & Tobias, P. (1995). Receptor-dependent mechanisms of cell stimulation by bacterial endotoxin. *Annual Review of Immunology, 13*(1), 437-457.

Vallieres, L., Campbell, I. L., Gage, F. H., & Sawchenko, P. E. (2002). Reduced hippocampal neurogenesis in adult transgenic mice with chronic astrocytic production of interleukin-6. *The Journal of Neuroscience : The Official Journal of the Society for Neuroscience, 22*(2), 486-492.

Van Aelst, L., & D'Souza-Schorey, C. (1997). Rho GTPases and signaling networks. *Genes & Development, 11*(18), 2295-2322.

Vawter, M. P., Dillon-Carter, O., Tourtellotte, W., Carvey, P., & Freed, W. J. (1996). TGFβ1 and TGFβ2 concentrations are elevated in parkinson's disease in ventricular cerebrospinal fluid. *Experimental Neurology, 142*(2), 313-322.

Vereker, E., Campbell, V., Roche, E., McEntee, E., & Lynch, M. A. (2000). Lipopolysaccharide inhibits long term potentiation in the rat dentate gyrus by activating caspase-1. *The Journal of Biological Chemistry, 275*(34), 26252-26258.

Visnagri, A., Kandhare, A. D., Chakravarty, S., Ghosh, P., & Bodhankar, S. L. (2014). Hesperidin, a flavanoglycone attenuates experimental diabetic neuropathy via modulation of cellular and biochemical marker to improve nerve functions. *Pharmaceutical Biology, 52*(7), 814-828.

Wahl, S., Barth, H., Ciossek, T., Aktories, K., & Mueller, B. K. (2000). Ephrin-A5 induces collapse of growth cones by activating Rho and Rho kinase. *The Journal of Cell Biology, 149*(2), 263-270.

Walder, C. E., Green, S. P., Darbonne, W. C., Mathias, J., Rae, J., Dinauer, M. C. (1997). Ischemic stroke injury is reduced in mice lacking a functional NOX. *Stroke; a Journal of Cerebral Circulation, 28*(11), 2252-2258.

Wallach, T., & Segal, A. (1997). Analysis of glycosylation sites on gp91PHOX, the flavocytochrome of the NOX, by site-directed mutagenesis and translation in vitro. *Biochem.J, 321*, 583-585.

Walmsley, S. (2005). Print C, farahi N, peyssonnaux C, johnson RS, Cramer T, sobolewski A, condliffe AM, cowburn AS, johnson N, chilvers ER. hypoxia-induced neutrophil survival is mediated by HIF-1alpha-dependent NF-kappab activity. *J Exp Med, 201*(1), 105-115.

Walters, C. E., Pryce, G., Hankey, D. J., Sebti, S. M., Hamilton, A. D., Baker, D. (2002). Inhibition of rho GTPases with protein prenyltransferase inhibitors prevents leukocyte recruitment to the central nervous system and attenuates clinical signs of disease in an animal model of multiple sclerosis. *Journal of Immunology (Baltimore, Md.: 1950), 168*(8), 4087-4094.

Wei, Y. H., & Lee, H. C. (2002). Oxidative stress, mitochondrial DNA mutation, and impairment of antioxidant enzymes in aging. *Experimental Biology and Medicine (Maywood, N.J.), 227*(9), 671-682.

Wettschureck, N., & Offermanns, S. (2002). Rho/Rho-kinase mediated signaling in physiology and pathophysiology. *Journal of Molecular Medicine, 80*(10), 629-638.

Weydt, P., Yuen, E. C., Ransom, B. R., & Möller, T. (2004). Increased cytotoxic potential of microglia from ALS-transgenic mice. *Glia, 48*(2), 179-182.

Whishaw, I. Q., O'Connor, W., & Dunnett, S. (1985). Disruption of central cholinergic systems in the rat by basal forebrain lesions or atropine: Effects on feeding, sensorimotor behaviour, locomotor activity and spatial navigation. *Behavioural Brain Research, 17*(2), 103-115.

Wientjes, F., Panayotou, G., Reeves, E., & Segal, A. (1996). Interactions between cytosolic components of the NOX: P40PHOX interacts with both p67PHOX and p47PHOX. *Biochem.J, 317*, 919-924.

Wiessner, C., Bareyre, F. M., Allegrini, P. R., Mir, A. K., Frentzel, S., Zurini, M. (2003). Anti–Nogo-A antibody infusion 24 hours after experimental stroke improved behavioral outcome

and corticospinal plasticity in normotensive and spontaneously hypertensive rats. *Journal of Cerebral Blood Flow & Metabolism, 23*(2), 154-165.

Willson, C. A., Irizarry-Ramíacrez, M., Gaskins, H. E., Cruz-Orengo, L., Figueroa, J. D., Whittemore, S. R. (2002). Upregulation of EphA receptor expression in the injured adult rat spinal cord. *Cell Transplantation, 11*(3), 229-239.

Wu, C., Chen, Y., Yu, L., Chen, H., Jen, C. J., Huang, A. (2007). Treadmill exercise counteracts the suppressive effects of peripheral lipopolysaccharide on hippocampal neurogenesis and learning and memory. *Journal of Neurochemistry, 103*(6), 2471-2481.

Yamamoto, T., & Yamada, K. (2004). Specific NADPH oxidase inhibitor. U.S. Patent Application 10/552,340, filed April 8, 2004.

Yang, S., & Kim, H. (2012). The RhoA-ROCK-PTEN pathway as a molecular switch for anchorage dependent cell behavior. *Biomaterials*, *33*(10), 2902-2915.

Yates, S. L., Burgess, L. H., Kocsis-Angle, J., Antal, J. M., Dority, M. D., Embury, P. B. (2000). Amyloid β and amylin fibrils induce increases in proinflammatory cytokine and chemokine production by THP-1 cells and murine microglia. *Journal of Neurochemistry, 74*(3), 1017-1025.

Yoshihara, T., Ishigaki, S., Yamamoto, M., Liang, Y., Niwa, I., Takeuchi, H. (2002). Differential expression of inflammation-and apoptosis-related genes in spinal cords of a mutant SOD1 transgenic mouse model of familial amyotrophic lateral sclerosis. *Journal of Neurochemistry, 80*(1), 158-167.

Yoshinaga, S., Kohjima, M., Ogura, K., Yokochi, M., Takeya, R., Ito, T. (2003). The PB1 domain and the PC motif-containing region are structurally similar protein binding modules. *The EMBO Journal, 22*(19), 4888-4897.

Yu, L., Quinn, M. T., Cross, A. R., & Dinauer, M. C. (1998). Gp91(PHOX) is the heme binding subunit of the superoxide-generating NOX. *Proceedings of the National Academy of Sciences of the United States of America, 95*(14), 7993-7998.

Zhan, Y., He, D., Newburger, P. E., & Zhou, G. W. (2004). p47PHOX PX domain of NOX targets cell membrane via moesin-mediated association with the actin cytoskeleton. *Journal of Cellular Biochemistry, 92*(4), 795-809.

Zhou, Y., Su, Y., Li, B., Liu, F., Ryder, J. W., Wu, X. (2003). Nonsteroidal anti-inflammatory drugs can lower amyloidogenic Abeta42 by inhibiting rho. *Science (New York, N.Y.), 302*(5648), 1215-1217.

Appendix

List of publications

FROM THESIS WORK

1. **Alokam R**, Singhal S, Srivathsav GS, Garigipati S, Puppala S, Sriram D, Perumal Y. Design of dual inhibitors of ROCK-I and NOX2 as potential leads for the treatment of neuroinflammation associated with various neurological diseases including autism spectrum disorder. Mol Biosyst. 2015 Feb 20;11(2):607-17.
2. Mishra RK, **Alokam R**, Singhal SM, Srivathsav G, Sriram D, Kaushik-Basu N, Manvar D, Yogeeswari P. Design of novel rho kinase inhibitors using energy based pharmacophore modeling, shape-based screening, in silico virtual screening, and biological evaluation. J Chem Inf Model. 2014 Oct 27;54(10):2876-86.
3. **Alokam R**, Battu MB, Gangadhar M, Srikanth R, Sriram D, Yogeeswari P. Identification of dual inhibitors of ROCK-I and NOX-2 useful in the treatment of neurodevelopmental and neurodegenerative diseases. J Neur Res. (Communicated)

OTHER PUBLICATIONS

1. Jeankumar VU, **Alokam R**, Sridevi JP, Suryadevara P, Matikonda SS, Peddi S, Sahithi S, Alvala M, Yogeeswari P, Sriram D. Discovery and structure optimization of a series of isatin derivatives as Mycobacterium tuberculosis chorismate mutase inhibitors. Chem Biol Drug Des. 2014 Apr;83(4):498-506.
2. **Alokam R**, Jeankumar VU, Sridevi JP, Matikonda SS, Peddi S, Alvala M, Yogeeswari P, Sriram D. Identification and structure-activity relationship study of carvacrol derivatives as Mycobacterium tuberculosis chorismate mutase inhibitors. J Enzyme Inhib Med Chem. 2014 Aug;29(4):547-54.
3. Mishra RK, **Alokam R**, Sriram D, Yogeeswari P. Potential role of Rho kinase inhibitors in combating diabetes-related complications including diabetic neuropathy--a review. Curr Diabetes Rev. 2013 May;9(3):249-66. Review.

PAPERS PRESENTED AT NATIONAL AND INTERNATIONAL CONFERENCES

1. Matharasala G., **Reshma A**., Sriram D., Yogeeswari P. MG2, a novel semicarbazone derivative, reduces neuropathic pain by inhibiting the expression levels of neuroinflammatory mediators. Pathways of Neurodevelopmental Disorders, March 16 - March 20, 2015, Granlibakken Resort, Tahoe City, California, USA.
2. Gaus, A., Mishra, R.K., **Alokam, R**., Singhal, S.M., Sriram, D., Yogeeswari, P., Evaluation of 2,6-diaminopyrimidines as novel Rho kinase inhibitors using animal models of treatment of neurological disorders. 66th Indian Pharmaceutical Congress: India- Pharmacy of the World, 23-25 January 2015, Hyderabad, India.
3. Srikanth, R., **Reshma, A**., Kulkarni, P., Sriram, D., Yogeeswari, P., Structure-based drug design, synthesis and screening of Adenosine A2A antagonists as novel antiepileptic agents. 11th European Congress on Epileptology, 29th June-3rd July 2014, Stockholm, Sweden.
4. Saketh, S.D., **Reshma, A**., Srikant, V., Sriram, D., Yogeeswari, P., BIA-6: A novel AKT inhibitor with potent activity in lung cancer, 15th World Conference on Lung Cancer, 27-30 October 2013, Sydney, Australia.
5. M. Siddharth Sai, V.U. Jean Kumar, **A. Reshma**, P. Yogeeswari, D. Sriram, In-Silico design, Synthesis and in-vitro screening of novel inhibitors of Chorismate mutase enzyme involved in Shikimate pathway of Mycobacterium tuberculosis, 2nd UK-India MedChem Congress, 22-23 March 2013, Hyderabad.
6. P. Santosh, V.U. Jean Kumar, **A. Reshma**, D. Sriram, P. Yogeeswari, Development of carvacrol derivatives as potential inhibitors of MTB chorismate mutase, 2nd UK-India MedChem Congress, 22-23 March 2013, Hyderabad.
7. Ram Kumar Mishra, **Reshma Chowdary**, D. Sriram, P. Yogeeswari, Design of Novel Rho Kinase Inhibitors for the treatment of Diabetic Complications using Energy-based Pharmacophore Modelling, In-silico screening and Docking studies, 3rd World Congress on Diabetes & Metabolism,24-26 Septemeber 2012, Hyderabad, India.
8. P. Sripriya, M. Soumya, **Reshma Alokam**, P. Susruta, D. Sriram, P. Yogeeswari, Structure Guided Design of Inhibitors for SH3 domain of p47PHOX subunit of NOX 2 implicated in various human disorders, 3rd World Congress on Diabetes & Metabolism,24-26 Septemeber 2012, Hyderabad, India.
9. **Reshma Alokam**, Jean Kumar, D. Sriram, P. Yogeeswari, Identification of novel inhibitors of Chorismate mutase enzyme involved in Shikimic pathway of Mycobacterium tuberculosis: Design and In-vitro screening, 3rd World Congress on Biotechnology,13-15 Septemeber 2012, Hyderabad, India.

BIOGRAPHY OF RESHMA CHOWDARY ALOKAM

Reshma Chowdary Alokam completed her Bachelor of Science in Microbiology from The St.Ann.s women college; Osmania University in the Year 2008 and M.Sc (Microbiology) from Avanti PG college, Osmania University also awarded gold medal from the same college. She has been appointed as a Research assistant in Biological sciences department in January 2011, Birla Institute of Technology and Science. Later, in August-2011 joined in Pharmacy department as a BITS-institute fellow under the supervision of Prof. P. Yogeeswari. She was awarded CSIR-Travel grant to attend the 8^{th} Brain international confernce from HRDG-CSIR, New Delhi in October 2014. She has published three scientific publications in well-renowned international journals and few more are in communication. She had presented papers at various national and international conferences.

BIOGRAPHY OF PROF.P.YOGEESWARI

Dr. P. Yogeeswari is presently working in the capacity of Professor and Associate Dean (Sponsored Research and Consultancy Division), Department of Pharmacy, Birla Institute of Technology and Science, Pilani, Hyderabad Campus. She received her Ph.D. degree in the year 2001 from Banaras Hindu University; Varanasi. She has been involved in research for the last 14 years and in teaching for 13 years. APTI honoured her with YOUNG PHARMACY TEACHER AWARD for the year 2007. In 2010, ICMR honored her by awarding "Shakuntala Amir Chand Award" for her excellent biomedical research. She has been awarded for IASP 2014 "Excellence in Pain Research and Management in Developing Countries" under the basic science research category at Argentina in October 2014. She has collaborations with various national and international organizations that include National Institute of Health, Bethesda, USA, National Institute of Mental Health and Neurosciences, Bangalore, Karolinska Institute, Stockholm, Sweden, National Institute of Immunology, New Delhi, India, Pasteur Institute, University of Lille, France, Bogomoletz Institute of Physiology National Academy of Science, Ukraine, and Faculty of Medicine of Porto, Porto, Portugal,. She has to her credit more than 190 research publications and one Indian Patent, Application No: 1138/CHE/2009. She is an expert reviewer of many international journals like Journal of Medicinal Chemistry (ACS), Journal of Chemical Information & Modeling (ACS, USA), Bioorganic Medicinal Chemistry (Elsevier), Recent Patents on CNS Drug Discovery (Bentham), etc. She has also co-authored a textbook on organic medicinal chemistry with Dr. D Sriram titled "Medicinal Chemistry" published by Pearson Education and one book chapter in in Jan 2013 by IGI Global. She is a lifetime member of Association of Pharmacy Teachers of India and Indian Pharmacological Society. She has successfully completed many sponsored projects and currently handling projects sponsored by DST, DBT INDO-BRAZIL, ICMR-INSERM, and CSIR. She has guided ten Ph.D students and currently nine students are pursuing their Ph.D. work.